UNIVERSIDAD
DE GRANADA

Doctoral Thesis

Modeling avascular tumor dynamics and low-intensity ultrasound therapeutics

---

Beatriz Blanco Besteiro

Advisors:
Guillermo Rus Carlborg
Juan Manuel Melchor Rodríguez

Doctoral Programme in Civil Engineering
2023

Editor: Universidad de Granada. Tesis Doctorales
Autor: Beatriz Blanco Besteiro
ISBN: 978-84-1195-464-8
URI: https://hdl.handle.net/10481/95847

La doctoranda Beatriz Blanco Besteiro, el director de la tesis Guillermo Rus Carlborg y el codirector Juan Manuel Melchor Rodríguez garantizamos, al firmar esta tesis doctoral, que el trabajo ha sido realizado por la doctoranda bajo la dirección del director y codirector de la tesis y hasta donde nuestro conocimiento alcanza, en la realización del trabajo, se han respetado los derechos de otros autores a ser citados cuando se han utilizado sus resultados o publicaciones.

En Granada, en marzo de 2023.

Director de la Tesis	Codirector de la Tesis	Doctoranda
Guillermo Rus Carlborg	Juan Manuel Melchor Rodriguez	Beatriz Blanco Besteiro

"It is our choices, Harry, that show what we truly are, far more than our abilities."

Albus Dumbledore

Acknowledgements

Thanks to the Ministry of Science, Innovation and Universities of Spain, for supporting this work through FPU17/01415 grant.

I really acknowledge my advisor, Guillermo Rus, for opening the doors of his research group and offering me four years of academic excellence. To my co-advisor, Juan Melchor, for introducing me to research and showing me a world that I am passionate about. I deeply appreciate their guidance and dedication, especially during this last challenging year. My heartfelt appreciation to Juan Soler and Roberto Palma for their immense investment of time in my thesis, and for the care and enthusiasm with which they have taught me. My most sincere gratitude to my stay advisor, Héctor Gómez, for granting me the great privilege of being a part of his outstanding work and team. I profess great admiration, respect, affection, and deep gratitude to these five excellent researchers. Their support has been invaluable and has enabled me to grow both academically and personally.

My appreciation also extends to my dear lab colleagues, Antonio G, Antonio C, Dani, Rafa, Manu, Hirad, Jose, and again Guillermo and Juanma for making the research enjoyable, and for their scientific and emotional support. Huge thanks to Inas and Jorge. Our team made Granada my second home. Thanks to collaborators Juan Campos, Francisco Gámiz, and Juan Marchal and their teams who also contributed to this thesis. I am indebted to Mario and Marina, for their great welcome and help during my time at Purdue.

Á xente que máis quero, a miña familia e amigos máis próximos. Grazas pola paciencia e a comprensión polo tempo que – moito ó meu pesar – non gozamos xuntos. Ós meus pais, Ángel e Chus, por regalarme as súas ás para voar e agardarme sempre. Débolles todo. Ó meu Susiño, por ser o meu gran apoio incondicional na búsqueda do futuro que desexamos. Ás miñas fermosas irmás, Noelia e Anita, por acompañarme en cada pequeno paso. Ós meus avoíños, Manuel e Pilar e ó meu amor Pablito, por iluminar as nosas vidas. Ás persoas que nos coidan alá onde vaiamos, Benjamín e Hortensia.

Abstract

Cancer is a complex process that is influenced by a combination of genetic and environmental factors. It stands as the second leading cause of death globally and constitutes a major public health concern with far-reaching implications for patient outcomes and healthcare costs. Despite the considerable strides that have been made in the diagnosis and research of this disease, our understanding of the mechanisms involved is still incomplete, leaving much to be elucidated. Despite the recent improvement in survival rates, treating cancer remains a challenging endeavor as cancer stem cells are resistant to traditional therapies like chemotherapy or radiotherapy.

The role of mechanics has emerged as a critical component in the development of tumors, alongside biochemical studies. Mechanical forces have been identified as both active and passive players in the progression of the disease, regulating a variety of cellular functions, including duplication, motility, growth, reorganization, and remodeling. Therefore, a comprehensive understanding of the interplay between biochemical and mechanical cues in tumor development is criticals for the development of effective strategies for cancer treatment and management.

Mechanical therapy is a novel therapeutic approach for cancer treatment that uses mechanotransduction to convert mechanical signals into cellular responses. One of the emerging mechanical treatments is low-intensity ultrasound waves, which is being investigated as a potential target therapy that can complement existing treatments. However, the various configurations used for ultrasound waves result in diverse mechanical and biological effects, which must be carefully considered and optimized to maximize their therapeutic potential.

In the current scientific landscape, mathematical oncology is proving to be a promising tool for understanding mechanotransduction, cellular communication, and other complex events that underlie the oncogenic process. In this context, this thesis aims to advance our understanding of cancer by introducing three self-coded numerical models that facilitate the study of tumor behavior through a mechanical perspective. By utilizing these models, the mechanical forces that govern cell fate can be more accurately quantified

and characterized, enabling the development of more effective intervention strategies and treatments.

Firstly, we study how migration, a process controlled by specific speed, competes with proliferation and possible mutations that give rise to non-homogeneous volume changes, generating stresses that modify tumor evolution. To unveil the competition, we develop mechanical-growth coupled equations and we solve the system using the Weighted Essentially Non-Oscillatory method in finite differences. Our findings suggest the need to use non-linear flows to limit the propagation velocity. Additionally, if cells are deprived of movement, non-homogeneous growth slows down proliferation while causing instabilities in cell density in a phenomenon known as retrograde diffusion, which is mitigated by the possibility of movement.

After studying these phenomena, we investigate the effect of mechanotherapy on tumor dynamics using finite-element models. We first study how ultrasound waves propagate through a spheroid embedded in a culture medium. A Kelvin-Voigt viscoelastic model with different parameters is used to conduct a parametric study of the frequency range (1-20MHz), acoustic pressure (0.1-5kPa), and viscosities (0.05-10Pa $\cdot$ s). The sensitivity analysis suggests that neglecting viscoelasticity can lead to an overestimation of the energy that reaches the tissue, as it fails to account for the dissipation of ultrasound waves caused by the viscosity of the tissue, while high acoustic pressure can lead to irreversible damage or cell death, and low acoustic pressure may not produce the desired therapeutic effects. Selecting the appropriate frequency depends on various factors, such as target tissue geometry, medium properties, and desired intensity. The study concludes that numerical simulations of wave propagations can help determine the optimal mechanical parameters for different cell types and disease states, which can guide the development of safe and effective LIUS treatments for cancer and other diseases.

Finally, this thesis proposes a novel quantitative multiscale model that integrates the effects of mechanical waves on tumor development through mechanotransduction. The model is based on coupled stress-growth equations and operates on two main timescales: fast-scale, where the wave propagates and mechanotransduction occurs, and slow-scale, where the tumor grows and adapts to the microenvironment as a poroelastic medium. The hypothesis put forth is that dynamic pressure is more effective in generating a cellular response than static stress, due to the complex mechanisms of stress redistribution involving the cytoskeleton and interstitial fluid flow through pores. Then, this model of mechanotransduction provides a quantitative explanation

for the difference in the threshold of dynamic and static stimulation, without the need for ad-hoc relationships.

To test the model, we have conducted preliminary experiments with in vitro spheroids and performed a sensitivity analysis of the impact of ultrasound on mechanotransduction. The outcomes demonstrate that the model can accurately reproduce experimental data with a high degree of accuracy, and predict both the growth of the spheroids, as well as the stress and deformation states of the medium and the spheroids. Specifically, our findings suggest that ultrasound generates stress fields that hinder and slow down both the development and migration of the tumor cells. This leads to selective treatment and patterns based on shadow areas of applied stress and cell sensitivity ranges, which alter both gradients of stress and interstitial fluid pressure.

Resumen

El cáncer es un proceso complejo que está influenciado por una combinación de factores genéticos y ambientales. Es la segunda causa de muerte a nivel mundial y constituye una importante preocupación en la salud pública con implicaciones significativas para los resultados del paciente y los costes de atención médica. A pesar de los importantes avances que se han logrado en el diagnóstico y la investigación de esta enfermedad, nuestra comprensión de los mecanismos involucrados sigue siendo incompleta, y todavía queda mucho por elucidar. Aunque en los últimos años se ha visto una mejora en las tasas de supervivencia, el tratamiento del cáncer sigue siendo un desafío debido a la insensibilidad de las células madre cancerosas a tratamientos convencionales como la quimioterapia o la radioterapia.

Además de los estudios bioquímicos, la mecánica surge como un componente decisivo en el desarrollo de tumores. Se ha identificado que las fuerzas mecánicas son parte activa y pasiva en la progresión de la enfermedad, regulando una variedad de funciones celulares que incluyen la duplicación, la movilidad, el crecimiento, la reorganización y la remodelación. Por lo tanto, es esencial alcanzar una comprensión integral de la interacción entre señales bioquímicas y mecánicas en el desarrollo de tumores para el desarrollo de estrategias efectivas para el tratamiento del cáncer.

La mecanoterapia representa un enfoque terapéutico novedoso para el tratamiento del cáncer, y que se basa en la mecanotransducción para convertir señales mecánicas en respuestas celulares. Entre los tratamientos mecánicos emergentes, se está investigando el uso de ondas de ultrasonido de baja intensidad como una potencial herramienta que puede mejorar el conjunto de tratamientos existentes. Sin embargo, las diversas configuraciones utilizadas para las ondas mecánicas dan lugar a diversos efectos mecánicos y biológicos, que deben considerarse y optimizarse cuidadosamente para maximizar su potencial terapéutico.

En el actual panorama científico, la oncología matemática está demostrando ser una herramienta prometedora para comprender la mecanotransducción, la comunicación celular y otros fenómenos complejos que subyacen al proceso oncogénico. En este contexto, la presente tesis se esfuerza por avanzar en

nuestra comprensión del cáncer mediante la introducción de tres modelos numéricos que facilitan el estudio del comportamiento del tumor desde una perspectiva mecánica. Al emplear estos modelos, las fuerzas mecánicas que gobiernan el desarrollo celular pueden cuantificarse y caracterizarse con mayor precisión, lo que permite el desarrollo de intervenciones y tratamientos más efectivos.

En primer lugar, estudiamos cómo la migración, un proceso controlado por una velocidad específica, compite con la proliferación y las posibles mutaciones que dan lugar a cambios de volumen no homogéneos, generando tensiones que modifican la evolución del tumor. Para examinar esta competencia, planteamos ecuaciones biacopladas de crecimiento y mecánico y las resolvemos utilizando el método de diferencias finitas ponderadas esencialmente no oscilatorias (método WENO). Nuestros hallazgos sugieren la necesidad de utilizar flujos no lineales para limitar la velocidad de propagación. Además, si las células se ven privadas de movimiento, el crecimiento no homogéneo ralentiza la proliferación al tiempo que provoca inestabilidades en la densidad celular en un fenómeno conocido como difusión retrógrada, que se mitiga mediante la posibilidad de movimiento.

Después de estudiar estos fenómenos, investigamos el efecto de la mecanoterapia en la dinámica del tumor utilizando modelos de elementos finitos. Primero, se observa cómo las ondas de ultrasonido se propagan a través de un esferoide embebido en un medio de cultivo. Se utiliza un modelo viscoelástico de Kelvin-Voigt con diferentes parámetros para realizar un estudio de sensibilidad del rango de frecuencia (1-20MHz), presión acústica (0.1-5kPa) y viscosidades (0.05-10Pa $\cdot$ s). El estudio paramétrico sugiere que no contemplar la viscoelasticidad puede conducir a una sobreestimación de la energía que llega al tejido, ya que no se tendría en cuenta la disipación de las ondas de ultrasonido causada por la viscosidad del tejido. Por otra parte, una alta presión acústica puede provocar daños irreversibles y citodisrupción, mientras que una presión acústica baja podría no producir los efectos terapéuticos deseados. La selección de la frecuencia adecuada depende de diversos factores, como la geometría del tejido a tratar, las propiedades mecánicas del medio y la intensidad deseada. El estudio concluye que las simulaciones numéricas de propagaciones de onda pueden ayudar a determinar los parámetros mecánicos óptimos para diferentes tipos celulares y estados de enfermedad, lo que puede guiar el desarrollo de tratamientos de LIUS seguros y efectivos para el cáncer y otras enfermedades.

Finalmente, esta tesis propone un nuevo modelo cuantitativo multiescala

que integra los efectos de las ondas mecánicas en el desarrollo de tumores a través de la mecanotransducción. El modelo se basa en ecuaciones de crecimiento y tensión acopladas, y opera en dos escalas de tiempo principales: la escala rápida, donde la onda se propaga y ocurre la mecanotransducción, y la escala lenta, donde el tumor crece y se adapta al microambiente como un medio poroelástico. La hipótesis planteada en mecanotransducción es que la tensión dinámica es más efectiva en generar una respuesta celular que la tensión estática, debido a los complejos mecanismos de redistribución de esfuerzos que involucran al citoesqueleto y al flujo de fluido intersticial a través de los poros. Por lo tanto, este modelo de mecanotransducción proporciona una explicación cuantitativa para la diferencia en el umbral de estimulación dinámica y estática, sin necesidad de introducir relaciones *ad hoc*.

El modelo predice la evolución de experimentos preliminares con esferoides in vitro y permite realizar un análisis de sensibilidad del impacto del ultrasonido en la mecanotransducción. Los resultados indican que el modelo puede reproducir con precisión los datos experimentales y predecir tanto el crecimiento de los esferoides como los estados de tensión y deformación del medio y los esferoides. Específicamente, nuestros hallazgos sugieren que el ultrasonido genera campos de tensión que ralentizan tanto el desarrollo como la migración de las células tumorales selectivamente. Además, se demuestran patrones de crecimiento y migración basados en áreas de sombra de tensión y rangos de sensibilidad celular, que alteran tanto los gradientes de tensión lenta como la presión de fluido intersticial.

Contents

List of Figures

List of Tables

List of Symbols

ρ	Tissue mass density
K_d	Bulk drained modulus
K_u	Bulk undrained modulus
μ	Shear modulus or Lame's second constant
ν	Poisson ratio
E	Young's modulus
η_μ	Shear solid viscosity
η_κ	Volumetric solid viscosity
W	Strain energy
I	First Invariant
II	Second Invariant
III	Third Invariant
J	Deformation jacobian
g	Growth stretch function
$\boldsymbol{x}$	Eulerian position vector
$\boldsymbol{X}$	Lagrangian position vector
$\boldsymbol{u}$	Displacement vector
$\boldsymbol{F}$	Total gradient deformation tensor
$\boldsymbol{F}_e$	Elastic deformation tensor
$\boldsymbol{F}_g$	Growth deformation tensor
$\boldsymbol{\lambda}_g$	Growth tensor
$\boldsymbol{I}$	Second-order identity tensor
$\boldsymbol{E}$	Green-Lagrange strain tensor
$\boldsymbol{S}$	Second Piola-Kirchoff pseudo-stress tensor
$\boldsymbol{P}$	First Piola-Kirchoff pseudo-stress tensor
$\boldsymbol{C}$	Right Cauchy-Green deformation tensor
$\boldsymbol{B}$	Left Cauchy-Green deformation tensor
$\boldsymbol{\varepsilon}$	Small Strain tensor
$\boldsymbol{\sigma}$	Cauchy Stress tensor
$\boldsymbol{\sigma}_e$	Elastic Stress tensor
$\boldsymbol{\sigma}_g$	Growth Stress tensor
$\boldsymbol{\sigma}_p$	Fluid Stress tensor
ε_v	Volumetric Strain tensor
σ_h	Hydrostatic Stress
σ_{vm}	Von-Mises Stress

Specific to Chapter 3

n	Cell density
α_n	Coupling volumetric growth function
c_n	Propagation speed front
$\boldsymbol{\mathcal{J}}_n$	Flux of cell density
D_n	Diffusion of cell density
m	PME parameter
β_n	Proliferation rate of cell density
C	Carrying capacity
$\boldsymbol{v}_n$	Velocity of cell density
$\mathbb{R}^N$	Real natural domain

Specific to Chapters 4 and 5

f	Frequency
T	Period
λ	Wavelength
c_p	Pressure wave speed
A	Acoustic pressure

ϕ_T	Tumor cell phase
ϕ_H	Healthy cell phase
ϕ_M	ECM phase
ϕ_F	Interstitial fluid phase
ζ	Fluid strain
$\boldsymbol{q}$	Flux of interstitial fluid
p	Interstitial fluid pressure
p_0	Initial interstitial fluid pressure
α	Biot constant
M	Biot modulus
k_h	Conductivity
κ	Permeability
ν_F	Fluid viscosity
k_v	Vessel conductivity
p_v	Vessel pressure
ω	Reflection coefficient
$\pi_v - \pi_e$	Interstital osmotic pressure
k_l	Lymphatic conductivity
p_l	Lymphatic vessel pressure
Γ_T	Source of tumor cell phase
Γ_H	Source of healthy cell phase

Γ_M	Source of ECM phase
Γ_F	Source of fluid
α_{TT}	Tumor cell phase decay
α_{TH}	Tumor-health cell phase exchange
α_{TM}	Tumor-ECM phase exchange
α_{HT}	Healthy-tumor cell phase exchange
α_{HH}	Healthy cell phase decay
α_{HM}	Healthy-ECM phase exchange
α_{MH}	ECM-health phase exchange
α_{MT}	ECM-tumor phase exchange
β_T	ECM production rate from tumor phase
β_H	ECM production rate from healthy phase
$\delta_M \alpha_{MT}$	ECM degradation rate from tumor phase
$\delta_M \alpha_{MH}$	ECM degradation rate from healthy phase
D_T	Diffusion of cell tumor phase
$\mathcal{M}_{\mathcal{B}}$	Mechanotransduction function
$\mathcal{M}$	Promedio of mechanotransduction function
T_T	Duplication rate of tumor phase
T_H	Duplication rate of healthy phase
q	Mechanotransduction parameter to fit maximum proliferation decrease
T_K	Maximum of the cells' viability
χ_σ	Smoothing coefficient of mechanotransduction
σ_L	Critical or limit stress perceived by cells
β_s	Dynamic stress correction coefficient

Abbreviations

ABC	Absorbing Boundary Conditions
ARF	Acoustic Radiation Force
CCM	Classical Continuum Mechanics
CSC	Cancer Stem Cells
DNA	Deoxyribonucleic Acid
ECM	Extracellular Matrix
EMT	Epithelial to Mensenchymal Transition
FAK	Focal Adhesion Kinase
FDA	Food and Drug Administration
FDM	Finite Difference Method
FEAP	Finite Element Analysis Program
FEM	Finite Element Method
FOEC	Fourth Order Elastic Constants
FSS	Fluid Shear Stress
GCM	Generalized Continuum Mechanics
Hh-Gli	Hedgehog-Gli
HIFU	High-Intensity Focused Ultrasound
IFP	Interstitial Fluid Pressure
ISPTA	Spatial Peak Temporal Average Intensity
KV	Kelvin-Voigt
LIUS	Low-Intensity Ultrasound
LIPUS	Low-Intensity Pulsed Ultrasound
MET	Mesenchymal to Epithelial Transition
MI	Mechanical Index
MAPK/ERK	Mitogen-Activated Protein Kinase/Extracellular Signal-Regulated
P1K3-AKT	Phosphatinositide—-3– Kinase–Protein Kinase
PME	Porous Medium Equation
SWE	Shear Wave Elastography
SWS	Shear Wave Speed
TGF-β	Transforming Growth Factor β
US	Ultrasound
RHO–ROCK	RHO– Associated Protein Kinase
WENO	Weighted Essentially Non-Oscillatory
WHO	World Health Organization

Part I

INTRODUCTION AND BACKGROUND

Chapter 1

Introduction

1.1 Context and Motivation

Cancer is the second leading cause of death worldwide. According to data published in reference [1], 19.3 million new cases were detected and 10.0 million deaths occurred in 2020 worldwide, accumulating almost a quarter of them in Europe (4.3 million cases), and it is projected to continue to rise in the coming years. In Spain, data estimates 282 thousand new cases and 113 thousand deaths in 2020, being prostate, breast, colorectum, and lung cancer the most incident [2, 3].

Cancer is a major public health concern with a significant impact on both patient outcomes and healthcare costs. In fact, cancer is one of the leading causes of economic and health burden among chronic diseases in the European Union [4, 5, 6, 7]. The cost of cancer care is expected to continue to rise in the future, making it a significant concern for healthcare systems and policymakers [6, 8, 9, 10].

The comprehension of the molecular processes involved in cancer cell transformation has significantly advanced in recent years [11, 12, 13, 14, 15]. However, despite the notable progress that has been made, our understanding of these mechanisms is still far from comprehensive and there is much yet to be discovered.

The multifactorial cause of cancer is related to genome alterations and mutations that result in the abnormal growth of cells. Overall, the origin of cancer is a complex process that can be influenced by a combination of genetic and environmental factors. Mutations are irreversible modifications of DNA that can be inherited while alterations refer to epigenetic changes that modify the expression of the genome without modifying DNA [16, 17, 18, 19, 20, 21, 22, 23, 24]. There are several risk factors that can contribute to the development of these mutations, including inherited genetic mutations, environmental factors, infections, radiation, obesity, sedentary lifestyle, aging, diet, alcohol, and tobacco consumption [25, 26, 27, 28, 29, 30, 31].

The existing treatments for cancer, including conventional chemotherapy and

radiotherapy, can have significant side effects and may not effectively eliminate cancer precursor cells known as cancer stem cells (CSCs) [32, 33, 34, 34], which are widely considered to have a significant impact on cancer metastasis and are frequently blamed for relapse due to their self-renewal and differentiation capabilities [35, 36, 37, 38, 39].

New therapies are on the horizon, such as immunotherapy, but patient stratification is challenging, and costs are high [40, 41, 42, 43, 44]. Therefore, new ways to interact with cells are needed to develop novel therapies to improve patient outcomes.

Among chemical processes, mechanical forces have a critical role in carcinogenesis. Recent literature provides ample evidence that cells are both passive and active players in the mechanical homeostasis of the body and that alterations in mechanical forces can derail cell function [45, 46, 47, 48, 49, 50].

Then, cells require a specific balance of mechanical forces to develop, and any abrupt or smooth alteration in the cell stress state could affect changes in volume –*growth*–, reorganization and shape –*morphogenesis*–, and in material properties –*remodeling*– [51, 52, 53, 54]. In this context, uniform growth is not a default state but a result of active regulation and competition of cell proliferation, motility, chemical agents, and mechanical feedback, in which growth modify stress – stress-driven growth– and stress regulates growth and patterns [55, 56, 57, 58].

Thus, cancer cells mechanics is recently highlighted as a critical controller of their progression and fate, and *mechanobiology* studies how cells biologically respond to mechanical stimuli. In particular, the potential of *mechanotransduction* principles is emerging [59, 60, 61] to support other therapies.

The importance of translating mechanotransduction into therapy has become increasingly clear, and some mechanical technologies emerged to battle cancer. Different laboratories are developing a variety of principles to actively impact cell behavior by modifying the mechanical microenvironment. They range mainly from ultrasound (US) to drugs that alter the elasticity of the remodeled microenvironment and cell stiffness [62, 63]. These principles are both translatable to the patient, since the US can be applied using transducers or patches, and the second one is based on drug delivery.

Regarding the US and leaving aside thermal therapies such as high-intensity focused ultrasound (HIFU) and sonoporation [64, 65, 66, 67, 68, 69], since they rely on different mechanisms that require carefully targeting confined tumors since they aimless destroy tissue, low-intensity ultrasound (LIUS) and its pulsed version (LIPUS), has been proposed to impact cancer cells by two main

mechanisms: i) selectively resonating the right diameter cells under the name of *oncotripsy*, what lies on destroying the cytoskeleton [70, 71, 72, 73, 74], and ii) triggered response produced in mechanotransduction via signaling pathways [73, 74, 75, 76, 77, 78, 79, 80].

Although these studies have repeatedly evidenced significant potential effects, the lack of understanding of the mechanism, and the even opposing responses triggered by diverse frequencies, energies, and configurations, make the concept still useless at its current state.

Hence, the understanding of the mechanical wave configuration is rising attention, although the mechanisms of how LIUS affects cancer cell behavior have been significantly restricted. The main reason lies in the high experimental cost, the stochastic effects associated with biological experiments, and the technical complexity of obtaining data from *in-vivo*.

In this context, mathematical oncology and *predictive medicine* appear to be valuable tools to complement experiments. Although predictions of a mathematical model for a biological system can not be, unfortunately, fully trusted [51], developing multiphysics models of the mechanical-biological interactions are key to unveiling tumor behavior [81, 82, 83, 45, 63, 84, 85].

Then, computational mechanobiology models could be a leading point for understanding the progression of the disease [86, 87, 52]. Indeed, a model can accurately describe and represent a biological system if it follows the qualitative trends of experimental tests [51]. In the last approximation, tailored models (realistic morphology and inherent properties of the tumor) could help clinicians in diagnostic and decision-making [88, 89, 90, 91, 92]. Thus, models could be used as complement medical strategy in pre-diagnostic. For instance, a combination of drugs [93, 94] and different mechanical waves could be tested and even combined for treatment optimization. Ensuring the appropriate proportions, the effectiveness of the treatment could be maximized, and health care costs would be minimised [63].

The key reason to investigate cancer from computational mechanics lies in the need to understand the fundamental behavior of growth and mechanics interaction regarding motility and proliferation in normal and changing situations and identify new targets for treatments to fight CSCs considering the signaling cascade of mechanotransduction pathways from mechanical signals generation at tissue scale to cell and molecular level.

Notwithstanding, modeling is challenging. The tumor morphology, the co-existence of different cell types, the bio-chemo-mechanical interactions, and the nonlinearity of tissues involve multi couple high-order partial differen-

tial equations which demand efficient methods of resolution in terms of computational cost and memory. The numerical procedures for obtaining approximated solutions to the system of equations are mainly based on the Finite Differences Method (FDM), which can help in more simplified models by directly approximating the unknown solution by finite difference approximation in nodes, and Finite Element Method (FEM), which is a useful tool to handle more computational challenges by using standard polynomials to interpolate functions to approximate the unknown solution within an element [95, 96, 97, 98, 99].

Therefore, the *Mechanotherapy* project pursued by our research group at the University of Granada represents a novel strategy in the fight against carcinogenesis. This approach seeks to comprehend and manipulate cellular mechanics through the integration of experiments and modeling, utilizing the latest advancements in mechanics, genomics, transcriptomics, proteomics, and metabolomics.

This interdisciplinary dissertation is a crucial component of the Mechanotherapy project. Specifically, it represents the initial effort to establish a theoretical framework that comprehends mechanically induced signaling pathways and stress states in the progression of tumors and to develop multiscale computational models that incorporate phenomena such as proliferation, controlled migration, stress-driven growth, and mechanical wave interactions to better understand tumor dynamics.

1.2 Research Objectives

The main scope of this thesis is to develop computational tools for understanding and tackling carcinogenesis from mechanics. To succeed, specific objectives must be accomplished. These are as follows:

1. **Set the framework of tumor mechanobiology and its theoretical models.** Describe the main characteristics of avascular tumors and review the current knowledge of tumor mechanobiology, providing a common framework for the different theoretical approaches that have emerged in the literature from the Continuum perspective and giving insight into emerging mechanotherapies and in particular LIUS.

2. **Unveil the competition between mechanics and migration in response to an abrupt change in cell density.** Compare the impacts of linear, non-linear, and non-linear saturated flux effects on migration. We aim to develop a model that accounts for non-homogeneous growth resulting from sudden changes and investigate

how these variations compete with proliferation and migration.

3. **Model the ultrasound interaction at spheroid level**. Model the wave propagation in tumor spheroids, taking into account the inherent attenuation of the waves. To accomplish this objective, we conduct a sensitivity analysis of wave propagation with regard to acoustic pressure, viscosity, and frequency.

4. **Develop a multiscale model of mechanotherapy where low-intensity ultrasound impacts tumor dynamics via mechanotransduction**. Propose a multiscale computational model that simulates the therapeutic effect that LIUS causes on a growing poroelastic tumor spheroid through mechanotransduction that accounts for both static and dynamic stress. Validate the model through comparison with experimental data, and use numerical simulations to explore patterns formation and selective proliferation, and migration inhibition.

1.3 Thesis overview

Following this introduction, Chapter 2 reviews the current knowledge of solid tumor growth from the biological mechanisms to the latest advances in the mathematical modeling of cancer, including the basics of Classical Continuum Mechanics, the leading works of theoretical models of tumor growth, and the low-intensity ultrasound application to tumors.

Depending on the specific purpose of the study and focusing on each objective, different theoretical models have been contributed in a hierarchal way, from simple to complex.

Then, in Chapter 3, we present a mathematical model to evaluate the competition between migration, proliferation, and non-homogeneous growth in regulating the reorganization of tumor cell density in its evolution. In particular, this Chapter firstly studies the differences between linear, non-linear, and non-linear saturated flux. Then, we assume migration as a controlled process in which the speed of the front propagation can be regulated through a saturated flux to compete with proliferation and non-homogeneous growth. To develop an accurate and efficient method to solve the set of equations in one dimension, we develop the Weighted Essentially Non-Oscillatory (WENO) method in finite differences in one dimension.

Once we highlight the role of controlled propagation in stress-driven non-homogeneous growth, we improve and modify the forward model developing a multiscale model in which LIUS affects tumor growth.

In particular, Chapter 4 aims at modeling the mechanical wave propagation through a tumor spheroid, considering the Kelvin-Voigt properties, that try to emulate the rheological behavior of spheroids seeded in a culture medium. We perform a parametric study, evaluating frequencies, amplitudes, and viscosities to finally obtain the hydrostatic stress state of the tumor after LIUS treatment. We use the Finite Element Method (FEM) in two dimensions considering plane strain.

In Chapter 5, we combine the wave propagation model developed in the previous Chapter with tumor dynamics. In particular, we generate a theoretical framework to understand mechanically induced proliferation and migration in tumor progression and treatment. We develop a multiscale temporal model in which LIUS hinders tumor proliferation and migration via mechanotransduction, accounting for slow and fast hydrostatic stress. We fit mechanotransduction parameters with experimental data and we then perform numerical simulations to explore patterns formation and selective proliferation and migration inhibition. We use FEM to implement the system of equations in two dimensions.

Finally, Chapter 6 presents a discussion of the results and main conclusions of this dissertation. Furthermore, some future lines are outlined and the limitations of the present study, such as dynamic Biot's poroelasticity propagation, are also pointed out.

At the end of the document, there is a list of publications and contributions that emerged from this thesis. Furthermore, the appendices and the references are also included.

Chapter 2

Background

2.1 Cancer dynamics

The cell cycle is a precisely regulated sequence of events that result in the replication and division of a single cell into two genetically identical daughter cells. Under normal circumstances, a delicate balance is maintained between cell division and programmed cell death (apoptosis), ensuring that only healthy cells are allowed to proliferate. However, in the case of tumor cells, this balance is disrupted as they express anti-apoptotic proteins or inactivate pro-apoptotic proteins, thereby evading programmed cell death and proliferating uncontrollably [100, 101, 102, 103].

Benign tumors are characterized by a lack of invasive properties and the absence of metastasis. In contrast, malignant tumors possess the ability to invade surrounding tissue and disseminate to distant sites in the body and are overcalled cancer.

The stages of cancer describe the extent to which a tumor has grown and spread in the body. The TNM system is the most extensively utilized method for categorizing the extent of cancer, in which T stands for the primary size of tumor and how far it has invaded nearby tissue, N refers to the lymph node involvement, and M to whether cancer has metastasized, or spread, to distant sites in the body [104]. The stages are also usually represented by Roman numerals, with stage I being the earliest, localized and least advanced stage and stage IV being the most advanced and widespread stage [104]. It is important to note that each type of cancer has different TNM staging systems and that other specific grading systems can also coexist, such as the Gleason score for prostate cancer [105].

The process of metastasis typically occurs in several stages [106, 107]: firstly, cancer cells begin to invade surrounding tissue and break away from the primary tumor (invasion) to later enter the blood and lymphatic vessels (intravasation). The circulatory system transports cancer cells passively throughout the organism in a process known as dissemination. Although cancer cells may stay dormant in the bloodstream for a long time without

producing any harm, if extravasation occurs, cancer cells escape from the vessels into other distant tissues through transendothelial migration [107]. Once outside the vessels, cancer cells form small nodules (micro-metastasis), and finally colonize the new tissue, multiplying, and forming a new macroscopic tumor at the secondary site if they are able to survive and proliferate in their new emplacement. In fact, not all cancer cells that break away from the primary tumor will successfully complete the process of metastasis and form new tumors. Also, different types of cancer may have different pathways for metastasis and some stages of metastasis can be more difficult to detect and treat than others, especially the early stages, being one of the reasons why cancer can be so challenging to treat [108].

In light of our discussion on metastasis, it is crucial to also comprehend the significance of the presence of vessels in tumors. Avascular tumors are tumors that do not contain blood vessels. They tend to grow slowly and are often relatively small, but as it progresses, they may begin to secrete tumor angiogenesis factors (TAF) which can promote the formation of new blood vessels [109]. This transition from an avascular to a vascular growth phase can enable the tumor to invade and spread to other parts of the body. In fact, vascularized tumors are capable of rapidly growing and spreading. They lead to the formation of new blood vessels from existing blood vessels in a process known as angiogenesis [110, 111, 112].

This thesis focuses on the primary stages of tumors, where they remain avascular without angiogenesis or angiogenic factors. Furthermore, we account for tumors without distinguishing between the histological features, location of the tumor, and cell origin, i.e. carcinomas (epithelial), melanoma (skin), sarcomas (connective), glioblastoma (nervous system), etc.

Regarding physiology, avascular tumors are mainly composed of interstitial fluid, which fills the spaces between cells, and solid components which are mainly different cells, extracellular matrix (ECM), filaments, and proteins.

ECM is a complex network of molecules, including structural proteins, that surrounds and supports cells. In tumors, the ECM is often disrupted and remodeled to create a microenvironment that is favorable to cancer cell growth [113, 114, 48]. This can include the overproduction of ECM components such as collagen, which can provide structural support for the tumor and make it more resistant to therapy [115, 116]. Additionally, cancer cells can secrete enzymes that degrade the ECM, allowing them to migrate and invade surrounding tissue [117, 113].

Cells attach to ECM to anchor themselves in place and regulate their behavior. However, in cancer, these cell-ECM interactions can be disrupted and contrib-

ute to the abnormal behavior of cancer cells. One of the main proteins involved in cell-ECM adhesion is a transmembrane protein called integrin, which helps in transmitting signals from the ECM to the cell, regulating cell behavior. In cancer, this expression can be altered, leading to changes in cell-ECM adhesion and increased invasive behavior [118, 119, 120]. Another relevant protein that plays a role in cell-ECM adhesion is matrix metalloproteinases (MMPs), which are key enzymes that promote ECM degradation allowing cancer cells to migrate and invade surrounding tissue [121, 122, 123, 124].

Furthermore, cells adhere to each other creating links that help to hold them together and maintain the integrity of tissues. In normal tissue, cell-cell adhesion is tightly regulated and helps to prevent the uncontrolled growth of cells. This regulation is often disrupted in cancer and cells can lose their normal cell-cell adhesion properties. One of the main proteins involved in cancer cell-cell adhesion is a transmembrane protein called E-cadherin, whose expression is often reduced or lost, allowing cancer cells to detach from each other and migrate away from the primary tumor [125, 126].

This process is related to epithelial-mesenchymal transition (EMT), in which cancer cells lose their epithelial characteristics and cell-cell adhesion and acquire mesenchymal properties, such as increased motility and invasiveness [127, 128, 129]. Another protein called N-cadherin is often upregulated in cancer cells, which can promote cell-cell adhesion and contribute to the formation of more aggressive tumors. Overall, the regulation of cell-cell adhesion is critical in cancer and the loss of E-cadherin and the increased expression of N-cadherin are key events in the development and progression of cancer [130, 131].

Cancer cells can form three-dimensional spheroids (MCTS), which mimic the microenvironment and interactions of solid tumors, and are extensively utilized in vitro for investigating cancer development, drug resistance, and the effectiveness of new therapeutic agents.

The formation of spheroids is influenced by surface tension, which is related to the cadherin expression level of the cells. The relative surface tensions determine the spreading of the cells, resulting in the rearrangement of the spheroid such that the cell line with lower cadherin expression spreads over the other [132, 133]. Thus, the accumulation of surface stress can contribute to the spheroid formation by altering cell adhesion properties, leading to cell detachment and self-aggregation [134]. For instance, the Hanging Drop technique uses surface tension and gravitational force to produce spheroids in vitro [135, 136].

The composition and proportion of the cells can vary depending on the type

and stage of the tumor, and the microenvironment in which it is growing. The different types of cells include differentiated cancer cells, immune cells, endothelial cells, and fibroblasts. Furthermore, there are cancer-associated fibroblasts, macrophages, adipocytes, endothelial and pericytes (CAFs, CAMs, CAAs, CAECs, CAPs), which are cells that have undergone changes in response to the tumor and can contribute to the growth and progression of the tumor [137, 138].

The subpopulation of cancer stem cells (CSCs) are considered to be the most crucial player cells within tumors, as they possess properties that promote the progression of the tumor [139, 140, 35, 36, 37]. CSCs are capable of self-renewal, differentiation into other cancer cell types, forming new tumors, evading the host immune system, migration, pumping out cytotoxic drugs, and resisting conventional therapy, making them a major contributor to cancer recurrence [44, 33, 38, 39]

When it comes to cancer treatment, the options available are varied and complex. Each therapy carries its own set of advantages and disadvantages, making it crucial to carefully evaluate the specific needs and circumstances of each individual patient. The type and stage of cancer, as well as the patient's overall health, all play a vital role in determining the most appropriate treatment plan. That being said, the most widely utilized and proven cancer therapies currently available are:

- Surgery is often the first line of defense. The goal of surgery is to excise as much of the malignant tissue as possible. Resection offers the benefit of potentially achieving complete removal of the tumor in a localized manner, although surgical intervention carries certain risks, including the potential for complications and the possibility of incomplete tumor removal due to indistinct tumor boundaries.
- Chemotherapy is a treatment modality that employs drugs to destroy cancer cells by disrupting the cell cycle. It is commonly employed in cancers that have metastasized to various locations in the body, such as leukemia and lymphoma. Chemotherapy offers the benefit of being able to target cancer cells that have spread to distant locations in the body. Notwithstanding, it also has certain drawbacks, such as the non-localized nature of the treatment, which can result in significant side effects and the possibility of cancer cells developing resistance to the drugs used.
- Radiation therapy is a treatment that uses high-energy rays to kill cancer cells. It is often used for cancers that are difficult to remove with surgery. Radiation therapy has the advantage of being able to

reach cancer cells that are hard to reach with surgery while localized, but it also has some disadvantages, such as the risk of side effects, like fatigue and skin irritation.

- Hormonal therapy is a treatment option for specific types of cancer such as breast and prostate cancer, which are sensitive to hormones. It aims to inhibit the production or action of hormones that promote cancer growth. Hormonal therapy can be administered orally, via injection, or as an implant and can be used alone or in conjunction with other treatments. It offers the advantage of targeting cancer cells specifically and lowers the risk of recurrence in certain types of cancer. However, it is only effective for tumors that have hormone receptors, and have the risk of side effects such as hot flashes and bone loss, and the possibility of cancer becoming resistant to the therapy over time.
- Immunotherapy leverages the immune system of the body to combat the disease. It is often used for cancers that are difficult to treat, such as melanoma and lung cancer. The use of immunotherapy has been a topic of intense research and development, due to its numerous advantages, including the specificity of target cancer cells, reducing the risk of harming healthy cells, and the durability of response, as the immune system can continue to attack cancer cells even after the treatment has ended. Despite its potential benefits, immunotherapy can also result in certain side effects, including fatigue, skin irritation, and allergic reactions.
- Cryoablation and thermal ablation are two types of minimally invasive procedures that use extreme temperatures to destroy cancer cells and they are typically used as secondary treatments or for patients who are not suitable for surgery or radiation therapy. Cryoablation uses cold to freeze and kill cancer cells, for instance in uterus cancer. Thermal ablation uses heat to destroy cancer cells, and can also be used to treat a variety of cancers, such as prostate cancer. In particular, high-intensity focused ultrasound (HIFU) has widespread use. Both procedures have the advantage of being able to reach cancer cells that are difficult to reach with surgery and have a relatively low risk of complications. However, both also carry some risks of side effects such as pain and swelling, and there is a possibility that not all cancer cells may be killed during the procedure.

In short, the main features of cancer have been made clear, including its components and current treatments. Specifically, the issues of CSCs are highlighted, as they are not eliminated by traditional treatment methods.

As such, there is a need to research new forms of treatment that can better target CSCs, and mechanotherapy is a potential solution in this regard. The next section explores how mechanics can be used then to improve prognosis disease, through an examination of recent experimental research in the field.

2.1.1 Role of mechanics

In addition to well-studied chemobiological factors [141, 142, 143, 144, 145, 146], mechanical stress is key in tumor development. Growing tumors can be considered as a poroelastic medium that deforms according to the stresses they are subjected to, depending not only on the duration and direction of the forces but also on the mechanical properties of the tumor and its environment [147, 148, 149]. The literature has used the term *pressure* in different contexts [150, 82, 151, 152, 153, 55, 58].

Some refer to the internal tumor stresses that keep the homeostatic state of the tissue, to the possible external stress applied to tumors, to the interstitial fluid pressure, to the mutual pressure exerted by two dynamic cell populations across their interface, and even to the fluxes of cells. Here, we refer to *pressure* as compression stress. We denote by stresses the internal and external forces applied to different tumor surfaces, regardless of their solid or fluid nature. Finally, the flow of cells is called flux.

Growing tumor behavior depends on both solid and fluid stress regarding its poroelastic nature. Solid stress increases as a function of tumor gain volume and internal interaction between cells, ECM, and cell components that cause elastic rearrangements. In particular, external forces also affect tumor behavior. Externally imposed static or dynamic compressive stresses on tumors cause proliferation inhibition and induce cell apoptosis. The first evidence of mechanical stress induction was confirmed in 1997 when Helmlinger et al. reported measurements of adenocarcinoma spheroids embedded in agarose gel matrices with different concentrations [154]. The results suggested that spheroid growth was completely inhibited at 1% of gel concentration. However, [154] also demonstrated the reversible behavior of the inhibitory effect, which implies that cells remain in a quiescent state as long as stress does not stop. Further experiments carried out in successive years for different cancer cell lines supported the results of [154]. Roose et al. performed experiments for spheroids of the human melanoma (MU89) cancer cell line at concentrations of 0.5% and 1% of type VII agarose [151]; Cheng et al. embedded monolayer cells of metastatic murine breast carcinoma (EMT6) and not metastatic murine mammary carcinoma (67NR) in agarose gel [155]; Montel et al. experimented with carcinoma cell spheroids (CT26) [156] and [157]

used multicellular spheroids of HT29, CT26, and BC52 cells. All analyses reached the same conclusion: the growth reduction resulted from compressive stress. To quantify the relationship between the concentration of the agarose gel (% w/w of Dextran) and the pressure (Pascals) exerted by the gel, the studies of [156, 157, 158] adapted the empirical formula proposed by [159]. From stress quantification, it is inferred that the compression applied in the above experiments reached values between 5-10kPa, achieving at least a 50% reduction in proliferation compared to stress-free growth and a 30% increase in apoptotic cell activity. Numerous techniques are available for quantifying cell proliferation, including cell counting, PCNA (proliferating cell nuclear antigen), Blue Alamar assay, and many others, while there are multiple methods for measuring apoptosis, such as TUNEL assay (Terminal deoxynucleotidyl transferase dUTP nick end labeling) or Caspase activity assays.

These findings reveal that not only the surrounding medium can exert pressure on the tumor but that any external or internal stress could affect the dynamics of the tumor. In particular, it has been shown that if compression is exerted externally by a piston with adjustable weights, the direction of stress affects the final shape of the tumor, as proliferation is inhibited in areas of high pressure, resulting in different patterns [155]. Furthermore, monolayer peripheral cells can undergo a phenotypic transformation that causes cells to become leader cells and initiate collective migration [160], although other studies show that compressive stresses through low ultrasound slow migration [77]. Another method of compressing tumors relies on seeding spheroids in permeable microcapsules. Indeed, reference [161] found that not only the difference in stiffness affects growth, but also the thicknesses of the matrix.

Some of these studies are reviewed in [162], where their findings are summarized according to the source of the stresses. The relevance of these findings lies in their potential to design new cancer therapies. How could we modify the tumor microenvironment and alter the tumor fate? In the following section, we will delve deeper into these questions, providing a comprehensive and detailed examination of mechanotherapy and contributing to the understanding of this area in Part II of this dissertation.

In addition to external stresses, growth and reorganization, as well as cell-cell and cell-ECM interactions, cause internal stresses within the tumor. Stresses generated during growth alter tumor patterning [46, 155] as well as biochemical components and drug delivery [163, 87, 164, 165]. Compressive radial and circumferential stresses can be distinguished in the core of the

tumor, while at the interface the stress is compressive in the radial direction and tensile in the circumferential direction [147, 45, 166]. Forces generated can be quantified by traction microscopy, micropillars, cantilevers, and other force sensors based on unknown material properties [58].

The interaction of the cell components and their environment also causes different levels of stress within the tumor. Existing forces between cell bounds keep the tumor stable in a homeostatic state. However, if adjacent groups of cells have significantly different mechanical parameters, e-cadherins could sense the stiffness of the cells and activate pathways that regulate cell adhesion [125, 152, 167]. Thus, the stiffest cluster of cells will compress the softest, generating forces that may allow the progression of pulled fronts and displacement of the softest tissue [147, 152, 168]. Furthermore, a patch of cells with identical mechanical properties could mutate and grow faster or slower than its environment, i.e., not uniformly compared to the rest of the tissue [55, 169]. As cells adhere to each other, cell patches transmit and accumulate stresses in a feedback mechanism: nonuniform growth generates pressure, which self-regulates growth [55, 58]. The underlying biological theory of these local mechanical interactions is based on cytonemes (a structure similar to a filopodia) that mediate the mechanosensing of cellular communication between the closest cells [170, 171].

The strength and contractility of adhesions have been shown to regulate durotaxis [172, 173], explaining why adhesion forces are considerably more robust in metastatic cells compared to non-metastatic cells [174, 175]. In fact, the mechanical state of cells depends on the stiffness and the amount of elastic energy stored [176, 177, 92, 63].

Studies have shown that cells grown on a stretched substrate exhibit a stiffer cytoskeleton compared to cells grown on unstretched gels. Furthermore, these cells display a reciprocal elongation with the substrate [176, 173] With respect to the primary tumor tension state, cells rearrange and modify their microenvironment, generating internal forces that interact with the external ones. These solid stresses that accumulate in the tumor during growth conform to the residual stress. Computational and experimental methods, such as tumor excision and opening, have been employed to quantify the residual stress in tumors. [178, 45, 179, 163, 180, 181].

From a fluid perspective, the primary fluid stresses that affect tumor dynamics are the interstitial fluid pressure of the tumor (IFP or TIF) and the capillary pressure (blood vessels and lymphatic system) [165], which interact with the extracellular medium by perfusion. These movements of perfusion and flow generate mainly fluid shear stresses (FSS) within the tumor and prevent fluid

accumulation in interstitial spaces under normal conditions [147].

Fluid shear stress is an essential regulator of tumor cell adhesion and extravasation [182], which affects fluid mechanics and metastatic potential since tumor cells are primarily exposed to interstitial and blood shear stress during metastasis to target secondary organs [183]. FSS levels are variable in the fluid microenvironment related to tumor metastasis [182]. Invading tumor cells can take advantage of interstitial flow to generate autologous chemokine gradients, guiding their migration to draining lymphatic vessels. At the same time, cells in the microenvironment also respond to elevated interstitial flow caused by tumors, precipitating a cascade of changes in cell phenotype, secretion of pro-invasive cytokines, and matrix remodeling, all of which improve tumor invasion [184]. However, there are other critical factors in extravasation and metastasis, such as the necessary cooperation of EMT cells that alter the surrounding matrix through MMP and non-EMT cells that establish colonies at secondary sites [185].

Hyperpermeability of blood vessels and loss of lymphatic drainage within the tumor [186] represent barriers to drug delivery and transport [63]. As a result of this high vascular permeability, the interstitial shear stress can reach approximately 0.01Pa [182, 187]. Blood shear stress levels are higher than those produced by interstitial and lymphatic flow, obtaining pressure values in veins, capillaries, and arteries of 0.1-0.4 Pa, 1-2 Pa, and 0.4-3 Pa, respectively [182, 188]. The lymphatic system drains and allows reentry of body fluid into the circulatory system, reaching an average pressure of 0.1Pa [182], less than the other FSS.

The interstitial fluid pressure within tumors is raised and isotropic due to the overall tumor stress, and this increase is a result of the hyperpermeability of blood vessels in the tumor [45]. The IFP is heterogeneous, with higher values in the core and lower values at the borders [189, 45]. The raised IFP has been established as a modulatory factor for tumor proliferation, as it results in hypoxia and nutrient deprivation, thereby promoting tumor growth [190]. In fact, interstitial fluid drainage in a tumor xenograft model reversibly decreases tumor cell proliferation by improving drug uptake, modifying patterning, and increasing the relaxation of the cortex [191].

Fluid forces can be measured by microfluidic traction force microscopy, confocal microscopy, and flow magnetic resonance imaging [182]. Furthermore, the classical Wick-in-needle (WN) and pressure catheter (PC) are the two most commonly used methods to measure fluid pressure directly [192], and magnetic resonance imaging (MRI) has been used to measure wall shear stress [193, 194].

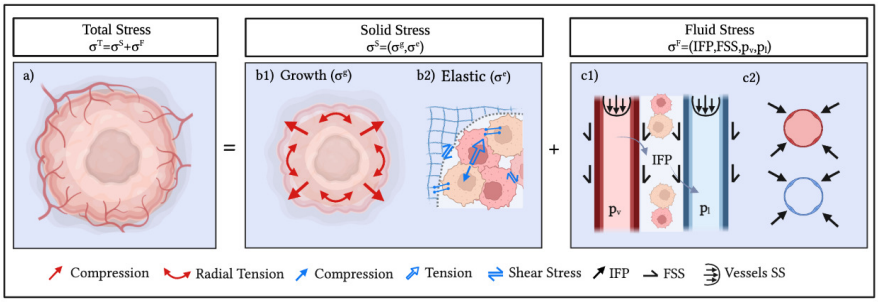

Figure 2.1: Stresses in a poroelastic tumor. a) Total stress is the sum of solid and fluid stresses generated during growth. b) Solid stress accounts for growth and elastic stresses. In particular, b1) shows the tensional growth state, which decomposes into radial compression and tension on the rims, while b2) accounts for the elastic rearrangement produced during growth: compression, shear, and tension forces that maintain equilibrium. Note that homeostasis is maintained if the cell-cell and cell-ECM adhesion forces are equilibrated. Finally, the fluid stresses c1) are mainly shear and account for the FSS in the interstitial medium and the shear stress of the blood and lymphatic vessels. IFP arises with growth compressing the vessels (see the cross section of vessels in Figure c2).

The interplay between microscale changes, such as cell-cell and cell-extracellular matrix interactions, and macroscale changes through mechanotransduction pathways results in a dynamic reciprocity [195]. Solid stresses in the tumor can cause compression of the vessels, leading to a decrease in vascular perfusion and hindering the flow of nutrients and lymphatic drainage. This results in an increase in interstitial fluid pressure, posing a barrier to drug delivery and enhancing the release of proangiogenic factors, contributing to the malignancy of tumor cells [196].

In summary, the dynamics of the tumor is involved in the accumulation of stress and the mechanical properties of the tumor and its environment, which in turn induces feedback into the biochemical pathways. Although the described solid and fluid effects are not mutually exclusive and a combined effect between stiffness and viscosity may coexist, in this review we propose to classify tumor dynamics into two major groups according to the leading nature of their progression: solid and fluid behavior of tumors.

The first scenario to be considered is when the matrix, surrounding tissue, or external forces inhibit tumor growth or migration by applying compressive stress on tumor tissue, as depicted in Figure 2.2a. This phenomenon has been

observed in experiments with agarose gels, where tumor growth is slowed if the tumor is embedded in a rigid medium. This relationship has also been demonstrated in vivo for prostate cancers, where benign prostatic hyperplasia applies compressive stress to the tumor, slowing its progression [92, 197, 198].

In the opposite case, the more rigid tumor causes compressions in the surrounding environment, thus displacing the surrounding tissue in a process called the mass effect, in which it gains volume and grows (Figure 2.2b). This phenomenon could explain why stiffer tumors can progress over surrounding tissue, creating joint forces that will depend on the relative stiffness of both tissues and accumulate throughout the growth process. Although tumor stiffness is characteristic of each cell line, the average stiffness of tumors ranges from 0.5-3kPa for spheroids [199] to 10-60kPa for consolidated tumors [200, 201, 202]. A suitable explanation of the difference between spheroids and consolidated tumors may be based on their function: cells and spheroids tend to adhere more slowly to each other, promoting motility, while consolidated tumors behave as solid masses with strong links and fibers. To characterize the mechanical properties of tumors, some techniques such as static and dynamic nanoindentation, micropipette aspiration, and optical tweezers are used in vitro [203, 204, 199]. The latter technology combines the mechanical characterization of cells with incubation and imaging to provide conditions similar to those in vivo (Pavone by ©Optic11). At the macroscale level, elastography is used [205, 206, 207].

However, the hypothesis regarding the displacement of the surrounding tissue by the growing tumor or vice versa remains controversial when the medium and tumor exhibit similar stiffness. Why can the tumor then migrate and proliferate? Recent studies propose a possible explanation based on the fluid dynamics of tumors, specifically, viscosity differences between the medium and the tumor [208, 209]. The phenomenon has been investigated in fluid systems, where a fluid with lower viscosity is introduced into a fluid with higher viscosity. This experiment has resulted in the formation of Saffman-Taylor instabilities, commonly referred to as viscous fingering, due to its characteristic pattern. Conversely, instabilities do not occur when viscosities are reversed [208, 210, 211].

Finally, these processes show a new perspective on tumor dynamics: growth and migration may be caused by differences in viscosities rather than differences in stiffness. Therefore, the tumor grows homogeneously if the viscosity of the medium is higher than that of the tumor (see Figure 2.2c) analogously to the case of the mass effect and heterogeneously if the tumor is less viscous than the medium, forming a patterning characteristic of viscous fingering and

more aggressive tumors, as shown in Figure 2.2d. Across these lines, recent reports show that glioblastoma (aggressive and metastatic tumor) has less viscosity compared to healthy brain parenchyma [208, 212]. On the contrary, viscosity differences do not appear to be helpful in breast tissue, almost twice as stiff as surrounding healthy tissue [205, 213].

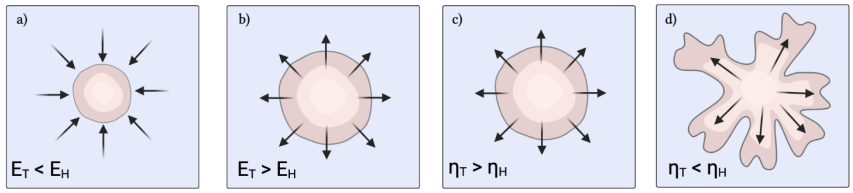

Figure 2.2: Difference in the patterning of tumor growth. a) and b) for solid growth behavior, and c) and d) for fluid growth behavior. In particular, a) shows the inhibition of growth due to compressive solid stress, b) growth as a solid mass effect, c) homogeneous tumor growth due to similar fluid properties, and d) the viscous fingering effect. The symbol E refers to the Young modulus, while η indicates viscosity. Subscripts T and H refer to the tumor and healthy medium, respectively.

2.1.2 Mechanotransduction as target therapy

The quest to unveil the molecular mechanisms by which mechanical forces modulate signal transduction and gene expression has been raised in the 21^{st} century to understand the mechanisms of cellular responses to the physiological environment [214, 147, 215, 216, 217, 47]. Although the exact mechanisms of responses remain unclear and are inherent to each type of cell line, in this section, we try to elucidate the main premises that have regulated the state of tumor stress to date, outlining an example of the leading hypotheses underlying mechanotherapy.

Mechanotransduction begins with the transmission of forces to tissue or cellular elements and ends with the integrated response of the cell cluster [215, 218]. The initial mechanical signal, mechanotransmission, occurs locally and is channeled to other mechanosensors along the linked cytoskeleton network extremely quickly, on the order of hundreds of milliseconds [218, 219]. If the forces are significant and are transmitted for a long enough time, mechanical stimuli cause deformation of cellular structures, which increase and strengthen in response to tension [220]. Conformational changes are followed by the selective mechanosensing or activation of intracellular biochemical signaling events [61, 221]. Then, cytoskeletal components are one of the leading

mechanisms in helping to transmit a complete array of chemical and physical signals that turn into a controlled mechanoresponse that regulates the cell prognosis [222, 223].

Mechanoresponsive pathways integrate the cellular response to force over space and time. The mechanism of response develops on slower time scales than other signals: transmission signaling pathways occur in minutes, and gene expression pathways can occur in hours to days [224, 218]. The leading network of cellular mechanotransduction comprises mainly transmembrane receptor proteins and the cytoskeleton, as well as extracellular matrix (ECM) protein complexes [47, 225]. Several hypotheses aim to explain outside-in mechanotransduction activation and how forces could enhance apoptosis, decrease proliferation, and prevent migration. Numerous studies detail the extensive biological pathways of mechanotransduction [223, 226, 215, 227], so in this thesis, we only focus on the core components – shown in Figure 2.3– that can be used as a targeted mechanical therapy to subsequently understand and propose mathematical frameworks that attempt to model them.

In this thesis, the focus is on the key components of outside-in mechanotransduction[1] activation and how forces can impact apoptosis, proliferation, and migration. While there is a wealth of research on the various biological pathways of mechanotransduction [223, 226, 215, 227], this study endeavors to isolate and analyze the critical elements involved in the process under investigations, as represented in Figure 2.3. These core components could be used as targeted mechanical therapy, and to subsequently understand and propose mathematical frameworks that attempt to model them.

- **Transforming Growth Factor β**: Transforming Growth Factor TGF-β is a family of cytokines that display a dual role in the tumor: at the early stages of the disease, acting as a tumor suppressor inhibiting cell cycle progression, and in advanced stages, promoting the Epithelial to Mesenchymal Transition (EMT), inducing the pro-tumorigenic response [228, 229, 230, 231]. Molecular events triggered by TGF-β drive the activation of canonical cascade signaling using SMADs [232], although noncanonical pathways, such as mitogen-activated protein kinase/extracellular signal-regulated (MAPK/ERK), have also been shown to influence tumor progression [233, 234, 235]. At later stages, tumor cells avoid the antitumor properties of TGF-β by inactivating TGF-β receptors, SMAD genes, or selectively silencing the properties of

[1] Note that only outside-in and isolation mechanisms are considered here. We assume neither the cell-cell interactions nor the existing links, which frequently act as hubs for other signaling regulations.

apoptotic TGF-β properties [234]. Furthermore, the feedback between ECM remodeling and the TGF-β signaling cascade [236] is critical in tumor control [237]. Experiments proved that soft ECM and increased TGF-β induced apoptosis, while increasing stiffness resulted in EMT employing non-canonical signaling pathways [237, 238, 239, 240]. Considering that in advanced disease, increasing the stiffness of the ECM of the microenvironment promotes tumor invasion and metastasis through the EMT, it clearly states that it is crucial to be aware of the stage at which action is required to regulate TGF-β action.

- **Integrin-focal adhesions**: Integrins are transmembrane receptors that regulate mainly cell-ECM adhesion. Integrins are activated by responding to the forces exerted by the alignment and stiffness of fibronectin in the ECM [120]. Once the stimulus is transmitted, the talin and kindlin proteins connect the tail of the integrin to the actin fibers. Focal adhesion is complete with binding of Focal Adhesion Kinase (FAK) [119, 241]. This activation promotes the linkage of vinculin [242, 243, 244], which adheres to actin in the cytoskeleton. The regulators of the actin cytoskeleton act downstream of Rho GTPase, triggering the activation of cascade signaling pathways: RHO–associated protein kinase (RHO–ROCK) and phosphatinositide—-3–kinase–protein kinase B (P1K3-AKT), which act as pro-oncogenes that induce lamellipodia protrusions, migration, motility, and decreased apoptosis [245, 246, 223, 118, 247]. Therefore, it is clear that blocking FAK overexpression, P13K-AKT, and RHO / ROCK pathways is a therapeutic target to investigate [248].

- **Wnt − Frizzled**: Wnt glycoprotein ligands adhere to Frizzled receptor proteins and trigger modulation of the β-catenin protein and co-receptors [249] through the canonical pathway [250]. This activation involves its translocation to the nucleus, where cell growth, motility, and differentiation are regulated [251, 252, 249]. Furthermore, there are non-canonical pathways independent of β -catenin: One of the most relevant in tumor development is the Wnt-Capathway $^{2+}$ [253, 250], where binding of Wnt to receptors causes a temporary increase in Ca concentration^{2+}. In particular, it is remarkable to point to the rise of cytoplasmatic Ca^{2+} via Piezo1 Ion Channel as a promoter of Wnt and P13K-AKT vias [254, 255, 256, 80, 257]. Wnt inactivation reduces migration by down-regulating matrix metalloproteinase (MMP) expression [258, 259, 260] and reduces EMT expression [260, 261, 262]. Furthermore, Wnt inhibitory factors (WIF-1) have also been shown to significantly reduce tumor growth [260, 263, 264]. Therefore, it could

be hypothesized that the mechanical stimulus could knock down the Wnt pathway, regulating tumorigenesis and cell invasion.

- **Hippo**: The Hippo pathway is a highly conserved kinase pathway that regulates cell proliferation, size, migration, and angiogenesis [265, 266, 267, 268]. Downstream regulation begins with the NF2 kinase protein and the serine / threonine protein kinases MST1 / 2 and the large tumor suppressor (LATS1 / 2), which activate the adapter proteins SAV1 and MOB1 [267, 269]. The Hippo pathway suppresses downstream transcriptional coactivators: the Yes-associated protein and transcription regulator protein 1 (YAP / TAZ) [270, 271], phosphorylating and sequestering them in the cytoplasm and inhibiting their nuclear transcription [272, 273, 274]. The localization of YAP-TAZ in the nucleus is identified as an oncogene that promotes EMT, malignancy, and secondary tumors [266, 267]. Nuclear activation of YAP-TAZ is also related to other vias (e.g., PI3K-AKT and Wnt) through high ECM stiffness, heterogeneous cell shape, loss of cell adhesions, and disturbed flow [275, 276, 272]. Therefore, blocking YAP-TAZ nuclear transcription and regulating the Hippo pathway is critical in mechanotherapy [269, 277, 278].

- **Hedgehog-Gli (Hh-Gli)**: Hedgehog proteins (in particular Sonic Hedgehog -SHh-) silence the Patched1 transmembrane protein (PTCH1), release Smoothened protein (SMO), and regulate the transcriptional activity of the glioma-associated oncogene (GLI)[279]. Hh-Gli pathway has been shown to be critical in tumorogenesis [280, 281, 282, 279], affect cytoneme stabilization and guidance [170], and negatively regulate EMT [283, 284, 285] in crosstalk with Wnt [286], TGF-β [287], and P13K-AKT [288, 289]. Furthermore, the orientation and guidance mechanisms followed by the Hh-Gli pathway have recently been studied [290], as well as the role of the Hh co-receptor interference hedgehog (Ihog) in contributing to integrin-mediated focal adhesions [291].

To conclude, we summarized and unified examples of biological pathways currently being studied to open a perspective that connects mechanotransduction mechanisms with biomechanical and mathematical models. Although we give short insights into possible mechanotransduction pathways, a complete proteomics analyses should test the therapeutic hypotheses in different tumor cells, stages, and stress states. Targeting these proteins and the pathways that regulate their expression is an active area of research for the devel-

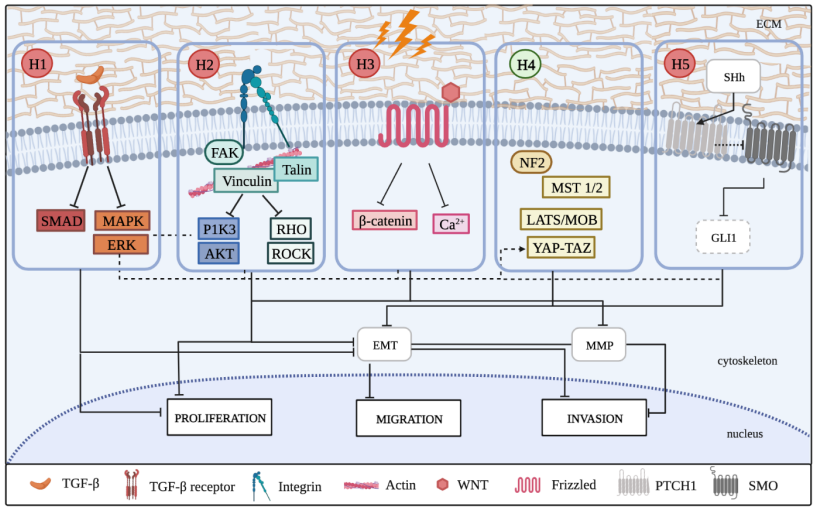

Figure 2.3: Examples of the therapeutical targets to impact cancer cells via mechanotransduction. From left to right, the mechanisms proposed are H1) Inhibition of TGF-β in advanced stages of the disease, H2) Deregulation of Integrins-focal adhesions to prevent the activation of P13K-AKT and RHO-ROCK pathways and its associated malignancy behavior, H3) Knockdown of Wnt-Frizzled to hinder poor prognosis, H4) Keep Hippo-pathway regulation to inhibit the YAP-TAZ nuclear localization and H5) Block overexpression of Hedgehog to prevent the inactivation of PTCH1 or Ihog. Mechanotherapy should account for these or other target mechanisms to selective block tumor progressor and the pathways that upregulate cancer propagation.

opment of new cancer therapies. In particular, the structure of the ECM emerges as a critical therapeutic driver, as the stiffness of the ECM is closely related to a poor prognostic disease in the proposed pathways. Therefore, mechanotherapy must focus on altering the biochemical and biomechanical properties of the tumor microenvironment and balance the pathways that prevent tumor progression in a non-invasive way.

2.2 Tumor modeling

Mathematical oncology is both a well-established and a rapidly-evolving field of research. The origins of this field date back to the differential equations that have been used to model and predict the uncontrolled proliferation of cancer cells and the effects of treatment for many years.

The pioneering works of Greenspan and McElwain remained an isolated case of mathematical oncology for two decades [292, 293, 294, 295]. In the 1990s, a large number of mathematical models were developed to describe the spatial growth of tumors, using approaches that ranged from simple diffusive models to complex multiphase models. Later, the interactions between the tumor and the immune system, mechanics, as well as the angiogenesis process, also became the focus of extensive theoretical research. Since then, comprehensive reviews on the advancements in mathematical oncology can be found in the references provided [296, 109, 297, 86, 298, 83, 299, 45, 300, 63, 301, 85, 302].

In cancer modeling, mathematical models can be broadly categorized into two types: discrete and continuum. Discrete models represent cancer as a collection of individual cells, whereas continuum models represent cancer as a continuous distribution of cells.

Discrete models simulate cancer at the subcellular and individual cellular scale, including protein synthesis, mutations, proliferation, apoptosis, cell adhesions, and migration. The most commonly used discrete models are based on whether cells are on a structured mesh (on-lattice models) or not (off-lattice models). Specifically, in on-lattice models, multiple cells can occupy a single lattice position (lattice-gas cellular automata), or each cell can occupy a single lattice position (cellular automata), or multiple positions (cellular Potts). Off-lattice models represent cells as autonomous agents that can move freely in a space without the use of a grid. These models can better represent the motility of agents and biomechanics, such as center-based and boundary-based models. For further reading on discrete models, we recommend [303], which provides a clear review of discrete models in cancer, including available open-source toolkits.

Continuum models, on the other hand, describe the distribution of clusters of cells and tissues in a given region at the macroscale. These models can provide a macroscopic view of cancer progression and can be used to predict how cancer will respond to treatment. They are based on systems of partial differential equations (PDE) which mainly include terms of reaction, diffusion, and convection.

Reaction terms are the source or sink functions of cells to mainly model

proliferation and apoptosis. These reaction terms can range from simple exponential equations to more complex models, such as gomperztian, logistic, and even functions that consider the competition between cells using predator-prey dynamics or Volterra-Lotka equations [304, 84]. Furthermore, the inherent uncertainty and variability in biological systems can be considered including stochastic functions as react terms in the model. The effect of therapies is usually modeled by altering parameters of proliferation or apoptosis or adding new reaction terms in the model [305, 168].

Convection and diffusion terms usually model motility and migration. In particular, Darcy's law is widely utilized for the diffusion of cells, despite its linearity and infinite speed of propagation hindering the regulation of the propagation front –inherent to each cell species–. To address this limitation, some studies incorporate the finite speed of the tumor's leading edge [306, 307, 308, 169, 309, 310, 311, 312].

These terms can be used also to model cellular movement in response to established gradients, such as chemical or mechanical signals (chemotaxis and mechanotaxis) [313, 314, 315]. Substances such as nutrients, growth factors, drugs, and proteins cascade are widely modeled as reaction-diffusion equations, coupled with other terms of PDE related to migration, proliferation, and even other agents to account for cell metabolism [316, 92]

The time scales also vary greatly depending on the type of process being studied. Proliferation, for example, can take hours to days as cancer cells divide and multiply. The formation and growth of a tumor can take weeks to months, as the cancer cells continue to divide and infiltrate surrounding tissue. In addition, while near invasion can take days, the complete process of metastasis can take weeks to years as cancer cells travel through the blood vessels or lymphatic system to reach new sites [317].

While continuum models are efficient in terms of computational cost, they may not be able to fully capture the intricate interactions between individual cells. This is where challenging hybrid and multiscale models come in - they blend the events happening at a subcellular, cellular, and tissue level, all while considering appropriate time and length scales [318].

Recent research in the field of mathematical oncology has also considered tumor growth dynamics from a mechanical continuum perspective. Tissues can be modeled using continuum mechanics since they can be understood as homogenized multiphase materials.

In this dissertation, we describe the main approaches of the macroscale continuum from finite growth theory and its simplification into infinites-

imal growth theory, which neglects the discontinuities on microscopic levels considering the tumor microenvironment as continuously distributed in the entire space it occupies. The fundamental theory underpinning the growth of tissues from the mechanics emerges from the works of [319, 179, 81] and the subsequent literature review performed by [54]. Since then, studies have primarily focused on the growth and remodeling theory of soft tissues [150, 82], without specific application to tumor modeling. However, some authors have specialized in cancer, considering growth with solid and fluid phases [86, 151, 180, 63]. More recently, [63, 45] summarized their comprehensive approach to tumor modeling from different angles: fluid and solid mechanical models, drug delivery, vascularization, and angiogenesis. The main equations of these models include multiphase systems, momentum balance, constitutive behavior, the mass balance that account for net proliferation and motility, and reaction-diffusion laws for biochemical components. In the following sections, we discuss the fundamental principles of continuum mechanics and their large application to the study of cancer.

2.2.1 Framework of Continuum

To elucidate the growth of tumors from a mechanical perspective, we initiate the discussion with the fundamentals of the Finite Strain theory [320] rooted in Classical Continuum Mechanics (CCM). This theory constitutes a preliminary approximation, as it assumes the material to be perfectly continuous. Then, we simplify here Generalized Continuum Mechanics (GCM) for which each material point P transmits both forces t_i and moments m_i. Therefore, under CCM, each material point P within the domain Ω only transmits forces, which are represented by the traction vector t_i.

Let P be a point in the undeformed body B at the initial time t=0 and in the undeformed configuration k_o, which deforms to the point p in the deformed body b at time t in the current configuration k_t (Figure 2.4). The point P is located at the material or Lagrangian coordinates $\mathbf{X}$, and p is located at the spatial or Eulerian coordinates $\mathbf{x}$. Thus, the initial position is represented by $\mathbf{X}$ while $\mathbf{x}$ denotes the position after a time t when the body is deformed. The displacement of particles, referred to as the undeformed coordinates (material coordinates), is expressed by Equation (2.2.1).

$$\mathbf{u}(\mathbf{X}, t) = \mathbf{x}(\mathbf{X}, t) - \mathbf{X}. \tag{2.2.1}$$

Material deformation at a material point is given by the gradient tensor $\mathbf{F}$,

which relates the reference and current configuration by Equation (2.2.2).

$$\mathbf{F} = \frac{d\mathbf{x}}{d\mathbf{X}}. \tag{2.2.2}$$

Consider dV the volume occupied by a particle and $\rho_o(\boldsymbol{X})$ the density in

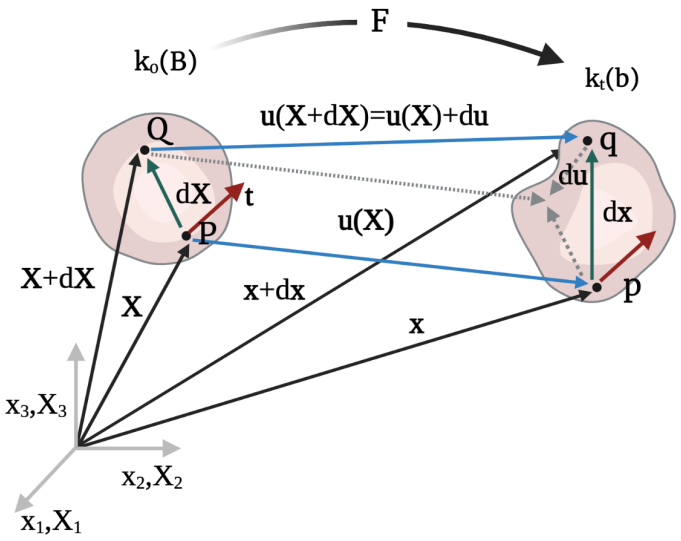

Figure 2.4: Fundamentals of Classical Continuum Mechanics. Configurations, Displacements, and Deformations.

the initial undeformed configuration $k_o(B)$. Thus, the mass of the particle is given by $dM_o = \rho_o dV$. After a time interval, dv and ρ are the volume and density of the current deformed configuration $k_t(b)$. The change in volume or density due to deformation is described by the determinant of the deformation gradient as J=$|\mathbf{F}|$ or in terms of volume or density variation between the current and initial configuration $\mathrm{J} = \left|\frac{dv}{dV}\right| = \left|\frac{\rho_o}{\rho}\right|$. Then, the conservation of mass for a single constituent in Lagrangian and Eulerian coordinates is:

$$\begin{aligned} \rho_o(\mathbf{X}) &= \mathrm{J}(\mathbf{X}, t)\rho(\mathbf{X}, t), \\ \frac{\partial \rho}{\partial t} + \nabla \cdot (\rho \mathbf{v}) &= 0, \end{aligned} \tag{2.2.3}$$

where the velocity of the particle is given by $\mathbf{v} = \dfrac{d\mathbf{x}}{dt}$. The finite deformation of the Green-Lagrange symmetric tensor $\mathbf{E}$ is defined to account for the strains.

$$\mathbf{E} = \frac{1}{2} \cdot \left(\mathbf{F^T F} - \mathbf{I}\right), \tag{2.2.4}$$

where $\mathbf{I}$ is the second-order identity tensor. Furthermore, the symmetric Green-Lagrange tensor $\mathbf{E}$ can be expressed in terms of displacements $\mathbf{u}$, as:

$$\mathbf{E} = \frac{1}{2}\Big(\nabla \mathbf{u} + \nabla \mathbf{u}^{\mathrm{T}} + \nabla \mathbf{u}^{\mathrm{T}} \cdot \nabla \mathbf{u}\Big). \tag{2.2.5}$$

The strain energy density is the energy stored in the tissue during stretching, and the use of different strain energy functions W depends on the tumor behavior. Stresses are obtained by deriving the strain energy density to $\mathbf{E}$ or strain deformation invariants, obtaining different constitutive equations. Invariants are tensors that satisfy the principle of material-frame indifference and do not change with Eulerian or material-frame rotations. The invariants used in this review are mainly used in non-linear elasticity; see equation (2.2.6). They are applied to a selected tensor $\mathbf{A}$.

$$\begin{aligned} \mathrm{I_A} &= \mathrm{tr}(\mathbf{A}) \\ \mathrm{II_A} &= \frac{1}{2}\Big((\mathrm{tr}(\mathbf{A}))^2 - \mathrm{tr}(\mathbf{A}^2)\Big), \\ \mathrm{III_A} &= |\mathbf{A}|. \end{aligned} \tag{2.2.6}$$

Regarding stresses, it is common to use the second Piola-Kirchoff pseudo-stress tensor $\mathbf{S}$:

$$\mathbf{S} = \frac{\partial \mathrm{W}}{\partial \mathbf{E}} = \frac{\partial \mathrm{W}}{\partial \mathrm{I_E}} \frac{\partial \mathrm{I_E}}{\partial \mathbf{E}} + \frac{\partial \mathrm{W}}{\partial \mathrm{II_E}} \frac{\partial \mathrm{II_E}}{\partial \mathbf{E}} + \frac{\partial \mathrm{W}}{\partial \mathrm{III_E}} \frac{\partial \mathrm{III_E}}{\partial \mathbf{E}}, \tag{2.2.7}$$

where the invariants here refer to the finite Green-Lagrange deformation tensor. However, other stresses are commonly used for convenience of configuration. In the Lagrangian approach, it highlights the first Piola-Kirchoff stress tensor $\mathbf{P}$, which associates the undeformed body with the stresses in the current configuration. In the Eulerian formulation, the Cauchy stress tensor –real stress– $\boldsymbol{\sigma}$ is referred to as the deformed body b in the current configuration. The relation between pseudo-stresses and the Cauchy stress tensor is given by Equation (2.2.8).

$$\begin{aligned} \mathbf{P} &= \mathrm{J}\boldsymbol{\sigma}\mathbf{F^{-T}}, \\ \mathbf{S} &= \mathrm{J}\mathbf{F^{-1}}\boldsymbol{\sigma}\mathbf{F^{-T}}. \end{aligned} \tag{2.2.8}$$

Another widely used notation is that described by the Cauchy-Green deformation tensors: the right Cauchy-Green deformation tensor $\mathbf{C} = \mathbf{F^T F}$, and the left Cauchy-Green deformation tensor $\mathbf{B} = \mathbf{F F^T}$. Considering the deformation tensor and the relation among pseudo-stresses, other formulas that can be found in the literature are:

$$\begin{aligned} \mathbf{P} = \mathbf{FS} = \frac{\partial \mathrm{W}}{\partial \mathbf{F}} = \mathbf{F}\frac{\partial \mathrm{W}}{\partial \mathbf{E}} = 2\mathbf{F}\frac{\partial \mathrm{W}}{\partial \mathbf{C}}, \\ \mathbf{S} = \mathbf{F^{-1}P} = \mathbf{F^{-1}}\frac{\partial \mathrm{W}}{\partial \mathbf{F}} = \frac{\partial \mathrm{W}}{\partial \mathbf{E}} = 2\frac{\partial \mathrm{W}}{\partial \mathbf{C}}. \end{aligned} \tag{2.2.9}$$

Last, the equilibrium of the system is achieved if the balanced momentum is guaranteed:

$$\nabla \cdot \mathbf{P} + \mathbf{b} = \rho_{\mathrm{o}} \frac{\partial^2 \mathbf{u}}{\partial \mathrm{t}^2}, \tag{2.2.10}$$

where $\mathbf{P}$ depends on the behavior of the constitutive material of each tissue, ρ_o is the material density, $\mathbf{b}$ are the body forces, and the term on the right represents the terms of inertia. Note that the characteristic velocities in biological tissues and growth are small – growth is relatively slow compared to elastic or viscoelastic response of tissues [51]–, so inertia terms can be neglected, and quasi-static equilibrium imposes.

2.2.2 Growth from Continuum

Once the mechanical basics are established, tumor growth is included in the mechanics framework similar to the thermoelastic problem [320]. Then, the expansion or resorption of the tumor causes deformation from the initial zero-stress state (ZSS) and there is a subsequent elastic rearrangement to ensure the equilibrium of the medium to current stress state [51]. Consequently, the deformation gradient tensor multiplicatively decomposes into the growth tensor $\mathbf{F_g}$ and the elastic tensor $\mathbf{F_e}$ (Figure 2.5a), although a third component could also be included to account for residual stresses accumulated in tumors [45, 179, 321, 158]. This residual stress works similar to prestressed concrete in Civil Engineering, making the tissue skeleton more efficient to loads [51].

$$\mathbf{F} = \mathbf{F_e F_g}, \tag{2.2.11}$$

where $\mathbf{F}$ is the total gradient deformation, $\mathbf{F_e}$ is the elastic rearrangement produced after the tumor dynamics and $\mathbf{F_g}$ considers the gain or resorption of the tumor mass described by the stretch rate g, $\mathbf{F_g} = g\boldsymbol{\lambda_g}$, with $\boldsymbol{\lambda_g}$ the anisotropy tensor that distributes growth in different directions through different weights. If the growth tensor is taken as isotropic, then $\boldsymbol{\lambda_g} = \mathbf{I}$. Just as it happened with the Jacobians of the deformation, the changes in

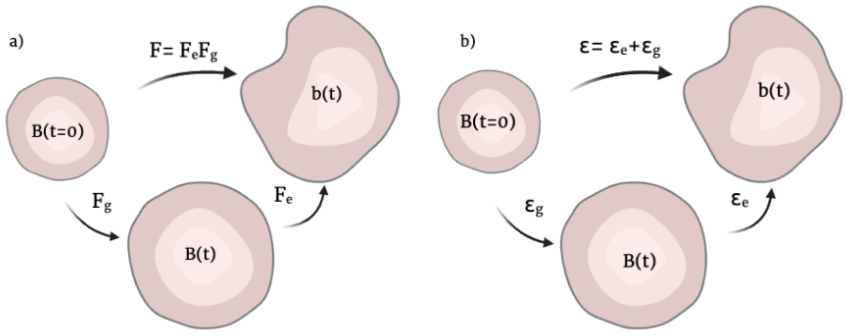

Figure 2.5: Theoretical framework of growth theory. a) Finite growth theory. b) Infinitesimal growth theory.

volume or density produced by growth are described by the determinant of gradient deformation J_g=$|\mathbf{F_g}|$. Then, if $J_g > 1$ growth takes place, while if $J_g < 1$, resorption occurs. The mass conservation that now accounts for mass gain or resorption can be expressed in a Lagrangian or Eulerian frame reference:

$$\begin{aligned} \frac{d(\rho \mathrm{J})}{dt} &= \mathrm{J}\rho\Gamma, \\ \frac{\partial \rho}{\partial t} + \nabla \cdot (\rho \boldsymbol{v}) &= \rho\Gamma, \end{aligned} \tag{2.2.12}$$

where the source term Γ accounts for the gain or loss of tumor mass. Some describe growth as an increase in the mass of already existing cells in the body [150, 53], *hypertrophy*, while others account for the increase in the number of cells – proliferation or duplication of cells – and its motion – motility or migration–, *hyperplasia*. Furthermore, growth dynamics can also be a function of the availability and concentration of nutrients [150, 180, 151], the generation or degradation of some cellular components [321, 322, 323], proteins [309, 92], drugs [324, 180] and stress as it is pointed in the next section. The relationship between the term of the isotropic growth strain and the proliferation rate is given by [150]:

$$\frac{dg}{dt} = \frac{1}{3} g\Gamma. \tag{2.2.13}$$

Additionally, volumetric fractions are used to model the multiphase tumor system. Considering that the constant density of each phase is $\rho_i = \dfrac{\partial m_i}{\partial v}$,

the volumetric fraction occupied by a phase can be represented by $\phi_i = \dfrac{\partial v_i}{\partial v}$, see details in references [325, 326, 81]. The classical theory of the growth of mixtures implies that the mass densities of each phase can change, but only in such a way that the mass is conserved [326, 150], which means that there can be mass interchange, but not true mass production [327, 328]. This overcomes the limitation of the theory of growth, in which there is a violation of the Continuum principle by creating new points [51]. The existence of different phases can be expressed as:

$$\phi_F + \sum_{i=1}^{n} \phi_i = 1, \tag{2.2.14}$$

where the subindex F refers to the interstitial fluid and the subindex i denotes the constituents of the solid tumor. In this context, the phase-field models are useful tools for solving interfacial problems, where fluid and solid phases would be changed between two values in the zone around the interface, avoiding abrupt changes between phases and allowing the diffuse nature interface [91, 92, 329]. In addition, some authors support the creation of mass-produced during tumor growth, so the previous equation is no longer satisfied, and the sum of the constituents would exceed the unit [84, 330]. Specifically, the mass conservation of the fluid and solid phases is a function of time and space:

$$\begin{aligned} \frac{\partial \phi_F}{\partial t} + \nabla \cdot (\phi_F \boldsymbol{v_F}) &= \phi_F \Gamma_F; \\ \frac{\partial \phi_i}{\partial t} + \nabla \cdot (\phi_i \boldsymbol{v_i}) &= \phi_i \Gamma_i. \end{aligned} \tag{2.2.15}$$

In addition to the reaction term of proliferation Γ_i, multiphase systems can involve feedback and interactions between different solid phases as explained previously. Lastly, the migration of the solid phases includes a diffusion term $\boldsymbol{\mathcal{J}}_i$:

$$\frac{\partial \phi_i}{\partial t} + \nabla \cdot (\phi_i \boldsymbol{v_i}) = \nabla \cdot \boldsymbol{\mathcal{J}}_i + \phi_i \Gamma_i, \tag{2.2.16}$$

where $\boldsymbol{\mathcal{J}}_i$ is the flux. Regarding the different phases that make up the continuum, equation (2.2.11) should be described for each phase as $\mathbf{F}_i = \mathbf{F}_{\mathbf{e}i}\mathbf{F}_{\mathbf{g}_i}$.

2.2.2.1 Infinitesimal growth theory

Since tumor deformation is a quasistatic process that occurs over a much larger time scale than elastic rearrangements, the continuum is widely modeled

considering infinitesimal theory and linear elasticity [92, 91, 331, 332, 90, 89], considering small strains and rotations. As such, linear elasticity provides a suitable mechanical framework for investigating the effects of mechanotransduction. Notwithstanding However, the choice of strain theory depends on the specific purpose of the study. To move from the multiplicative decomposition of large strains to the additive decomposition of small strains (Figure 2.5b), we define the polar decomposition of the gradient tensor $\mathbf{F}$:

$$\mathbf{F} = \mathbf{RU}, \tag{2.2.17}$$

with $\mathbf{U}$ the right stretch tensor and $\mathbf{R}$ the rotation tensor. In particular, the stretch tensor is defined by :

$$\mathbf{U} = \sqrt{\mathbf{F^T F}} \approx \mathbf{I} + \boldsymbol{\varepsilon} + h.o.t., \tag{2.2.18}$$

where the small strain tensor is defined by $\boldsymbol{\varepsilon} = \frac{1}{2}\left(\nabla\mathbf{u} + \nabla\mathbf{u}^{\boldsymbol{T}}\right)$ and $h.o.t.$ refers to high-order terms. The rotation tensor is:

$$\mathbf{R} = exp(\boldsymbol{\Theta}) \approx \mathbf{I} + \mathbf{e}\boldsymbol{\Theta} + h.o.t., \tag{2.2.19}$$

with $\mathbf{e}$ is the Levi-Civita tensor and $\boldsymbol{\Theta}$ the rotation tensor. Combining equations (2.2.17), (2.2.18) and (2.2.19), and assuming $\boldsymbol{\Theta} \ll 1$, then:

$$\mathbf{F} = (\mathbf{I} + \boldsymbol{\varepsilon})(\mathbf{I}) = (\mathbf{I} + \boldsymbol{\varepsilon}) + h.o.t. \tag{2.2.20}$$

Notice that the spatial derivative of displacements in equation (2.2.1) can be described as:

$$\frac{\partial \mathbf{u}}{\partial \mathbf{X}} = \frac{\partial \mathbf{x}}{\partial \mathbf{X}} - \mathbf{I} = \mathbf{F} - \mathbf{I} \longrightarrow \varepsilon \approx \frac{\partial \mathbf{u}}{\partial \mathbf{X}} = \mathbf{F} - \mathbf{I}. \tag{2.2.21}$$

Using (2.2.20), assuming small deformations and rotations, the multiplicative decomposition of (2.2.11) reads:

$$\mathbf{F} = \mathbf{F_e F_g} = (\mathbf{I} + \boldsymbol{\varepsilon}_\mathbf{e})(\mathbf{I} + \boldsymbol{\varepsilon}_\mathbf{g}) = \mathbf{I} + \boldsymbol{\varepsilon}_\mathbf{g} + \boldsymbol{\varepsilon}_\mathbf{e}. \tag{2.2.22}$$

Finally, the infinitesimal growth theory is based on:

$$\boldsymbol{\varepsilon}_\mathbf{e} + \boldsymbol{\varepsilon}_\mathbf{g} + \mathbf{I} = \boldsymbol{\varepsilon} + \mathbf{I} = \mathbf{F}. \tag{2.2.23}$$

Then, Equation (2.2.11) simplifies into the additive equation (2.2.24):

$$\boldsymbol{\varepsilon} = \boldsymbol{\varepsilon}_\mathbf{e} + \boldsymbol{\varepsilon}_\mathbf{g}, \tag{2.2.24}$$

where $\boldsymbol{\varepsilon_e} = \frac{1}{2}(\nabla \mathbf{u} + \nabla \mathbf{u}^{\mathrm{T}})$ is the elastic small deformation that guarantees mechanical equilibrium and the volumetric growth deformation is $\boldsymbol{\varepsilon_g} = g\boldsymbol{\lambda_g}$. Taking into account small strains, the elastic Cauchy stress tensor may be expressed as:

$$\boldsymbol{\sigma_e} = \boldsymbol{\sigma} - \boldsymbol{\sigma_g}, \tag{2.2.25}$$

where $\boldsymbol{\sigma}$ is the total tensional state obtained from equation (2.2.7) and $\boldsymbol{\sigma_g}$ is the induced growth stress. Assuming the volumetric growth of the tumor, $\boldsymbol{\sigma_g} = K\boldsymbol{\varepsilon_g}$, with K the bulk modulus. Finally, note that the advective term of the mass continuity equation (2.2.16) would be negligible under the assumption of small displacements, small strains, and gradual changes in tumor phases.

2.2.2.2 Governing equations: elasticity and poroelasticity

Due to the heterogeneous nature of the tumor, it is important to model the mechanical behavior according to it. We denote by $\mathrm{W_e}$ the strain energy density of the solid skeleton drained, and $\mathrm{W_p}$ the contribution of saturated pores to the strain energy density. The total contribution reads $\mathrm{W} = \mathrm{W_e} + \mathrm{W_p}$. Most of the constitutive relations of solid elastic used in the literature are the Blatz-Ko, Neo-Hookean, Exponential, and Ciarlet equations, as shown in Table 2.1. Although viscosity is a fundamental parameter in reorganization at small scales, viscosity is no longer relevant over long times – intrinsic to growth. Therefore, the equations of tumor behavior do not include the solid viscosity of the cells that could be described by the Kelvin-Voigt, Maxwell, or Burgers models. However, viscosity can be a crucial parameter in fluid behavior, as outlined in Section 2.1.1. Despite the different constitutive relations proposed in the literature, [321] concluded that the evolution of stress appeared to be independent of the chosen constitutive relation [321], although exponential law better fitt cancer breast and colon adenocarcinoma experiments.

In addition to the elastic properties of the tumor, the fluid component is usually taken into account. Studies widely used the Biot theory of porooelasticity [337], which is based on the assumption that the deformation of the tumor is caused by both the solid matrix and the fluid that fills its pores. Although the theory was initially developed to describe the mechanical behavior of soil, it has also been widely applied to other porous materials such as bone, and tumor tissues.

Then, Biot's theory allows us to model the elastic behavior of the tumor, the fluid flow inside the pores, and the interaction between the solid matrix and the fluid-filled pores [325]. To model poroelasticity, several possibilities

Table 2.1
Essential strain energy functions used in tumor growth modeling. Constants λ and μ are the first Lamé parameter and the shear modulus, respectively[a]. The invariants described above are related to the right Cauchy tensor (C) and the left Cauchy tensor (B). J_e is the elastic determinant and f, z, A_1, A_2 and C are constants.

Law	Main equation	Source
C. Neo-Hookean	$W_e = 0.5\mu(I_C - 3 + 2\ln J_e) + 0.5\lambda(J_e - 1)^2$	[321, 323]
C. Blatz-Ko	$W_e = \frac{\mu f}{2}\left[(I_C - 3) - \frac{2}{z}(III_C{}^{z/2} - 1)\right] + \frac{\mu(1-f)}{2}\left[\frac{II_C}{III_C} - 3 - \frac{2}{z}(III_C{}^{-z/2} - 1)\right]$	[321, 150, 333]
C. Ciarlet	$W_e = \frac{\lambda}{4}\cdot(III_B - \ln III_B - 1) + \frac{\mu}{2}\cdot(I_B - \ln III_B - 3)$	[334, 335, 166]
Exponential	$W_e = A_1\left(e^{C_1(-3+I_C J_e^{-2/3})} - 1\right) + A_2(-1 + J_e)^2$	[321]
C. Linear	$W_e = 0.5\lambda(I_E)^2 + \mu I_E^2$	[331, 336, 92, 91]

[a]Note that elastic parameters should be drained if poroelasticity is considered.

arise to model the solid displacement and the fluid displacement $\mathbf{u} - \mathbf{u}_F$, the solid displacement and the relative solid-fluid displacement $\mathbf{u} - w$, or a combination of the solid displacement and the pore pressure $\mathbf{u} - p$. This last approximation is the most used in tumor growth due to the reduction of degrees of freedom and allows focusing on the influence of fluid pressure on the solid skeleton.

According to this formulation, the fluid strain energy can be modeled by a quadratic potential $W_p = -\frac{\alpha}{2}(p - p_o)^2$, where α is the Biot coefficient, which represents the volume of fluid gained or lost when the pore pressure returns to its initial state [338], The variation in fluid content ζ assuming constant density is related to elastic volumetric strain ε_v, and the pore pressure p:

$$\zeta = \phi_F - \phi_{F0} = \frac{1}{M}(p - p_0) + \alpha\varepsilon_v, \tag{2.2.26}$$

where ϕ_F is the current fluid phase, ϕ_{F0} is the initial fluid content, and M is the Biot modulus, which considers the increase in fluid amount as a result of a unit increase in the pore pressure, under constant volumetric stress [338, 339]. Then, the fluid mass conservation can be rewritten as the Storage equation:

$$\frac{\partial\zeta}{\partial t} = \nabla\cdot\boldsymbol{q} + \Gamma_F \longrightarrow \frac{1}{M}\frac{\partial p}{\partial t} + \alpha\frac{\partial\varepsilon_v}{\partial t} = \nabla\cdot\boldsymbol{q} + \Gamma_F. \tag{2.2.27}$$

where the pressure flux is represented by $\boldsymbol{q}$, and the parabolic Darcy law generally defines it, $\boldsymbol{q} = k_h\nabla p$, with k_h denoting conductivity, which is a function of the viscosity of the dynamic fluid, the porosity, and the permeability of the medium [337, 338]. The term Γ^F considers the fluid interchange between the lymphatic and vascular systems and the interstitial fluid described, which is usually defined by the Starling equation [340, 186, 341, 304, 342].

As pointed out at the beginning of the section, it is relevant to consider the multiscale scale of the problem. Thus, some authors have also considered the microscale of biochemical interactions by reaction or reaction-diffusion equations, as described in (2.2.16). From these equations, the dependence of growth on local oxygen [151, 324, 343], nutrients [333, 344], proteins [92, 309, 91] and even the effect of therapy such as drug delivery [324, 180]. Notably, slight variations of these substances prolonged in time can produce the same effect as a sizeable instantaneous fluctuation. For instance, reference [170] shows that hypoxia processes and small flow (apparently negligible) of Hh prolonged in time significantly influence the growth or migration.

2.2.2.3 Modeling mechanotransduction

Based on growth theory, studies have advanced in research proposing that growth modifies tumor stress and strain state and that stress acts as a regulator of proliferation and migration –mechanotransduction–, as has been demonstrated experimentally (see Section 2.1.1). Then, growth-induced stress models as a bidirectional coupling.

The first biomechanical models that involve mechanotransduction in tumors were proposed by [151], who formulated and validated a linear poroelastic model that accounts for the inhibition of proliferation of the melanoma tumor spheroid line (MU89) embedded in agarose gel matrices. Since then, mechanotransduction $\mathcal{M}$ has been modeled as a phenomenological function that affects migration and proliferation rates through stress.

The key idea is that the forces present in the tumor are pressure-like, and directly proportional to tumor cells through a function that describes the dependence of growth on solid stress. Considering the previous Eulerian equation of mass continuity described (2.2.16), mechanotransduction is usually included in mass continuity as follows:

$$\frac{\partial \phi_i}{\partial t} + \nabla \cdot (\phi_i v_i) = \nabla \cdot (\mathcal{M} \boldsymbol{\mathcal{J}}_i) + \mathcal{M} \phi_i \Gamma_i, \tag{2.2.28}$$

being $\mathcal{M}$ the mechanotransduction function that can affect migration (first term on the right) and proliferation (second term on the right). Table 2.2 shows the main mechanotransduction functions used in the literature to date. Specifically, the contribution of modeling mechanotransduction translates into different approaches which fit the experimental data described in 2.1.2. Some computational studies found that growth-induced stress promotes higher levels of solid stress in the tumor interior and lower in the periphery [186]. Furthermore, high compressive solid stress can collapse blood vessels in the

Table 2.2
Mechanotransduction laws used in recent years. The fitting parameters β_i, q, and χ_σ are related to the size of the cell and the fitting of proliferation to relieve stress. Hydrostatic stress that accounts for volumetric changes is $\sigma_{\mathrm{h}} = 1/3\mathrm{tr}(\boldsymbol{\sigma})$, Σ refers to the adhesion forces of the cells and Von-Misses stress, which is a measure of the energy of distortion, is defined by $\sigma_{\mathrm{vm}} = \sqrt{\frac{(\sigma_1-\sigma_2)^2+(\sigma_2-\sigma_3)^2+(\sigma_3-\sigma_1)^2}{2}}$, where σ_i refers to main stresses. The compressive stress threshold that cells sense is defined by σ_h^{crit} is characteristic of each cell line. The choice of what type of stress is considered depends on the purpose of the study, so other proposals such as Tresca stress could be included if the main source of mechanotransduction is shear stress.

Affected term	**Mechanotransduction law**	**Source**
Growth	$\mathcal{M} = 1 - \beta\sigma_h$	[151, 186, 321, 324, 322, 84]
Growth	$\mathcal{M} = \left(1 - (\beta_1\sigma_h{\beta_2}^{-1} + \sigma_h)\right)$	[343]
Growth	$\mathcal{M} = \left[q + \frac{\left(1-q\right)e^{\chi_\sigma\left(\sigma_h - \sigma_h^{crit}\right)}}{1 + e^{\chi_\sigma\left(\sigma_h - \sigma_h^{crit}\right)}}\right]$	[84, 330]
Growth	$\mathcal{M} = 1 - \beta_1\frac{\Sigma}{\Sigma + \beta_2}$	[158]
Migration	$\mathcal{M} = e^{-\beta\sigma_{vm}}$	[89, 90, 332]
Migration and Growth	$\mathcal{M} = e^{-\beta_1(\sigma_{vm} + \beta_2\lvert\sigma_h\rvert)}$	[92]

tumor interior [186], negatively affecting drug delivery [322]. However, a highly vascularized region in the tumor periphery is associated with better oxygenation and positive drug delivery such as chemotherapy [324] and nanomedicine [322].

Furthermore, [343] proved that stiffer cells propagate through softer tissue and [321] quantified 1.5 the number of times the tumor must be more rigid than its surrounding to displace it. Reference [321] also suggested that solid stress involves tumor inhibition independently of the constitutive equation chosen, although it strongly depends on mechanical interactions with the surrounding host tissue. References [84, 330] showed the interspecific competition of species that defines the Volterra-Lotka or predator-prey equations that describe the dynamics of tumor and healthy cells. Indeed, tumor cells are inhibited if stress exceeds a critical threshold value.

Some studies also propose a pseudopotential stress law based on cell repulsive interactions and attractive forces. In particular, reference [326] developed a switch function in which mechanotransduction occurs if there is compression on the membrane of proliferative cells. The works of [345, 346] change the law for a monotonic mollifier of the step function, and more recently [158] propose four mechanotransduction functions (linear, exponential, inversely propor-

tional, and Michaelis-Menten-like equation – which is shown in Table 2.2) fitting experiments.

Considering also the effect of mechanotransduction on migration, [89] reconstructed the coupling parameter β from Magnetic Resonance Imaging (MRI). This could be one of the critical points in personalized mechanotransduction models, including chemotherapy effects. More recently, the intra-tumoral heterogeneity of gliomas [90] and the impact of drug delivery in breast tumors were also included in the mechanically coupled equations [332]. Lastly, [92] proposed a personalized prostate cancer model in which not only stress-driven growth but also the mechanics produced by benign hyperplasia slow tumor growth. This is the only function of mechanotransduction known, as far as we are aware, that accounts for migration and proliferation terms and for both Hydrostatic and Von-Misses stress.

These pioneering studies serve as powerful tools to simulate and analyze the complex biological and physiological processes underlying cancer development and progression. These models have demonstrated the potential to make predictions about cancer progression, and response to treatment, and ultimately would improve patient outcomes.

The application of mathematical and engineering techniques in oncology is expected to become increasingly important as we strive to understand the underlying mechanisms of cancer, identify novel therapeutic strategies, and personalize treatment plans. The integration of mathematical and computational models into clinical decision-making has the potential to transform the field of oncology and revolutionize the way we approach cancer diagnosis and treatment.

2.3 Ultrasound in mechanotherapy

Mechanotherapy, also known as mechanical signaling therapy, is an emerging cancer treatment that uses mechanics to target and destroy cancer cells. This approach is based on the idea that cancer cells have a heightened sensitivity to mechanical forces and that applying these forces can disrupt their function and promote their death.

As detailed below, a variety of techniques are nowadays being developed by different laboratories to actively impact cell behavior by altering microenvironment. They range from drugs that modify the elasticity of the remodeled microenvironment and cell stiffness, to mechanical waves. These principles serve as valuable tools for research and understanding and are currently translatable to clinical applications, as mechanical waves can be applied using transducers or patches and drugs can be administered to patients. Furthermore, this potential therapies can be combined to increase the efficacy of treatments and improve overall prognosis of the disease.

In altering the tumor microenvironment, a drug-loaded hydrogel matrix selectively captured and eliminated cancer cells, since they are attracted to the modified extracellular matrix (ECM), where they are eliminated [347]. Hence, the matrix acts as a stiffness filter, differentiating between tumor and healthy cells, independently of the applied drug load. In addition, normalizing the tumor matrix by degrading its collagen with bacterial collagenase treatment [348], and by pirfenidone [349], alleviates the solid stress and reduces the interstitial fluid pressure improving vascular density and the supply of drugs to the tumor. This supply can be remoted regulated by magnetic nanoparticles (MNP) [350, 351] and also mechanical waves [352, 353, 354].

In biomechanics, mechanical waves have been usually used to study and characterize the mechanical properties of biological tissues. Mechanical waves are a promising technique that opens a line in therapy since they can be remotely focused and they minimize side effects. They are disturbances that propagate through a medium transferring energy without the transference of mass. These waves are caused by oscillations or vibrations of the particles of the medium and can be classified into two main categories: longitudinal or compressional waves, in which the motion of the particles is parallel to the direction of wave propagation and are characterized by the alternation of compression and rarefaction of the medium through which they travel; and transverse or shear waves, in which the motion of the particles is perpendicular to the direction of wave propagation.

In particular, ultrasound is longitudinal mechanical waves with frequencies

higher than the upper audible limit of human hearing (20 kHz). The primary application of ultrasound in Engineering was monitoring health structures in nondestructive testing, although its application to diagnostic and screening in medical imaging is clear.

In addition, its therapeutic potential has been demonstrated in recent years. Depending on the wave parameters, ultrasound is used for tissue regeneration, stimulation, thermal ablation, gene delivery, drug-mediated, and to selectively impact cancer cells [355, 356, 313, 68, 357].

In Figure 2.6, we illustrate the relation of frequency of the ultrasound with the wavelength and their relation to length and time scales in cancer.

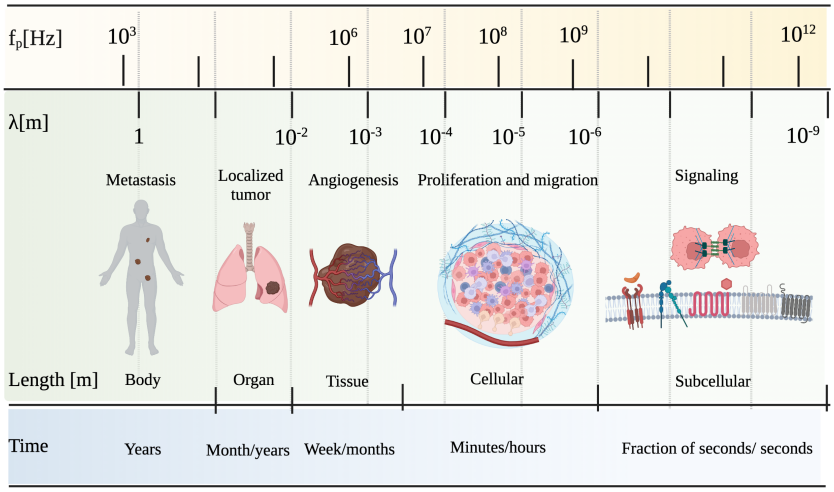

Figure 2.6: Relation of the frequency with wavelength, size, and time-scale of cancer. We have considered the relation $\lambda = c_p f^{-1}$, where ultrasound wave speed is assumed $c_p \approx 1490\text{ms}^{-1}$.

The Mechanical Index (MI) is a measure of the power of an ultrasound beam. It is derived from the need for an indicator for the possible non-thermal bioeffects of the acoustic field. It is defined as:

$$\text{MI} = \frac{p_r}{\sqrt{f}}, \tag{2.3.1}$$

where p_r is the rarefactional pressure amplitude measured in MPa and f is the center frequency of the transducer, in [MHz] Furthermore, the Intensity Spatial Peak Temporal Average (ISPTA) measures the average intensity

during the entire sonication and is thus a good measure of tissue heating, which scales in proportion to sonication duration. The definition of ISPTA yields:

$$\text{ISPTA} = \frac{1}{t_p} \int_0^{t_p} \frac{1}{A} \int_A I(t, x, y, z)\ dA\ dt, \tag{2.3.2}$$

where t_p is the pulse duration and $I(t, x, y, z)$ is the temporal and spatial distribution of the acoustic intensity. In the context of therapeutic ultrasound, ISPTA is an important parameter for determining the potential for non-thermal effects of ultrasound, such as cavitation, tissue heating, and mechanical disruption of tissue.

As pointed out in Section 2.1, HIFU is a type of thermal ablation therapy that uses high-energy ultrasound waves to heat and destroy cancer cells. In particular, HIFU uses high-intensity ultrasound with ISPTA values in the range of 10^2-10^4Wcm^{-2} to produce thermal and mechanical effects in tissue.

One of the main advantages of HIFU is that allows for real-time monitoring of the tissue due to its dependence on MRI guidance. HIFU has been shown to be effective in treating early-stage prostate cancer, with reported long-term cancer-specific survival rates of up to 90% [358, 68]. However, the high energy of the sound waves can result in the destruction of both healthy and cancerous tissue, leading to unintended harm. Thus, HIFU is only used to treat small and localized tumors, and it may not be effective in treating larger or more advanced cancers.

To avoid indiscriminately destroy of healthy tissue as well as tumors, an alternative approach involves low intensity ultrasound (LIUS), or its pulsed version (LIPUS).

Currently, there is no universally accepted definition of low-intensity ultrasound. Some studies indicate restricted used of LIUS to ISPTA$< 0.3\text{Wcm}^{-2}$ [359, 74], while others consider a more broad range where ISPTA $< 3 - 5\text{Wcm}^{-2}$. For the purpose of this thesis, we include the more permissive ISPTA values, to have a complete broad range of biomechanical effects in cancer including mainly mechanotransduction and cytodisruption.

In therapeutics, FDA limits the maximum allowable ISPTA for most medical ultrasound therapy applications in the range of 10^2-10^4Wcm^{-2}. However, these limits can vary widely depending on the specific therapy being used and the conditions under which it is applied.

LIUS has been explored for a range of therapeutic purposes [360, 359]. From sonodynamic therapy, low-intensity ultrasound applied to cancer cells in combination with a sonosensitizer triggers cavitation – phenomenon wherein

bubbles form in a liquid material when the local pressure (such as might be produced by the rarefaction part of a passing ultrasound wave) falls below the vapor pressure of the liquid sufficient to pull the material apart. Stable cavitation refers to the oscillation of bubbles in response to the ultrasound, while transient cavitation refers to the violent collapse of bubbles, which can cause tissue damage–, generating free radicals and causing cell death.

Furthermore, in ultrasound-mediated chemotherapy, the insonation of a tumor with the presence of a chemotherapeutic agent enhances its delivery to cancer cells while reducing its cytotoxic impact on surrounding normal tissues. This is achieved through the use of ultrasound alone, in conjunction with microbubbles, and through the use of drug-loaded microbubbles or liposomes attached to microbubbles.

Regarding gene delivery, it is suggested that focused ultrasound can induce sonoporation, resulting in temporary permeation of cell membranes. This allows for the introduction of therapeutic molecules into cancer cells, although the exact mechanism by which genetic material crosses the endothelial barrier to reach the tumor is yet to be determined.

More recently, LIUS has been demonstrated to selectively kill cancer cells while sparing healthy tissue. This specificity makes LIUS a highly promising candidate for cancer therapy and will be discussed in greater detail in the following subsection.

Although literature reveals a wide range of sonication conditions utilized in various studies, making it difficult to draw precise comparisons between the findings, in Figure 2.7 we summarize the key insights into the main mechanical and biological effects produced at different intensities and acoustic pressures. Thus, LIUS therapy can include a wide range from cytodisruption to mechanotransduction, and even it can result in a combination of effects.

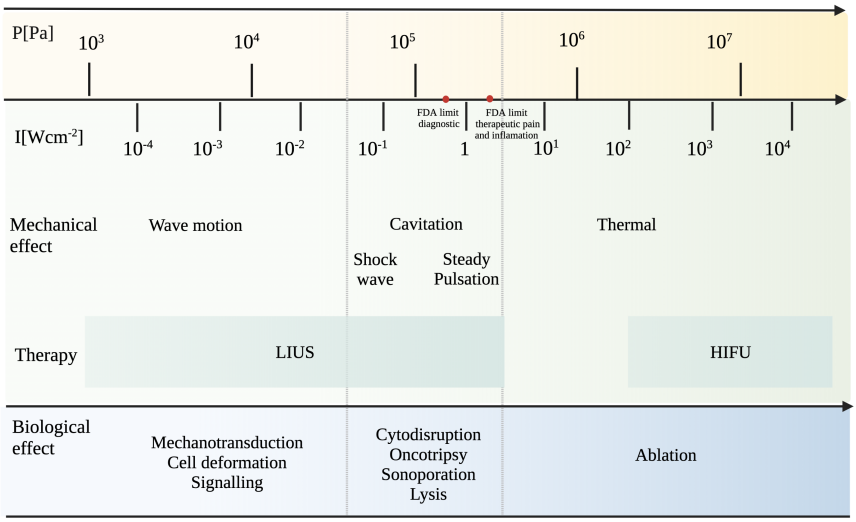

Figure 2.7: Relation between pressure and energy and bioeffects. Intensity has been calculated through $I = p^2/\rho c_p$, being p the root mean square pressure amplitude. Note that not only intensity hinders mechanical or biological effects but also frequency.

2.3.1 Low-intensity ultrasound as target therapy in cancer

LIUS has been theoretically proposed to mainly cytodisrupt cancer cells by selectively resonating the right diameter cells under the name of *oncotripsy* [71]. Furthermore, the viscoelasticity of the microenvironment was theoretically proposed to reduce the natural frequencies of cells, which increases the time to lysis [72].

On the experimental side, LIUS has been associated with an increase in apoptotic human cancer cells; see Table 2.3 for a detailed setup of experiments. In particular, researchers found that the cytoskeleton is disrupted after sonification. Cytodisruption is highly dependent on frequency, cell type, and pulse duration, increasing with a longer pulse duration (PD) despite the same total energy applied [74, 70].

In this line, US stimulation in a continuous waveform at lower intensities can generate mechanical stimulation similar to that in a pulsed form at higher intensity [75]. In addition, standing waves, reflection, and cavitation are mechanistically necessary for cytodisruption [70, 75], while high stiffness or viscosity of the medium significantly affects the propagation of waves [70], promoting patternings in growth as a result of the distribution of field

stress [73]. Remarkably, LIUS has also significantly reduced the ability to induce osteoclastic differentiation [76], suggesting a possible effective treatment of bone metastasis.

In addition to the cytodisruption mechanism of oncotripsy, LIUS has been shown experimentally to affect proliferation via mechanotransduction. Although the detailed mechanisms of the inhibitions pathways are not yet clear and the number of experiments is quite low, novel reports investigate LIUS mechanotransduction pathways proposing that LIUS promotes Piezo-1 activation that allows calcium entry upstream [80, 79].

Regarding migration, in recent studies, [78, 77] found that LIUS inhibits the collective migration of cancer cells, specifically pancreatic tumor cells, in wound healing processes while fibroblasts are not selectively inhibited. Results showed a collective response to the acoustic performance, with more prominent effects on non-starved cells.

These studies are proof-of-concept for the physical effects of ultrasound stimulation on tumor cell growth and migration, demonstrating significant therapeutic potential. However, the mechanism of action and the varying responses triggered by different frequencies, energies, and configurations are not fully understood, so the further biological study is ongoing to understand the underlying mechanisms. The current state of LIUS research is costly and time-consuming due to the need for empirical experimentation.

In order to fully understand the mechanism of LIUS and optimize its therapeutic potential, mathematical modeling can be utilized to simulate the complex interactions between the ultrasound waves and the tumor microenvironment, and in combination with other treatments. Ultrasound-tumor interaction models can provide valuable insights into the underlying mechanisms of LIUS and aid in the development of more effective treatment strategies. In the long term, these models could be combined with relevant patient information to create customized treatment plans that optimize the effectiveness of LIUS for each individual patient [89, 91, 90].

Recent advancements in the field have revealed not only the potential of ultrasound but also shear waves as a promising therapeutic option, following mechanotransduction principles. Our research group and the group led by Ralph Sinkus at King's College London have made significant strides in this area [361, 362, 363], demonstrating the effectiveness of shear wave therapy in cancer.

As highlighted in Figure 2.6, shear waves operate at lower frequency ranges than ultrasound, allowing mechanotransduction while minimizing the pos-

Table 2.3
Main setups in LIUS therapy in vitro. The relation between intensity and acoustic pressure has been established. The notation [−] is used when there is no information.

Cell line	Frequency [MHz]	Intensity [mW/cm^2]	Acoustic pressure [MPa]	Setup and Comments	Bioeffects[a]	N	Source
CT-26, K562, U937, T cell (in suspension)	0.3-0.67	$< 9.7 \cdot 10^4$	<1.2	TUS= 2 min/day for 2 days. PD=2-40ms. DC= 10%. Requires standing waves and reflection for cavitation. Selective growth inhibition	Cytodisruption	3-9	[70]
T47D, MCF-12A (monolayers)	1.5	10,30, 50,100	0.012, 0.021, 0.027, 0.039	TUS=10min/day for 3 days. PD = 200μs. DC= 20%. Decreasing proliferation with increasing intensity, PD, and DC. Selective growth inhibition	Mechanotransduction	1	[75]
HT29, Caco2	0.65-4.5	$87.4 - 6.7 \cdot 10^4$	0.036-1	TUS= 10min/day for 1 day. PD= 30s. DC= 25% Inhibition of growth with intensity and frequency	Mechanotransduction - Cytodisruption	2	[74]
MDA-MB-231, Raw264.7	1.5	30	0.021	TUS=20min/day for 10 days. PD = 200μ. DC= 20% Viability is not affected. Reduction of osteoclastic differentiation	Mechanotransduction	3	[76]
A375, A549, Hela, Hacat	0.67	254	0.061	TUS = 2min for 2 days, PD=30ms, DC= 10%. Importance of stress field distribution. Selective growth inhibition	Mechanotransduction - Cytodisruption	[−]	[73]
MDA-MB-231, A375P, HT180 (in suspension on matrigel, in vivo in CAM models, organoids)	0.33	7.7	0.011	TUS= 2h/day for 3 days. PD = [−]. DC= 50%. Growth inhibition	Mechanotransduction: Piezo1 channel	2-3	[80]
MDA-MB-231, MCF10A (monolayers in matrigel)	0.33	7.7	0.011	TUS= 2h/day for 3 days. PD = [−]. DC= 50%. Growth inhibition	Mechanotransduction: Piezo1 channel	4	[79]
PANC-1 (monolayers)	1	< 100	0.038	TUS= 10-20-30min. DC= 100%. Migration inhibition	Mechanotransduction	4	[78, 77]

[a]We use the term mechanotransduction if there is no mechanical cavitation and cytodisruption if there is, although in some studies there is not clear and combined effect could coexist.

sible cytodisruption and resonance of cells caused by ultrasound at more higher frequencies and intensities [71, 72]. Moreover, as LIUS, SW avoids the indiscriminate ablation of cells produced by HIFU. Regarding another oscillatory shear stress, it can be noted the use of shear stress through perfused interstitial fluid pulses [364]. The shear stresses could be generated indirectly from LIUS by multiscale interactions and mode conversions such as acoustic radiation force, microstreaming, or cavitation jetting.

This thesis is focused on the use of ultrasound, but the successful efforts in utilizing shear waves as a therapy demonstrate the importance of continuing to explore and develop new techniques in the field of mechanotherapy. The ability to harness the power of these mechanical waves opens up new possibilities

for the treatment of a variety of conditions, and further research in this area holds great potential for improving patient outcomes.

With that in mind, in the following section, we present different models used in literature to model wave propagation in soft tissues, with approaches for both shear and longitudinal waves.

2.3.2 Wave propagation modeling in tumors

The propagation of waves in tumors is modeled using the basic equations that govern the continuum: compatibility, dynamic balance momentum, and constitutive equation. Due to the intrinsic behavior of each tissue, as well as in growth, different models arise to evaluate the tumor response. In soft tissue wave propagation, it is usually assumed small displacements and null mass transport in propagation.

Viscoelastic propagation models take into account the solid elastic phase and the associated viscosity and are commonly used in the field of medical imaging for the evaluation of soft tissues.

The most widely used viscoelastic propagation models in soft tissues are the Maxwell and Kelvin-Voigt constitutive equations, although more viscoelastic models exist [365, 366, 367, 368]. The Maxwell model represents a material as a combination of a spring and a dashpot in series, while the Kelvin-Voigt model represents a material as a combination of a spring and a dashpot in parallel. The spring represents the elastic behavior of the material, while the dashpot represents the viscous behavior.

The Voigt model is more accurate in predicting creep than the Maxwell model as it predicts a constant strain in the long term, while the Maxwell model predicts linear strain-time behavior. Therefore, to study how the material behaves while the wave propagates through it, it is accurate to assume that the Kelvin-Voigt can be a reliable approximation. The equations that govern wave propagation are:

$$\begin{aligned} \nabla \cdot \boldsymbol{\sigma} + \mathbf{b} &= \rho \frac{\partial^2 \mathbf{u}}{\partial \mathrm{t}^2} \\ \boldsymbol{\sigma} &= \boldsymbol{C^e} \boldsymbol{\varepsilon} + \boldsymbol{C^v} \frac{\partial \boldsymbol{\varepsilon}}{\partial t} \end{aligned} \tag{2.3.3}$$

where the small strain is $\boldsymbol{\varepsilon} = \frac{1}{2}(\nabla \mathbf{u} + \nabla \mathbf{u}^{\mathrm{T}})$, and $\boldsymbol{C^e}$ and $\boldsymbol{C^v}$ are the fourth elastic range tensor and the fourth viscous range tensor, which account for the undrained material properties of the tissue.

The selection of a suitable model for the analysis of wave propagation in

tumors is a critical step that requires careful consideration of various factors, including the specific loading conditions, the mechanical and physical properties of the tumor and surrounding medium, and the geometries involved. In order to obtain accurate results, it is essential to gather the necessary input data through experiments and performs inverse problem analyses, which can inform the choice of the most appropriate model and deepen our understanding of the underlying mechanics.

By utilizing models of wave propagation in tumors, we can analyze and understand the response of tumors to ultrasound waves in terms of mechanical variables such as stress, strain, and displacement. However, it is important to note that these models do not incorporate the effects of ultrasound on biological processes.

In order to understand the impact of ultrasound on tumor dynamics, including the patterns and effects on cell migration and proliferation, new models are needed that couple ultrasound and tumor mechanics. This requires the integration of mathematical equations that accurately capture both the wave propagation and tumor mechanics, rather than treating them as separate phenomena.

2.4 Key points to contribute

Having established the state-of-the-art in the field of mathematical and mechanical oncology, the key starting points from which contributions are made in the following section are summarized:

- Abrupt changes in cell growth can impact and compete with mechanics and migration patterns. Biologically, the focus is on understanding the potential formation of these patterns, while mathematically and computationally, there is a lack of models that analyze controlled migration together with non-homogeneous growth from Continuum.
- Cancer stem cells have been found to be resistant to conventional therapies, so there is a clear need for new treatments to overcome this challenge.
- Low-Intensity Ultrasound is highlighted in recent years as a potential target mechanotherapy that could be combined with conventional therapies to improve treatment efficacy.
- There is currently a lack of models that integrate Low-Intensity Ultrasound with tumor dynamics.

Part II

CONTRIBUTIONS

Chapter 3

Controlled propagation flux and non-homogeneous growth

3.1 Introduction

Cells sense their environment and adapt their growth and reorganization to the adjacent cells, in terms of division –hyperplasia– , cell enlargement – hypertrophy, cell motility – migration –, and ECM reorganization.

The development and maintenance of tissues and organs heavily rely on migration and growth processes, which require a reorganization of cellular distribution and often result in significant morphological changes, such as in the case of epithelial-mesenchymal transition [369]. These changes can impact remodeling and stress levels, leading to alterations in intracellular and extracellular pressure that affect both the biomechanical and biochemical properties of the cell and its surrounding environment.

Under these conditions, Shraiman introduced a theoretical mechanical feedback mechanism that modulates growth, disrupting the state of balance between proliferation and apoptosis. This approach postulates that even in homogeneous mechanical environments, cells can undergo mutations that result in differences in their proliferation and growth rates relative to the surrounding tissue, leading to cellular competition and mechanical stresses. As a result, each cell can assess its own proliferation and growth rate relative to the microenvironment and adjust its growth accordingly [55, 57].

In Part I of this dissertation, the phenomenon of growth-induced stress – i.e. the stress produced by cells during growth – was presented. If the growth process is non-homogeneous, it can be accurately postulated that heterogeneous stress is a consequence of the non-uniform growth of the tissue.

In the presence of uniform growth rate and free boundary conditions, tissue elasticity responds by adjusting tissue strain growth through uniform

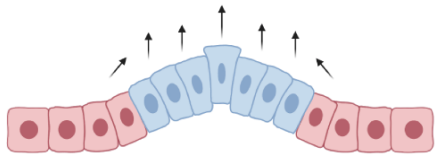

(a) Cluster of cells growing faster than its surroundings could cause the loss of cell–cell adhesion.

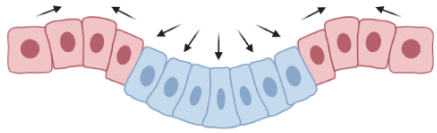

(b) Rearrangement of growth and pressure affects both mutant cluster cells and adjacent cells.

Figure 3.1: Heterogeneous cluster growth.

dilatation, without introducing additional stresses. However, with non-homogeneous growth, clusters of cells may experience slower or faster growth rates compared to their surrounding cells, resulting in strain or compression within the cluster or its surrounding tissue. The extent of this strain depends on the stress level, and cells may lose their adhesion and become disaggregated from the tissue as shown in Figure 3.1(a), or potentially causing buckling in adjacent cells as well, as ilustrated in Figure 3.1(b).

Cytonemes, which are membrane nanotubes, not only mediate cellular communication but also sense mechanical stimuli from neighboring cells, as many studies have shown [370, 371, 372, 373, 374, 170]. Therefore, cells can perceive pressure and growth from surrounding cells differently, depending on their intercellular connections. Typically, cytonemes have a range of approximately 3-7 cell units, which equates to around 60μm [374]. Cytoneme-cytoneme or cytoneme-membrane interactions facilitate cell-to-cell communication, as depicted in Figure 3.2.

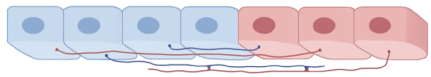

Figure 3.2: Cytonemes mechanosensing. Outline of the cytoneme–cytoneme or cytoneme–membrane interactions of the adjacent cells, which are assumed to be spatially consistent with the mechanical transmissions due to growth and internal regulation of pressure.

However, the situation changes when motion is introduced to the growth-stress process. If cells are able to move within the tissue, the non-uniform stress induced by heterogeneous growth may be partially alleviated and reorganized. Consequently, the drive toward homeostasis may not be prevalent throughout the entire tissue.

The migration of collective cells is propelled by traction forces produced by some cells located behind the propagation front [56]. These forces exert a localized impact on the environment and communicate with adjacent cells through both biochemical and biomechanical signaling pathways that interact and modify gradients.

As pointed out in Section 2.2.2, the diffusion term of continuum equations has been widely modeled as linear and isotropic, despite migration being a controlled speed process in which a propagation front appears. To overcome this drawback, some studies suggest adding a relaxation term that limits the infinite propagation speed characteristic of linear diffusion using relaxation terms [375]. In contrast, others define a finite-speed tumor propagation front through the porous medium equation (PME)[1] [306], and its limitation through second-order terms by Brinkman's law [376]. References [307, 308, 309, 310, 311, 312] use a flux-saturated PME with measurable propagation speed.

Flux-saturated models are essentially equations in divergence form so that their flux saturates at a constant value as long as the size of the gradients is large enough. These models frequently appear in some areas of mathematical physics (radioactive transport theory and astrophysics, for example) and are gaining relevance in mathematical biology (morphogenesis and tumor dynamics). This flux model allows us to combine both the diffusion of porous media and flux-saturated mechanisms to obtain a deeper understanding of each of them and their mutual interaction that opens the possibility of new emerging behaviors.

The main advantage of including the effects of saturated flow compared to PME is that saturated flow terms introduce a new biological parameter: the speed of the tumor propagation front, which enables to control and regulate the profile of tumor progression both from a qualitative point of view defining the characteristics of the front and quantitatively since the speed of the tumor can be regulated from experimental data. [311].

This limited speed also affects the evolution of the rest of the terms involved

[1]The Porous Medium Equation owes its name to its use in describing the flow of an ideal gas in a homogeneous porous medium. In biology, PME refers to a non-linear cell flux that accounts for a finite propagation.

in the process: growth and stress. Then, the strength of this Chapter lies in joining some of the most relevant items of the current oncological models: controlling the tumor propagation front [153, 377] and including the role of non-homogeneous growth in mechanics [319, 54, 378, 55, 82].

In particular, we focus on how abrupt changes in tumor cell density leads to a competition of non-homogeneous growth and its driven-stress, proliferation, and migration.

3.2 Mathematical model

We follow the principles of Finite Growth theory and its simplification into small strains, where strains are additive, as explained in Section 2.2.2. We rewrite the Neo-Hookean elastic strain energy function described in Table 2.1 in terms of bulk K and shear modulus μ, considering small strains and growth. Then:

$$W = \int \left(\mu\Big(\boldsymbol{\varepsilon} - \frac{1}{3}tr(\boldsymbol{\varepsilon})\mathbf{I}\Big)^2 + \frac{K}{2}\Big(tr(\boldsymbol{\varepsilon})\mathbf{I} - \boldsymbol{\varepsilon}_g\Big)^2\right)dx. \tag{3.2.1}$$

The first term on the right represents pure shear, and the second term is the bulk compression affected by the volumetric strain growth of the tissue. The growth strain is described now as non-homogeneous:

$$\boldsymbol{\varepsilon}_g = \int_0^t (g - \langle g\rangle)\boldsymbol{\gamma}\, ds, \tag{3.2.2}$$

where $\boldsymbol{\gamma}$ is the tensor that distributes the growth in different directions. In this study, we have assumed isotropic or volumetric growth, so $\boldsymbol{\gamma} = 1/3\mathbf{I}$ results to be driven by the hydrostatic pressure.

The growth stretch function is defined by $g = \alpha_n n$, where n is the cell density and α_n is the coupling factor that accounts for the volume or mass gain ratio. The local average growth rate is $\langle g\rangle(x,t)$. We have applied the theory of cell communication to model the local interaction of growth and its influence on internal homeostatic growth regulation. Then, the average stretch growth is a regular function for each cell, which has support on the range within which cytonemes operate:

$$\langle g\rangle(x,t) = \int_{-\epsilon}^{\epsilon} g(x-y,t)\delta(y)\, dy, \tag{3.2.3}$$

where δ is a regularizing function with compact support on $(-\epsilon,\epsilon)$, being ϵ the cytoneme zone of influence and sensitivity of each cell to its environment. The regularizing function is described by $\delta_\epsilon(x) = \epsilon^{-N}\delta\left(\frac{x}{\epsilon}\right)$, with $\epsilon > 0$ and

δ measurable, positive and bounded function with integral one, supported in the unit ball in $\mathbb{R}^N$.

The governing equation is obtained by deriving strain elastic energy function to strains. Then, the Cauchy elastic stress is:

$$\boldsymbol{\sigma}_e = 2\mu\Big(\boldsymbol{\varepsilon} - \frac{1}{3}\boldsymbol{\varepsilon}\mathbf{I}\Big) + \kappa\Big(\boldsymbol{\varepsilon}\mathbf{I} - \boldsymbol{\varepsilon}_g\Big). \tag{3.2.4}$$

On the other hand, researchers have investigated the mechanisms of cell proliferation by studying the relationship between the number of cells N, time t, and spatial variable x. Cell division is typically modeled using a logistic function that governs the process of cell duplication until the tumor reaches its carrying capacity C, which is defined as the maximum number of cells that can be supported per unit volume. The temporal evolution of the cell population can be described using the following differential equation:

$$\frac{dN}{dt} = NT_n\Big(1 - \frac{N}{C}\Big), \tag{3.2.5}$$

To account for heterogeneous proliferation, the duplication rate has been treated as spatially and temporally dependent, i.e. $T_n(x,t)$.

The number of cells relates to cell density by the relation $n(x,t) = NV^{-1}$. Then, deriving equation 3.2.5 considering this relationship, and including migration, the conservation of mass in terms of cell density that responds to an abrupt change in cell density is governed by:

$$\frac{dn}{dt} + n\frac{\partial V}{\partial t}V^{-1} = \nabla\cdot\boldsymbol{\mathcal{J}} + T_n n\Big(1 - \frac{nV}{C}\Big). \tag{3.2.6}$$

In this chapter, we propose an alternative method to address the problem of solving the entire system of equations of mechanics and tumor dynamics. Instead, we seek to determine the precise volumetric elastic strain at which momentum balance is achieved. Following the approach introduced in previous studies [55, 57], we minimize the strain energy function – equation (3.2.1) – with respect to the displacement vector to ensure that the energy balance is satisfied, and subsequently, to meet two additional conditions: that the divergence of the stress tensor is zero and that the small strain compatibility equation is fulfilled. This strategy enable us to establish a direct and rigorous relationship between the elastic strain and the evolution of cell density.

In the minimization of the functional, boundary conditions must be included. These conditions lead to the emergence of an additive scalar term $\chi(x)$ as

follows:

$$\frac{\partial tr(\boldsymbol{\varepsilon})}{\partial t} = g - \frac{\mu}{K+\mu}\Big(g - \langle g \rangle\Big) + \chi, \tag{3.2.7}$$

where χ satisfies $\dfrac{\partial^2 \chi_1}{\partial x^2} = 0$. Considering free boundary conditions, then it is deduced that $\chi = 0$. The hydrostatic stress can be easily obtained by $\sigma_h = K\mathrm{tr}(\boldsymbol{\varepsilon}_e)$ or $\sigma_h = 1/3\mathrm{tr}(\boldsymbol{\sigma}_e)$, leading to:

$$\frac{\partial \sigma_h}{\partial t} = -\frac{K\mu}{K+\mu}\Big(g - \langle g \rangle\Big). \tag{3.2.8}$$

Finally, the volumetric strain can be related to volume – V – deformation by:

$$\frac{\partial V}{\partial t} V^{-1} = \frac{\partial tr(\boldsymbol{\varepsilon})}{\partial t} = \nabla \cdot \boldsymbol{v}_n. \tag{3.2.9}$$

Taking into account now the definition of the growth stretch function and described relations 3.2.7 and 3.2.9, we can rewrite the cell density evolution as:

$$\frac{dn}{dt} = \nabla \cdot \boldsymbol{\mathcal{J}} + T_n n\Big(1 - \frac{nV}{C}\Big) - \alpha_n n^2 + \frac{\mu}{K+\mu} n\Big(\alpha_n n - \langle \alpha_n n \rangle\Big). \tag{3.2.10}$$

This equation describes the evolution of cell density, resulting from the interplay between migration, proliferation, and non-homogeneous growth. The term representing non-homogeneous growth, which is derived from mechanical equations, can be interpreted as a retrograde diffusion term that considers non-homogeneous stress-driven growth, as will be discussed in more detail later. The volume gain of cells evolve according to equations 3.2.7 and 3.2.9, impacting the stress state of the cells and vice versa.

We aim to clear control the speed of propagation of the front with the so-called flux-saturated equations. The purpose is to combine two non-linear diffusion mechanisms: porous media and the flux–saturated terms, which results in a saturated flow as long as the gradient size is large enough. The proposed flux is defined by the equation:

$$\boldsymbol{\mathcal{J}} = D_n \frac{n^m \nabla n}{\sqrt{n^2 + \Big(\dfrac{D}{c_n}\Big)^2 |\nabla n|^2}}, \tag{3.2.11}$$

where the coefficient of diffusion for cells is conventionally represented as D_n and is commonly known as viscosity in Helle-Shaw type models. However, in this specific context, the term viscosity will not be employed to prevent any

erroneous association with tissue viscosity. The coefficient m is an empirical parameter related to the propagation and the medium porosity, with $m \geq 1$, and c_n the speed of propagation of the solution support.

The solutions of the flux-saturated equations preserve the migration fronts and provide a qualitative and quantitative fit with the experimental data [309, 170], in the sense of maintaining compactness of the support and the finite speed of propagation. It also preserves the possible discontinuities, allowing the appearance of emerging invasion profiles. This class of concepts has often been used in similar contexts, such as cell communication [170, 379] and morphogenesis processes associated with the equations of Keller–Segel [380, 381].

3.3 Numerical methods

To carry out numerical computations, we have utilized a custom code developed in Matlab (©MathWorks Inc., Natick, MA, USA) based on the method of finite differences.

The requirement for preserving the tumor propagation front and avoiding numerical noise from the saturated flux calls for high approximation orders. To meet this requirement, we utilize the Weighted Non-Oscillatory method (WENO), which aims to achieve high-order accuracy by blending multiple low-order numerical approximations through the use of weights. Smoothness indicators are calculated for each approximation and are then used to determine the weights. The final solution is obtained by taking a combination of the weighted approximations [310, 382, 383, 384, 385]. The WENO method provides accurate high-order stability resolution while maintaining non-oscillatory, stable, and sharp discontinuity transitions. In our implementation, we adapt the fifth-order WENO method [384, 385, 386] with 1000 points to perform spatial discretization. For time domain discretization, we employ the third-order explicit Runge–Kutta method.

We consider a range of parameter values to computationally analyze the different types of patterns caused by the proliferation-migration-growth interaction. For parameter selection, we base on the literature data: (i) growth rate of human colon adenocarcinoma obtained experimentally [387] for a range of α parameter; (ii) dynamics in front of glioblastomas [309] for the diffusion, speed of propagation and carrying capacity, which is defined in 10^6cells; (iii) data of LN229 glioma for mechanical parameters reported by [388], where Elastic Young modulus is considered $E = 1$kPa. Assuming the Poisson coefficient $v \approx 0.45$, the bulk and shear moduli are $K = 3.33$kPa and $\mu = 0.34$kPa. The equations are solved in one dimension.

3.4 Results

3.4.1 Linear, non-linear and non-linear saturated flux

To provide a more robust and grounded analysis of the non-linear propagation models, it is advisable to perform qualitative results that showcase the differences between linear, non-linear, and non-linear saturated fluxes. These demonstrations will help highlight the strengths and unique features of each model and provide a clearer understanding of the mechanisms at play.

Then, we define the linear flux as $\boldsymbol{\mathcal{J}} = D_n \nabla n$, where D_n is the linear diffusion coefficient of cells. The non-linear flux is described by the equation $\boldsymbol{\mathcal{J}} = D_n n^m \nabla n$, in which the non-linear relationship between the flux and cell density is established and more complex interactions between cells and their environment can be captured. Finally, the non-linear saturated flux is described by equation (3.2.11). This model takes into account both the non-linear relationship between the flux and cell density and the effect of saturation on the flux.

To analyze the propagation of the different cell fluxes, we perform simulations from three different initial conditions, namely the step function, the triple step function and the sigmoid function. These initial conditions are selected as they provide a diverse range of mathematical profiles, each with unique characteristics and behaviors.

The two first functions are useful for capturing sudden transitions in cell density and are represented mathematically as a piecewise function. In particular, the step function represents a sudden and sharp change in cell density, where the value of cell density is constant in one region and abruptly changes to a different constant value in another region, which could occur under mutations. For instance, mutations in genes that regulate the cell cycle, such as tumor suppressor genes or oncogenes, can result in selective uncontrolled cell growth and proliferation, which suddenly begin to grow at a much faster rate than normal tumor cells, leading to sudden transitions.

The triple step function contains three discontinuities in its graph. These jumps result in rapid changes in the values of the function at specific points, which can be used to model rapid changes in a quantity over time, not only in the borders but also in the inner regions.

On the other hand, the sigmoid function models a gradual and smooth change in cell density over time, with a characteristic S-shaped curve. This function is useful for modeling biological processes where growth occurs in a smooth and continuous manner without sharp discontinuities.

As shown in Figure 3.3, linear flux completely breaks down the propagation front for the three initial conditions, with the most notable being piecewise functions, where the discontinuity and the front are completely lost. The most important difference between non-linear and saturated non-linear flux lies in the verticality of the propagation front, which is maintained in the saturated flux and lost in the non-linear.

Focusing on the saturated flow, the parameter m holds a significant importance in characterizing the non-linear diffusion dynamics of the system. The value of m has an impact on the speed of the propagation front, with $m = 1$ indicating a finite propagation speed that is bounded by the c_n veloctity. When m exceeds 1, the velocity of the front is limited and partially suppressed, resulting in a decrease in speed while maintaining stability independently of the initial condition (see Figure 3.4).

Therefore, solutions of the flux-saturated equations can maintain the features of the initial data, including the compactness of its support and the presence of potential jump discontinuities. This results in the formation of steep invasion profiles characterized by a sudden increase in cell density, which are essential for a comprehensive understanding of tumor cell behavior when non-homogeneous growth occurs.

Steep invasion profiles can manifest in a variety of biological processes beyond invasive cancers. For instance, during immune responses, T cells and macrophages infiltrating tissues to combat infections or injuries can lead to such profiles. Similarly, embryonic development entails cell migration and proliferation, often resulting in steep invasion profiles, especially at the interfaces between different tissue types. Lastly, wound healing involves the migration of cells to the wound site, causing steep invasion profiles and an abrupt rise in cell density in the vicinity of the injury.

3.4.2 Proliferation and non-homogeneous growth

In this subsection, we analyze the behavior of cell density in the absence of migration, as represented by $\boldsymbol{\mathcal{J}} = 0$ in equation (3.2.10). Assuming constant parameters α_n and T_n, we found that the effect of parameter α_n slows the evolution of cell density compared to classical logistic growth, where $\alpha_n = 0$ (see Figure 3.5(a)).

However, the cells located in front regions are impacted by stress-driven growth discrepancies arising from the absence of neighboring cells, leading to a rise in cell density at the corners over time, as shown in Figure 3.5(a). When volume rate acquisition surpasses a critical threshold, defined as $\alpha_n \geq 1 \cdot 10^{-1}$ mm^2 cell^{-1} h^{-1}, the system is unable to mitigate the non-

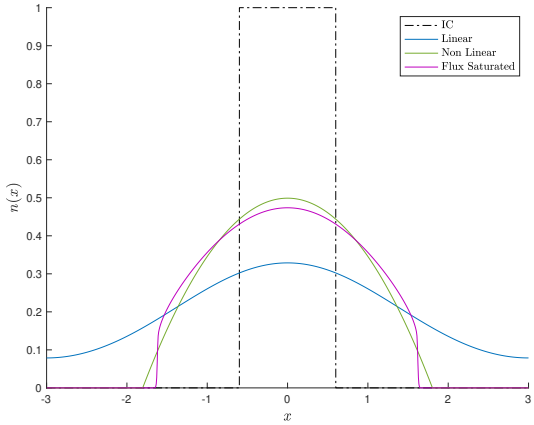

(a) Cell density evolution in step function

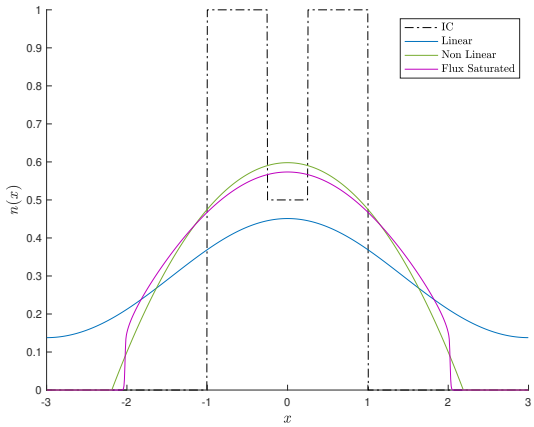

(b) Cell density evolution in triple step function

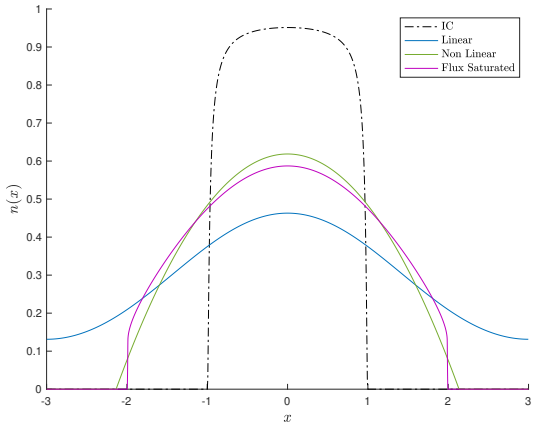

(c) Cell density evolution in sigmoid function

Figure 3.3: Cell density evolution from different initial conditions and fluxes. Simulations performed at time t=11 days, with $D = 1$ $\mathrm{mm^2 h^{-1}}$, $c_n = 1$ $\mathrm{ms^{-1}}$ and $m = 1$.

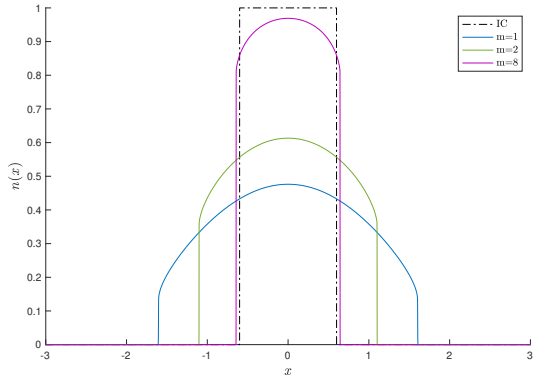

(a) Cell density evolution in triple step function

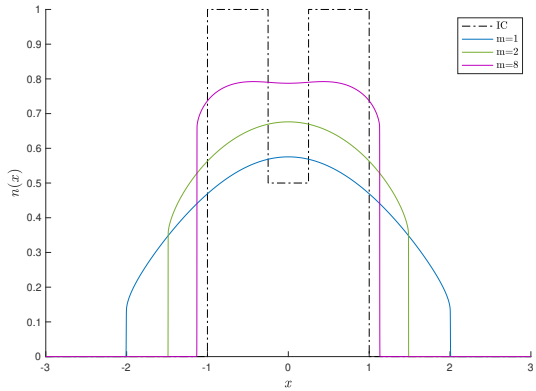

(b) Cell density evolution in sigmoid function

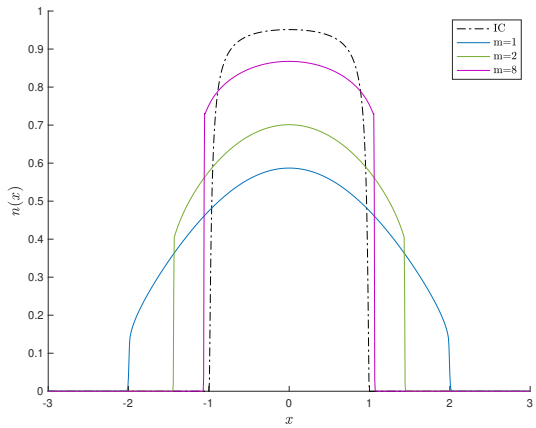

(c) Cell density evolution in sigmoid function

Figure 3.4: Cell density evolution for flux-saturated equation from different initial conditions and m parameter, varying between 1,2 and 8.

homogeneous growth, leading to a concentration of density at zones where the growth stress changes abruptly.

The aggregation of cells in response to non-homogeneous growth differences is a result of the retrograde diffusion process governing the dynamics of cell density, which becomes more pronounced with growth, leading to an increase in concentration over time. The cell density remains bounded for each value of α_n, in agreement with previous studies [58]. This phenomenon can be observed at jump zones or at the corners of the domain (see Figure 3.5(b)), and its underlying mechanism is the homeostatic adjustment of non-homogeneous stress and proliferation.

The study also explores heterogeneous growth scenarios that may occur when a group of cells grows at a different rate than the surrounding cells, as shown in Figure 3.6(a) and Figure 3.6(b). In these scenarios, stress-driven growth varies and is manifested as higher or lower α_n values in the core region

Instabilities in cell density also emerge and the proposed dynamic is inadequate to mitigate their impact. Over time, these instabilities escalate to reach a maximum value that is limited by the carrying capacity. This can only be alleviated through the implementation of a migration process that can diffuse the cell concentration or density instabilities, which will be explored in the subsequent section.

To establish the reliability of the observed cell density fluctuations, we compare them with solutions obtained from higher discretizations, including those with a finer resolution than the fluctuations under consideration. This comparison eliminates the impact of numerical errors. It is worth noting that we do not normalize the results with respect to the carrying capacity, which is the product of density and volume. Therefore, changes in carrying capacity may arise from alterations in both density and volume.

3.4.3 Saturated flux, proliferation and non-homogeneous growth

In this susection, we evaluate the performance of the complete cell flux model incorporating the flux-saturated dispersion term. This term regulates the effects of non-uniform cell growth on the density of the cell population. Our results show that the speed of the tumor front is largely independent of the value of the parameter α_n, as demonstrated in Figure 3.7(a), which compares the speed of the front for different values of α_n.

However, we observe significant qualitative differences in the evolution of the tumor front as a result of non-uniform growth. These differences are reflected in the tendency to lose the convex shape of the tumor density, as seen in

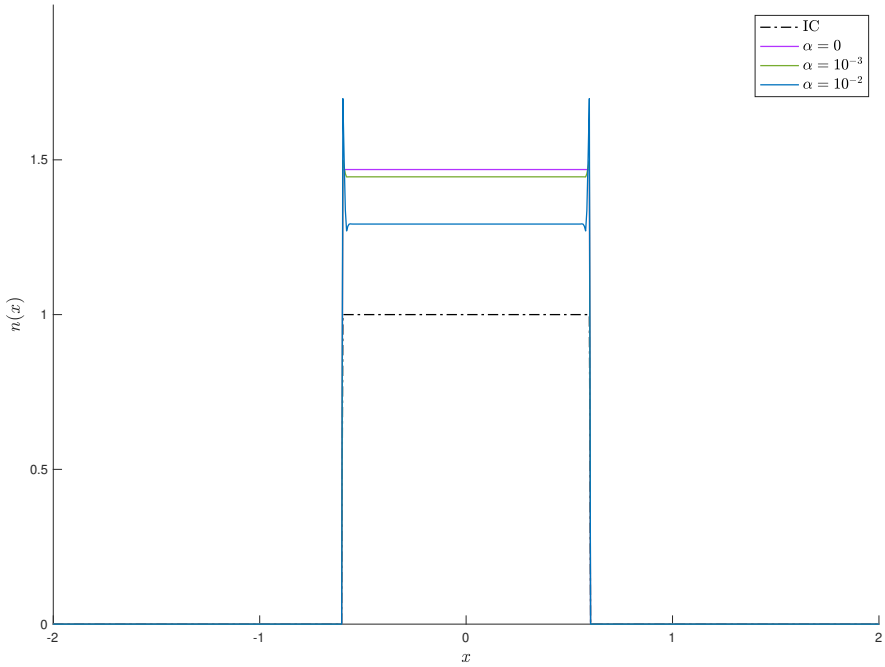

(a) Non-homogeneous growth leads to abrupt changes in cell density, which do not occur if $\alpha_n = 0$, t = 11.25days.

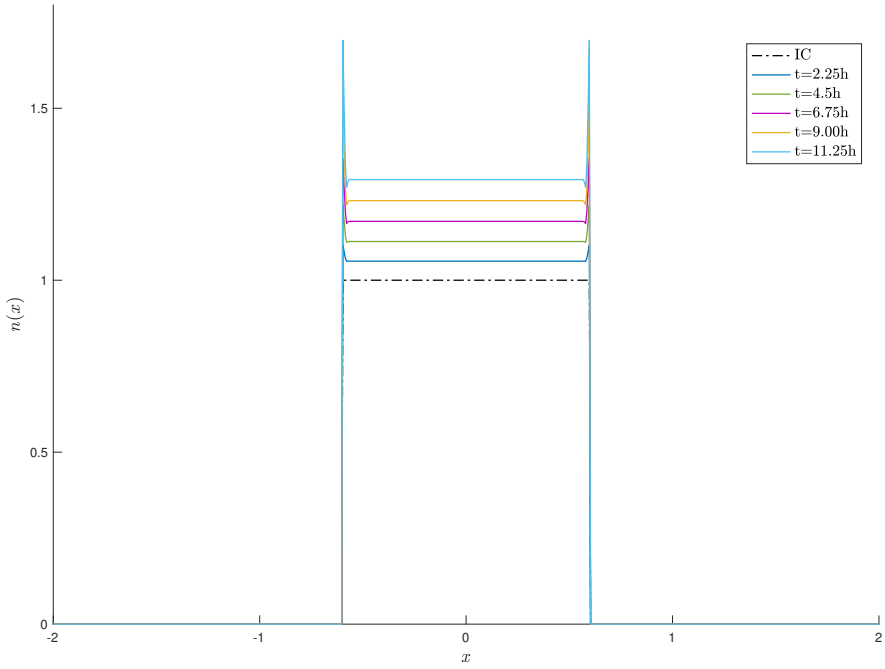

(b) Increase of cell density differences with time, with $\alpha_n = 1 \cdot 10^{-2}\text{mm}^2\text{cell}^{-1}\text{h}^{-1}$.

Figure 3.5: Cell density evolution in sharp discontinuities. Proliferation parameter $T_n = 3.45 \cdot 10^{-2}\text{h}^{-1}$ and $\mathcal{J} = 0$.

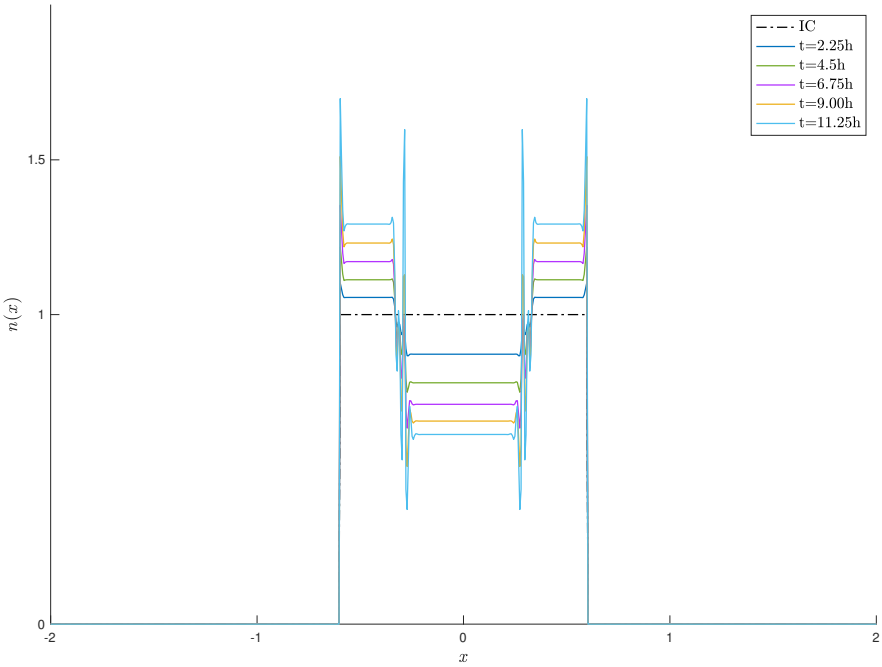

(a) Cluster of cells growing slower than its surroundings. Parameter $\alpha_n = 1 \cdot 10^{-1}\text{mm}^2\text{cell}^{-1}\text{h}^{-1}$ in the core and $\alpha_n = 1 \cdot 10^{-2}\text{mm}^2\text{cell}^{-1}\text{h}^{-1}$ in inner region.

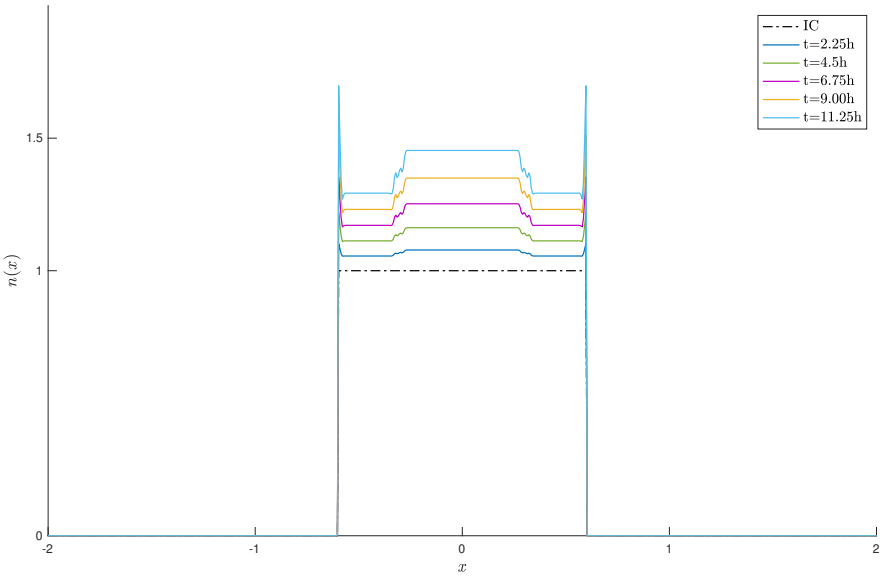

(b) Cluster of cells growing faster than its surroundings. Parameter $\alpha_n = 1 \cdot 10^{-3}\text{mm}^2\text{cell}^{-1}\text{h}^{-1}$ and $\alpha_n = 1 \cdot 10^{-2}\text{mm}^2\text{cell}^{-1}\text{h}^{-1}$ in the core and the inner region.

Figure 3.6: Heterogeneous cell density evolution. Proliferation parameter $T_n = 3.45 \cdot 10^{-2}\text{h}^{-1}$ and $\boldsymbol{\mathcal{J}} = 0$.

Figures 3.7(a) and 3.8, particularly when growth differences are substantial.

Our findings also suggest that cell migration regulates the stress differences caused by cells growing slower than their surroundings for $m = 1$, which was not observed in the absence of flux, as reported in Figure 3.5. The results indicate that mechanical feedback leads to an equilibrium state of the cell cluster, identified as a quiescent state regulated by internal pressure and local growth (see Figure 3.7(b)).

Interestingly, if the proliferation rate T_n decreases over time – at t = 30h and t = 50h –, the mechanism is delayed, leading to the asymptotic achievement of the local homeostatic state, as shown in Figure 3.8(a). Conversely, the effect becomes reversible if the parameters of non-uniform growth and/or proliferation are modified in the cell group. For example, if growth differences decrease or local proliferation increases, the cell density in the mutated zone tends to converge with the rest of the tumor, even if the difference in parameters is substantial (see Figure 3.8(b)), consistent with the biological characteristics of the quiescent state [155].

Furthermore, this model suggests that when non-homogeneous growth is not taken into account, excessive proliferation can cause a sudden increase in density evolution, as the tumor's support system cannot keep up with its internal growth rate. This was demonstrated in the case study of traveling waves associated with flux saturation [307]. Extreme values of proliferation or non-homogeneous growth could also result in the loss of damping of density instabilities, or even the emergence of new discontinuities, as seen in Figures 3.7 and 3.8.

3.4.3.1 Role of m parameter

The parameter m has been shown to be a crucial factor in regulating the progression of the tumor front, its shape, and the distribution of cell density. As we have observed, increasing the value of m may lead to keep growth instabilities and density fluctuations within the tumor (Figure 3.9) when $m \geq 2$.

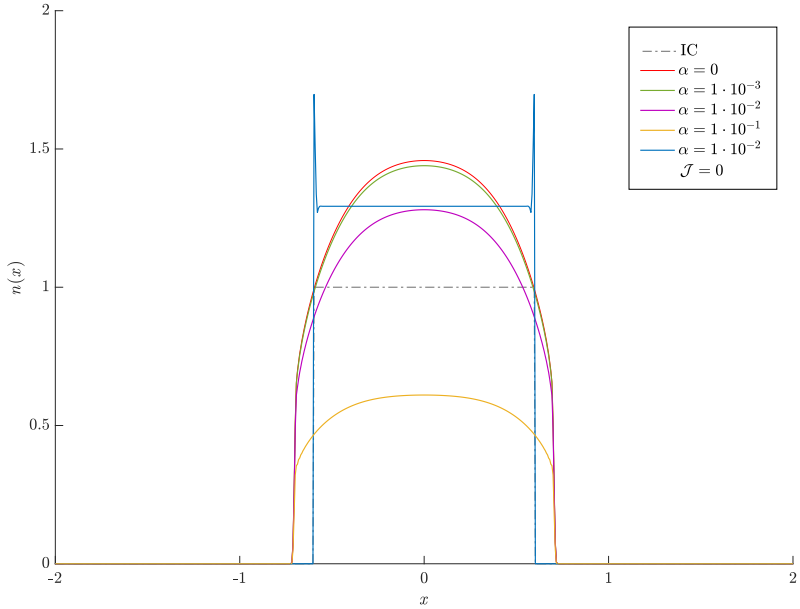

(a) Effect of constant α_n parameter on proliferation and migration at time t = 11.25h.

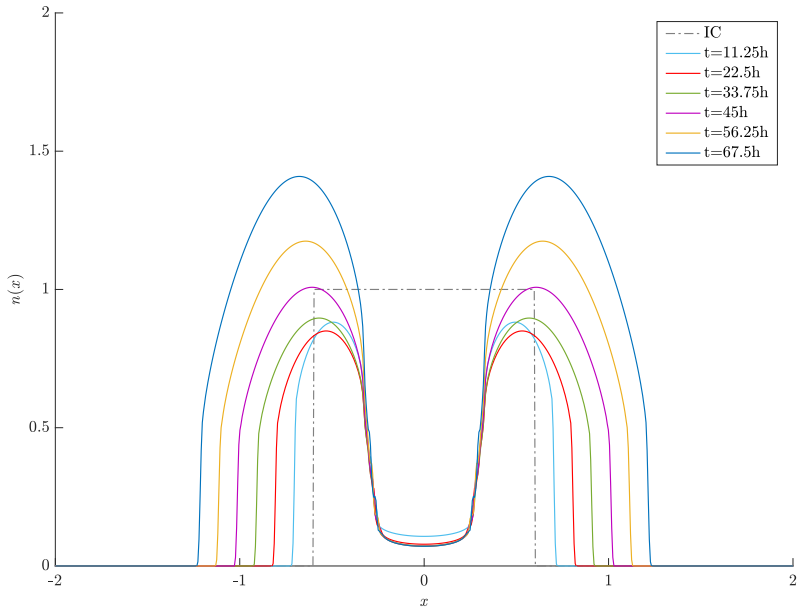

(b) Cluster of cells with high parameter α_n in the core (α_n=$1 \cdot 10^{-2}$mm^{2}cell^{-1}h^{-1}) than its surroundings (α_n=$1 \cdot 10^{-3}$mm^{2}cell^{-1}h^{-1}).

Figure 3.7: Cell density evolution considering flux-saturated migration, non-homogeneous growth and proliferation. Parameters: $T_n = 3.45 \cdot 10^{-2}\text{h}^{-1}$, $D = 0.348 \cdot 10^{-2}\text{mm}^2\text{h}^{-1}$, $c_n = 0.87 \cdot 10^{-2}$ and $m = 1$.

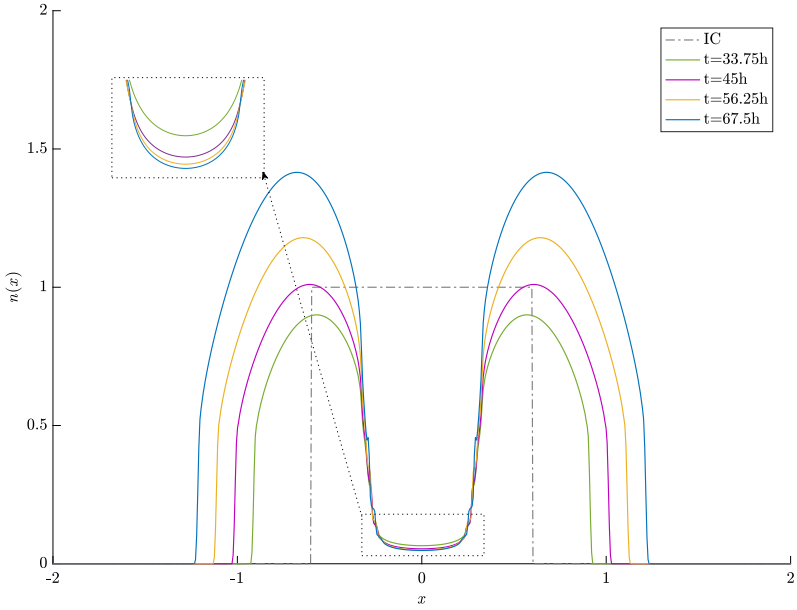

(a) Heterogeneous proliferation rate is considered in space at time, with α_n parameters of Figure 3.7(b). In the inner regions, and at time t = 30h, $T_n = 3.45 \cdot 10^{-3} \mathrm{h}^{-1}$. At t = 50h, proliferation is totally inhibited, $T_n = 0 \mathrm{h}^{-1}$. In the corner regions, $T_n = 3.45 \cdot 10^{-2} \mathrm{h}^{-1}$.

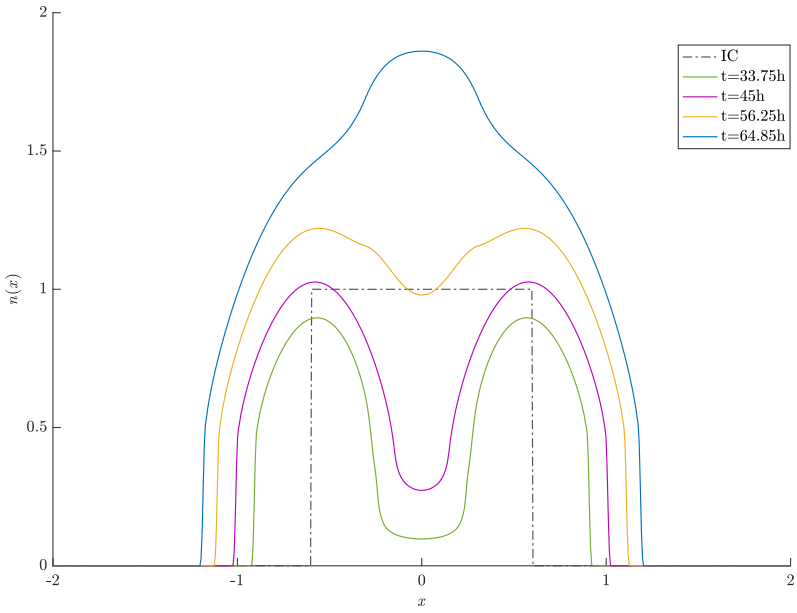

(b) Non-homogeneous stress is relieved at time t = 30h, where $\alpha_n = 1 \cdot 10^{-3} \mathrm{mm}^2 \mathrm{cell}^{-1} \mathrm{h}^{-1}$ and $T_n = 3.45 \cdot 10^{-2} \mathrm{h}^{-1}$. At t = 50 h, tendency of α_n and T_n changes: $\alpha_n = 1 \cdot 10^{-3} \mathrm{mm}^2 \mathrm{cell}^{-1} \mathrm{h}^{-1}$, $T_n = 6.9 \cdot 10^{-2}$ h^{-1} and $\alpha_n = 5 \cdot 10^{-3} \mathrm{mm}^2 \mathrm{cell}^{-1} \mathrm{h}^{-1}$, $T_n = 3.45 \cdot 10^{-2}$ h^{-1} for the core and inner region, respectively.

Figure 3.8: Cell density evolution considering flux-saturated migration, non-homogeneous growth and heterogeneous proliferation. Parameters: $D = 0.348 \cdot 10^{-2} \mathrm{mm}^2 \mathrm{h}^{-1}$, $c_n = 0.87 \cdot 10^{-2}$ and $m = 1$.

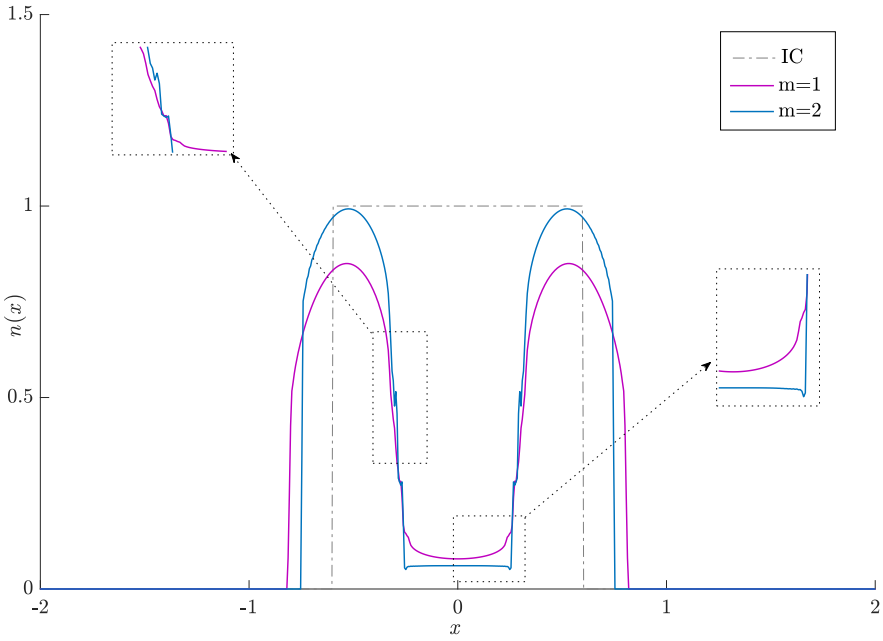

Figure 3.9: Cell density evolution considering flux-saturated migration, non-homogeneous growth and proliferation, with different m parameter. Simulations at time t = 22.5h.

Moreover, it is conceivable to alleviate these instabilities by elevating the velocity of tumor expansion, denoted by c_n, as opposed to enhancing the diffusion coefficient, referred to as D_n. Nonetheless, it is essential to acknowledge that achieving such enhancement may not be practical based on experimental evidence, as reported by reference [309]. Specifically, when the value of the growth exponent m surpasses unity ($m > 1$), there may be a requirement for an increased pace of tumor propagation to mitigate the internal growth instabilities.

3.5 Conclusions

In this study, we investigated the role of non-homogeneous growth, proliferation, and migration in regulating the reorganization of tumor cell density during its evolution.

The selection of the cell flux model is contingent upon the level of detail desired in the analysis. The linear Darcy flux is straightforward in implementation and analysis but may not sufficiently capture the intricate interactions between

cells and their surroundings. On the other hand, the non-linear flux provides a more complete representation of these interactions but may overlook the saturation's influence, i.e. it restricts infinite propagation but cannot regulate the speed of propagation.

In contrast, the non-linear saturated flux offers the most in-depth comprehension of the interactions and effectively accounts for the effect of saturation on the flux, controlling migration dynamics and allowing for instabilities, when $m \geq 1$. Hence, the saturated flow was deemed appropriate for this study. However, in cases where instabilities due to non-uniform growth are not a concern, it can be simplified to non-linear flow to reduce computational complexity and cost.

The results of our investigation demonstrate that growth-induced stress generates a dual effect of aggregation and homeostasis, playing a crucial role in regulating growth and motility.

Through numerical simulations, we demonstrate that differences in growth can lead to a decrease in proliferation. Our analysis shows that, in the absence of migration, growth mechanisms combined with non-homogeneous stress can result in significant oscillations in cell density, which are bounded by the rates of proliferation, stress-driven growth, and the carrying capacity of the logistic model.

This study investigates how non-homogeneous growth affects the migration process. The results suggest that this process can counteract retrograde diffusion oscillations resulting from proliferation and non-homogeneous stress-driven growth. Our findings emphasize the competition between retrograde diffusion and non-linear diffusion through flux saturation in porous media.

Moreover, the proposed system could replicate many evolutionary patterns seen in experiments, making it a useful tool for future research. From a mathematical modeling perspective, introducing non-homogeneous growth terms cause cell density discontinuities that alter the convexification tendency of flux-saturated processes.

Our proposed system could accurately reproduce observed evolutionary patterns in experiments, which makes it a valuable tool for further research. In summary, our study underscores the importance of considering non-homogeneous growth, proliferation, and migration as competitors in the regulation of tumor cell density reorganization

Chapter 4

Ultrasound propagation in tumor spheroid

4.1 Introduction

Ultrasound propagation through biological tissue is a complex process that is influenced by a variety of biomechanical factors. In this chapter, we focus on simulating ultrasound propagation through an in vitro tumor spheroid, with a particular emphasis on the effect of viscoelasticity.

Our proposal is to employ low-intensity ultrasound (LIUS) at high frequencies, utilizing lower acoustic pressures to prevent cavitation. Previous studies have indicated that cells are able to perceive and respond to static pressures as low as 5-10kPa [154, 151, 155], while numerical studies suggest even low values of 1kPa [330, 84, 304]. These findings suggest that cells possess the ability to sense and convert even lower dynamic pressures into chemical and biological signals, without the risk of cytodisruption. By utilizing LIUS at high frequencies with lower acoustic pressures, we can leverage this mechanosensing capability to potentially achieve therapeutic effects without causing cavitation to cells.

The concept behind this approach is based on the hypothesis that static stress necessitates more intensity to evoke a response, due to the dissipation of stress, while dynamic pressure does not have sufficient time to dissipate. For instance, in static rheology, when a material is subjected to a constant force and reaches a steady state, the redistribution of stresses can cause mechanoreceptors to sense a fraction of the transient stresses.

The mechanisms involved in stress redistribution are intricate and may include multiple factors. One of these factors is the cytoskeleton, which provides structural support to cells and plays a critical role in distributing mechanical loads within the cell. Another factor is the viscosity of the solid phases of the material, as well as the dissipation of stresses through the flow of interstitial fluid through pores.

Thus, using LIUS with lower acoustic pressure and higher frequencies can avoid potential uncontrollability issues in in-vivo experiments and at high-length scales associated with cytodisruption and standing waves.

The primary goal of our study is to conduct a comprehensive parametric investigation of the effects of various frequencies, acoustic pressures, and viscosities on ultrasound propagation.

We focus on developing a model for ultrasound propagation in a Kelvin-Voigt viscoelastic medium with an embedded tumor spheroid. As outlined in the Background section, we assume that the time scale for wave propagation is significantly shorter than the fluid flow within the tumor, thereby warranting the use of a viscoelastic model as a simpler and more accurate representation as compared to a poroelastic model. However, it is pertinent to acknowledge that alternative models may also be considered, and the efficacy of utilizing viscoelastic propagation can be further evaluated through comparative analyses. Through this study, we aim to gain a deeper understanding of how these mechanical factors modify ultrasound propagation and how they can be potentially leveraged to influence tumor dynamics.

To achieve our objective, we propose to model ultrasound propagation independently of its duty cycle, whether it is continuous or pulsed. We make this decision since we apply the mechanical wave throughout the entire cell growth process, and the duty cycle operates on a timescale of milliseconds that depends on persistence. Consequently, once a mechanical stimulus is applied, the response persists for a few seconds, much like how vision allows us to see individual frames as part of a motion picture. As a result, even during the silent period of the duty cycle, signaling remains activated, enabling us to consider the stress field.

By modeling the ultrasound wave until it reaches a stationary state, in which stress remains constant irrespective of the duty cycle, we can efficiently investigate the effects of ultrasonic stress on tumor dynamics. The stationary stress state achieved in our simulations is an important input for the model presented in the next Chapter, where we investigate how ultrasound-induced stress, in combination with the stress generated during tumor growth, influences tumor dynamics via mechanotransduction.

4.2 Mathematical model

The ultrasound wave travels in the direction of wave propagation, compressing the medium along that direction. We formulate the displacement of the wave as a boundary condition, for instance, in a lateral face (x = a). Then,

displacements generated by a transducer in the y-axis direction are described in the simplified form:

$$\mathbf{u}_u = \Big(0, A\sin\left(2\pi f t_u\right)\Big), \tag{4.2.1}$$

where A is the wave amplitude in terms of displacements and f is the central frequency. Before natural wave dissipation, the wave travels at constant speed $c_p = \sqrt{\frac{K + \frac{4}{3}\mu}{\rho}}$, where K and μ are the undrained bulk and shear modulus, and ρ stands for medium density.

The dynamic balance equation that accounts for the inertial terms produced during sonication reads:

$$\nabla \cdot \boldsymbol{\sigma}_u = \rho \frac{\partial^2 \mathbf{u}_u}{\partial {t_u}^2}, \tag{4.2.2}$$

where $\boldsymbol{\sigma}_\mathrm{u}$ is the stress produced by mechanical wave propagation. To accurately model the complex attenuation that occurs on a fast time scale, we utilize the Kelvin-Voigt governing equation (KV), as described in Section 2.3.2 and presented below:

$$\boldsymbol{\sigma}_u = 2\mu\Big(\boldsymbol{\varepsilon}_u - \frac{1}{3}\mathrm{tr}(\boldsymbol{\varepsilon}_u)\mathbf{I}\Big) + K\mathrm{tr}(\boldsymbol{\varepsilon}_u)\mathbf{I} + 2\eta_\mu\Big(\frac{\partial \boldsymbol{\varepsilon}_u}{\partial t_u} - \frac{1}{3}\mathrm{tr}\Big(\frac{\partial \boldsymbol{\varepsilon}_u}{\partial t_u}\Big)\mathbf{I}\Big) + \eta_K \frac{\partial \mathrm{tr}(\boldsymbol{\varepsilon}_u)}{\partial t_u}\mathbf{I}, \tag{4.2.3}$$

where the small strain is $\boldsymbol{\varepsilon}_u = \frac{1}{2}(\nabla \mathbf{u}_u + \nabla {\mathbf{u}_u}^\mathrm{T})$. In our analysis, the weakening of ultrasound waves is described by the shear viscosity η_μ and volumetric viscosity η_K. To incorporate the effect of bulk viscosity, we consider the attenuation coefficient α_η of an ultrasonic wave at a given frequency, as previously described in the literature [389, 390]:

$$\eta_K = \frac{\alpha_\eta 2\rho {c_p}^3}{(2\pi f)^2} - \frac{4}{3}\eta_\mu. \tag{4.2.4}$$

Notwithstanding, the contribution of the shear viscosity can be neglected due to the low order of magnitude of the shear component of the compressional waves.

Attenuation is frequency dependent. At 5MHz, fat tissue and parenchyma exhibit dissipation values ranging from $\alpha_\eta \in [0.2, 1.2]\mathrm{dBmm}^{-1}$ [391], corresponding to viscosities of $\eta_K \in [0.15, 1]\mathrm{Pa}\cdot\mathrm{s}$. Leukemia cells, on the other hand, exhibit values of $\alpha_\eta = 0.5\mathrm{dBmm}^{-1}$ and a viscosity of $\eta_K = 0.37\mathrm{Pa}\cdot\mathrm{s}$ [392]; while blood can reach values of $\alpha_\eta = 0.05\mathrm{dBmm}^{-1}$, corresponding to a viscosity of $\eta_K = 0.047\mathrm{Pa}\cdot\mathrm{s}$ [393], and the microscopic viscosity of the plasma membrane is $\eta_K = 0.21\mathrm{Pa}\cdot\mathrm{s}$ [394].

At the macro scale, the viscosity increase and it can reach values of $\eta_K \in [0.7, 4.1]\text{Pa} \cdot \text{s}$ in breast cancer [205], and even $\eta_K \in [5.56, 6.56]\text{Pa} \cdot \text{s}$ in prostate cancer [395]. For further details on viscosity measurements, we refer to study [213].

4.3 Numerical methods

The self-developed computational model is solved in the Finite Element Analysis Program [396] – FEAP – and Matlab (©MathWorks Inc., Natick, MA, USA). We solve the system assuming a two-dimensional problem and plane strain.

The sensibility analysis includes range of frequencies of $f = [1 - 20]$MHz, acoustic pressures of $A = [0.1 - 5]$ kPa, and viscosities of η_i =[0-10]Pa·s, being i the culture medium c or tumor viscosities T . These ranges of frequencies and intensities are well below those established by the FDA, which significantly minimizes the possibility of collateral damage. Specifically, we have verified that the spatial-peak temporal-average intensity ISPTA $< 100\text{mW} \cdot \text{cm}^{-2}$, and the mechanical index MI<1.9.

For the purpose of simulations, we consider a melanoma tumor spheroid of 200μm embedded in culture medium within a bioreactor of 2 cm in each direction. To limit computational expense, we confine our modeling to a 2mm region of the culture medium, as illustrated in Figure 4.1. In addition, we employ the Lysmer-Kuhlemyer Boundary Conditions to account for non-reflecting boundaries which absorb the 90% of the wave, and where the normal stress is expressed as $\boldsymbol{\sigma_n} = k_l \rho c_p \dfrac{\partial \mathbf{u}}{\partial t}$, being k_l a constant between $[1 - 100]$ [397].

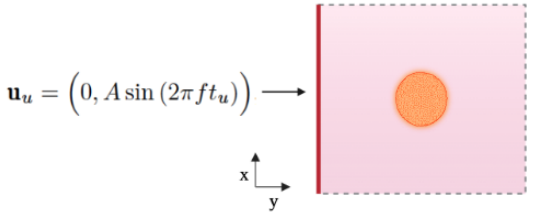

Figure 4.1: Wave propagation simulation simplification. The displacement boundary condition time dependent is set in a face x=a, while absorbing boundary conditions are applied in all faces.

We propagate continuous ultrasound through the spatial domain thrice to reach stationary state. The quantity of elements necessary for the simulations

is dependent on both the space and time intervals. The spatial discretization is assumed as $dx = \lambda/30$, where the wavelength is $\lambda = \frac{c_p}{f}$. As for the time interval, it is taken as $dt = f^{-1}{m_h}^{-1}$, being m_h the number of elements in each direction.

4.4 Results

4.4.1 Viscosity

The conducted simulations varying viscosities demonstrate the importance of taking into account dissipation in therapeutic ultrasound. As shown in Figure 4.2, ultrasound waves propagate uniformly through elastic media at a constant wave speed that does not depend on frequency.

However, introducing viscosity in the simulations results in a frequency-dependent wave speed, wave attenuation, and wave dispersion, which is a time-dependent behavior that increases with viscosity.

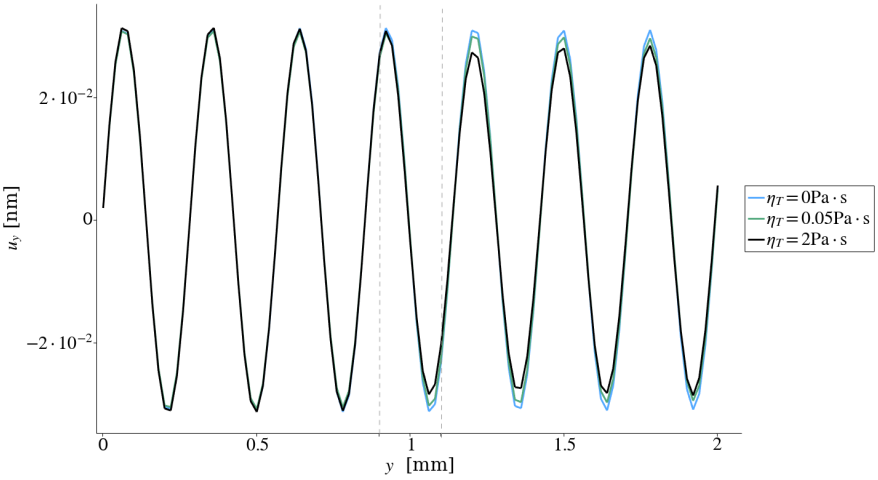

Figure 4.2: Viscosity-attenuation dependence. Homogeneous and elastic propagation maintains amplitude constant while viscosity attenuates wave propagation. Higher viscosity of the tumor produces a decrease in wave amplitude. All cases are shown for $\eta_c = 0.05\text{Pa} \cdot \text{s}$, $f = 5\text{MHz}$, and $A = 1.5\text{kPa}$.

When the viscosity of a tumor exceeds that of the surrounding medium, it leads to diffraction of the ultrasound wave, resulting in regions where the maximum acoustic pressure cannot be achieved, as demonstrated in Figure 4.3. The degree of this diffraction effect relies on the disparity in viscosity between

the tumor and its surrounding environment. This phenomenon has the potential to influence the growth patterns of the tumor, as elaborated in the subsequent chapter.

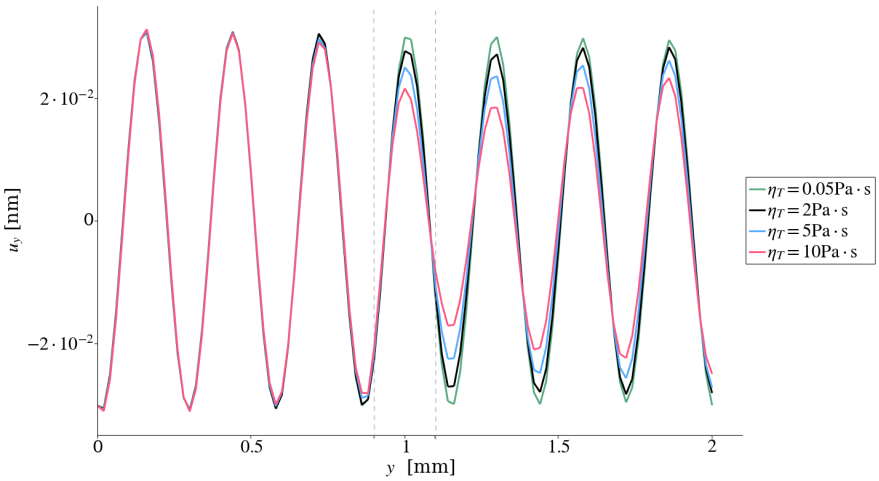

Figure 4.3: Viscosity and attenuation in less viscous medium. The diffraction and the loss of amplitude wave increase with higher tumor viscosities. All cases are shown for $\eta_c = 0.05\text{Pa} \cdot \text{s}$, $f = 5\text{MHz}$, and $A = 1.5\text{kPa}$. Note that the last cycles of waves gain amplitude because of the absorbing conditions used, which reflect the 10% of the energy[a].

[a]This issue could be overcome by modifying the absorbing boundary conditions or by increasing the size of the sample.

Conversely, when the viscosity of the surrounding medium is greater than that of the tumor, the ultrasound wave is attenuated before reaching the tumor spheroid, as shown in Figure 4.4. It is important to note that increasing the viscosity of the medium leads to a reduction in wave amplitude, which may necessitate an increase in acoustic pressure to achieve higher stress levels in the tumor under higher viscosity conditions.

4.4.2 Acoustic pressure

e conducted an investigation to examine the effects of varying acoustic pressure on wave amplitudes in a viscoelastic medium with heterogeneous viscosity. The findings, illustrated in Figure 4.5, reveal that increasing the acoustic pressure, while maintaining a constant frequency and viscosity, leads to higher wave amplitudes and, thus, higher levels of generated stress.

When propagating waves through a viscoelastic medium, the response of the

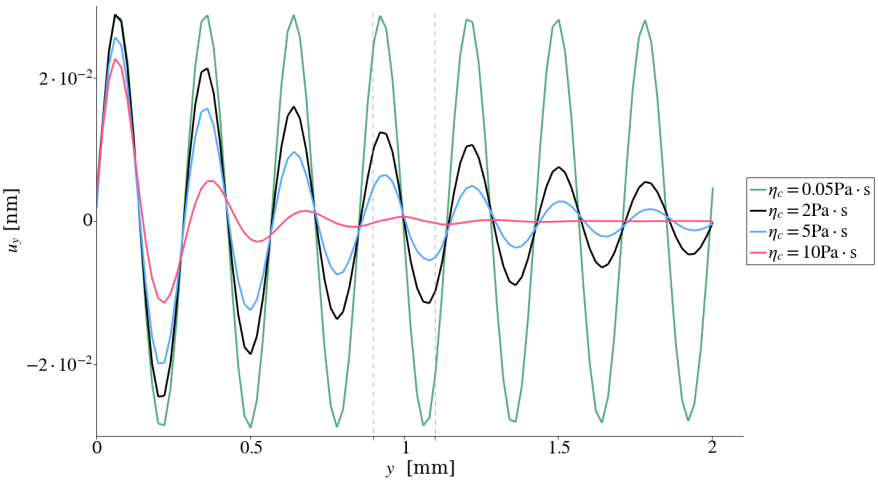

Figure 4.4: Viscosity and attenuation in more viscous medium. Higher viscosities of the medium imply higher attenuation before reaching the tumor spheroid. All cases are shown for $\eta_T = 0.05\text{Pa} \cdot \text{s}$, $f = 5\text{MHz}$, and A =1.5kPa.

medium to different acoustic pressures is contingent on both the frequency of the waves and the magnitude of the acoustic pressure. At low acoustic pressures, the response of the medium is primarily elastic, and the waves propagate through the medium with minimal energy dissipation. As the acoustic pressure increases, the medium starts to exhibit viscoelastic behavior, with energy dissipation becoming more pronounced as the waves propagate.

At high acoustic pressures, the viscoelastic response of the medium can become predominant, resulting in intense wave weakening. This underscores the significance of selecting the appropriate acoustic pressure carefully in low-intensity therapeutic ultrasound treatments to avoid overly attenuating or absorbing the waves, which could compromise the optimal therapeutic outcomes.

4.4.3 Frequency

As the frequency of an ultrasonic wave increases, its wavelength generally decreases, enabling higher intensities to be achieved without altering the acoustic pressure of the wave. However, the impact of frequency on wave propagation is influenced by the material properties of the medium. At lower frequencies, materials exhibit greater elasticity, while at higher frequencies, they become more viscous, leading to amplitude wave loss.

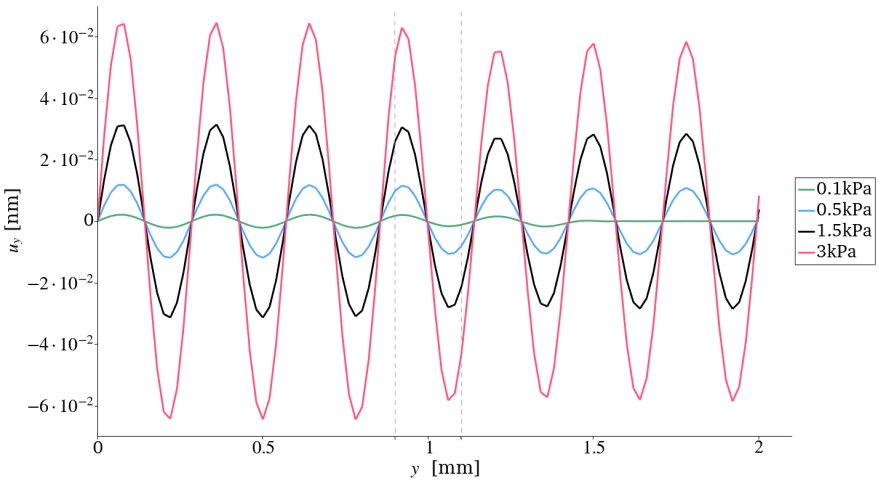

Figure 4.5: Acoustic pressure analysis. An increase in acoustic pressure lead to increased wave amplitude. All cases are shown for $\eta_c = 0.05\text{Pa} \cdot \text{s}$, $\eta_T = 2\text{Pa} \cdot \text{s}$, and $f = 5\text{MHz}$.

Simulations reveal that a frequency of 20 MHz results in significantly greater dissipation compared to lower frequencies. In contrast, for a frequency of 1 MHz and given the dimensions of the tumor spheroid, the viscosity of the medium appears to have little effect on wave attenuation, as depicted in Figure 4.6. It is important to consider the material properties of the medium when selecting the appropriate frequency to ensure optimal therapeutic outcomes.

If we aim to use a high frequency in a viscous medium to induce therapeutic effects, we would need to increase the emitted acoustic pressure to mitigate the effects of viscosity, as demonstrated in Figure 4.7. However, an extreme increase in frequency and intensity could potentially exceed the established safety limits.

To conclude, we present the temporal evolution of mechanical waves in both elastic and viscoelastic media with varying frequencies, specifically focusing on cases where the tumor has a higher viscosity than the surrounding medium. Two different frequencies, 5MHz and 20MHz were considered, and the evolution of the wave behavior was visualized in Figure 4.8.

The maps show the hydrostatic stress at different times during sonication, including before the wave reaches the tumor after it reaches the tumor, and when a stationary state is achieved. Our findings indicate that for elastic cases,

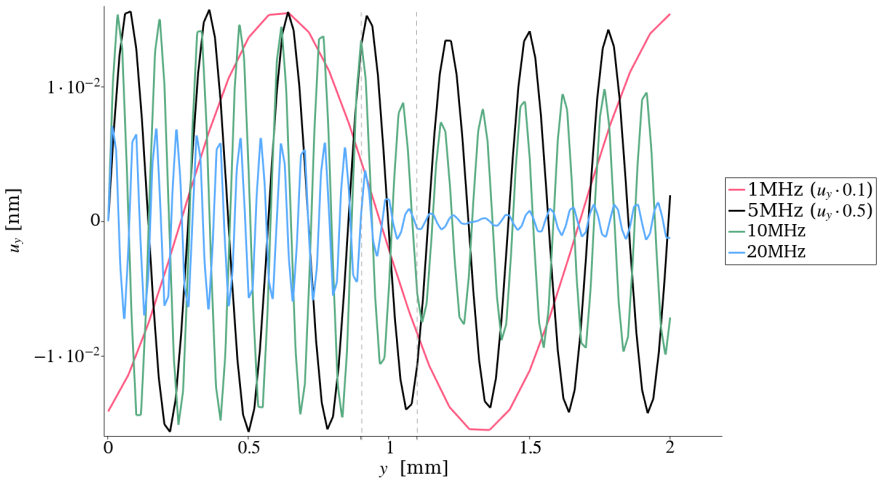

Figure 4.6: Frequency analysis. Higher frequencies show greater wave dissipation and less wavelength. Note that frequencies of 1 and 5 MHz are scaled to present them in the same range of amplitudes. Parameters of $\eta_T = 2\text{Pa} \cdot \text{s}$ and $\eta_c = 0.05\text{Pa} \cdot \text{s}$ and A=1.5kPa.

the amplitude and speed of wave propagation remain constant. However, when viscoelasticity is considered, there is a slight decrease in hydrostatic stress.

Moreover, we observed that increasing the frequency results in greater amplitude decay resulting in lower tension areas and a decrease in wave speed. Additionally, the diffraction effect highlighted in earlier discussions can also be achieved at equal frequencies if the tumor's viscosity is even higher than that of its surrounding medium. These results emphasize the importance of carefully selecting the appropriate frequency and considering the material properties of the medium in low-intensity ultrasound treatments for optimal therapeutic outcomes.

Stress has been identified as an important parameter in the promotion of mechanotherapy. Table 4.1 presents a summary of the peak hydrostatic pressure achieved at the central point of a tumor by a stationary wave, implying that higher peak pressures could lead to a greater reduction in cell proliferation, i.e. configurations of f =1MHz and f = 5MHz with A =1.5-3kPa, and considering η_c=0.05Pa·s and η_c=2Pa·s.

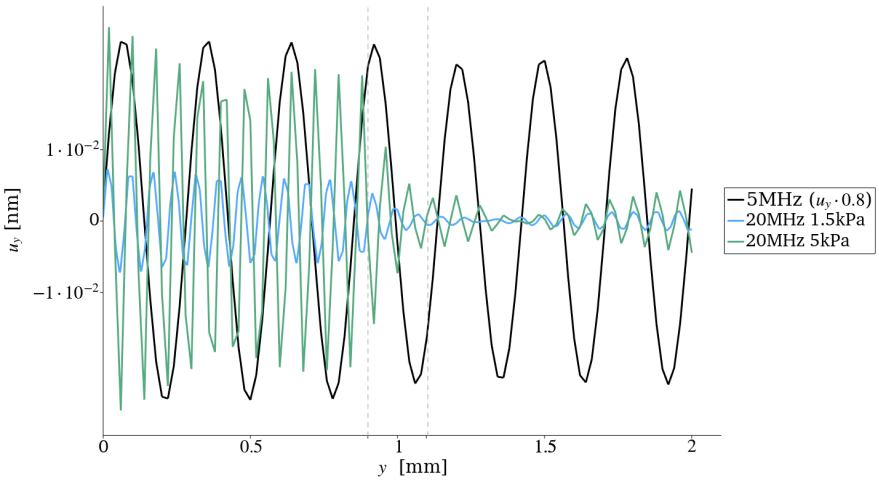

Figure 4.7: Frequency with increased acoustic pressure. Increased pressure in high frequencies lead to a decrease in wave attenuation. Parameters of $\eta_T = 2\text{Pa} \cdot \text{s}$ and $\eta_c = 0.05\text{Pa} \cdot \text{s}$. For $f = 5\text{MHz}$, the acoustic pressure is $A = 1.5\text{kPa}$.

Table 4.1
Numerical results of peak pressures in LIUS therapy.

f [MHz]	A [kPa]	η_c[Pa · s]	η_T[Pa · s]	p_r [kPa]
1	1.5	0.05	2	1.342
5	1.5	0.05	2	1.227
10	1.5	0.05	2	0.775
20	1.5	0.05	2	0.193
20	5	0.05	2	0.742
5	0.1	0.05	2	0.075
5	0.5	0.05	2	0.471
5	3	0.05	2	2.550
5	1.5	0	0	1.340
5	1.5	0.05	0.05	1.298
5	1.5	0.05	5	1.107
5	1.5	0.05	10	0.920
5	1.5	2	0.05	0.500
5	1.5	5	0.05	0.262
5	1.5	10	0.05	0.022

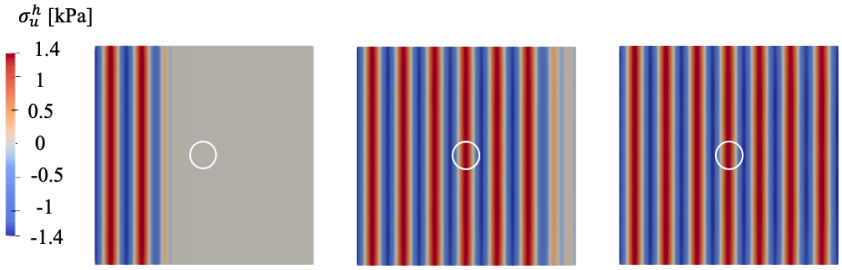

(a) Elastic wave propagation, with f = 5MHz and A=1.5kPa. The speed of the wave remains constant over propagation.

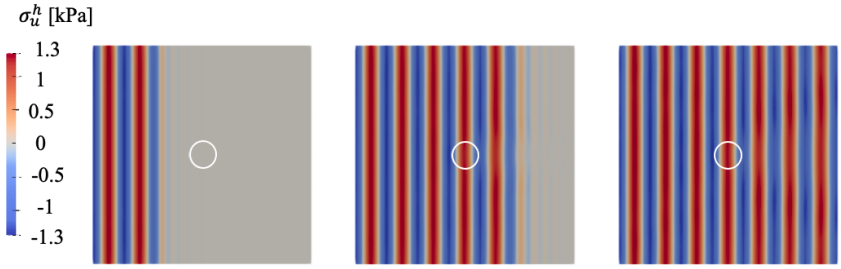

(b) Viscoelastic wave propagation, with f = 5MHz, A = 1.5kPa, η_T = 2Pa · s and η_c = 0.05Pa · s. Decrease in the speed and amplitude of wave compared with elastic case. Subtle areas of shadow are becoming discernible.

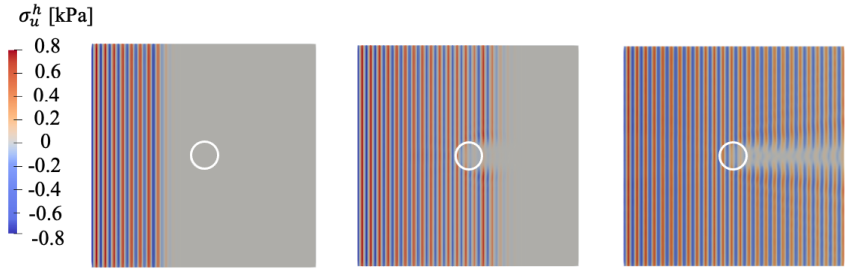

(c) Viscoelastic wave propagation, with f = 20MHz, A =1.5kPa, and η_T = 2Pa · s and η_c = 0.05Pa · s. Higher decrease in speed and attenuation compared with f =5MHz propagation. Distinct stress-induced shadow areas are readily discernible.

Figure 4.8: Ultrasound hydrostatic stress in different wave propagations. Simulations are shown including pre-tumor, post-tumor, and upon reaching steady-state conditions.

4.5 Conclusions

Our findings underscore the significance of accounting for the viscoelastic behavior of tissue when designing and optimizing LIUS treatments. Failing to consider these effects can result in inaccurate predictions of wave dissipation and overestimation of the stress experienced by cells, leading to unrealistic scenarios.

In our simulations, we have observed that the higher viscosity of the tumor tissue resulted in shadow zones behind the sonicated area, where the wave energy dissipates due to the viscosity of the tumor spheroid.

Acoustic pressure is a fundamental parameter that significantly influences the efficacy and safety of LIUS treatments. Excessive acoustic pressure can trigger cavitation and heating effects, leading to mechanical disruption of tissues and irreversible damage. In contrast, inadequate acoustic pressure may not produce the desired therapeutic effects, allowing cells to proliferate and migrate to regions with lower stress levels.

In addition to acoustic pressure, the selection of the appropriate frequency for LIUS is required to achieve optimal therapeutic outcomes, such as apoptosis or quiescence in cancer treatments. The choice of frequency depends on various factors, such as the target tissue geometry, medium properties, and desired intensity. Lower frequencies are associated with deeper penetration into tissues, making them ideal for treatments targeting structures located deeper in the body. However, as the frequency increases, the wave energy is increasingly absorbed and dissipated, resulting in greater weakening of the wave. The degree of absorption depends on the properties of the medium through which the wave propagates, such as its viscosity.

The findings of this numerical in vitro study are highly relevant for the potential translation of LIUS into potential effective clinical treatments. For instance, in the treatment of superficial cancers like melanoma, higher frequencies can be used since the target tissue is closed to the skin surface, and the attenuation of the wave is minimal. On the other hand, for deep-seated cancers such as pancreatic cancer, lower frequencies may be studied to achieve optimal focused therapeutic effects due to the need for deeper penetration into the body. The selection of an appropriate frequency should also consider the desired precision of the treatment, as higher frequencies provide better resolution and hence more focused treatment.

Taking into consideration the range of frequency, acoustic pressure, and intensity parameters, our study indicates that in order to effectively induce mechanotransduction, the tumor size should be larger than the wavelength of

the material or, at the very least, the wavelength should be able to propagate through the tumor without significant attenuation due to medium viscosity, provided that the acoustic pressure remains above a certain threshold. The relationship between these parameters is complex and must be carefully optimized to ensure that the desired therapeutic outcomes are achieved while minimizing the potential for adverse effects such as tissue damage.

Based on our data, we conclude that a frequency of $f = 1 - 5$MHz could be an appropriate choice for treating a 200μm tumor spheroid, given its viscosity range of $\eta_T \in [1, 3]$Pa·s and the viscosity of the culture medium two orders of magnitude lower. While the optimal acoustic pressure depends on the specific cell type, our findings suggest that static hydrostatic stresses within the range examined could be sufficient to inhibit spheroid growth, and acoustic pressures greater than $A = 1.5$kPa may be effective for the stated frequencies.

Therefore, selecting the appropriate mechanical parameters depend on specific medium properties, desired intensity, and target tissue geometry. Numerical studies could provide insights into the optimal mechanical parameters for different cell types and disease states, which can guide the development of in vitro and in vivo studies and future clinical applications.

In conclusion, our findings have the potential to inform the design of ultrasound-based cancer therapies, improve our ability to predict and manipulate the ultrasound-tissue interaction, and ultimately guide and contribute to the development of safe and effective LIUS co-treatments for cancer or other diseases while minimizing the risk of adverse effects.

Chapter 5

LIUS therapy in a growing tumor spheroid

5.1 Introduction

Once we have simulated different ultrasound propagations, we aim at joining ultrasound propagation to tumor evolution. Then, this chapter is focused on developing a biomechanical multiscale model that includes the therapeutic effect that LIUS seems to cause on growing tumors. The mathematical model is proposed at two different scales: i) slow-time scale in which the tumor grows and migrates and ii) fast-time scale in which ultrasound propagates through the tumor. Both scales are coupled by mechanotransduction, which occurs at an ultrasonic time interval and triggers tumor dynamics response at a slow-scale.

Firstly, we reconstruct the mechanotransduction parameters of our mathematical model approach with a preliminary experiment conducted in the laboratory using A375 melanoma cancer stem cell spheroids exposed to 5 MHz ultrasound with varying acoustic pressures. To reproduce the experiment in silico, we simplify the degrees of freedom in the mathematical model and adjust the parameters for proliferation, cellular decay, mechanotransduction, and ultrasound wave propagation.

After contrast with preliminary experimental procedures, we aim to further investigate the mechanotransduction process in cancer stem cell spheroids. Specifically, we focus on varying the mechanical parameters studied in Chapter 4, such as frequency, acoustic pressure, and viscosity, to establish potential biological outcomes such as apoptosis or quiescences with different mechanical configurations. By systematically varying these parameters and analyzing their effects on mechanotransduction, we hope to gain a deeper understanding of the underlying mechanisms involved in ultrasound-induced mechanotransduction in cancer stem cell spheroids.

This sensibility analysis is performed to our overall understanding of how ultrasound can be used to potentially impact cancer by reducing the pro-

liferation and dissemination of tumors. By identifying the key mechanical parameters that influence mechanotransduction, we can better design ultrasound protocols to achieve specific therapeutic outcomes.

Lastly, we have conducted simulations based on published data without ultrasound [84, 330]. Using the mechanotransduction parameters reconstructed from the previous study, we suggest how growth, migration, and patterning can be modified by ultrasound application. Moreover, the insights achieved from this study may also inform the development of novel strategies for cancer co-treatment based on ultrasound-induced mechanotransduction.

5.2 Mathematical model

We propose a multiscale model that accounts for the low-intensity ultrasound influence (microsecond-second time scale, t_u) on a growing tumor (hour-day time scale t) via mechanotransduction function. The multiscale method is a strategy for capturing the long-term effects that are not visible on a small scale but become significant at a larger and slower scale.

As described in Chapter 2, tumors are poroelastic materials composed of different phase components, including nutrients, healthy cells, tumor cells, interstitial fluid, proteins, and ECM. For the purposed study, the tumor is assumed to have a fluid phase (ϕ_F) of interstitial fluid and different solid phases (ϕ_i) which provide the elastic stiffness. The solid phases included here are tumor cells (ϕ_T), healthy cells (ϕ_H), and the extracellular matrix (ϕ_M).

The proposed model is based on the well-studied thermodynamic framework of Biot's poroelasticity and growth theory, and we refer to [337, 151, 84, 330] to deep into the fundamentals of the equations, in which the model of poroelastic cell competition and mechanotransduction are based. We use the $\boldsymbol{u} - p$ poroelastic notation, neglecting the relative fluid-solid displacement to focus on how fluid pressure affects the dynamic of solid phases. We assume infinitesimal strain theory and linear elasticity since there is no large deformation during ultrasound insonification [70] and growth does not develop great deformation.

The balance momentum that describes the dynamic mechanical equilibrium is:

$$\nabla \cdot \boldsymbol{\sigma} = \rho \frac{\partial^2 \mathbf{u}}{\partial t^2}, \tag{5.2.1}$$

where ρ is the medium density and $\mathbf{u}$ are the displacements. The Cauchy multiscale stress tensor in a sonicated growing tumor is described by:

$$\boldsymbol{\sigma}(\boldsymbol{x}, t) = \boldsymbol{\sigma}_s(\boldsymbol{x}, t) + \boldsymbol{\sigma}_u(\boldsymbol{x}, t_u), \tag{5.2.2}$$

where the slow-scale stress $\boldsymbol{\sigma}_s(\boldsymbol{x}, t)$ accounts for the growth and the poroelastic rearrangements while the fast-scale stress $\boldsymbol{\sigma}_u(\boldsymbol{x}, t_u)$ refers to ultrasonic stress which occurs at time t_u. To isolate the governing equations at each temporal scale, we define the average of the multiscale stress over an ultrasonic spatial and temporal cycle [398, 399], i.e. reference ultrasonic wavelength λ and period T:

$$\langle \boldsymbol{\sigma} \rangle = \frac{1}{\lambda T} \int_0^T \int_0^\lambda \boldsymbol{\sigma} \, d\boldsymbol{x} \, dt_u. \tag{5.2.3}$$

Considering the definition of multiscale stress, the above reads:

$$\langle \boldsymbol{\sigma} \rangle = \frac{1}{\lambda T} \int_0^T \int_0^\lambda \boldsymbol{\sigma}_s \, d\boldsymbol{x} \, dt_u + \frac{1}{\lambda T} \int_0^T \int_0^\lambda \boldsymbol{\sigma}_u \, d\boldsymbol{x} \, dt_u, \tag{5.2.4}$$

being the slow stress independent of the ultrasonic scale, $\langle \boldsymbol{\sigma}_s \rangle = \boldsymbol{\sigma}_s$. On the other hand, ultrasonic stress is a function of the sinus over λ and T, as denoted in equation 4.2.1, so $\langle \boldsymbol{\sigma}_u \rangle = 0$. Then, the average of the multiscale stress is the slow-scale stress, $\langle \boldsymbol{\sigma} \rangle = \boldsymbol{\sigma}_s$, and subsequently, the average of the slow-scale stress is the total multiscale stress, $\langle \boldsymbol{\sigma}_s \rangle = \boldsymbol{\sigma}$. Finally, regarding equation (5.2.2) and the independence of the slow-scale stress from the ultrasonic scale, the ultrasonic stress is $\boldsymbol{\sigma}_u = \boldsymbol{\sigma} - \langle \boldsymbol{\sigma} \rangle$.

Once the multiscale approach is formalized, we define the slow-scale stress as an additive decomposition:

$$\boldsymbol{\sigma}_s = \boldsymbol{\sigma}_e + \boldsymbol{\sigma}_p + \boldsymbol{\sigma}_g, \tag{5.2.5}$$

being $\boldsymbol{\sigma}_\mathrm{e}$ the so-called effective solid stress tensor, $\boldsymbol{\sigma}_\mathrm{p}$ the fluid pressure contribution, and $\boldsymbol{\sigma}_\mathrm{g}$ the stress generated during growth. Hence, the equation of dynamic equilibrium (5.2.1) applied to slow-scale stress can be considered as a quasistatic process since characteristic velocities are small and inertia terms can be neglected. For an elastic isotropic material, the constitutive equation for the effective solid stress that accounts for the elastic rearrangements yields:

$$\boldsymbol{\sigma}_e = 2\mu_d \Big(\boldsymbol{\varepsilon} - \frac{1}{3} \mathrm{tr}(\boldsymbol{\varepsilon}) \mathbf{I} \Big) + K_d \mathrm{tr}(\boldsymbol{\varepsilon}) \mathbf{I}, \tag{5.2.6}$$

where the small strain is $\boldsymbol{\varepsilon} = \frac{1}{2}(\nabla \mathbf{u} + \nabla \mathbf{u}^\mathrm{T})$, with $\mathbf{u}$ the displacements, $\mathbf{I}$ the second-order identity tensor, and K_d and μ_d the drained bulk and shear modulus. We can neglect the viscous solid contribution at the slow-scale governing equation since the relaxation terms of rearrangements are on a

smaller time scale than growth. The stress produced by the fluid is:

$$\boldsymbol{\sigma}_p = -\alpha\Big(p - p_0\Big)\mathbf{I}, \tag{5.2.7}$$

with α the Biot coefficient, p the fluid pore pressure, and p_0 the initial fluid pore pressure. The evolution of the fluid pressure p is regulated by the Storage equation:

$$\frac{\partial \zeta}{\partial t} = \frac{1}{M}\frac{\partial p}{\partial t} + \alpha\frac{\partial tr(\boldsymbol{\varepsilon})}{\partial t} = \nabla \cdot \Big(k\nabla p\Big) + \Gamma_{\mathrm{F}}, \tag{5.2.8}$$

being ζ the dimensionless variation of fluid content defined by the difference between the actual and initial fluid phase $\zeta = \phi_{\mathrm{F}} - \phi_{\mathrm{F0}}$. The parameter M is the Biot modulus, and k is the conductivity, $k = \kappa {\nu_f}^{-1}$, where κ is the permeability of the medium, and the dynamic fluid viscosity is described by ν_f. The source term Γ_F accounts for the fluid interchange between vessels and capillaries. Considering Starling's theory [330, 84, 400, 304, 186], the fluid flow source yields:

$$\Gamma_F = k_v\Big[(p_v - p) - \omega(\pi_v - \pi_l)\Big] - k_l(p - p_l), \tag{5.2.9}$$

where p_v relates to the vessel pressure, ω is the reflection coefficient which weights the interstitial osmotic pressure $(\pi_v - \pi_l)$, and p_l is the lymphatic pressure drainage working in the opposite direction of the vessel pressure system. The k_v and k_l parameters are the conductivity coefficients of the vessel and lymphatic system respectively. Following the recent trends in literature, the conductivity of the lymphatic system can be described as a function of tumor cells that includes decreasing drainage of the lymphatic system caused by tumor growth:

$$k_l = \Big[1 - (\phi_T - \phi_{T0})\Big]k_{ln}, \tag{5.2.10}$$

with k_{ln} the conductivity of the lymphatic system under normal conditions [330, 400]. Finally, the stress produced by growth reads:

$$\boldsymbol{\sigma}_g = -K_d g\boldsymbol{\gamma}, \tag{5.2.11}$$

where g is the growth strain function and $\boldsymbol{\gamma}$ is the tensor that distributes the growth in different directions. In this study, we have assumed isotropic or volumetric growth, so $\boldsymbol{\gamma} = 1/3\mathbf{I}$, which is also utilized in Chapter 3. Additionally, homogeneous growth is considered for the sake of simplicity in

this particular investigation. The growth function reads:

$$g = \phi_T + \phi_H + \phi_M - \phi_{T0} - \phi_{H0} - \phi_{M0}, \tag{5.2.12}$$

with the zero subindexes denoting the initial volume fractions. The volumetric fractions evolve and interact with the mechanical environment and, among others, by:

$$\begin{aligned} \frac{\partial \phi_T}{\partial t} &= \nabla \cdot (\mathcal{M}_T D_T \phi_T \nabla \phi_T) + \phi_{\mathrm{F}} \mathcal{M}_{\mathrm{T}} \phi_{\mathrm{T}} \Gamma_{\mathrm{T}} \mathrm{T}_{\mathrm{T}}, \\ \frac{\partial \phi_H}{\partial t} &= \phi_F \mathcal{M}_H \phi_H \Gamma_H T_H, \\ \frac{\partial \phi_M}{\partial t} &= \beta_T \phi_T + \beta_H \phi_H - \delta_M \phi_M \Gamma_M, \end{aligned} \tag{5.2.13}$$

where the first equation describes the tumor phase dynamics. In particular, the first term on the right accounts for tumor the non-linear tumor phase flux, described here by a finite-speed tumor propagation front limited by the diffusion coefficient D_T. The second term considers the competitive interaction among other species – Γ_{T}, fluid phase ϕ_F and proliferation T_T–. Both migration and source terms account for mechanotransduction function – $\mathcal{M}_{\mathrm{T}}$ –. Mechanotransduction, competition, fluid phase and proliferation are also described for healthy cells by $\mathcal{M}_{\mathrm{H}}$, Γ_{H} and T_H. The ECM evolution depends on i)the species interaction Γ_{M}, ii) the ECM synthesis promoted by the cells by the production rates β_T and β_H, and iii) the ECM degradation processes enabled by the loss rate δ_M [330]. The competition terms Γ_T, Γ_H and Γ_M are defined by the following predator-prey or Volterra-Lokta dynamics [401]:

$$\begin{aligned} \Gamma_T &= \Big(1 - \alpha_{TT}\phi_T - \alpha_{TH}\phi_H - \alpha_{TM}\phi_M\Big), \\ \Gamma_H &= \Big(1 - \alpha_{HT}\phi_T - \alpha_{HH}\phi_H - \alpha_{HM}\phi_M\Big), \\ \Gamma_M &= \alpha_{MT}\phi_T + \alpha_{MH}\phi_H \end{aligned} \tag{5.2.14}$$

where the coefficients α_{ii}, with $i = \{T, H, M\}$, represent the interaction among the cell species. To complete the system of equations, we define the mechanotransduction function. Based on time scales at which mechanotransduction occurs, we propose that cells perceive the promedio of the sigmoid function $\mathcal{M}_{B_i}$ at an ultrasonic time interval, in which cells could sense perturbations and activate mechanotransduction pathways that alter proliferation above a certain stress threshold [221, 225, 215]. Then, mechanotransduction

can be expressed as:

$$\mathcal{M}_i = \frac{1}{T}\int_0^T \mathcal{M}_{B_i} dt_u, \tag{5.2.15}$$

where $\mathcal{M}_{B_i}$ is based on already published works summarized in Table 2.2:

$$\mathcal{M}_{B_i} = \left[q_i + (1-q_i)e^{b_i(|\sigma_{\mathcal{M}}|-\beta_u\sigma_{L_i})}\left(1+e^{b_i(|\sigma_{\mathcal{M}}|-\beta_u\sigma_{L_i})}\right)^{-1}\right]. \tag{5.2.16}$$

Indeed, the initial proliferation or migration of cells decreases to the maximum of the viability of the cells, achieving the factor of q_i when the stress $\sigma_{\mathcal{M}}$ perceived by the cells in the environment exceeds a threshold σ_{L_i}. In literature, this threshold is obtained for static stress and values around $[1-10]$kPa [154, 151, 155, 330, 84, 304]. However, to also account for dynamic stress, we adopt a linear parameter β_u, which reduces the sensitivity limit of cells. Parameter b_i refers to the smoothness of the transition zone of the sigmoid function, i.e., how fast or slow cells adapt their proliferation to stress.

We assume that cells sense both static hydrostatic growth-induced and dynamic ultrasonic-induced stress via mechanotransduction pathways. Then:

$$\sigma_{\mathcal{M}} = \left(\sigma_s^h + \sigma_u^h\right), \tag{5.2.17}$$

where the superscript h is the hydrostatic stress defined by $\sigma^h = \frac{1}{3}\mathrm{tr}(\boldsymbol{\sigma})$ for each time-scale stress. We neglect the shear stress contribution because its order of magnitude is much smaller than the normal components due to the plane ultrasound wave and the isotropic growth. In Figure 5.1, we schematize how the mechanotransduction function works.

To conclude the formalization, we obtain $\boldsymbol{\sigma}_u^h$ over a period of time from the propagation of a P-wave emitted by a transducer through the medium, as previously explained in Chapter 4.

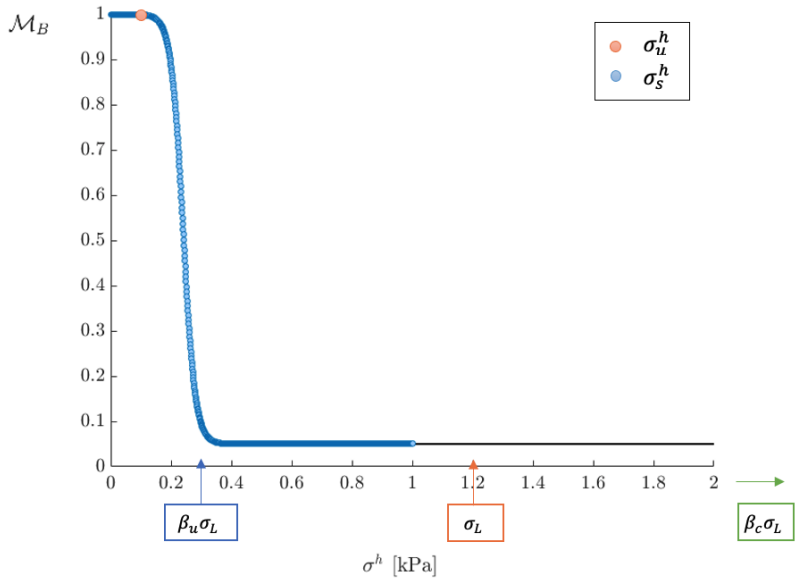

Figure 5.1: Mechanotransduction function. Cells perceive the promedio of the sigmoid function $\mathcal{M}_B$. The slow ultrasound stress is constant at an ultrasonic time interval, while ultrasound stress exhibits dynamic behavior, oscillating between rarefaction and compression – for this case, we have plotted the absolute stress of a wave with an amplitude of 1kPa –. To account for the dynamic nature of ultrasound stress, the static stress limit, σ_L, is decreased by a coefficient, β_u. However, if the limit is exceeded, it may result in cell disruption and cessation of proliferation, indicated by $\mathcal{M}_B = 0$.[a]

[a]Note that our current function does not account for the cytodisruption effect.

5.3 Methods

5.3.1 Numerical methods

Regarding the initial conditions, the initial fluid phase is defined by equation $\phi_{\mathrm{F0}} = 1 - \phi_{\mathrm{T0}} - \phi_{\mathrm{H0}} - \phi_{\mathrm{M0}}$. The initial fluid pressure guarantees the equilibrium of the Storage equation, so p_0 causes the source term to be null at the initial time instant t = 0h. Furthermore, the initial components of the tumor and healthy cells are distributed in space according to a smoothing

function S proposed in reference [330]:

$$\begin{aligned} \phi_{T0} &= \overline{\phi}_{T0} S, \\ \phi_{H0} &= \overline{\phi}_{H0}\Big(1 - S\Big), \\ S &= \Big[1 + e^{b_S \frac{(r - l_t)}{l}}\Big]^{-1}, \end{aligned} \tag{5.3.1}$$

where the parameter $\overline{\phi}_{i0}$ is the initial concentration rate, l_t represents the tumor size, r the radius of the tumor, and l the total length size of the medium, while b_S is the smoothing coefficient.

Regarding boundary conditions (BC), we adopt Winkler-inspired Boundary Conditions to adopt the confinement of the tumor spheroid at slow scales $\boldsymbol{\sigma_n} = -k_w \mathbf{u}$, where $\mathbf{n}$ is the outer normal vector and k_w is a constant [92]. For fast-scale ultrasound propagation, we use the Lysmer-Kuhlemyer Boundary Condition to account for nonreflecting boundaries or absorbing boundary conditions [397], as discussed in Chapter 4. The normal stress reads $\boldsymbol{\sigma_n} = k_l \rho c_p \dfrac{\partial \mathbf{u}}{\partial t}$, where k_l is a constant between $[0 - 100]$.

The self-developed computational model is solved in finite elements using Finite Element Analysis Program [396] – FEAP 8.6– and Matlab (©MathWorks Inc., Natick, MA, USA). We solve the multiscale system assuming a two-dimensional problem and plane strain.

As explained in Section 5.2, the different scales model can be considered independent, and the flowchart of the numerical simulations is reported in Figure 5.2.

We conducted a set of simulations using a multiscale model that includes mechanotransduction effects, with different mechanical parameter values according to Chapter 4. The parameter values used in each simulation are summarized in Table 5.1 and the specific parameters for fast-scale ultrasound were described in Chapter 4. In some cases, certain parameters were kept constant across simulations, while in others, they were varied to explore their impact on the outcome. Specifically, in our preliminary experiments prediction, we simplify the model. We make sure to specify which parameters are being modified for each simulation in the corresponding figures or results.

5.3.2 Experimental method

In this section, we provide a detailed account of the cell culture method, cell line acquisition, and setup used in our experiments. The cell culture setup

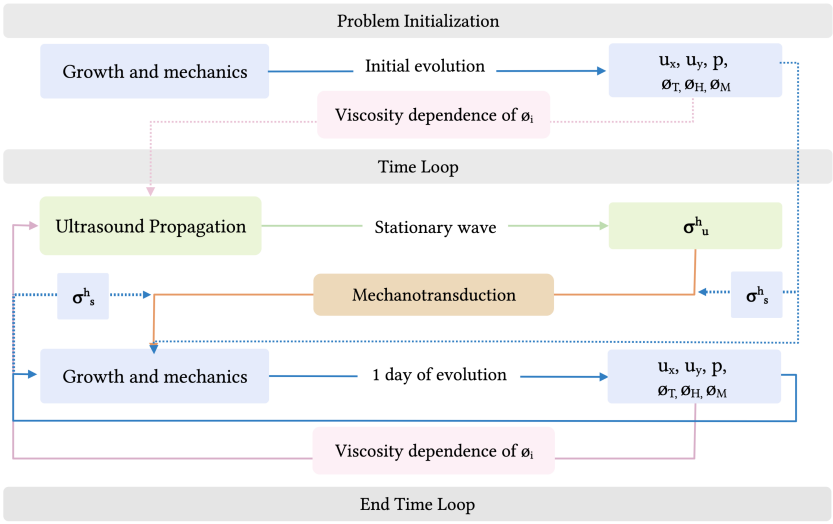

Figure 5.2: Flowchart of the multiscale model. The system is initialized at slow-scale, where the displacements, fluid pressure, and solid phases are obtained. The solid phases are added into fast-scale model of wave propagation to consider the viscosity medium of the tumor cell phase dependence. The fast-scale model evolves until the stationary waves are achieved, and ultrasonic hydrostatic stress is computed. Together with the hydrostatic slow stress, the ultrasonic stress is considered to compute the evolution of the system accounting for mechanotransduction. The results are again included at slow and fast-scale to complete the time loop until the final time of simulations is achieved.

has been performed and extensively improved over the years by members of our collaborating group *Advanced therapies: differentiation, regeneration, and cancer* of the University of Granada. Our team, on the other hand, is at the forefront of using mechanical waves in soft tissues [398, 213].

5.3.2.1 Experimental setup

The bioreactor in which CSCs are located is subjected to a 70% alcohol spray and subsequently placed in a chamber designed for ultraviolet (UV) sterilization. This process lasts for 30 minutes and ensures disinfection of the bioreactor by effectively eliminating potential contaminants with the use of UV light. The water and attenuating material chambers are filled with caution to prevent overflow and avoid any form of contamination or interference. Additionally, the chambers are covered with insulating tape.

Table 5.1
Multiscale modeling parameters for numerical simulations

Description	Symbol	Data	Units	Reference
Young modulus	E	8	kPa	[151, 114, 330]
Undrained Poisson modulus	ν_u	0.49999	[-]	[151, 114]
Drained Poisson modulus	ν	0.4	[-]	[151, 114, 92]
Mass density	ρ	1000	$\mathrm{kg \cdot m^{-3}}$	[-]
Hydraulic conductivity	k_h	$3.1 \cdot 10^{-14}$	$\mathrm{m^2 \cdot Pa^{-1} s^{-1}}$	[151, 114, 186, 340, 342]
Biot coefficient	α	$9.91 \cdot 10^{-1}$	[-]	[330, 402]
Biot modulus	M	1.79	MPa	[330, 402]
Vessel conductivity	k_v	$2.70 \cdot 10^{-8}$	$\mathrm{Pa^{-1} \cdot s^{-1}}$	[340, 186, 400]
Vessel pressure	p_v	$3.33 \cdot 10^{3}$	Pa	[186]
Reflection coefficient	ω	$9.00 \cdot 10^{-1}$	[-]	[340, 400]
Interst osmotic pressure	$\pi_v - \pi_e$	$1.33 \cdot 10^{3}$	Pa	[340, 400]
Lymphatic conductivity	k_{lo}	$9.98 \cdot 10^{-8}$	$\mathrm{Pa^{-1} \cdot s^{-1}}$	[186]
Lymphatic vessel pressure	p_l	$1.33 \cdot 10^{2}$	Pa	[84]
Exchange coefficient	α_{TT}	1.30	-	[330]
Exchange coefficient	α_{TH}	1.00	-	[330]
Exchange coefficient	α_{TM}	1.00	-	[330]
Exchange coefficient	α_{HH}	3.00	-	[330]
Exchange coefficient	α_{HT}	2.00	-	[330]
Exchange coefficient	α_{HM}	1.00	-	[330]
Coefficient	β_T	$5.79 \cdot 10^{-7}$	$\mathrm{s^{-1}}$	[330]
Coefficient	β_H	$1.16 \cdot 10^{-6}$	$\mathrm{s^{-1}}$	[330]
Coefficient	$\delta_M \alpha_{MT}$	$2.89 \cdot 10^{-6}$	$\mathrm{s^{-1}}$	[330]
Coefficient	$\delta_M \alpha_{MH}$	$2.89 \cdot 10^{-6}$	$\mathrm{s^{-1}}$	[330]
Initial condition ϕ^T	ϕ^{T0}	$1.50 \cdot 10^{-1}$	-	[330]
Initial condition ϕ^H	ϕ^{H0}	$1.50 \cdot 10^{-1}$	-	[330]
Initial condition ϕ^M	ϕ^{M0}	$4 \cdot 10^{-1}$	-	[330]
Proliferation rate ϕ^T	T_T	$1.26 \cdot 10^{-5}$	$\mathrm{s^{-1}}$	[330]
Proliferation rate ϕ^H	T_H	$1.26 \cdot 10^{-5}$	$\mathrm{s^{-1}}$	[330]
Common lower rate	q	0.05	[-]	[330]
Smootheness mechanotransduction	χ_σ	-0.05	$\mathrm{Pa^{-1}}$	[330]
Dynamic stress coefficient	β_s	0.2	[–]	Fitted
Tumor Limit stress	σ_L	$1.2 \cdot 10^{3}$	Pa	[330, 154, 151, 155]

The complete setup is shown in Figure 5.3. The Arduino is connected to the computer and the software is loaded, which enables the switch of mechanical signals. The Arduino also serves as a trigger to restart the signal and prevent

any time delay. The wave is generated using Matlab software and then loaded onto the wave generator. Before connecting the wave generator to the amplifier, the signal is first verified using an oscilloscope to ensure that the frequencies and connections are correct. Once the signals have been tested, the transducer is connected and placed on the support, and coupling gel is extended on the transducers and bioreactor faces as a coupling material to avoid air bubbles. The relays are then connected.

As the final step, the cells are transferred to their designated chambers in the bioreactor and placed in the incubator until the subsequent analysis. To conduct the examination, the bioreactor is taken out of the incubator and moved into a UV sterilization chamber with laminar flow to avoid contamination.

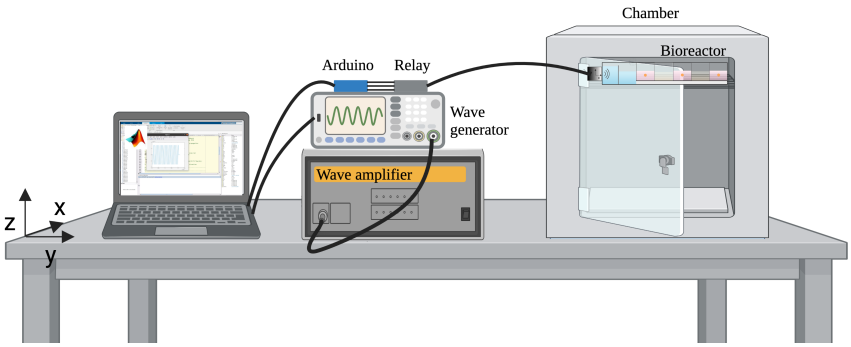

Figure 5.3: Setup of the preliminar measurements.

The bioreactor utilized for cell culture consists of five sequentially arranged Petri dishes containing A375 melanoma cells embedded in culture medium and an attenuating medium (oil), as depicted in Figure 5.4. This experimental setup is designed to enable the generation of various wave amplitudes using a single transducer, as the emitted wave loses energy while propagating through different media. To prevent heating effects, a water-filled region is included at the beginning of the bioreactor. Acoustic pressure values are measured in each culture using a hydrophone probe, which is submerged in a replica of the bioreactor to capture acoustic pressure values without affecting tumor response. Through this method, we have determined that the first culture experiences 15.5 kPa, the second 7.5 kPa, and the third 1.5 kPa.

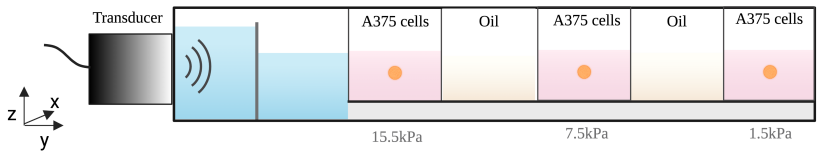

Figure 5.4: Sonication scheme. The transducer emits the ultrasonic wave through a first medium of water, which prevents the temperature from increasing. The wave then travels through the culture containing cells and then attenuating media, causing the acoustic pressure to decrease as it encounters different materials. As a result, the same bioreactor can be used for a given frequency and various amplitudes.

5.3.2.2 Cell culture

Melanoma cancer cell line (A375) are acquired from the American Type Culture Collection (ATCC) and arecultured according to the recommended procedures by the ATCC. The cell lines are passaged for a period of less than 6 months and were regularly screened for mycoplasma contamination. Cells were maintained in advanced DMEM (Sigma-Aldrich) supplemented with 10% FBS (Gibco) and 5% Penicillin/Streptomycin (Sigma-Aldrich).

To obtain tertiary spheres, melanoma cells are cultured in suspension using low-attachment plates containing DMEM-F12, 1% streptomycin-penicillin, 1 mg/mL hydrocortisone (Sigma-Aldrich), 4 ng/mL heparin (Sigma-Aldrich), 1X ITS (Gibco), 1X B27 (Gibco), 10 ng/mL EGF (Sigma-Aldrich), 10 ng/mL FGF (Sigma-Aldrich), 10 ng/mL HGF, and 10 ng/mL IL6 (Miltenyi Biotec). The cells are cultured for 6 days and the spheres are disaggregated every 72 hours until tertiary spheres are obtained. To achieve this, the spheres are collected by centrifugation at 1500 rpm for 5 minutes, incubated with trypsin-EDTA (Sigma-Aldrich) at 37°C for 5 minutes, and then inactivated with FBS. The cells are then washed with PBS and reseeded in the same culture conditions.

5.3.2.3 Cell proliferation assay

To evaluate cell proliferation, we employ the Alamar blue assay (Biorad) as the measurement method. Cell growth is monitored on days 0, 1, and 3. To ensure reliable results, two parallel experiments are conducted. In the first experiment, a bioreactor is exposed to 24 hours of ultrasound, and measurements were taken. In the second experiment, a bioreactor is utilized where cells underwent the 72-hour treatment without interruption. This approach is implemented to avoid any potential interference or damage during

the manipulation of the spheroids.

The experimental procedure consists of adding 10μl of Alamar blue solution per 100μl of media to the cells and incubating them for 2 hours. Following the incubation period, the fluorescence intensity is measured using the Synergy HT instrument (BIO-TEK) at an excitation wavelength of 530nm and emissions of 590nm.

5.4 Results

5.4.1 Multiscale mechanotherapy *in-vitro*

The experimental configuration used in this study was based on previous knowledge of how stress can impact cell growth, as discussed in Chapter 4. The selection of the ultrasound frequency is important to achieving optimal therapeutic outcomes, as very low frequencies would not penetrate the tumor, while high frequencies could potentially cause cytodisruption through resonance. Therefore, we select a frequency of 5MHz, which is within the range that can partially penetrate the tumor and enhance mechanotransduction without causing cytoskeleton damage.

In reference to the acoustic pressure, we apply acoustic pressures of 1.5kPa, 7.5kPa, and 15.5kPa, as illustrated in Figure 5.4. These values fall within a safe range, as they are sufficient to induce mechanotransduction without causing tissue disruption.

5.4.1.1 Experimental results

For the preliminary analysis of the data, a non-parametric methodology is developed under the assumption of non-normality in the growth rate variables. The choice is performed as a consequence of the small size of the sample per group. It should be understood that experiments in medical engineering are expensive and costly in terms of design, time, and setup. The rates are standardized from the initial growth quantities, where the control group is not exposed to any ultrasound propagation and the effect group was sonicated to a frequency of 5MHz.

Our preliminary experiments suggest that tumor cells diminish their net proliferation if they are sonicated at 5MHz compared with non-sonicated cells for three days, as shown in Figure 5.5. Furthermore, the different acoustic pressures do not show significant differences between them – data not shown – but evidence of statistical significance, indicating that the sensitivity limit of the cells is reached before 1.5kPa, which is in agreement with the hypothesis that the sensitivity limit of cells is lower for dynamic stress than for static

stress [330, 84, 304, 154].

For the methodology, the hypothesis contrast is analyzed by the Wilcoxon-Mann-Whitney test for small samples and independent means with the exact distribution. A p-value of 0.018 is obtained with a fixed 5% of type I error. This probability reveals a statistically significant inference for the difference of means in the groups, observing a less rate for the cellular population exposed to high-frequency ultrasound.

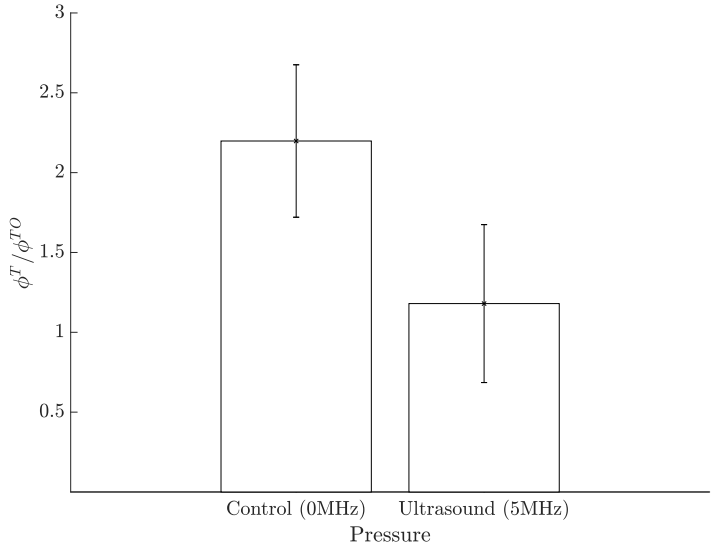

Figure 5.5: Preliminar experiments for non-sonicated and sonicated cells. Cell proliferation diminishes if the tumor spheroid is sonicated at 5MHz for three days, compared with non-sonicated cells. $^*p < 0.05$ in the Wilcoxon-Mann-Whitney test, n=3.

5.4.1.2 Multiscale mechanotherapy model

We have reduced the degrees of freedom of the mathematical model to fit our experimental data and reconstruct the mechanotransduction parameters. For sake of simplicity, we have assumed the absence of the extracellular matrix and healthy phases, and we only consider the coexistence of proliferative tumor cells and fluid within the tumor spheroid, meaning that$D = \alpha_{TH} = \alpha_{TM} = \Gamma_F = \Gamma_H = \Gamma_M = \beta_T = \beta_H = 0$.

We have chosen specific mechanical parameters for our experiment, including a frequency of $f = 5$MHz, a tumor viscosity of η_T=2Pa·s, a culture medium viscosity of η_c=0.05Pa·s, and an acoustic pressure of A =1.5kPa. The selection

of acoustic pressure is based on the results of our preliminary experiments, which have indicated no significant differences between the different acoustic pressures applied.

To begin with, the simulation parameters are calibrated using the results obtained from the control experiment, which have considered the observed deceleration of cell proliferation on the first day. This decline is linked to the rearrangement and development of spheroid clusters. Therefore, it is plausible that the absence of notable distinctions between the control and sonication groups on the first day of the experiment is a result of the cellular reorganization. A constant and higher proliferation rate is maintained from the first to the third day. Once the growth parameters are calibrated, we proceed to adjust the mechanotransduction parameters to match the experimental results.

From a computational standpoint, the hydrostatic stresses characterizing the stress state of the tumor manifest themselves at two distinct scales: the slow and the ultrasonic stress, as illustrated in Figure 5.6. With regard to the slow-scale stress, compression is predominantly concentrated in the core of the tumor, while tension begins to be present in the inner regions, as depicted in Figure 5.6(a). These results are consistent with prior research examined in [147, 45, 166].

It is noteworthy that the stress scales involved in this study exhibit significant differences, with the tumor-induced growth stress being in the order of Pascals, while the ultrasound stress is three orders of magnitude higher. The considerable difference in stress scales between the ultrasound and slow-scale stress implies that ultrasound stress is expected to exert a more prominent impact on mechanotransduction than slow-scale stress. Thus, slow-scale stress contribution to mechanotransduction is comparatively less significant than that of ultrasound stress.

Furthermore, numerical simulations suggest that ultrasound diffraction through the tumor can result in shadow areas with lower displacements and stresses, as expounded in Chapter 4.

For this particular case study, diffraction is attributed to the difference in viscosities between the culture medium and the tumor spheroid, as well as the applied frequency, resulting in a heterogeneous stress distribution within the bioreactor. These findings fit previous studies reported in the literature [73]. On the experimental front, these results could be verified through the use of a high-speed camera.

Then, propagation patterns of mechanical waves are the key players in

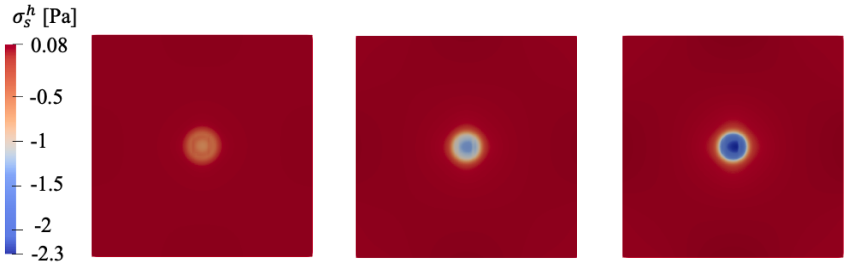

(a) Slow hydrostatic stress evolution at t=1,2,3 days. Compression increases at the center of the spheroid as it grows.

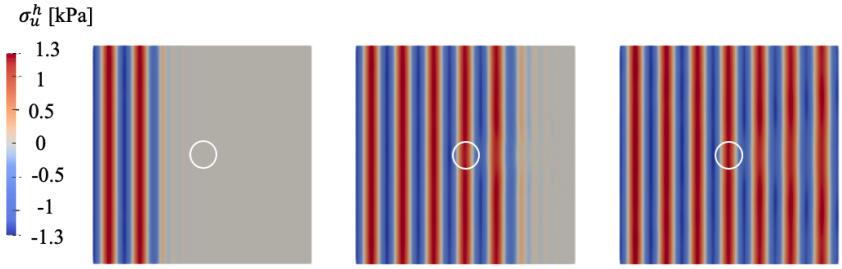

(b) Fast ultrasound stress before reach tumor spheroid, after and when stationary state is reached.

Figure 5.6: Hydrostatic stresses during growth.

mechanotransduction. According to simulations, the mechanotransduction function $\mathcal{M}_T$ remains spatially constant in the control culture since the total stress generated during the three-day growth remained well below the threshold stress of cells over a period of time.

On the other hand, the application of low-intensity ultrasound results in the formation of stress shadow areas due to tumor diffraction, leading to spatial heterogeneity of mechanotransduction (as shown in Figure 5.7). However, in our experiments, the stress shadow is not strong enough to cause any growth or migration patterns of the cells through pressure gradients towards areas of lower stress. Nevertheless, it is important to note that the development of such patterns in the tumor is possible with different parameters of sonication or mechanotransduction, as numerically suggested in the following section.

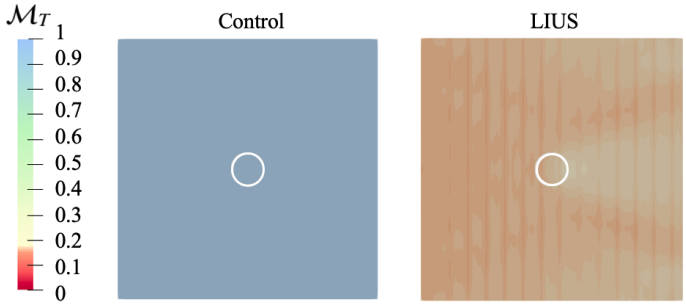

Figure 5.7: Mechanotransduction maps. Control culture exhibits constant mechanotransduction values in space, while dynamic LIUS hydrostatic stress causes shadow areas that are translated into patterns in mechanotransduction. The main parameters used for these simulations are $\alpha_{TT} = 2.9$, $\beta = 0.2$, $t = 3$ days. The key US parameters are $A = 1.35$kPa, $f = 5$MHz, $\eta_T = 2\text{Pa} \cdot \text{s}$ and $\eta_c = 0.05\text{Pa} \cdot \text{s}$.

Numerical results suggest that tumor cell proliferation is reduced when subjected to $f = 5$MHz sonication, as compared to control experiments and based on the mechanotransduction described. Figure 5.8 shows that the overall tumor phase decreases, which is more visible when the tumor cell phases are normalized along the y-axis.

Despite the lack of experimental cell count localization, it is feasible to estimate the total number of cells by integrating the tumor phase over space at a given time, i.e., $\int_A \phi_T(x, y, t) dA$, and compare it with the experimental findings. Indeed, the numerical simulations presented in this study closely replicate the initial experimental findings, as illustrated in Figure 5.9.

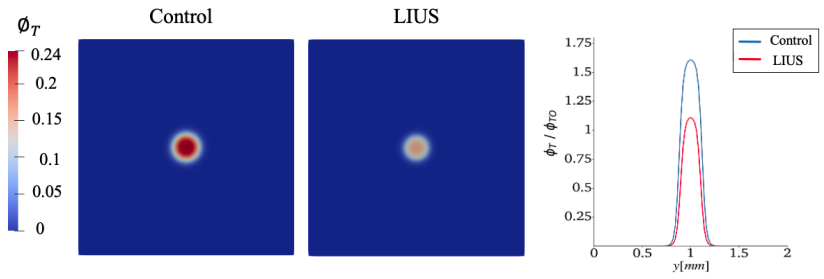

Figure 5.8: Computational simulations show a decrease in cell proliferation of sonicated cells. The main parameters used for these simulations are $\alpha_{TT} = 2.9$, $\beta = 0.2$, $t = 3$ days. The key US parameters are $A = 1.35$kPa, $f = 5$MHz, $\eta_T = 2\text{Pa} \cdot \text{s}$ and $\eta_c = 0.05\text{Pa} \cdot \text{s}$

Chapter 4 presents a sensitivity analysis of frequencies, amplitudes, and viscosities to investigate the behavior of the mechanical wave under different assumptions. The findings of the study are then utilized to explore how cells may respond to various sonication conditions through mechanotransduction.

It is important to note that the mechanotransduction parameters are adjusted for the reference experiment model, which has a frequency of 5 MHz, an acoustic pressure of 1.5 kPa, and viscosities $\eta_T = 2\text{Pa} \cdot \text{s}$ and $\eta_c = 0.05\text{Pa} \cdot \text{s}$. As such, the results presented below are based on these reference parameters.

Firstly, we investigate the dependence of acoustic pressure, as shown in Figure 5.10. Considering the reference acoustic pressure, higher amplitudes could lead to a greater decrease in proliferation, although the sensitivity limit of the cells is reached before the limit of perceived stress. Consequently, higher acoustic pressure would not result in substantial changes.

Notwithstanding, further increasing the acoustic pressure well above the limit could result in the extreme case of cytodisruption, where the maximum stress perceived by the cells is reached, leading to their destruction through phenomena such as cavitation or resonance.

On the other hand, reducing stress to 0.1 and 0.5kPa could lead to a lower growth rate compared to the control, as cells would continue to proliferate in regions with higher stress, while their growth would be hindered in areas that have reached the dynamic limit of sensitivity. Our analysis indicates that tumor proliferation could be diminished within a range of acoustic pressures between 0.5-3kPa at a frequency of 5MHz.

Figure 5.12 illustrates the parametric investigation of viscosity, which has

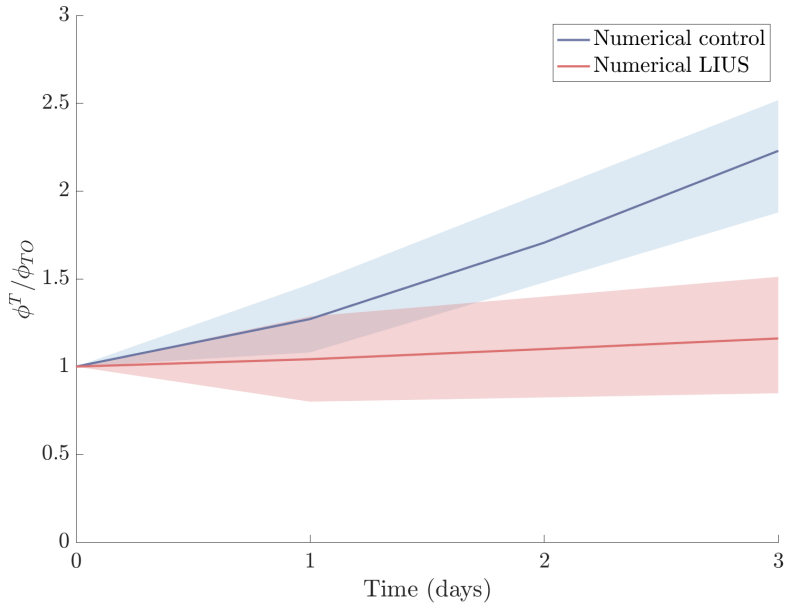

Figure 5.9: Computational model can reproduce in vitro experiments. Simulations suggest a reduction of cell viability for sonicated spheroids at frequency $f = 5$MHz, $A = 1.5$kPa, tumor viscosity $\eta_T = 2\text{Pa}\cdot\text{s}$ and culture medium viscosity $\eta_c = 0.05\text{Pa}\cdot\text{s}$. The shaded bands represent experiments while the solid lines denote numerical simulations. A change in trend is observed between control and sonicated cells, where cell proliferation decreases a 48% with the application of LIUS. The proliferation parameters used are $T_T = 0.58\cdot 10^{-5}\text{h}^{-1}$ at the first day, and $T_T = 0.77\cdot 10^{-5}\text{h}^{-1}$ from day one, while $\alpha_{TT} = 2.9$. Mechanotransduction parameters are $q_T = 0.05$, $b_T = 0.05$, $\beta_s = 0.2$, and $\sigma_{L_T} = 1.2$kPa.

been previously established to be directly proportional to wave attenuation. Specifically, when the tumor exhibits higher viscosity than its surrounding medium, and the medium viscosity is not too elevated, the intensity that reaches the tumor increases, resulting in more noticeable mechanotransduction effects. Additionally, a more viscous tumor will dissipate more energy, leading to more significant growth at the same acoustic pressures.

On the other hand, if the viscosity of the medium is higher than that of the tumor, the wave could potentially attenuate before reaching the tumor. This would result in tensions that are not significant enough to reduce proliferation.

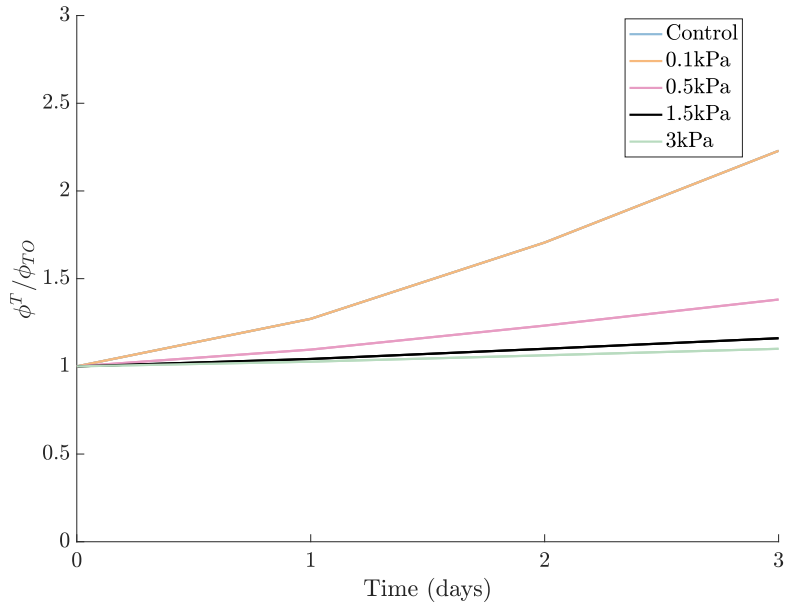

Figure 5.10: Acoustic pressure in growth. The increase of acoustic pressure reduces proliferation while low acoustic pressure may have not influence tumor duplication, as the A =0.1kPa, which overlaps with control. The main parameters used for these simulations are $f = 5$MHz, tumor viscosity $\eta_T = 2\text{Pa} \cdot \text{s}$ and culture medium viscosity $\eta_c = 0.05\text{Pa} \cdot \text{s}$. The proliferation parameters used are $T_T = 0.58 \cdot 10^{-5}\text{h}^{-1}$ at the first day, and $T_T = 0.77 \cdot 10^{-5}\text{h}^{-1}$ from day one, while $\alpha_{TT} = 2.9$. Mechanotransduction parameters are $q_T = 0.05$, $b_T = 0.05$, $\beta_s = 0.2$, and $\sigma_{L_T} = 1.2$kPa.

An example of this scenario could be when the viscosity of the medium is extremely high, such as 10Pa·s. As demonstrated in Chapter 4, Figure 5.12 reveals that high frequencies in viscous media are characterized by significant attenuation, leading to a higher amount of energy dissipation in the medium. Consequently, lower amplitudes and stresses can be expected, resulting in considerable tumor growth in comparison to the control at frequencies of 1MHz and 5MHz. These frequencies, when subjected to an acoustic pressure of 1.5kPa, generate stress fields comparable to the stress limit.

Remarkably, there are marginal differences between the frequencies of 1 MHz and 5 MHz, as both are capable of achieving the requisite amplitudes to achieve the stress limit. However, since the 1 MHz wave possesses much longer wavelengths, the mechanotransduction phenomenon is more likely to

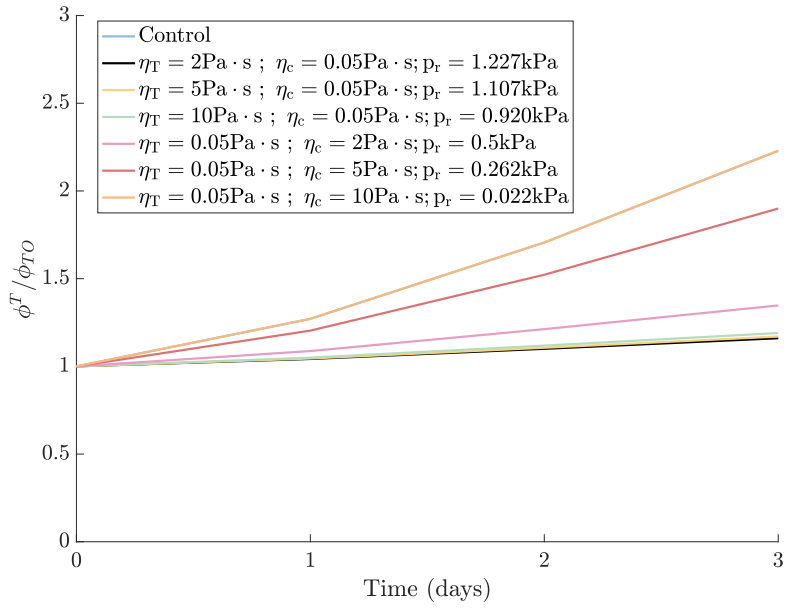

Figure 5.11: Viscosities in growth. The elevation of tumor viscosity results in greater stress shadow areas, thereby reducing proliferation rates. However, these shadows alone are insufficient to induce proliferation. When the viscosity of the surrounding medium increases, it leads to complete wave attenuation, which means that the acoustic pressures received by the cells are well below the stress threshold. As a consequence, the cells proliferate, even reaching values comparable to those of non-sonicated cells. The main parameters used for these simulations are $f = 5\text{MHz}$ and $A = 1.5\text{kPa}$. The proliferation parameters used are $T_T = 0.58 \cdot 10^{-5}\text{h}^{-1}$ at the first day, and $T_T = 0.77 \cdot 10^{-5}\text{h}^{-1}$ from day one, while $\alpha_{TT} = 2.9$. Mechanotransduction parameters are $q_T = 0.05$, $b_T = 0.05$, $\beta_s = 0.2$, and $\sigma_{L_T} = 1.2\text{kPa}$, $t = 3$ days.

result from shaking rather than wave penetration into the spheroid.

To achieve similar effects at f =20 MHz, assuming the same viscosity and mechanotransduction parameters, the acoustic pressure would need to be increased, resulting in higher intensity, as proposed in Figure 5.13, in which a frequency of f =20MHz and A = 5kPa decreases cell proliferation compared to A =1.5kPa. The interdependence of acoustic pressure, viscosity, and frequency parameters plays a crucial role in regulating the amplitude of the wave in a given domain, leading to the formation of heterogeneous stress fields

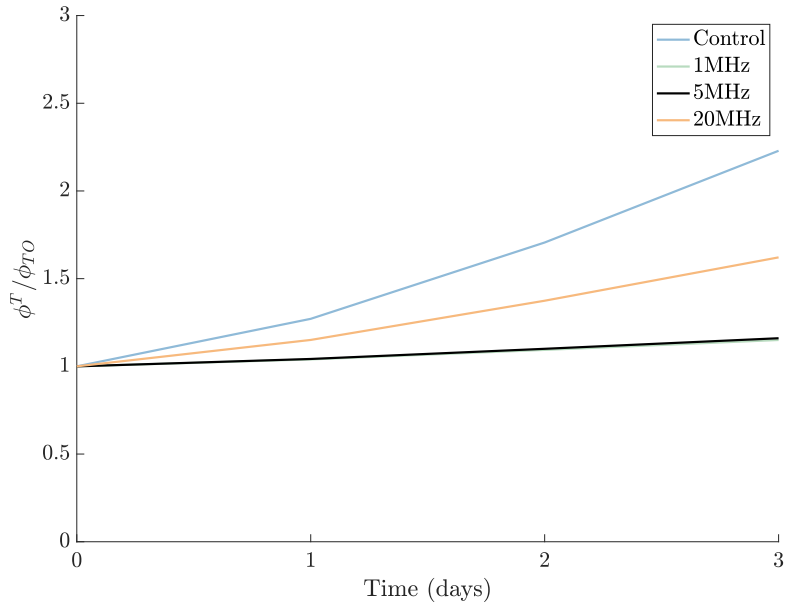

Figure 5.12: Frequencies in growth. High frequencies generate stress shadow areas in which cells can proliferate, whereas lower frequencies do not produce significant changes in the mechanical transduction, resulting in cells growing at similar rates and receiving acoustic pressures below the stress threshold. The main parameters used for these simulations are $A = 1.5$kPa, tumor viscosity $\eta_T = 2\text{Pa} \cdot \text{s}$ and culture medium viscosity $\eta_c = 0.05\text{Pa} \cdot \text{s}$. The proliferation parameters used are $T_T = 0.58 \cdot 10^{-5}\text{h}^{-1}$ at the first day, and $T_T = 0.77 \cdot 10^{-5}\text{h}^{-1}$ from day one, while $\alpha_{TT} = 2.9$. Mechanotransduction parameters are $q_T = 0.05$, $b_T = 0.05$, $\beta_s = 0.2$, and $\sigma_{L_T} = 1.2$kPa, $t = 3$ days.

that generate diverse mechanotransduction outcomes. The main findings are summarized in Table 5.2.

Specifically, our numerical simulations suggest that acoustic pressures of 1.5kPa can reduce proliferation rates by 46.6-48% when the frequency ranges between 1-5MHz, and for medium viscosity values of $\eta_c = 0.05\text{Pa} \cdot \text{s}$. For higher frequency values, such as 20 MHz, the acoustic pressure needs to be increased to 5kPa to achieve a decrease of 52.5%.

On the other hand, an increase in the viscosity of the medium leads to a corresponding increase in attenuation, which may limit the reduction in proliferation rates significantly, reaching values comparable to control

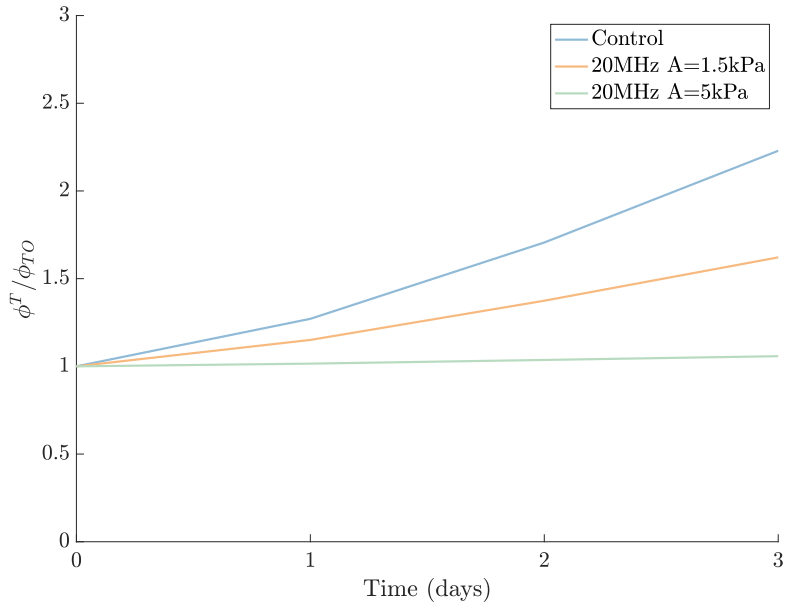

Figure 5.13: Frequencies and acoustic pressure in growth. High frequencies with high acoustic pressure could decrease duplication compared with lower acoustic pressures. The main parameters used for these simulations are tumor viscosity $\eta_T = 2\text{Pa} \cdot \text{s}$ and culture medium viscosity $\eta_c = 0.05\text{Pa} \cdot \text{s}$. The proliferation parameters used are $T_T = 0.58 \cdot 10^{-5}\text{h}^{-1}$ at the first day, and $T_T = 0.77 \cdot 10^{-5}\text{h}^{-1}$ from day one, while $\alpha_{TT} = 2.9$. Mechanotransduction parameters are $q_T = 0.05$, $b_T = 0.05$, $\beta_s = 0.2$, and $\sigma_{L_T} = 1.2\text{kPa}$, $t = 3$ days.

conditions (0-39.6% reduction compared to non-sonicated cells). In such cases, it would be necessary to increase the acoustic pressure if the medium is highly viscous.

Our findings are consistent with previous studies [154, 151, 156, 157, 158], which have reported at least a 50% reduction in proliferation rates compared to stress-free growth and a 30% increase in apoptotic cell activity with static tension values of 5-10kPa. Accordingly, our results lend support to the hypothesis that comparable reductions in proliferation rates can be attained through the application of lower dynamic stress.

Further studies exploring the coupling and interplay between these parameters can provide valuable insights into the mechanism of mechanotransduction

Table 5.2
Numerical results of LIUS therapy and proliferation reduction in comparison to the control group on the third day.

f [MHz]	A [kPa]	η_c[Pa · s]	η_T[Pa · s]	Proliferation decrease [%]
1	1.5	0.05	2	48.4
5	1.5	0.05	2	48
20	1.5	0.05	2	27.3
20	5	0.05	2	52.5
5	0.1	0.05	2	0.0
5	0.5	0.05	2	38.1
5	3	0.05	2	50.7
5	1.5	0.05	5	47.5
5	1.5	0.05	10	46.6
5	1.5	2	0.05	39.6
5	1.5	5	0.05	14.8
5	1.5	10	0.05	0.21

and its role in tumor growth and proliferation.

5.4.2 Selectively patterns in growth and migration

To evaluate the complete model, we propose to apply LIUS to a previously validated model [330]. For these simulations, we use all the equations described in Section 5.2 and the mechanotransduction parameters fitted to our experimental data.

We no longer evaluate the growth rate quantitatively but instead focus on the spatial and temporal distribution of tumor cells, considering the various phases mentioned earlier. This approach allows for a more comprehensive and nuanced understanding of the effects of mechanotransduction on tumor growth and proliferation, including the dynamics of spheroid formation and progression. Overall, this approach provides a more holistic view of the complex interplay between physical and biological factors in tumor growth and progression.

In these simulations, a tumor tissue with a radius of 3mm is considered, surrounded by healthy cells, extracellular matrix, and fluid phase. The tumor viscosity is assumed to be 5Pa · s, which is representative of the complex microenvironment in which tumors grow and interact.

5.4.2.1 Cross-diffusion

To explore the impact of flux in the tumor phase, we initially conduct simulations without incorporating ultrasound. We observe a cross-diffusion phenomenon in this scenario, as depicted in Figure 5.14. Tumor cells are able to move while healthy cells and extracellular matrix adjust their growth to respond to tumor motility, while they do not account for their own flux. In our modeling of this system, we adopt the parameters proposed in reference [330] and set the tumor phase diffusion coefficient to $D_T = 6 \cdot 10^{-12}\text{mm}^2\text{h}^{-1}$.

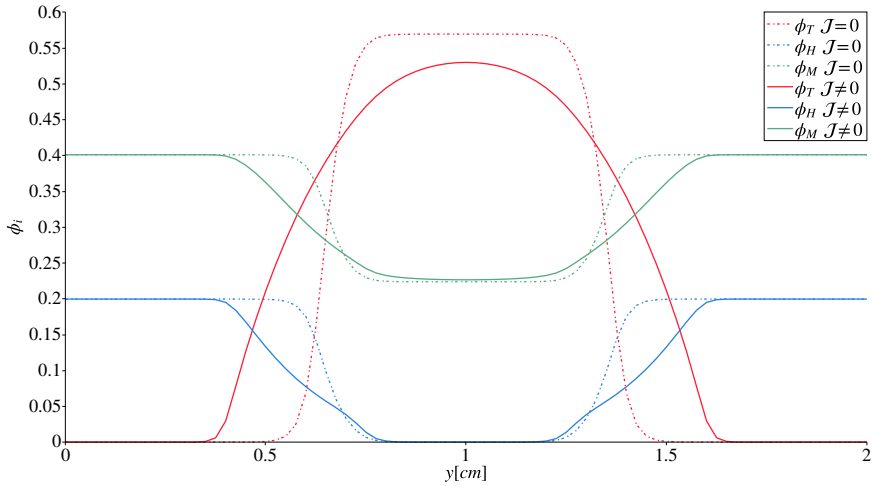

Figure 5.14: Cross-diffusion of cells phases. Non-linear flux facilitates the migration of the tumor phase, allowing cells to disperse in space, in contrast to immobilized cells with fixed support. This tumor diffusion process is then transmitted to other solid phases through a cross-diffusion effect. Dash lines refer to growth without flux, while solid lines refer to growth considering the flux of cells. In both cases, sonication is neglected. Results at time $t = 21$days.

5.4.2.2 Selective therapy and patterning

In this study, we aim to explore the feasibility of selectively modifying tumor cells through the application of ultrasound. Specifically, we utilize a frequency of 1MHz, which we have found to have similar effects as 5MHz for small spheroid dimensions when the same amplitude and viscosity are considered. However, for larger spheroid dimensions, the use of 1 MHz may be sufficient to induce mechanotransduction with similar parameters as previously indicated, while the wave dissipation with 5MHz may not reach the required limit stresses, leading to continued proliferation.

Simulation studies suggest that ultrasound does not exert a direct impact on the proliferation and production of healthy cells, for healthy cell mechanotransduction parameters of $\sigma_L \geq 10$kPa and β_s=0.2. The level of stress experienced by healthy cells is significantly lower than that experienced by tumor cells, indicating that ultrasound limits the stress on healthy cells to a greater extent than on tumor cells.

The growth of the tumor and healthy cells is interdependent due to predator-prey relations, and a decrease in the growth of tumor cells affects healthy cells but does not impact their net proliferation since the threshold for healthy cell proliferation is higher. It should be noted that the interaction of ultrasound with cells may lead to the remodeling of the extracellular matrix (ECM) structure.

In the absence of movement, the presence of zones with different stress levels may lead to instabilities. The tumor phase then grows by breaking the initial tumor symmetry, leading to a concentration of cells at points of lower stress, as depicted in Figure 5.15. This stress is transmitted to the ECM phase, which in turn deregulates its growth.

These observations shed light on why some experimental studies have reported the continued proliferation of cells. Tumor cells may proliferate in shadow zones where the threshold stress is heterogeneously reached, resulting in no significant difference in total cell count compared to the control. However, the spatial distribution of cells could be a critical factor for investigation.

Taken together, these findings suggest that ultrasound may selectively affect health cells more than on tumor cells. Nevertheless, the interplay between the growth of tumors and healthy cells could influence their spatial distribution, emphasizing the importance of further investigation in this regard.

If migration is allowed, a similar effect to that observed in Chapter 3 occurs, where migration dissipates and homogenizes differences in growth or stress. This is supported by the findings of [78, 77], where a decrease in migration was observed compared with non-sonicated cells. Furthermore, tumor cells migrate in a predetermined direction while regulating growth internally.

In particular, cells leading in areas of lower stress may be able to incentivize migration. Cells could use cytonemes to sense the stress state of their environment and respond accordingly, for example by extending cytonemes towards stiffer regions or retracting them from areas of high stress.

These results suggest that allowing for migration can impact the distribution of cells and may be an important factor to consider in the regulation of growth and stress. These findings also highlight the importance of understanding

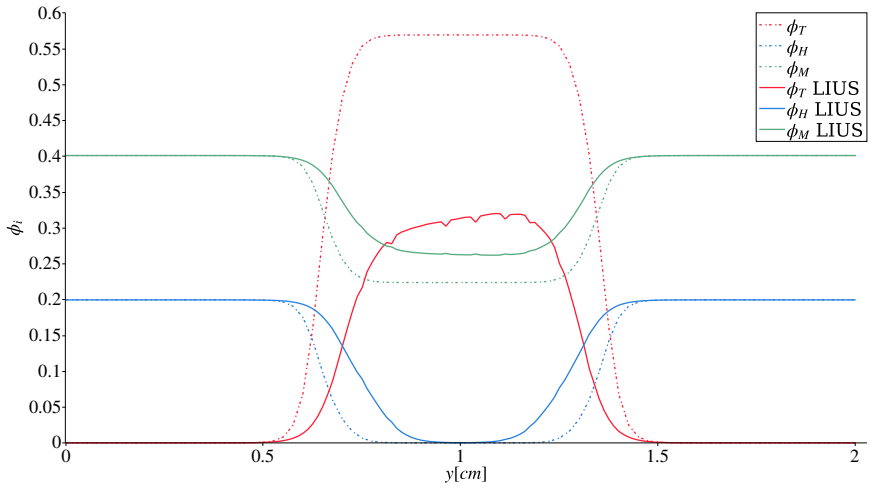

Figure 5.15: Patterns in growth. LIUS selectively reduces the proliferation of the tumor cell phase, causing patterns in low-stress areas that translate to the ECM phase while the healthy phase remains unaltered. Dash lines refer to growth without sonication and considering the null flux of cells, while solid lines refer to sonicated tumor phase with the null flux of cells. The used parameters are $f = 1$MHz, $A = 1.5kPa$, and $\eta_T = 5$Pa·s. Results at time $t = 21$days.

the role of mechanical parameters in these processes. Further investigation is needed to fully understand the complex interplay between migration, growth, stress, and cytoneme signaling in the context of ultrasound therapy.

Theoretically, it is possible for cells to evade apoptosis or quiescence by migrating through areas of lower stress. This phenomenon could be opposite to durotaxis, where cells move towards areas of higher pressure gradients. In fact, if the tumor viscosity increases to $10\text{Pa} \cdot \text{s}$ or if the higher frequency and acoustic pressure are applied, the resulting patterns and effects would be more pronounced. In the following section, we demonstrate the evolution of tumor cells, fluid pressure, and both fast and slow stresses over time with a sonication of $f = 1$MHz and an acoustic pressure of $A =$1.5 kPa.

Our findings suggest that significant differences in perceived limit stress between different areas of the tumor can lead to distinct growth phases during tumor evolution. In Figure 5.17, we present the results when migration is not allowed, while Figure 5.18 shows the effects of natural cell movement. As expected, the cells tend to concentrate in areas of lower stress, with the ECM responding by adjusting to the tumor cells, while healthy cells occupy

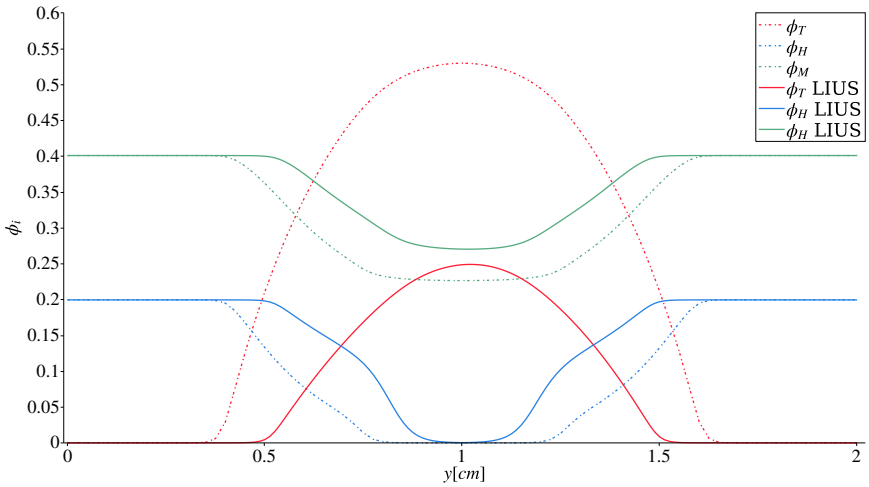

Figure 5.16: Patterns in migration. LIUS inhibits migration, while flux disperses the patterns that LIUS causes in the tumor cell phase. Dash lines refer to growth without sonication and considering the flux of cells, while solid lines refer to sonicated tumor phase with the flux of cells. The used parameters are $f = 1$MHz, $A = 1.5$kPa, and $\eta_T = 5$Pa·s. Results at time $t = 21$days.

the space left by the tumor cells.

Interstitial fluid pressure is known to increase with the tumor cell phase, resulting in a break in the symmetry of pressure. This pressure gradient may lead to the compression of blood vessels and hinder the delivery of oxygen and nutrients to tumor cells, leading to hypoxia and starvation in some areas. As the tumor grows and expands, the fluid pressure effects become more pronounced in the direction of its progression.

The existence of cell mobility amplifies the diffusion of tumor cells and directed migration, leading to a decrease in the total cell concentration but an increase in dispersion, which allows for stress dissipation and reduces the prominent elevation in interstitial pressure seen when migration is neglected.

Similarly, the slow stress generated by the tumor also shows a quantitative increase, although it is lower than in the case of only growth. The compression is more pronounced in the direction of tumor expansion, which is the preferred direction of migration. Meanwhile, the core exhibits tensile stress, which decreases over time.

For the purpose of illustration, we demonstrate the capacity of a higher

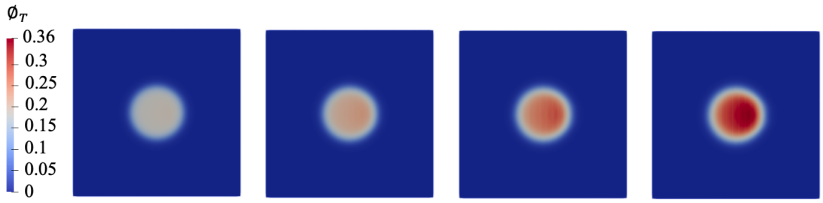

(a) Tumor phase growth creates pattern in response to the ultrasound direction of propagation.

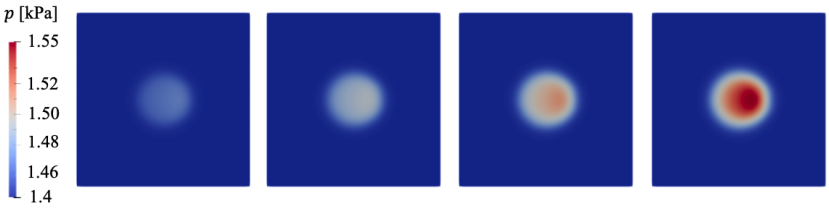

(b) Fluid pressure increase as a tumor phase function.

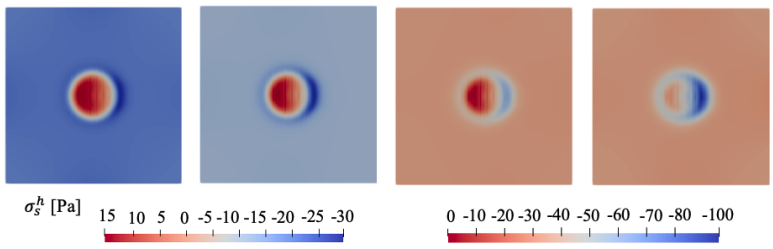

(c) Slow hydrostatic stress responds to ultrasound creating compression patterns in the direction of wave propagation.

Figure 5.17: Tumor phase, fluid pressure, and slow-stress evolution during sonication at $f = 1$MHz. The main parameters used for these simulations are $\eta_T = 10\text{Pa} \cdot \text{s}$, $f = 1\text{MHz}$, $A = 1.5\text{kPa}$. Results are shown for t=5,10,15 and 21 days.

(a) Migration dissipates non-homogeneous patterns inside tumor spheroid, although the migration gradient of the cells moves towards the propagation direction of the ultrasound.

(b) Migration dissipates the areas of higher fluid pressure accumulation compared with non-migration studies.

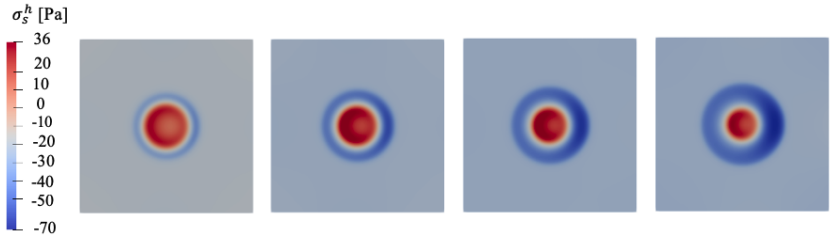

(c) Slow hydrostatic stress responds to ultrasound creating compression patterns in the direction of wave propagation, but they are mitigated compared with non-migration studies.

Figure 5.18: Tumor phase, fluid pressure, and slow-stress evolution during sonication with migration at $f = 1$MHz. The main parameters used for these simulations are $\eta_T = 10\text{Pa}\cdot\text{s}$, $f = 1\text{MHz}$, A =1.5kPa, and $D_T = 6\cdot 10^{-12}\text{mm}^2\text{h}^{-1}$. Results are shown for t=5,10,15 and 21 days.

frequency of $f = 5$ MHz and a viscosity of $\eta_T = 10\text{Pa} \cdot \text{s}$ to induce significant wave attenuations, leading to unrestricted growth in shadow zones. Consequently, proliferation and migration attain counts that approach those of the control, despite exhibiting completely distinct growth patterns. Specifically, proliferation continues to escalate in shadow zones while being impeded in close proximity to the ultrasound, resulting in discernible patterns in the direction of propagation, as demonstrated in Figure 5.19. Moreover, as previously observed, migration effectively dissipates the build-up of cellular and stress-related accumulations, albeit a predominant migration direction still prevails, as depicted in Figure 5.20.

To conclude our findings, we present the displacement of the center of gravity of the tumoral phase in the three numerically studied cases. Figure 5.21 demonstrates that, for the cases with f =1MHz, the center of gravity shifts 1% in the direction of propagation when considering η_T=5Pa $\cdot$ s, and 2-3% when η_T=10Pa $\cdot$ s, compared to the growth of the control without ultrasound applied. Additionally, the center of mass of the tumoral phase decreases by 10-16%. For $f = 5$MHz, the tumoral phase decrease is much less noticeable (1%), although the center of gravity shifts by 3-4% compared to the control.

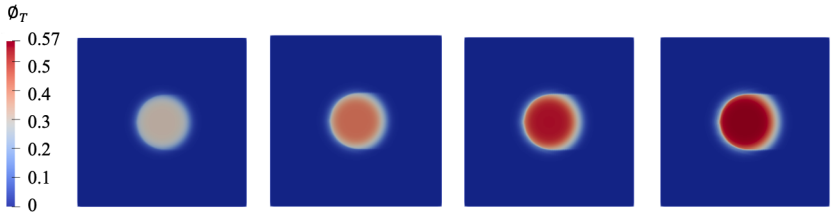

(a) Tumor phase growth creates pattern in response to the ultrasound direction of propagation.

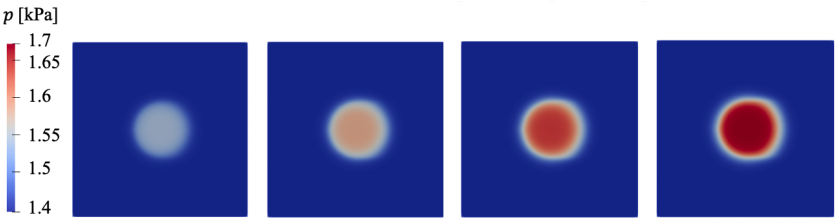

(b) Fluid pressure increase as a tumor phase function.

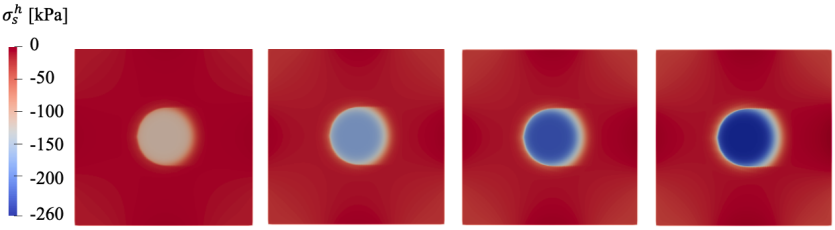

(c) Slow hydrostatic stress responds to ultrasound creating compression patterns in the direction of wave propagation.

Figure 5.19: Tumor phase, fluid pressure, and slow-stress evolution during sonication at $f = 5$MHz. The main parameters used for these simulations are $\eta_T = 10\text{Pa} \cdot \text{s}$, $f = 5\text{MHz}$, $A = 1.5\text{kPa}$. Results are shown for t=5,10,15 and 21 days.

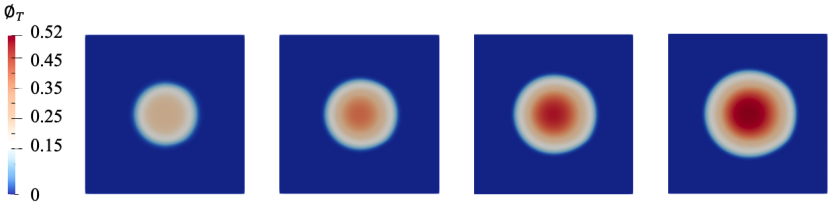

(a) Migration dissipates non-homogeneous patterns inside tumor spheroid, although the migration gradient of the cells moves towards the propagation direction of the ultrasound

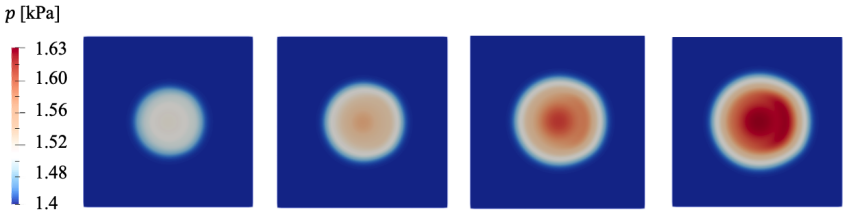

(b) Migration dissipates the areas of higher fluid pressure accumulation compared with non-migration studies.

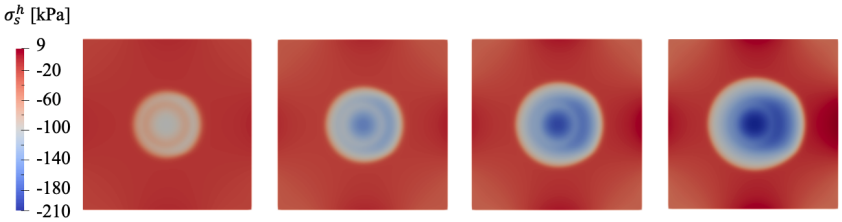

(c) Slow hydrostatic stress responds to ultrasound creating compression patterns in the direction of wave propagation, but they are mitigated compared with non-migration studies.

Figure 5.20: Tumor phase, fluid pressure, and slow-stress evolution during sonication with migration at $f = 5$MHz. The main parameters used for these simulations are $\eta_T = 10\text{Pa} \cdot \text{s}$, $f = 5\text{MHz}$, A =1.5kPa, and $D_T = 6 \cdot 10^{-12}\text{mm}^2\text{h}^{-1}$. Results are shown for t=5,10,15 and 21 days.

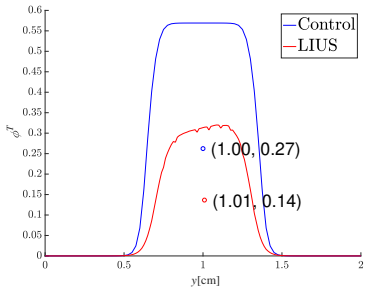

(a) $f = 1$MHz, η_T=5Pa · s, $\mathcal{J} = 0$.

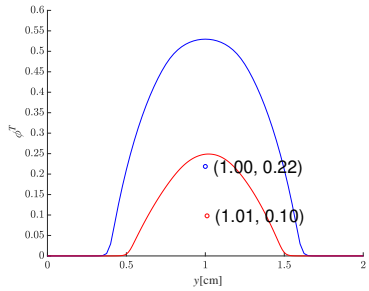

(b) $f = 1$MHz, η_T=5Pa · s, $\mathcal{J} \neq 0$.

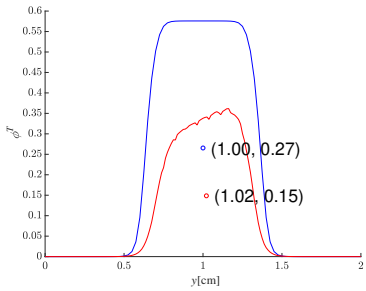

(c) $f = 1$MHz, η_T=10Pa · s, $\mathcal{J} = 0$.

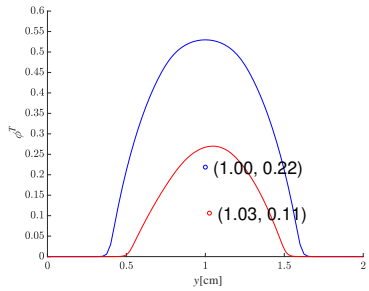

(d) $f = 1$MHz, η_T=10Pa · s, $\mathcal{J} \neq 0$.

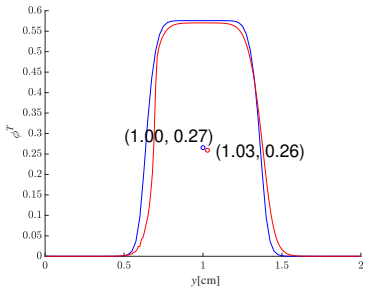

(e) $f = 5$MHz, η_T=10Pa · s, $\mathcal{J} = 0$.

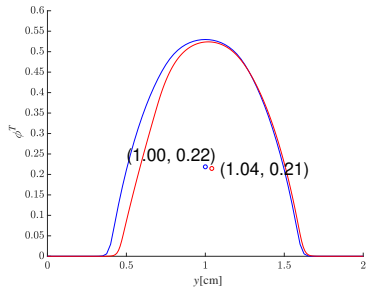

(f) $f = 5$MHz, η_T=10Pa · s, $\mathcal{J} \neq 0$.

Figure 5.21: Displacement of the center of gravity in the wave propagation direction. The first coordinate indicates the position of the center of gravity along the y-axis, while the second coordinate of the point refers to the tumoral phase.

5.5 Conclusions

We have proposed a novel multiscale model that can accurately reproduce the effects of LIUS mechanotherapy on cancer cells at the in-vitro level. The non-thermal nature of our proposed ultrasonic bio-effects allows for a less aggressive treatment of unconfined tumors, and in particular to directly target and remove CSCs responsible for tumor development and recurrence while inhibiting metastasis.

The presented model of mechanotransduction affords a precise and quantifiable account of the differential thresholds between dynamic and static stimulation. This circumvents the need for arbitrary and ad-hoc relationships, such as the calculation of the root mean square of ultrasonic stress, to explain the observed disparities.

Our preliminary experiments with therapeutic ultrasound suggest that CSC growth can be inhibited by using 5MHz and pressure amplitudes of more than 1.5kPa. This provides a starting point for further investigation in this area, potentially leading to new treatment options for cancer, suggesting that cancer cells are more sensitive to ultrasound-induced tension than static stress.

In addition, our model can predict the effects of LIUS therapy at different frequencies and acoustic pressures. Our preliminary research provides insight into acoustic pressure as the key parameter in selective therapy for tumor cells, patterns in growth, and thus computational modeling to aid in decision-making.

We have identified the importance of surpassing stress limits in all tumor zones to prevent the existence of preferred zones of growth and migration, highly undesired in therapy while keeping the safety limits.

Numerical results from our model suggest that the proliferation of healthy cells remains selectively activated while tumor cells undergo apoptosis, allowing for modeling selective therapy and that tumor cell migration regulates redistribution of the other solid components by the cross-diffusion process.

Our findings demonstrate that higher frequency ultrasound combined with differences in viscosity can induce patterning in both proliferation and migration, resulting in a break in the initial symmetry or isotropy of the model and displacing the center of gravity of tumor cell phase in the direction of wave propagation. These patterns not only impact growth, but also compressional stress-driven growth and interstitial fluid pressure, which increase the direction of tumor propagation and potentially lead to hypoxia and nutrient deprivation. Our results also suggest that migration plays an important role

in dissipating both growth and interstitial fluid stresses.

The multiscale model proposed provides a promising approach to exploring the effects of LIUS mechanotherapy on cancer cells. With further development and experimentation, this approach could offer a less aggressive, more effective, and cost-efficient treatment option for cancer.

Moving forward, it is necessary to fully elucidate the underlying mechanisms and develop targeted interventions that effectively disrupt tumor growth and progression while minimizing adverse effects on surrounding healthy tissue. Additionally, our model does not account for the remodeling of extracellular matrix (ECM) or proteins, which may be an important consideration for future modeling efforts. It should also be noted that our results are based on reconstructed mechanotransduction parameters, and different parameters could trigger more abrupt responses.

In summary, our multiscale model provides a promising approach for exploring the effects of LIUS mechanotherapy on cancer cells. With further development and experimentation, this approach could provide a novel complement treatment option for cancer that is less aggressive, more effective, and more cost-efficient than current therapies.

Part III

DISCUSSION AND CONCLUSIONS

Chapter 6

Discussion

In this dissertation, we have synthesized various mechanobiology approaches that have emerged in recent years, encompassing both biological and mechanical perspectives within the framework of continuum mechanics. The comprehensive background review covers the main hypotheses underlying mechanotransduction, the essential features of the theory governing growth modeling from mechanics, the equations that govern tumor behavior, the highlights of LIUS therapy, and the framework of wave propagation in soft tissues.

Following the literature review, we have identified several potential contributions, including investigating the interplay between non-homogeneous growth and migration, and the growing demand for innovative technological and computational tools that facilitate a deeper understanding of tumor evolution. Im we have highlighted the potential use of low-intensity ultrasound to target cancer stem cells.

This thesis proposes three computational models that enhance the understanding of mechanobiology and mechanotransduction by examining tumor dynamics in response to mechanical forces, as well as the effects of mechanotherapy on tumor development.

In summary, the first proposal investigates the competition between migration, proliferation, and mutations, which results in non-homogeneous volume changes that generate stresses that modify tumor evolution. The set of equations consists of coupled stress-growth equations with a migration term.

This study highlights, firstly, the need to use nonlinear flows to describe tumor migration, in contrast to the linear flows frequently used in mechanically-based growth approaches [89, 90]. This need arises from the requirement to control the velocity and front of migration, which is lost in linear flows, as observed for different scenarios in Figure 3.3, and as established in the literature [307, 308, 309, 310, 311, 312].

In particular, the saturated nonlinear flow controls the propagation front's advance through a biological parameter of finite velocity. Furthermore, the

porosity parameter m modifies the propagation front's speed, decreasing it as m increases, as depicted in Figure 3.4.

However, the need to preserve the tumor propagation front and avoid numerical noise from the saturated flow calls for high approximation orders. To obtain this requirement, we utilize the Weighted Non-Oscillatory method (WENO), which aims to achieve high-order accuracy by blending multiple low-order numerical approximations through the use of weights. Smoothness indicators are calculated for each approximation and are then used to determine the weights. The final solution is obtained by taking a combination of the weighted approximations [310, 384]. Thus, the WENO method provides accurate high-order stability resolution while maintaining non-oscillatory, stable, and sharp discontinuity transition

On the other hand, small changes in growth generate mechanical feedback that may lead to instabilities, as theoretically proposed in references [55, 57] and numerically demonstrated in this study, as shown in Figures 3.5 and 3.6. Furthermore, allowing for controlled cellular movement within the tumor can dissipate these stresses and regulate growth, as indicated in Figures 3.7 and 3.8.

To control this regulation, the use of the saturated non-linear flow is considered appropriate in this study. However, in cases where instabilities resulting from non-uniform growth are not a concern, it can be simplified to a non-linear flow to reduce computational complexity and cost, as we have done in the subsequent study.

Once these phenomena are studied, we have considered the effect of mechanotherapy on tumor dynamics by analyzing the ultrasound propagation in a spheroid embedded in a culture medium using a Kelvin-Voigt viscoelastic constitutive equation [365, 366, 367, 368]. We have performed a sensibility analysis including a range of frequencies of $f = [1 - 20]$MHz, acoustic pressures of $A = [0.1 - 5]$ kPa, and viscosities of η_i =[0-10]Pa·s, being i the culture medium c or tumor viscosities T. The set of equations has been solved in finite elements considering two dimensions.

Based on the propagation model, we have observed that higher viscosity of tumor tissue results in shadow zones behind the tumor spheroid, where wave energy dissipates due to the viscosity of the tumor spheroid. It is important to note that this effect could potentially be even more pronounced if the problem were considered in three dimensions.

Acoustic pressure plays a significant role in the efficacy and safety of LIUS treatments. Excessive acoustic pressure can trigger cavitation and heating

effects, leading to mechanical disruption of tissues and irreversible damage. In contrast, inadequate acoustic pressure may not produce the desired therapeutic effects, allowing cells to proliferate and migrate to regions with lower stress levels.

In addition to acoustic pressure, selecting the appropriate frequency for LIUS is necessary to achieve optimal therapeutic outcomes, such as apoptosis or quiescence in cancer treatments. The frequency choice depends on various factors, including target tissue geometry, medium properties, and desired intensity. Lower frequencies penetrate deeper into tissues, making them ideal for treatments targeting structures located deeper in the body. However, as the frequency increases, the wave energy is increasingly absorbed and dissipated, resulting in greater weakening of the wave. The degree of absorption depends on the properties of the medium through which the wave propagates, such as its viscosity.

Although the optimal acoustic pressure depends on the specific cell type, our findings suggest that dynamic hydrostatic stresses within the range examined could be sufficient to inhibit spheroid growth, and acoustic pressures greater than $A = 1.5\text{kPa}$ may be effective for the stated frequency.

Finally, we propose a multiscale model that integrates the effects of mechanical waves on tumor development through mechanotransduction. The proposal is based on equations grounded on Finite Growth Theory considering small deformations, similar to other studies [84, 330, 89, 90, 332, 92]. We have solved the model using Finite Elements in two dimension.

The multiscale system includes coupled stress-growth equations and two main timescales: a fast-scale where waves propagate and mechanotransduction occurs, and a slow-scale where tumor cells proliferate, migrate, and adapt to the microenvironment. The microenvironment is modeled as a poroelastic medium composed of solid components, including tumor cells, healthy cells, and ECM, as well as fluid phases.

In contrast to studies based on cytodisruption, [70, 71, 72, 73, 74], our idea of LIUS therapy is based on the triggered response of cells via mechanotransduction, where proliferation is partially inhibited [73, 74, 75, 76, 77, 78, 79, 80].

The hypothesis is that dynamic pressure is more effective in generating a cellular response than static stress due to the complex mechanisms of stress redistribution involving the cytoskeleton and interstitial fluid flow through pores. The mechanotransduction coupling function, described in equations 5.2.16 and 5.2.17 is based on functions of mechanotransduction described and validated in literature [151, 186, 321, 324, 322, 84, 343, 84,

330, 89, 90, 332, 92].

The contribution to the function of mechanotransduction is to add the difference in threshold between dynamic and static stimulation, without requiring ad-hoc relationships while providing a quantitative explanation for the observed differences. Thus, the function of mechanotransduction is defined in an ultrasonic time period in which cell mechanosensors could receive signaling linked to the cytoskeleton network extremely quickly [218, 219], and then respond triggering changes in proliferation and migration, as proposed in [224, 218].

In order to generate similar intensities to those reported in the literature, and to avoid possible cavitation phenomena, we have exceeded the frequencies and increased the acoustic pressure, as compared to current studies whose parameters are shown in Table 2.3.

Thus, we propose to experimentally sonicate melanoma A-375 cancer stem cells at a frequency of $f = 5$MHz and amplitudes ranging from $A = [1.5 - 15.5]$kPa, assuming a tumor viscosity of $\eta_T = 2\text{Pa} \cdot \text{s}$ and a culture medium viscosity of $\eta_c = 0.05\text{Pa} \cdot \text{s}$, in line with the viscosity ranges established in the literature [391, 392, 393, 205, 394, 213, 395].

The preliminary experiment indicates that the proliferation of melanoma cancer stem cells is inhibited by a percentage of change of 48% when sonicated at a frequency of $f = 5$MHz, which supports the feasibility of LIUS as a treatment, given that CSCs are currently resistant to conventional therapies [32, 33, 34, 34].

A simplified multiscale computational model can accurately reproduce this observed phenomenon for given mechanotransduction parameters, as shown in Figure 5.9.

These findings are consistent with previous studies [154, 151, 156, 157, 158, 84, 330], which have reported a 50% reduction in proliferation rates compared to stress-free growth and a 30% increase in apoptotic cell activity with static tension values of 1-10kPa. Accordingly, the results lend support to the hypothesis that comparable reductions in proliferation rates can be achieved through the application of lower dynamic stress.

Moreover, these results provide predictions for both the growth and stress and deformation states of the medium and spheroid. Specifically, we observed growing compressive stress in the core regions, as proposed by previous studies [147, 45, 166]. Additionally, the study also points out that the compressional state increases over time.

We have considered various scenarios where the fate of the tumor spheroid is differently affected by stress, and we have performed a parametric analysis of the effect of ultrasound on mechanotransduction, as summarized in Table 5.2.

The numerical simulations indicate that acoustic pressures of 1.5kPa may reduce proliferation rates by 46.6-48.4% when the frequency ranges between 1-5MHz, and for medium viscosity values of $\eta_c = 0.05\text{Pa} \cdot \text{s}$. For higher frequency values, such as 20 MHz, the acoustic pressure needs to be increased to 5kPa to achieve a decrease of 52.5%.

On the other hand, an increase in the viscosity of the medium leads to a corresponding increase in attenuation, which may limit the reduction in proliferation rates significantly, reaching values comparable to control conditions (0-39.6% reduction compared to control). In such cases, it would be necessary to increase the acoustic pressure if the medium is highly viscous.

Then, we studied the full multiscale system considering all solid phases and the migration of the tumor phase. This research indicates that therapeutic ultrasound not only suppresses tumor cell proliferation but also hinders their migration, which is in agreement with experimental results obtained by references [78, 77]. Moreover, the inclusion of migration to the tumoral phase in the model results in a cross-diffusion process, where the tumor cells move through the different phases and interact through a predator-prey scheme. This leads to competition between different tumor phases, and the migration of one phase propagates to the other phases.

The selective mechanotherapy function proposes that healthy cell proliferation remains unaffected due to their higher sensitivity threshold, while decreasing the tumor phase may increase the role of healthy cells due to the predator-prey system. This provides a potential strategy for selectively targeting cancer cells while preserving healthy tissue as reported in [70, 75, 73].

This preliminary research proposes that ultrasound may generate patterning in proliferation and migration, breaking the initial symmetry of the system based on the applied stress and cell sensitivity ranges, as experimentally studied in reference [73] and numerically corroborated in Figure 5.17 and 5.18. Furthermore, the results suggest that diffusion dampens slow stress, homogenizing the response of the tumor to the environment, as also pointed out in Chapter 3, but preserving migration towards areas of lower stress.

In particular, these models can describe the displacement of the center of gravity of the tumor, which, although does not reach large values in our study (1-4%), could increase with different parameters and geometries. Indeed, they can be used to propose different angles of sonication in order to avoid

directed migration to conflictive areas. Consequently, this approach allows for the optimization of therapeutic strategies, by analyzing and designing more precise and effective setups.

Interstitial fluid pressure increases with tumor growth. Under normal conditions, the IFP is heterogeneous, with higher values in the core and lower values at the borders [189, 45], in the order of kPa. On this basis, this thesis predicts the breakage of the stress symmetry since there are pressure gradients in the direction of ultrasonic propagation, as observed in Figure 5.17 and 5.18.

Finally, it is deduced that although the tumor initially grows by mass effect, the application of ultrasound generates compressive and rarefactive stresses which induce compressive stress states in the cells. This, in turn, leads to partial inhibition of proliferation and migration, depending on the ultrasound pressure gradients.

However, this thesis has some limitations. Tissue hyperelasticity has not been accounted for, and mechanical and biological properties have been relied upon from literature as a successful indentation or speed-camera-controlled experiments have not been conducted.

Although preliminary experiments in Chapter 5 have been numerically reproduced, the number of experiments is low due to the stochasticity and high experimental cost associated with CSC culture, and this dissertation mainly remains within the computational framework.

Therefore, further experiments at longer times are required to evaluate different computational responses, refine the models for improved accuracy, and determine the optimal use of frequency and acoustic pressure depending on the viscoelasticity of the medium. Furthermore, we have assumed viscoelasticity based on Kelvin-Voigt equations in propagation, and there is a need for a sensitivity analysis that accounts for the plausibility of the chosen constitutive equation.

Additionally, the mechanotransduction pathways of proteins have not been incorporated into our proposal, as they have not been experimentally validated. Instead, mechanotransduction has been applied directly to the duplication or diffusion ratio, even though cellular responses are triggered by proteins. We have neither considered the effect of co-therapies.

Finally, this study is a preliminary numerical approach to the mechanobiology and ultrasonic mechanotherapy of in vitro spheroids. The simple geometries used have not accounted for more complex formations, which may exhibit additional phenomena such as scattering. To create a more realistic in vivo

scenario, these phenomena and their associated patterns would need to be considered.

Chapter 7

Conclusions

With experimental costs remaining high and biological processes exhibiting significant stochasticity, mathematical oncology offers valuable insights and aid in the development of effective treatment strategies and understanding of tumor behavior. The importance of new cancer therapies, particularly low-intensity ultrasound, and the need for computational tools and technologies that can target cancer stem cells that are resistant to current therapies have been emphasized in this study.

In this context, this thesis represents an interdisciplinary investigation of mechanobiology in cancer. The specific contributions of this thesis are summarized as follows:

- **Non-linear saturated flux controls the biological speed of the invasion front**, while linear flux leads to an infinite speed of propagation, and non-linear fluxes keep the stability of the front. Furthermore, the porosity parameter m regulates the speed of migration, decreasing it while m increases.
- **Variations in growth may lead to instabilities that act as retrograde diffusion** in competition with proliferation due to the mechanical feedback.
- **Cell migration can avoid instabilities and dissipate abrupt changes** of non-homogeneous stress-driven growth.
- **Low-pressure and high frequencies acoustic waves stimulate signaling** while maintaining low intensity to trigger growth and migration inhibition while avoiding cytodisruption.
- **Acoustic pressure is the dominant parameter in mechanotransduction**. Low acoustic pressures may not be sufficient to alter tumor fate. However, once a threshold stress level is surpassed, further increases in acoustic pressure may not be necessary to induce signaling, while excessive levels of acoustic pressure could lead to the limit of cell disruption.

- **The interdependent parameters of acoustic pressure, viscosity, and frequency can be tuned to optimize the selectivity of therapeutic applications**. The energy dissipation increases with viscosity, and frequency selection is influenced by tumor size. Low-frequency waves generate longer wavelengths, resulting in tumor shaking. In contrast, high-frequency waves may interact with the components of the cells. The proposed computational model reduces the need for experimental testing of different mechanical parameter configurations, including transducer placement, angle of sonication, geometries, and tissue layers.
- **The proposed mechanotransduction function provides a quantitative explanation for the observed differences in the threshold between dynamic and static stimulation** without requiring ad-hoc relationships.
- **Dynamic pressure is more effective than static stress in generating a cellular response**, and it has been numerically and experimentally validated, as evidenced by the ability to achieve similar reductions in proliferation rates at 1.5kPa (46.6-48.4%).
- **Cancer stem cells growth can be inhibited in by using 5MHz and an acoustic pressures greater than 1.5kPa**, as suggested by the preliminary experiment of therapeutic ultrasound.
- **The migratory behavior of the tumor phase leads to a cross-diffusion process**, where the movement is propagated to other solid phases via a predator-prey interaction scheme.
- **Healthy cell proliferation remains selectively unaffected by LIUS** due to their higher sensitivity threshold, while the reduction of the tumor cell burden through LIUS may increase the role of healthy cells in the predator-prey system.
- **Ultrasound can generate patterning in proliferation and migration**, breaking the initial symmetry of the system and thus displacing the center of gravity of the tumor cells to areas of lower acoustic pressure.
- **Interstitial fluid pressure adapts to ultrasound patterns**, increasing in the direction of propagation due to the concentration of tumor cells. Furthermore, compressional slow stress increases over time.
- **Therapeutic ultrasound hinders cell migration**. In addition, migration dampens slow stress and fluid pressure homogenizing the response of the tumor to the environment.

Chapter 8

Ongoing and future work

Considering Chapter 3, some broad opportunities start with the analysis of this model. Specifically, it is possible to incorporate the aforementioned Brinkman's law and perform analytical studies on the qualitative aspects of the solutions (oscillations or non-convexification of shape in density, among others). In a short time, we are also interested in incorporating the biochemical interactions, which will modulate both growth and cell adhesion properties.

Regarding Chapters 4 and 5, the present study does not comprehensively describe the complex protein interactions that regulate the signaling pathways associated with cell proliferation and migration. Thus, to elucidate the specific molecular mechanisms underlying the observed changes in cellular behavior, future studies could incorporate a proteomic analysis. Such analysis would provide valuable insights into the altered signaling pathways and protein expression patterns that promote the decrease in cell proliferation observed in this study. Furthermore, nutrient consumption and hypoxia should also be taken into account.

In the short term, it is essential to incorporate the effect of chemotherapy into the models to aid in the determination of optimal drug and ultrasound doses, as well as mechanical parameters, for an effective treatment that minimizes collateral effects. For instance, we could numerically investigate the effect of combining some dose of chemotherapy with non-continuous ultrasound application, where we apply ultrasound for a few hours per day and allow proliferation without ultrasound for the remaining hours. By systematically varying these parameters, we can determine the optimal treatment regimen that maximizes treatment efficacy.

In addition to longitudinal mechanical waves, our group is also investigating the potential of shear waves. Within the numerical framework of this thesis, we can modify initial conditions, frequency ranges, and the associated mechanotransduction function, which would now be dependent on Von Mises or Tresca stress to account for shear components. With this study, we could compare the effects of shear waves with LIUS to investigate how the cell

sensitivity parameters change when the nature of the stress source is modified.

In addition, we have simulated the tumor as a viscoelastic material at the ultrasonic scale. While dynamic poroelasticity has primarily been studied in the context of bone tissue and earthquake engineering, we are striving to incorporate dynamic poroelasticity into wave propagation modeling to examine the different response patterns in comparison to viscoelastic propagation. In this regard, the fluid phase would be assumed to mainly absorb the stress.

Dynamic poroelasticity follows Biot principles and its equations are more complex than static poroelasticity [403, 404, 325, 405]. When considering both solid and fluid phases, two compression waves are obtained, one fast wave and one slow wave, and a third shear wave. In soft tissues, in which the solid phase lacks high stiffness, the wave tends to travel faster through the fluid and slower through the skeleton.

The set of equations for wave propagation in dynamic poroelasticity can be described again in three different formulations. However, the **u**-p formulation does not exist in the time domain, so the **u**-w or **u**-$\mathbf{u_F}$ formulation is usually used. The main equations that we are investigating are:

$$\begin{aligned}
\nabla \cdot \boldsymbol{\sigma_S} + (1-\phi_F)\,\boldsymbol{b} &= (1-\phi_F)\,\rho_s \frac{\partial^2 u}{\partial t^2} \\
&\quad - \rho_a \left(\frac{\partial^2 \mathbf{u_F}}{\partial t^2} - \frac{\partial^2 \mathbf{u}}{\partial t^2} \right) - \frac{\phi_F^2}{\kappa} \left(\frac{\partial \mathbf{u_F}}{\partial t} - \frac{\partial \mathbf{u}}{\partial t} \right) \\
\nabla \cdot \boldsymbol{\sigma_F} + \phi_F \boldsymbol{b_F} &= \phi_F \rho_F \frac{\partial^2 \mathbf{u_F}}{\partial t^2} \\
&\quad + \rho_a \left(\frac{\partial^2 \mathbf{u_F}}{\partial t^2} - \frac{\partial^2 \mathbf{u}}{dt^2} \right) + \frac{\phi_F^2}{\kappa} \left(\frac{\partial \mathbf{u_F}}{dt} - \frac{\partial \mathbf{u}}{dt} \right) \\
\boldsymbol{\sigma_S} &= \boldsymbol{C^e \varepsilon} + \frac{Q^2}{R} \mathrm{tr}(\boldsymbol{\varepsilon}) + Q \mathrm{tr}(\boldsymbol{\varepsilon_F}) \\
\boldsymbol{\sigma_F} &= -\phi_F p = Q \mathrm{tr}(\boldsymbol{\varepsilon}) + R \mathrm{tr}(\boldsymbol{\varepsilon_F})
\end{aligned} \tag{8.0.1}$$

where the small solid strain is $\boldsymbol{\varepsilon} = \frac{1}{2}(\nabla \mathbf{u} + \nabla \mathbf{u}^{\mathrm{T}})$ and the small fluid strain is $\boldsymbol{\varepsilon_F} = \nabla \cdot \mathbf{u}$. The densities of solid and fluid are denoted by ρ_s and ρ_f respectively. Porosity is described by ϕ_F, and Q and R are poroelastic coupling constants, while κ is the permeability. The apparent density is defined by $\rho_a = C\phi_F \rho_f$, where C is a constant depending on the frequency of excitation and the geometry of the pores, which is usually considered C=0.66.

At this point, we already computed and validated the model, as depicted

in Figure 8.1 and 8.2 in which a longitudinal wave propagates through a homogeneous poroelastic medium with different values of permeability. The results suggest that high permeability leads to a decrease in solid wave amplitude – energy dissipation – while lower permeability leads to similar wave amplitudes. Further efforts are necessary to understand the responses accounting for the heterogeneity of the medium and to study the relations of permeability, porosity, and coupling parameters.

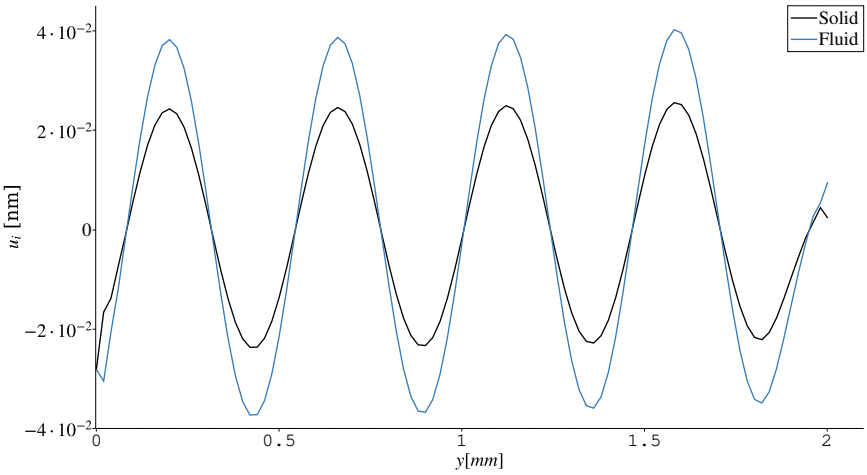

Figure 8.1: On going work: poroelastic wave propagation with high permeability. Results are shown for a homogeneous medium, with $\rho_F = \rho_s = 1000kg \cdot m^{-3}$, $\nu = 0.4$, $\phi = 0.3$, $Q = R = 1.2 \cdot 10^9$Pa, C=0.66, and $\kappa = 1 \cdot 10^9 \mathrm{m}^2\mathrm{Pa}^{-1}\mathrm{s}^{-1}$. For high values of κ, solid phase waves diminish their amplitude with respect to fluid phase waves.

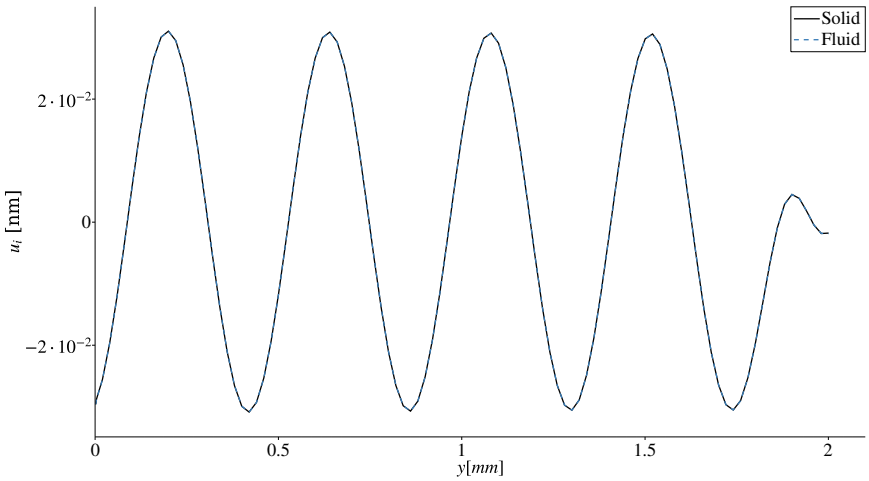

Figure 8.2: On going work: poroelastic wave propagation with low permeability. Results are shown for a homogeneous medium, with $\rho_F = \rho_s = 1000kg \cdot m^{-3}$, $\nu = 0.4$, $\phi = 0.3$, $Q = R = 1.2 \cdot 10^9$Pa, C=0.66, and $\kappa = 3.1 \cdot 10^{-14}\mathrm{m}^2\mathrm{Pa}^{-1}\mathrm{s}^{-1}$. For lower values of κ, solid and fluid phase waves have similar amplitude.

Finally, in the coming years, tumor reengineering is expected to become a challenging component in the analysis of tumor dynamics. Therefore, more mathematical proposals are needed regarding the topic addressed in this thesis in order to clarify questions about the action and consequences of co-therapies, ultimately translating the models to a patient-specific scale and contributing to clinical decision-making.

Part IV

APPENDICES

Appendix A

List of publications

The results of this dissertation have been published in peer-reviewed journals and they have been presented at different conferences.

A.1 Articles in peer-reviewed journals

- **B. Blanco**, H. Gomez, J. Melchor, R. Palma, J. Soler, G. Rus, Mechanotransduction in tumor growth modeling. *Physics of Life Reviews*. 2023; 44: 279-301https://doi.org/10.1016/j.plrev.2023.01.017. JCR score: D1. Associated with Chapter 2.
- **B. Blanco**, J. Campos, J. Melchor, J. Soler, Modeling Interactions among Migration, Growth, and Pressure in Tumor Dynamics. *Mathematics*. 2021; 9(12):1376. https://doi.org/10.3390/math9121376. JCR score: D1. Associated with Chapter 3.
- **B. Blanco** et al., Modeling LIUS therapy in a growing tumor spheroid. *In preparation*. 2023. Associated with Chapters 4 and 5.

A.2 Contributions in conferences

- **B. Blanco**, R. Palma, H. Gomez, J. Soler, G.Rus, A computational model for the therapeutic effect of low-intensity ultrasound on a growing tumor spheroid, (accepted for poster presentation) *ISTU*. April 2023 Lyon, France.
- **B. Blanco**, H. Gomez, J. Melchor, G. Rus, J. Soler, Biomechanical model for solid tumor growth. *14th Virtual Congress WCCM & ECCOMAS 2020*. International Association for Computational Mechanics (IACM) and European Community on Computational Methods in Applied Sciences (ECCOMAS).
- **B. Blanco**, H. Gomez, J. Melchor, G. Rus, J. Soler, Modelo biomecánico para crecimiento tumoral sólido in vitro. *IX Reunión del Capítulo Español de la Sociedad Europea de Biomecánica (ESB), Las Palmas de Gran Canaria, Spain, 2019*. Universidad de Las Palmas de Gran Canaria.

Appendix B

Collaborations in other works

Prostate cancer detection and characterization

This collaboration emerged in the first year of this thesis, starting from a dissertation of laboratory colleague [365], who patented a new transurethral medical technology for characterizing the mechanical properties of prostate tissues, proving promising preliminary in-silico results for the future detection of prostate cancer.

In particular, the technique of elastography has been utilized extensively since the 1990s to quantify tissue stiffness through the velocity of shear waves. However, the application of this technique is limited due to difficulties in separating longitudinal and shear waves, as well as the pressure applied during measurement. To address these limitations, a Transurethral Shear Wave Elastography sensor (TU-SWE) was developed to isolate pure shear waves, eliminating the risk of wave interference. This sensor consists of a rotational actuator disk and four piezoceramic receivers arranged circumferentially, which facilitate the transmission of shear waves that interact with the tissue prior to the reception.

The main aim of my work was to perform a proof-of-concept of the TU-SWE sensor in prostate-like gelatine phantoms through a two-part methodology. The first part consisted of an experimental setup for obtaining shear wave stiffness in the phantoms using the TU-SWE transducer, while the second part involved obtaining Verasonics dispersion curves for validation. The variables under investigation were the applied suction pressure and the distance between the emitter and receivers within the phantom. A series of phantoms were tested at various gelatine concentrations (ranging from 7.5% to 15%), suction pressures (ranging from 0 to 10 kPa), and emission-receiver distances (ranging from 0 to 10 mm).

The main conclusions drawn from this study are as follows: 1) careful calibration is necessary to compensate for the electromechanical cross-talk of

the TU-SWE probe; 2) Verasonics calibration curves are consistent with TU-SWE shear wave speed measurements; and 3) experimental results indicate that the applied suction pressure and emission-receiver distance do not affect the shear wave stiffness measurements. The preliminary results suggest that the proposed probe in reference [365] can effectively reconstruct the mechanical constants from the propagated shear wave.

This work was presented at three international conferences:

- **B.Blanco**, A. Gomez, J. Torres, I. H Faris, A. Callejas, J. Melchor, M. Carvajal, N. Saffari, G.Rus. Validation of the transurethral shear wave elastography probe in prostate like gelatine phantoms, *International Congress on Ultrasonics*, University of Leuven, Brugges, Belgium, 2019.
- **B.Blanco**, A. Gomez, J. Torres, I. H Faris, A. Callejas, J. Melchor, M. Carvajal, N. Saffari, G.Rus. Performance study of a transurethral shear wave probe in prostate phantoms, *27th Annual International Conference on Composites/ Nano Engineering*, Granada, Spain, 2019.
- **B.Blanco**, A. Gomez, J. Torres, I. H Faris, A. Callejas, J. Melchor, M. Carvajal, N. Saffari, G.Rus. Validation of the transurethral shear wave elastography probe in prostate like gelatine phantoms, *EUROSON - 31st Congress of the EFSUMB*, European Federation of Societies for Ultrasound in Medicine and Biology (EFSUMB) y la Federación Española de Sociedades de Ultrasonidos en Medicina y Biología (FESUMB), Granada, Spain, 2019.

Viscoelastic properties characterization of tumor spheroids with AFM

In a collaborative effort with the *Center for Research in Information and Communication Technologies* of the University of Granada, we conducted measurements on tumor spheroids to obtain their viscoelastic properties. The spheroids were provided by the collaborating group of *Advanced therapies: differentiation, regeneration, and cancer* – the same team who performed experiments described in Chapter 5 –, and the measurements were carried out by the laboratory head and technicians.

Our team assisted in the measurements by preparing the samples and identifying the spheroids using a microscope. Despite our efforts, the measurement process proved to be complex, and no conclusive results have been obtained thus far. For future endeavors, it is imperative to optimize the measurement protocol and ensure the viability of the cells during and after the experiment.

Teaching

Regarding teaching Mechanics in the Bachelor of Civil Engineering and Electronic Engineering, the following contributions in Book Chapters have been published:

- **B. Blanco**, J. Chiachio, M. Chiachio, A. Callejas, G. Rus, J. Melchor (2019). Teaching the 21st century Civil Engineering: research results and critical perspective, *Innovación docente e investigación en ciencias, ingeniería y arquitectura*, 52 (pp. 625-636), Dykinson, ISBN: 978-84-1324-559-1, 2019.
- **B. Blanco**, A. Callejas, J. Chiachio, M. Chiachio, G. Rus, J. Melchor (2019). Project-based learning in strength of materials: degree in Industrial Electronic Engineering in academic courses between 2015 and 2017, *Innovación docente e investigación en ciencias, ingeniería y arquitectura*, 61 (pp. 731-740), Dykinson, ISBN: 978-84-1324-559-1, 2019.

Appendix C

Extended summary in Spanish

C.1 Introducción

El cáncer es la segunda causa principal de muerte en todo el mundo. Según datos publicados en la referencia [1], se detectaron 19,3 millones de nuevos casos y se produjeron 10,0 millones de muertes en todo el mundo en 2020, acumulando casi una cuarta parte de ellas en Europa (4,3 millones de casos), y se prevé que siga aumentando en los próximos años. En España, los datos estiman 282 mil nuevos casos y 113 mil muertes en 2020, siendo el cáncer de próstata, mama, colon y pulmón el más incidente [2, 3].

El cáncer es una preocupación importante para la salud pública con un impacto significativo tanto en los resultados de los pacientes como en los costos sanitarios. De hecho, el cáncer es una de las principales causas de carga económica y de salud entre las enfermedades crónicas en la Unión Europea [4, 5, 6, 7]. Se espera que el coste del tratamiento del cáncer siga aumentando en el futuro, lo que lo convierte en una preocupación significativa para los sistemas de salud y los responsables políticos [6, 8, 9, 10].

La comprensión de los procesos moleculares involucrados en la transformación de las células cancerosas ha avanzado significativamente en los últimos años [11, 12, 13, 14, 15]. Sin embargo, a pesar del notable progreso que se ha logrado, nuestra comprensión de estos mecanismos sigue siendo muy limitada y aún queda mucho por descubrir.

La causa multifactorial del cáncer está relacionada con las alteraciones y mutaciones del genoma que resultan en el crecimiento anormal de las células. En general, el origen del cáncer es un proceso complejo que puede verse influido por una combinación de factores genéticos y ambientales. Las mutaciones son modificaciones irreversibles del ADN que se pueden heredar, mientras que las alteraciones se refieren a cambios epigenéticos que modifican la expresión del genoma sin modificar el ADN [16, 17, 18, 19, 20, 21, 22, 23, 24]. Hay varios factores de riesgo que pueden contribuir al desarrollo de estas mutaciones,

incluidas las mutaciones genéticas heredadas, los factores ambientales, las infecciones, la radiación, la obesidad, el estilo de vida sedentario, el envejecimiento, la dieta, el consumo de alcohol y tabaco [25, 26, 27, 28, 29, 30, 31].

Los tratamientos existentes para el cáncer, incluyendo la quimioterapia convencional y la radioterapia, pueden tener efectos secundarios significativos y pueden no eliminar eficazmente las células precursoras del cáncer conocidas como células madre del cáncer (CSC), [32, 33, 34, 34]. Las CSC tienen un impacto significativo en la metástasis y se les atribuye una gran influencia en las recaídas debido a sus capacidades de autorenovación y diferenciación [35, 36, 37, 38, 39].

Actualmente hay nuevas terapias en el horizonte, como la inmunoterapia, pero la estratificación de los pacientes es un desafío y los costes son altos [40, 41, 42, 43, 44]. Por lo tanto, se necesitan nuevas estrategias para interactuar con las células desarrollando nuevos tratamientos que mejoren el pronóstico de los pacientes.

Además de los procesos bioquímicos, las fuerzas mecánicas juegan un papel crítico en la carcinogénesis. La literatura reciente proporciona amplias pruebas de que las células son tanto jugadores pasivos como activos en la homeostasis mecánica del cuerpo y que las alteraciones en las fuerzas mecánicas pueden modificar la función celular [45, 46, 47, 48, 49, 50]. En este contexto, el crecimiento uniforme no es un estado predeterminado, sino el resultado de la regulación activa y la competencia de la proliferación celular, la movilidad, los agentes químicos y la retroalimentación mecánica, en la que el crecimiento modifica las tensiones –crecimiento impulsado por la tensión– y la tensión regula el crecimiento y sus patrones asociados [55, 56, 57, 58].

Recientemente, se ha destacado la importancia de la mecánica de las células cancerosas como un controlador crítico de la progresión de la enfermedad. En este contexto, la *mecanobiología* estudia cómo las células responden a estímulos mecánicos biológicamente. En particular, destaca el potencial de los principios de *mecanotransducción* como complemento de las terapias ya existentes [59, 60, 61]. La literatura sobre mecanotransducción es amplia, pero en su mayoría se limita a grandes vías biológicas y de proteínas.

La importancia de traducir la mecanotransducción en terapia se ha vuelto cada vez más visible y el desarrollo de tecnologías mecánicas para combatir el cáncer no ha hecho más que empezar. Diferentes laboratorios están desarrollando una variedad de principios para impactar activamente el comportamiento celular mediante la modificación del microambiente mecánico [62, 63]. Estos principios van desde el uso de ultrasonidos (US) hasta fármacos que alteran la elasticidad del microambiente y la rigidez celular. Estos principios son

traducibles al paciente, ya que el US se puede aplicar mediante transductores o parches, y el segundo se basa en la administración de fármacos.

En cuanto al US y dejando de lado las terapias térmicas como el ultrasonido focalizado de alta intensidad (HIFU) y la sonoporación [64, 65, 66, 67, 68, 69], ya que dependen de diferentes mecanismos que requieren dirigirse cuidadosamente a los tumores confinados ya que destruyen el tejido sano, el ultrasonido de baja intensidad (LIUS) y su versión pulsada (LIPUS) proponen impactar a las células cancerosas por dos mecanismos principales: i) resonancia selectiva de las células bajo el nombre de *oncotripsia*, que se basa en la destrucción del citoesqueleto[70, 71, 72, 73, 74], y ii) respuesta desencadenada de mecanotransducción a través de vías de señalización [73, 74, 75, 76, 77, 78, 79, 80].

Aunque estos estudios han evidenciado repetidamente efectos potenciales significativos, la falta de comprensión del mecanismo, y las diferentes respuestas desencadenadas por diversas frecuencias, energías y configuraciones, hacen que el concepto todavía no sea aplicable en su estado actual.

Por ello, la comprensión de la configuración de ondas mecánicas está suscitando cada vez más atención, aunque todavía, los mecanismos de cómo el LIUS afecta al comportamiento de las células cancerosas es considerablemente restringido. La razón principal radica en el elevado coste experimental, los efectos estocásticos asociados a los experimentos biológicos y la complejidad técnica de obtener datos *in-vivo*.

En este marco teórico, la oncología matemática y la *medicina predictiva* son herramientas valiosas para complementar el entendimiento de la biología experimental. Aunque, por desgracia, no se puede confiar plenamente en las predicciones de un modelo matemático para un sistema biológico [51], el desarrollo de modelos multifísicos de las interacciones mecánico-biológicas es clave para desentrañar el comportamiento tumoral [81, 82, 83, 45, 63, 84, 85].

Así, los modelos de mecanobiología computacional son un punto importante de partida para comprender la progresión de la enfermedad [86, 87, 52]. De hecho, un modelo puede describir y representar con precisión un sistema biológico si sigue las tendencias cualitativas de las pruebas experimentales [51]. En última aproximación, los modelos a medida (morfología realista y propiedades inherentes al tumor) podrían ayudar a los clínicos en el diagnóstico y la toma de decisiones [88, 89, 90, 91, 92]. Así, los modelos podrían utilizarse como estrategia médica complementaria en el prediagnóstico. Por ejemplo, se podría probar e incluso combinar una combinación de fármacos [93, 94] y diferentes ondas mecánicas para optimizar el tratamiento. Asegurando las proporciones adecuadas, se podría maximizar la eficacia del tratamiento y

minimizar los costes sanitarios [63].

La razón principal para investigar el cáncer desde la mecánica computacional radica en la necesidad de comprender el comportamiento de la dinámica tumoral en respuesta a la interacción mecánica en situaciones normales y cambiantes, e identificar nuevas dianas para los tratamientos destinados a combatir las CSC, teniendo en cuenta la cascada de señalización de las vías de mecanotransducción desde la generación de señales mecánicas a escala tisular hasta el nivel celular y molecular.

No obstante, la modelización es todo un reto. La morfología tumoral, la coexistencia de diferentes tipos celulares, las interacciones bioquímico-mecánicas y la no linealidad de los tejidos implican ecuaciones diferenciales parciales de alto orden que exigen métodos eficientes de resolución en términos de coste computacional y memoria. Los procedimientos numéricos para obtener soluciones aproximadas al sistema de ecuaciones se basan principalmente en el Método de las Diferencias Finitas (FDM), que puede ayudar en modelos más simplificados mediante la aproximación directa de la solución desconocida por aproximación de diferencias finitas en nodos, y Método de Elementos Finitos (FEM), que es una herramienta útil para resolver retos computacionales más complejos mediante el uso de polinomios estándar para interpolar funciones y así aproximar la solución desconocida dentro de un elemento [95, 96, 97, 98, 99].

En este escenario, el proyecto *Mecanoterapia* llevado a cabo por nuestro grupo de investigación en la Universidad de Granada representa una estrategia novedosa en la lucha contra la carcinogénesis. Nuestro enfoque busca comprender y manipular la mecánica celular combinando experimentos y modelado, utilizando los últimos avances en mecánica, genómica, transcriptómica, proteómica y metabolómica.

La tesis que se presenta es un componente esencial de dicho proyecto. En concreto, establece el marco teórico de referencia que incluye las principales vías de señalización relacionadas con la mecánica y los estados de tensión en la progresión de los tumores, con la finalidad de desarrollar modelos computacionales multiescala que ayuden a comprender la dinámica tumoral incorporando fenómenos como la proliferación, la migración controlada, el crecimiento impulsado por la tensión y las interacciones de las ondas mecánicas.

C.2 Objetivos

El principal objetivo de esta tesis es desarrollar herramientas computacionales para comprender y abordar la carcinogénesis desde la mecánica. Para lograrlo, es necesario cumplir una serie de objetivos específicos que se detallan a continuación:

1. **Establecer el marco de la mecanobiología tumoral y sus modelos teóricos.** Describir las principales características de los tumores avasculares y revisar el conocimiento actual de la mecanobiología tumoral, proporcionando un marco común para los diferentes enfoques teóricos que han surgido en la literatura desde la perspectiva de la Teoría Clásica de los Medios Continuos y dando una visión de las mecanoterapias emergentes, centrándose en los ultrasonidos de baja intensidad a nivel experimental y teórico.

2. **Estudiar la competición entre mecánica y migración en respuesta a un cambio abrupto en la densidad celular**. Comparar los efectos lineales, no lineales y no lineales de flujo saturado en la migración. Desarrollar un modelo matemático basado en mecánica para comprender la respuesta del crecimiento no homogéneo de células a cambios bruscos en la densidad celular controlando el frente de velocidad de propagación. Analizar la interacción entre la proliferación, la migración y el crecimiento impulsado por la tensión no homogénea.

3. **Modelar la interacción ultrasónica a nivel de esferoide**. Modelar la propagación de ultrasonidos en esferoides tumorales, considerando la atenuación inherente de las ondas mecánicas realizando un análisis de sensibilidad de la propagación de ondas con respecto a la presión acústica, la viscosidad y la frecuencia.

4. **Desarrollar un modelo multiescala de mecanoterapia en el que los ultrasonidos de baja intensidad influyan en la dinámica tumoral a través de la mecanotransducción**. Proponer un modelo computacional multiescala que simule el efecto terapéutico que los LIUS parecen causar en un esferoide tumoral poroelástico en crecimiento a través de la mecanotransducción. Validar el modelo mediante la comparación con datos experimentales, y utilizar las simulaciones numéricas para explorar la inhibición de la proliferación y migración selectiva, así como la formación de patrones.

C.3 Contribuciones

En esta tesis, hemos sintetizado diversos enfoques mecanobiológicos que han surgido en los últimos años, abarcando perspectivas tanto biológicas como mecánicas en el marco de la mecánica de los medios continuos. Nuestra exhaustiva revisión de los antecedentes abarca las principales hipótesis subyacentes a la mecanotransducción, las características esenciales de la teoría que fundamenta el modelado del crecimiento a partir de la mecánica, los modelos que rigen el comportamiento tumoral, los aspectos más destacados de la terapia LIUS y el marco de la propagación de ondas en tejidos blandos.

Tras la revisión bibliográfica, hemos identificado varias contribuciones potenciales, como la interacción entre el crecimiento no homogéneo y la migración y la creciente demanda de herramientas tecnológicas y computacionales innovadoras que faciliten una comprensión más profunda de la evolución tumoral. Además, hemos destacado el uso potencial de los ultrasonidos de baja intensidad para atacar las células madre cancerosas.

Esta tesis propone tres modelos computacionales que mejoran la comprensión de la mecanobiología y la mecanotransducción examinando la dinámica, la migración y el crecimiento tumoral en respuesta a fuerzas mecánicas, así como los efectos de la mecanoterapia en el desarrollo tumoral.

En resumen, nuestro primer modelo investiga la competencia entre migración, proliferación y mutaciones, que da lugar a cambios de volumen no homogéneos que generan tensiones que modifican la evolución tumoral. Para estudiar esta competición, desarrollamos ecuaciones acopladas de mecánica-crecimiento y resolvemos el sistema por minimización de la energía y utilizando el método esencialmente no oscilatorio ponderado (WENO) en diferencias finitas en una dimensión. Los resultados sugieren que deben utilizarse flujos no lineales para limitar la velocidad de propagación. Además, el estudio indica que el crecimiento no homogéneo ralentiza la proliferación a la vez que provoca inestabilidades en la densidad celular en un fenómeno conocido como difusión retrógrada, que se ve mitigado por la posibilidad de movimiento celular.

Una vez estudiados estos fenómenos, consideramos el efecto de la mecanoterapia en la dinámica tumoral investigando cómo se propagan las ondas ultrasónicas a través de un esferoide embebido en un medio de cultivo utilizando un modelo viscoelástico de Kelvin-Voigt con diferentes parámetros de frecuencias, presiones acústicas y viscosidades. El estudio paramétrico sugiere que no contemplar la viscoelasticidad puede conducir a una sobreestimación de la energía que llega al tejido, ya que no tiene en cuenta la disipación de las ondas de ultrasonido causada por la viscosidad del tejido, mientras que una

alta presión acústica puede provocar daños irreversibles o la muerte celular, y una presión acústica baja puede no producir los efectos terapéuticos deseados. La selección de la frecuencia adecuada depende de diversos factores, como la geometría del tejido diana, las propiedades del medio y la intensidad deseada. El estudio concluye que las simulaciones numéricas de propagaciones de onda pueden ayudar a determinar los parámetros mecánicos óptimos para diferentes tipos celulares y estados de enfermedad, lo que puede guiar el desarrollo de tratamientos de LIUS seguros y efectivos para el cáncer y otras enfermedades.

Por último, proponemos un modelo multiescala que integra los efectos de las ondas mecánicas en el desarrollo tumoral a través de la mecanotransducción. El modelo consiste en ecuaciones acopladas de tensión-crecimiento y dos escalas temporales principales: escala rápida, donde la onda se propaga y ocurre la mecanotransducción, y escala lenta, donde el tumor crece y se adapta al microambiente como un medio poroelástico. Para demostrar la validez del modelo, realizamos una validación experimental y preliminar con esferoides in vitro. Consideramos varios escenarios con diferentes parámetros de propagación para realizar un análisis de sensibilidad del efecto de los ultrasonidos en la mecanotransducción. Nuestros resultados sugieren que el modelo puede replicar los datos experimentales, permitiendo predicciones tanto del crecimiento como de los estados tensionales y de deformación del medio y del esferoide. Así, se ha comprobado numéricamente que los ultrasonidos generan campos de tensión que inhiben y ralentizan tanto el crecimiento como la migración, creando patrones basados tanto en las tensiones aplicadas como en los rangos de sensibilidad celular, y alterando los gradientes de tensión lenta de crecimiento y presión de fluido intersticial.

C.4 Discusión

En esta tesis, se han sintetizado los enfoques de mecanobiología que han surgido en los últimos años, abarcando tanto perspectivas biológicas como mecánicas dentro del marco de la mecánica de los medios continuos. La revisión exhaustiva de antecedentes engloba las principales hipótesis subyacentes a la mecanotransducción, las características esenciales de la teoría que fundamentan la modelización del crecimiento a partir de la mecánica, las ecuaciones que rigen el comportamiento tumoral, los aspectos más destacados de la terapia LIUS y el marco de propagación de ondas en tejidos blandos.

Después de la revisión de la literatura, se han identificado varias contribuciones potenciales, incluyendo la interacción entre el crecimiento y la migración no homogéneos, y la creciente demanda de herramientas tecnológicas y

computacionales innovadoras que faciliten una comprensión más profunda de la dinámica tumoral. También se ha destacado el novedoso uso de ultrasonido de baja intensidad para atacar a las células madre del cáncer.

Esta tesis propone tres modelos computacionales que mejoran la comprensión de la mecanobiología y la mecanotransducción examinando la dinámica del tumor en respuesta a las fuerzas mecánicas, así como los efectos de la mecanoterapia en el desarrollo del tumor.

En resumen, la primera propuesta investiga la competencia entre la migración, la proliferación y las mutaciones, lo que resulta en cambios de volumen no homogéneos que generan tensiones que modifican la evolución del tumor. El conjunto de ecuaciones consiste en ecuaciones de crecimiento y tensión acopladas con un término de migración de flujo saturado.

Este estudio destaca, en primer lugar, la necesidad de utilizar flujos no lineales para describir la migración del tumor, en contraste con los flujos lineales que se utilizan con frecuencia en los enfoques de crecimiento basados en la mecánica [89, 90]. Esta necesidad surge de la necesidad de controlar la velocidad y el frente de migración, perdido en los flujos lineales, como se observa para diferentes escenarios en la Figura 3.3, y como ya se ha establecido previamente en la literatura [307, 308, 309, 310, 311, 312].

En particular, el flujo no lineal saturado controla el avance del frente de propagación a través de un parámetro biológico de velocidad finita. Además, el parámetro de porosidad m modifica la velocidad del frente de propagación, disminuyéndola a medida que m aumenta, como se representa en la Figura 3.4.

Sin embargo, la necesidad de preservar el frente de propagación del tumor y evitar el posible ruido numérico del flujo saturado requiere órdenes de aproximación altos. Para lograr este requisito, se utiliza el método ponderado no oscilatorio (WENO), que tiene como objetivo lograr una precisión de alto orden mediante la combinación de múltiples aproximaciones numéricas de bajo orden a través del uso de pesos y coeficientes. En este método. se calculan indicadores de suavidad para cada aproximación y luego se utilizan para determinar los pesos. La solución final se obtiene formando una combinación de las aproximaciones ponderadas [310, 384]. Por lo tanto, el método WENO proporciona una resolución de estabilidad de alto orden precisa, a la vez que mantiene una transición no oscilatoria, estable y nítida de la discontinuidad.

Por otro lado, los pequeños cambios en el crecimiento generan retroalimentación mecánica que puede llevar a inestabilidades, como se propone teóricamente en las referencias [55, 57] y se demuestra numéricamente en este estudio, como se observa en las Figura 3.5 y 3.6. Además, permitir el

movimiento celular controlado dentro del tumor puede disipar estas tensiones y regular el crecimiento, de acuerdo a las Figura 3.7 y 3.8.

Para controlar esta regulación, se considera apropiado el uso del flujo no lineal saturado en este estudio. Sin embargo, en los casos en que las inestabilidades resultantes del crecimiento no uniforme no son una preocupación, se puede simplificar a un flujo no lineal para reducir la complejidad y el coste computacional, tal y como se ha hecho en el estudio posterior.

Una vez que se han estudiado estos fenómenos, hemos considerado el efecto de la mecanoterapia en la dinámica tumoral analizando la propagación de ultrasonidos en un esferoide embebido en un medio de cultivo, utilizando la ecuación constitutiva viscoelástica de Kelvin-Voigt [365, 366, 367, 368]. Se ha realizado un análisis de sensibilidad que incluye un rango de frecuencias de $f = [1 - 20]$MHz, presiones acústicas de $A = [0.1 - 5]$ kPa, y viscosidades de $\eta_i =$[0-10]Pa·s, siendo i las viscosidades del medio de cultivo c o del tumor T. El conjunto de ecuaciones se ha resuelto en elementos finitos considerando dos dimensiones.

Basándonos en el modelo de propagación, hemos observado que una mayor viscosidad del tejido tumoral favorece zonas de sombra detrás del esferoide tumoral, donde la energía de la onda se disipa debido a la viscosidad del esferoide. Cabe destacar que este efecto podría ser más pronunciado incluso si se considerasen las tres dimensiones del problema.

La presión acústica juega un papel significativo en la eficacia y seguridad de los tratamientos LIUS. Una presión acústica excesiva puede desencadenar efectos de cavitación y calentamiento, lo que lleva a la alteración mecánica de los tejidos y a un posible daño irreversible del mismo. Por el contrario, una presión acústica inadecuada puede no producir los efectos terapéuticos deseados, permitiendo que las células proliferen y migren a regiones con niveles de tensión más bajos.

Además de la presión acústica, la selección de la frecuencia adecuada para LIUS es necesaria para lograr resultados terapéuticos óptimos, como la apoptosis o la quiescencia en los tratamientos contra el cáncer. La elección de la frecuencia depende de varios factores, como la geometría del tejido a tratar, las propiedades del medio y la intensidad deseada. Las frecuencias más bajas penetran más profundamente en los tejidos, lo que las hace ideales para tratamientos dirigidos a estructuras ubicadas más profundamente en el cuerpo. Sin embargo, a medida que aumenta la frecuencia, la energía de la onda se absorbe y se disipa cada vez más, lo que resulta en una mayor debilidad de la onda. Además, el grado de absorción depende de las propiedades del medio a través del cual se propaga la onda, como puede ser su viscosidad.

Aunque la presión acústica óptima depende del tipo celular específico, nuestros hallazgos sugieren que las tensiones dinámicas hidrostáticas que se han examinado podrían ser suficientes para inhibir el crecimiento de esferoides, y que las presiones acústicas mayores que $A = 1.5$kPa podrían ser efectivas para la frecuencia indicada.

Finalmente, proponemos un modelo multiescala que integra los efectos de las ondas mecánicas en el desarrollo del tumor a través de la mecanotransducción. La propuesta se basa en ecuaciones fundamentadas en la Teoría de Crecimiento Finito considerando pequeñas deformaciones, de forma similar a otros estudios [84, 330, 89, 90, 332, 92]. Hemos resuelto el modelo usando Elementos Finitos en dos dimensiones.

El sistema multiescala incluye ecuaciones acopladas de crecimiento y esfuerzo y dos escalas de tiempo principales: una escala rápida donde las ondas se propagan y ocurre la mecanotransducción, y una escala lenta donde las células del tumor proliferan, migran y se adaptan al microambiente. El microambiente se modela como un medio poroelástico compuesto por componentes sólidos, incluyendo células tumorales, células sanas y la matriz extracelular, así como fases fluidas.

En contraste con los estudios basados en la citodisrupción [70, 71, 72, 73, 74], nuestro aport se basa en la respuesta desencadenada de las células a través de la mecanotransducción, donde la proliferación se inhibe parcialmente [73, 74, 75, 76, 77, 78, 79, 80].

La hipótesis es que la presión dinámica es más efectiva para generar una respuesta celular que la tensión estática debido a los complejos mecanismos de redistribución de tensión que involucran al citoesqueleto y al flujo de fluidos intersticiales a través de los poros. La función de acoplamiento de mecanotransducción, descrita en las ecuaciones 5.2.16 y 5.2.17, se basa en funciones de mecanotransducción descritas y validadas en la literatura [151, 186, 321, 324, 322, 84, 343, 84, 330, 89, 90, 332, 92].

La contribución a la función de la mecanotransducción se basa en incluir la diferencia en el umbral entre la estimulación dinámica y estática, sin requerir relaciones ad hoc, al mismo tiempo que proporciona una explicación cuantitativa de las diferencias observadas. Por lo tanto, la función de la mecanotransducción se define en un período de tiempo ultrasónico en el que los mecanosensores celulares podrían recibir señales relacionadas con la red del citoesqueleto extremadamente rápidamente [218, 219], y luego responder desencadenando cambios en la proliferación y migración, como se propone en [224, 218].

Con el fin de generar intensidades similares a las descritas en la literatura y evitar posibles fenómenos de cavitación, hemos superado las frecuencias e incrementado la presión acústica, en comparación con los estudios actuales cuyos parámetros se muestran en la Tabla 2.3.

Así, proponemos tratar experimentalmente células madre cancerosas de melanoma A-375 a una frecuencia de $f = 5$MHz y amplitudes que oscilan entre $A = [1.5 - 15.5]$kPa, asumiendo una viscosidad tumoral de $\eta_T = 2\text{Pa} \cdot \text{s}$ y una viscosidad del medio de cultivo de $\eta_c = 0.05\text{Pa} \cdot \text{s}$, en línea con los rangos de viscosidad establecidos previamente en otros estudios [391, 392, 393, 205, 394, 213, 395].

El experimento preliminar indica que la proliferación de las células madre cancerosas de melanoma se inhibe en un porcentaje del cambio del 48% cuando se sonican a una frecuencia de $f = 5$MHz, lo que respalda la viabilidad de LIUS como tratamiento, dado que las CSC son actualmente resistentes a las terapias convencionales [32, 33, 34, 34].

El modelo computacional multiescala propuesto y simplificado puede reproducir con precisión el decrecimiento de células observado para determinados parámetros de mecanotransducción, como se muestra en la Figura 5.9.

Estos hallazgos son consistentes con estudios anteriores [154, 151, 156, 157, 158, 84, 330], que han reportado una reducción del 50% en las tasas de proliferación en comparación con el crecimiento libre de tensión y un aumento del 30% en la actividad apoptótica de las células con valores de tensión estática de 1-10kPa. En consecuencia, los resultados respaldan la hipótesis de que reducciones comparables en las tasas de proliferación pueden lograrse a través de la aplicación de una tensión dinámica menor.

Además, estos resultados proporcionan predicciones tanto para el crecimiento como para los estados de tensión y deformación del medio y el esferoide. Específicamente, observamos un creciente tensión compresiva en las regiones centrales, como se propone en estudios anteriores [147, 45, 166]. Además, el estudio también indica que la compresión aumenta con el crecimiento.

Hemos considerado varios escenarios en los que el esferoide tumoral se ve afectado de manera diferente por la tensión y hemos realizado un análisis paramétrico del efecto del ultrasonido en la mecanotransducción, como se resume en la Tabla 5.2.

Las simulaciones numéricas indican que las presiones acústicas de 1.5kPa pueden reducir las tasas de proliferación en un 46.6-48.4% cuando la frecuencia oscila entre 1-5MHz, y para valores de viscosidad del medio de $\eta_c = 0.05\text{Pa} \cdot \text{s}$. Para valores de frecuencia más altos, como 20 MHz, la presión acústica debe

aumentarse a 5kPa para lograr una disminución del 52.5%.

Por otro lado, un aumento en la viscosidad del medio conduce a un aumento en la atenuación, lo que puede limitar significativamente la reducción en las tasas de proliferación, alcanzando valores comparables a las condiciones de control (reducción del 0-39.6% de las células). En tales casos, sería necesario aumentar la presión acústica si el medio es altamente viscoso.

Posteriormente, hemos estudiamos el sistema multiescala completo considerando todas las fases sólidas y la migración de la fase tumoral. Esta investigación indica que la terapia de ultrasonido no solo inhibe la proliferación de las células tumorales, sino que también ralentiza su migración, en concordancia con los resultados experimentales obtenidos en las referencias [78, 77]. Además, la inclusión de la migración en la fase tumoral del modelo resulta en un proceso de difusión cruzada, en el que las células tumorales se mueven a través de las diferentes fases e interactúan mediante un esquema de depredador-presa. Esto lleva a la competencia entre diferentes fases sólidas y la migración de una fase se propaga a las otras fases.

La función de mecanoterapia selectiva propone que la proliferación de células sanas permanece inalterada debido a su umbral de sensibilidad más alto, mientras que la disminución de la fase tumoral puede aumentar la concentración de las células sanas debido al sistema depredador-presa. Así, la terapia selectiva a través de mecanotransducción se ha propuesto como una estrategia potencial para dirigirse selectivamente a las células cancerosas y preservar el tejido sano, como se ha reflejado ya en las referencias [70, 75, 73].

Esta investigación preliminar propone que la terapia de ultrasonidos puede generar patrones en la proliferación y migración, rompiendo la simetría inicial del sistema en función de la tensión aplicada y los rangos de sensibilidad celular, como se ha estudiado experimentalmente en la referencia [73] y corroborado numéricamente en la Figura 5.17 y 5.18. Además, los resultados sugieren que la difusión amortigua la tensión lenta, homogeneizando la respuesta del tumor al entorno, como también se señaló en el Capítulo 3, pero preservando la migración hacia áreas de menor tensión.

En particular, estos modelos pueden describir el desplazamiento del centro de gravedad del tumor, el cual, aunque no alcanza grandes valores en nuestro estudio (1-4%), podría aumentar con diferentes parámetros y geometrías. De hecho, se pueden usar para proponer diferentes ángulos de sonicación para evitar la migración dirigida a áreas conflictivas. En consecuencia, este enfoque permitiría la optimización de las estrategias terapéuticas, mediante el análisis y diseño de configuraciones dirigidas y efectivas.

La presión del fluido intersticial aumenta con el crecimiento del tumor. En condiciones normales, la presión es heterogénea, con valores más altos en el núcleo y valores más bajos en los bordes, del orden de kPa, como se ha observado en [189, 45]. Bajo estas premisas, esta tesis predice la ruptura de la simetría de la tensión debido a los gradientes de presión en la dirección de la propagación ultrasónica, tal como se observa en la Figura 5.17 y la Figura 5.18.

Finalmente, se deduce que aunque el tumor crece inicialmente por efecto masa, la aplicación de ultrasonido genera tensiones compresivas y rarafactivas que inducen estados de compresión en las células. Esto, a su vez, conduce a la inhibición parcial de la proliferación y la migración, dependiendo de los gradientes de presión ultrasónica.

Sin embargo, esta tesis tiene algunas limitaciones. No se ha tenido en cuenta la hiperelasticidad del tejido, y las propiedades mecánicas y biológicas se han basado en la literatura, ya que no se han llevado a cabo experimentos de indentación o de control de velocidad con cámaras. ¡

Aunque se han reproducido numéricamente algunos experimentos preliminares del Capítulo 5, el número de experimentos es bajo debido a la estocasticidad y al alto coste experimental asociado con el cultivo de CSC, por lo que esta tesis se mantiene principalmente dentro del marco computacional.

Por lo tanto, se requieren más experimentos y a mayor largo plazo para evaluar diferentes respuestas computacionales, refinar los modelos para una mayor precisión y determinar el uso óptimo de la frecuencia y la presión acústica dependiendo de la viscoelasticidad del medio. Además, hemos supuesto la viscoelasticidad basada en las ecuaciones de Kelvin-Voigt en la propagación, y es necesario un análisis de sensibilidad que tenga en cuenta la plausibilidad de la ecuación constitutiva elegida.

Además, en nuestra propuesta no se han incorporado las vías de mecanotransducción de proteínas, ya que no se han podido validar experimentalmente. En su lugar, se ha aplicado la mecanotransducción directamente a la relación de duplicación o difusión, aunque las respuestas celulares son desencadenadas por las proteínas. Tampoco hemos considerado el efecto de las co-terapias.

Por último, este estudio es una aproximación numérica preliminar a la mecanobiología y la mecanoterapia ultrasónica de esferoides in vitro. Las geometrías simples utilizadas no han tenido en cuenta formaciones más complejas, que pueden exhibir fenómenos adicionales como la dispersión. Para crear un escenario in vivo más realista, sería necesario considerar estos fenómenos y sus patrones asociados.

C.5 Conclusiones

Para concluir, la oncología matemática es una valiosa herramienta de ayuda en el desarrollo de estrategias efectivas de tratamiento y comprensión del comportamiento tumoral, mitigando los altos costes experimentales y su significativa estocasticidad. La importancia de las nuevas terapias contra el cáncer, particularmente la terapia de ultrasonido de baja intensidad, y la necesidad de herramientas y tecnologías computacionales que puedan atacar selectivamente a las células madre cancerosas resistentes a las terapias actuales han sido enfatizadas en este estudio.

En este contexto, esta tesis representa una investigación interdisciplinar de la mecanobiología en el cáncer. Las contribuciones específicas de esta tesis se resumen a continuación:

- **El flujo no lineal saturado controla la velocidad biológica del frente de invasión**, mientras que el flujo lineal conduce a una velocidad de propagación infinita, y los flujos no lineales mantienen la estabilidad del frente. Además, el parámetro de porosidad m regula la velocidad de migración, disminuyéndola a medida que m aumenta.
- **Las variaciones en el crecimiento pueden conducir a inestabilidades que actúan como difusión retrógrada** en competencia con la proliferación debido a la retroalimentación mecánica.
- **La migración celular puede evitar inestabilidades y disipar cambios abruptos** de crecimiento impulsado por el estrés no homogéneo.
- **Las ondas acústicas de baja presión y alta frecuencia estimulan la señalización** mientras mantienen una baja intensidad para desencadenar la inhibición del crecimiento y la migración, evitando la citodisrupción.
- **La presión acústica es el parámetro dominante en la mecanotransducción**. Las presiones acústicas bajas pueden no ser suficientes para alterar el destino del tumor. Sin embargo, una vez que se supera un nivel de estrés umbral, aumentar aún más la presión acústica puede no ser necesario para inducir la señalización, mientras que niveles excesivos de presión acústica podrían llevar al límite de la citodisrupción.
- **Los parámetros interdependientes de presión acústica, viscosidad y frecuencia se pueden ajustar para optimizar la selectividad de las aplicaciones terapéuticas**. La disipación de energía aumenta con la viscosidad, y la selección de la frecuencia está influenciada por el tamaño del tumor. Las ondas de baja frecuencia

generan longitudes de onda más largas, lo que resulta en una agitación del tumor. En contraste, las ondas de alta frecuencia pueden interactuar con los componentes de las células. El modelo computacional propuesto reduce la necesidad de pruebas experimentales de diferentes configuraciones de parámetros mecánicos, incluyendo la ubicación del transductor, el ángulo de sonificación, las geometrías y las capas de tejido.

- **La función de mecanotransducción propuesta proporciona una explicación cuantitativa para las diferencias observadas en el umbral entre la estimulación dinámica y estática** sin necesidad de relaciones ad-hoc.
- **La presión dinámica es más efectiva que el estrés estático en generar una respuesta celular**, lo cual ha sido validado numérica y experimentalmente, como se evidencia en la capacidad de lograr reducciones similares en las tasas de proliferación a 1.5kPa (46.6-48.4%).
- **El crecimiento de las células madre cancerosas puede ser inhibido utilizando 5MHz y presiones acústicas mayores a 1.5kPa**, como sugiere el experimento preliminar de ultrasonido terapéutico.
- **El comportamiento migratorio de la fase tumoral conduce a un proceso de difusión cruzada**, donde el movimiento se propaga a otras fases sólidas a través de un esquema de interacción depredador-presa.
- **La proliferación de las células sanas permanece selectivamente inalterada por LUIS debido a su umbral de sensibilidad más alto**, mientras que la reducción de la carga celular tumoral a través de ULIS puede aumentar el papel de las células sanas en el sistema depredador-presa.
- **El ultrasonido puede generar un patrón en la proliferación y migración**, rompiendo la simetría inicial del sistema y desplazando el centro de gravedad de las células tumorales a áreas de menor presión acústica.
- **La presión del fluido intersticial se adapta a los patrones de ultrasonido**, aumentando en la dirección de propagación debido a la concentración de células tumorales. Además, la tensión lenta de compresión aumenta con el tiempo.
- **El ultrasonido terapéutico dificulta la migración celular**. Además, la migración amortigua la tensión lenta y la presión del fluido homogeneizando la respuesta del tumor al entorno.

C.6 Futuras líneas de investigación

En relación al Capítulo 3, es posible incorporar la ley de Brinkman mencionada anteriormente y realizar estudios analíticos sobre los aspectos cualitativos de las soluciones (como oscilaciones o la no-convexificación de la forma de densidad, entre otros). Además, en un corto plazo, estamos interesados en incorporar las interacciones bioquímicas que modulan tanto el crecimiento como las propiedades de adhesión celular.

En cuanto a los Capítulos 4 y 5, el presente estudio no describe de manera completa las complejas interacciones proteicas que regulan las vías de señalización asociadas con la proliferación y migración celular. Por lo tanto, para dilucidar los mecanismos moleculares específicos subyacentes a los cambios observados en el comportamiento celular, los estudios futuros podrían incorporar un análisis proteómico. Dicho análisis proporcionaría valiosas ideas sobre las vías de señalización alteradas y los patrones de expresión proteica que promueven la disminución en la proliferación celular observada en este estudio. Además, el consumo de nutrientes y la hipoxia también deberían tenerse en cuenta.

En el corto plazo, es esencial incorporar el efecto de la quimioterapia en los modelos para ayudar en la determinación de las dosis óptimas de fármacos y ultrasonido, así como de los parámetros mecánicos, para un tratamiento efectivo que minimice los efectos colaterales. Por ejemplo, podríamos investigar numéricamente el efecto de combinar una dosis de quimioterapia con la aplicación no continua de ultrasonido, donde aplicamos el ultrasonido durante algunas horas al día y permitimos la proliferación sin ultrasonido durante las horas restantes. Al variar sistemáticamente estos parámetros, podemos determinar el régimen de tratamiento óptimo que maximice la eficacia del tratamiento.

Además de las ondas mecánicas longitudinales, nuestro grupo también está investigando el potencial de las ondas de corte. Dentro del marco numérico de esta tesis, podemos modificar las condiciones iniciales, los rangos de frecuencia y la función de mecanotransducción asociada, que ahora dependería de la tensión de Von Mises o Tresca para tener en cuenta las componentes de corte. Con este estudio, podríamos comparar los efectos de las ondas de corte con el LIUS para investigar cómo cambian los parámetros de sensibilidad celular cuando se modifica la naturaleza de la fuente de tensión.

Además, hemos simulado el tumor como un material viscoelástico a escala ultrasonido. Si bien la poroelasticidad dinámica se ha estudiado principalmente en el contexto del tejido óseo y la ingeniería sísmica, nos esforzamos

por incorporarla en la modelización de la propagación de ondas para examinar los diferentes patrones de respuesta en comparación con la propagación viscoelástica. En este sentido, se asumiría que la fase líquida principalmente absorbe la tensión.

La poroelasticidad dinámica sigue los principios de Biot y sus ecuaciones son más complejas que la poroelasticidad estática [403, 404, 325, 405]. Al considerar ambas fases sólida y fluida, se obtienen dos ondas de compresión, una onda rápida y una onda lenta, y una tercera onda de corte. En los tejidos blandos, en los que la fase sólida carece de alta rigidez, la onda tiende a viajar más rápido a través del fluido y más lento a través del citoesqueleto.

El conjunto de ecuaciones para la propagación de ondas en la poroelasticidad dinámica puede describirse de nuevo en tres formulaciones diferentes. Sin embargo, la formulación **u**-p no existe en el dominio del tiempo, por lo que se suele utilizar la formulación **u**-w o **u**-$\mathbf{u_F}$. Las principales ecuaciones que estamos investigando son 8.0.1.

En este punto, ya hemos programado y validado el modelo, como se muestra en la Figura 8.1 y 8.2, en la cual una onda longitudinal se propaga a través de un medio poroelástico homogéneo con diferentes valores de permeabilidad. Los resultados sugieren que una permeabilidad alta conduce a una disminución en la amplitud de la onda sólida – disipación de energía – mientras que una permeabilidad baja conduce a amplitudes de onda similares. Se necesitan esfuerzos adicionales para comprender las respuestas que tienen en cuenta la heterogeneidad del medio y para estudiar las relaciones entre la permeabilidad, la porosidad y los parámetros de acoplamiento.

Por último, en los próximos años la reingeniería de tumores está destinada a convertirse en un componente desafiante en el análisis de la dinámica tumoral. Por lo tanto, se necesitan más propuestas matemáticas en relación a la temática abordada en la presente tesis con el fin de esclarecer preguntas sobre la acción y las consecuencias de las co-terapias, para finalmente traducir los modelos a una escala específica del paciente y contribuir en última instancia a la toma de decisiones clínicas.

Appendix D

Finite Difference formulation

In this Appendix, we show the finite difference formulation associated with Chapter 3. To solve the problem, we have followed the pioneering works of Shu [382, 383, 384, 385] and codes previously developed in reference [386].

For sake of simplicity, we have rewritten the equation 3.2.10 in one-dimension:

$$\frac{\partial u}{\partial t} = \frac{\partial}{\partial x}\left(D \frac{u^m \frac{\partial u}{\partial x}}{\sqrt{u^2 + \left(\frac{D}{c}\right)^2 |\frac{\partial u}{\partial x}|^2}} \right) + S(u) \tag{D.0.1}$$

where $u(x,t)$ is the solution, and x and t are the spatial and temporal variables, respectively. The source terms $S(u)$ yields:

$$S(u) = Tu\Big(1 - \frac{uV}{C}\Big) - \alpha u^2 + \frac{\mu}{K+\mu} u\Big(\alpha u - \langle \alpha u \rangle\Big). \tag{D.0.2}$$

The WENO method aims to provide a high-order accurate solution free from oscillations, even in the presence of shocks. The algorithm for calculating the non-linear flux is:

1. Compute the first flux approximation.
   We have assumed the first flux approximation as $w = \dfrac{\partial u}{\partial x}$, and we preliminary discretize it as $w_i = \dfrac{u_{i+1} - u_{i-1}}{2\Delta x}$, where w_i is the central finite difference approximation of $\dfrac{\partial u}{\partial x}$ at the point x_i, u_{i+1} and u_{i-1} are the values of u at x_{i+1} and x_{i-1} respectively, and Δx is the distance between x_{i+1} and x_{i-1}, which is the same as the distance between any

two neighboring points of the grid. Then we have:

$$f = \frac{\partial}{\partial x}\left(D \frac{u^m w}{\sqrt{u^2 + \left(\frac{D}{c}\right)^2 |w|^2}} \right) \tag{D.0.3}$$

and we assume w constant.

2. Compute the Lax-Friedrichs Flux Splitting:

$$\begin{aligned} g^+_{i+1/2} &= \frac{1}{2}(f_i + \beta u_i) \\ g^-_{i-1/2} &= \frac{1}{2}(f_i - \beta u_i), \end{aligned} \tag{D.0.4}$$

where $g^+_{i+1/2}$ is the approximation of the flux going from x_i to x_{i+1}, and $g^-_{i-1/2}$ is the approximation of the flux going from x_i to x_{i-1}, and β is a parameter that determines the strength of the flux splitting, which is taken as $\beta = \max(|f|)$. For simplification, from now we consider $h = g^-_{i+1/2}$ and $k = g^+_{i-1/2}$.

3. Approximate the solution in each subdomain using the following high-order polynomials:

$$\begin{aligned} p_{0n} &= \frac{2h_{i-2} - 7h_{i-1} + 11h_i}{6} \\ p_{1n} &= \frac{-h_{i-1} + 5h_i + 2h_{i+1}}{6} \\ p_{2n} &= \frac{2h_i + 5h_{i+1} - h_{i+2}}{6} \\ p_{0p} &= \frac{-k_{i-2} + 5k_{i-1} + 2k_i}{6} \\ p_{1p} &= \frac{2k_{i-1} + 5k_i - k_{i+1}}{6} \\ p_{2p} &= \frac{11k_i - 7k_{i+1} + 2k_{i+2}}{6} \end{aligned} \tag{D.0.5}$$

4. Compute a set of smoothness indicators that measure the degree of

non-smoothness of the solution in each subdomain.

$$
\begin{aligned}
B_{0n} &= \frac{13}{12}(h_{i-2} - 2h_{i-1} + h_i)^2 + \frac{1}{4}(h_{i-2} - 4h_{i-1} + 3h_i)^2 \\
B_{1n} &= \frac{13}{12}(h_{i-1} - 2h_i + h_{i+1})^2 + \frac{1}{4}(h_{i-1} - h_{i+1})^2 \\
B_{2n} &= \frac{13}{12}(h_i - 2h_{i+1} + h_{i+2})^2 + \frac{1}{4}(3h_i - 4h_{i+1} + h_{i+2})^2 \\
B_{0p} &= \frac{13}{12}(k_{i-2} - 2k_{i-1} + k_i)^2 + \frac{1}{4}(k_{i-2} - 4k_{i-1} + 3k_i)^2 \\
B_{1p} &= \frac{13}{12}(k_{i-1} - 2k_i + k_{i+1})^2 + \frac{1}{4}(k_{i-1} - k_{i+1})^2 \\
B_{2p} &= \frac{13}{12}(k_i - 2k_{i+1} + k_{i+2})^2 + \frac{1}{4}(3k_i - 4k_{i+1} + k_{i+2})^2
\end{aligned}
\tag{D.0.6}
$$

5. Compute a set of nonlinear weights that balance the contribution of each polynomial to the final reconstruction.

$$
\begin{aligned}
\alpha_{0n} &= \frac{d_{0n}}{(\epsilon + B_{0n})^2} \\
\alpha_{1n} &= \frac{d_{1n}}{(\epsilon + B_{1n})^2} \\
\alpha_{2n} &= \frac{d_{2n}}{(\epsilon + B_{2n})^2} \\
\alpha_n &= \alpha_{0n} + \alpha_{1n} + \alpha_{2n} \\
\alpha_{0p} &= \frac{d_{0p}}{(\epsilon + B_{0p})^2} \\
\alpha_{1p} &= \frac{d_{1p}}{(\epsilon + B_{1p})^2} \\
\alpha_{2p} &= \frac{d_{2p}}{(\epsilon + B_{2p})^2} \\
\alpha_p &= \alpha_{0p} + \alpha_{1p} + \alpha_{2p}
\end{aligned}
\tag{D.0.7}
$$

with:

$$
\begin{aligned}
d_{0n} = \frac{1}{10}, \quad d_{1n} = \frac{6}{10}, \quad d_{2n} = \frac{3}{10} \\
d_{0p} = \frac{3}{10}, \quad d_{1p} = \frac{6}{10}, \quad d_{2p} = \frac{1}{10}
\end{aligned}
$$

and $\epsilon = 1 \cdot 10^{-6}$.

6. Compute stencil weights.

$$\begin{aligned} w_{0n} &= \frac{\alpha_{0n}}{\alpha_n} \\ w_{1n} &= \frac{\alpha_{1n}}{\alpha_n} \\ w_{2n} &= \frac{\alpha_{2n}}{\alpha_n} \\ w_{0p} &= \frac{\alpha_{0p}}{\alpha_p} \\ w_{1p} &= \frac{\alpha_{1p}}{\alpha_p} \\ w_{2p} &= \frac{\alpha_{2p}}{\alpha_p} \end{aligned} \tag{D.0.8}$$

7. Combine the polynomials and weights to obtain a high-order accurate approximation of the solution.

$$\begin{aligned} f_n = h^-_{i+\frac{1}{2}} &= w_{0n} \cdot p_{0n} + w_{1n} \cdot p_{1n} + w_{2n} \cdot p_{2n} \\ f_p = g^+_{i-\frac{1}{2}} &= w_{0p} \cdot p_{0p} + w_{1p} \cdot p_{1p} + w_{2p} \cdot p_{2p} \end{aligned} \tag{D.0.9}$$

8. Combine the polynomials and weights to obtain a high-order accurate approximation of the solution at the interfaces and add the source term:

$$L_i = \frac{(f_p - f_{p_{i-1}}) + (f_n - f_{n_{i-1}})}{\Delta x} + S(u). \tag{D.0.10}$$

Finally, we use the third-order Runge-Kutta method to integrate in time:

$$\begin{aligned} u^{(1)} &= u^n + \Delta t L(u^n) \\ u^{(2)} &= \frac{3}{4}u^n + \frac{1}{4}u^{(1)} + \frac{1}{4}\Delta t L(u^{(1)}) \\ u^{(3)} &= \frac{1}{3}u^n + \frac{2}{3}u^{(2)} + \frac{2}{3}\Delta t L(u^{(2)}). \end{aligned} \tag{D.0.11}$$

Specifically, given the value of u at time t^n, the scheme calculates an intermediate value $u^{(1)}$ using a standard forward Euler step and a weighted combination of u^n and $u^{(1)}$ is used to estimate u at the midpoint of the time step. Finally, the scheme uses a weighted combination of u^n and $u^{(2)}$ to estimate the solution at the end of the time step.

Appendix E

Weak formulation of equations

E.1 General concepts

The numerical model is self-coded in FEAP 8.6, considering two dimensions and plane strain. The problem is defined in Cartesian coordinates. The MATErial set command is used to specify the parameters for each material as well as to specify the element type associated with the material set parameters.

First, we define an own-coded material, in which we defined the equations of the problem and set parameters. We then blend a square mesh with surface elements defined by quadrilateral (bilateral) shapes consisting of four nodes. The number of used elements depends on the dimensions and characteristics of the problem, ranging between 10^4 and $40 \cdot 10^4$.

For the boundary conditions, line elements (2-node element) are defined using the standard FEAP element library. These are assigned with the FEAP materials: LABC for absorbing boundary conditions in wave propagation and WINKler for Winkler boundary conditions in the slow-scale model.

The Newmark-β method with standard parameters is used as the numerical integration technique to solve the system of second-order differential equations while implicit Backward Euler integration is considered for first-order differential equations. The spatial discretization is performed with standard isoparametric shape functions of Lagrange type.

From now, we show the residuals and tangent matrices associated with Chapters 4 and 5. The total degree of freedoms (a) are six: the displacements (u_x,u_y), the fluid pressure (p), and the solid phases (ϕ^T, ϕ^H, ϕ^M), which we activate or deactivate them depending on the purpose study.

For sake of simplicity, we explain the process for the linear elastic problem and we then show directly the residuals and tangent matrices for all degrees of freedom. Furthermore, we assume that the double dot accounts for the second derivative of time.

To obtain the weak form, the balance of momentum equation is multiplied by test functions – virtual increments of the degrees of freedom – $\delta\boldsymbol{u}$ for displacements – and integrated over the problem domain Ω, by applying the divergence theorem and considering Neumann Boundary conditions. Then, the balance of momentum in weak form reads:

$$-\int_{\Omega}(\nabla^{s}\delta\boldsymbol{u}):\boldsymbol{\sigma}^{T}\,d\Omega+\oint_{\Gamma}\delta\boldsymbol{u}\cdot\boldsymbol{t}d\Gamma-\int_{\Omega}\delta\boldsymbol{u}\cdot(\boldsymbol{b}-\rho\ddot{\boldsymbol{u}})d\Omega=0. \tag{E.1.1}$$

To obtain an approximation solution of this weak form, the degree of freedom at node a given by $\mathtt{a}_a^u$, their corresponding time derivatives, the virtual increments $\delta\mathtt{a}_a^u$, and spatial coordinates $\mathtt{a}_a^x$ are discretized by using standard three-dimensional shape functions $\mathcal{N}$ based on isoparametric Lagrangian polynomials:

$$\begin{aligned}\boldsymbol{u}&\approx\mathcal{N}_a\mathtt{a}_a^u,\\ \ddot{\boldsymbol{u}}&\approx\mathcal{N}_a\ddot{\mathtt{a}}_a^u,\\ \delta\boldsymbol{u}&\approx\mathcal{N}_a\delta\mathtt{a}_a^u,\\ \boldsymbol{x}&\approx\mathcal{N}_a\mathtt{a}_a^x,\end{aligned} \tag{E.1.2}$$

where the Einstein summation convention is used. In addition to the above, we also need to discretize the derivatives of the displacement and test functions with respect to the spatial coordinates. In this case:

$$\begin{aligned}\nabla^{s}\boldsymbol{u}&\approx\nabla^{s}\mathcal{N}_a\mathtt{a}_a^u\approx\boldsymbol{\mathcal{B}}_a^s\mathtt{a}_a^u,\\ \nabla^{s}\delta\boldsymbol{u}&\approx\boldsymbol{\mathcal{B}}_a^s\delta\mathtt{a}_a^u,\end{aligned} \tag{E.1.3}$$

where $\boldsymbol{\mathcal{B}}_a^s$ is the derivative of the shape function with respect to the spatial coordinates. Considering two-dimension and plane strain, the matrix reads:

$$\boldsymbol{\mathcal{B}}_a^s=\begin{pmatrix}\mathcal{N}_{a,1}&0\\ 0&\mathcal{N}_{a,2}\\ 0&0\\ \mathcal{N}_{a,2}&\mathcal{N}_{a,1}\end{pmatrix}. \tag{E.1.4}$$

The residual at node a is directly obtained from the weak form, introducing the previous discretizations and integrating in the finite element of domain

Ω_e and boundary Γ_e:

$$\boldsymbol{\mathcal{R}}_a^u = -\int_{\Omega_e} (\boldsymbol{B}_a^s)^t \boldsymbol{\sigma}\, d\Omega_e + \oint_{\Gamma_e} \mathcal{N}_a \boldsymbol{t} d\Gamma_e - \int_{\Omega_e} \mathcal{N}_a \rho \ddot{\boldsymbol{u}} d\Omega_e \tag{E.1.5}$$

where the superscript t denote the transponse of the matrix. The residual is then differentiated with respect to the degrees of freedom and their time derivatives to obtain the tangent matrices:

$$\begin{aligned} \boldsymbol{\mathcal{K}}_{ab}^{ij} &= -\frac{\partial \boldsymbol{\mathcal{R}}_a^i}{\partial \mathsf{a}_b^j} \\ \boldsymbol{\mathcal{C}}_{ab}^{ij} &= -\frac{\partial \boldsymbol{\mathcal{R}}_a^i}{\partial \dot{\mathsf{a}}_b^j} \\ \boldsymbol{\mathcal{M}}_{ab}^{ij} &= -\frac{\partial \boldsymbol{\mathcal{R}}_a^i}{\partial \ddot{\mathsf{a}}_b^j} \end{aligned} \tag{E.1.6}$$

where $\boldsymbol{\mathcal{K}}$, $\boldsymbol{\mathcal{C}}$ and $\boldsymbol{\mathcal{M}}$ are the stiffness, capacity and mass matrices, respectively. The supra indices i, j denote the degree of freedom and and a and b are two arbitrary nodes. In the following and for sake of simplicity, we directly show the residuals and the tangent matrices used in this work for all degrees of freedom.

E.2 Dynamic balance equation

$$\nabla \cdot \boldsymbol{\sigma} = \rho \ddot{\boldsymbol{u}} \tag{E.2.1}$$

$$\boldsymbol{\mathcal{R}}_a^u = -\int_{\Omega_e} (\boldsymbol{B}_a^s)^t \boldsymbol{\sigma}\, d\Omega_e + \oint_{\Gamma_e} \mathcal{N}_a \boldsymbol{t} d\Gamma_e - \int_{\Omega_e} \mathcal{N}_a \rho \ddot{\boldsymbol{u}} d\Omega_e \tag{E.2.2}$$

considering the constitutive equation $\boldsymbol{\sigma} = \boldsymbol{C}^e : \boldsymbol{\varepsilon} - \boldsymbol{\sigma}_p - \boldsymbol{\sigma}_g$, we have:

$$\boldsymbol{\mathcal{K}}_{ab}^{uu} = \int_{\Omega_e} (\boldsymbol{B}_a^s)^t \boldsymbol{C}^e \boldsymbol{B}_b^s d\Omega_e \tag{E.2.3}$$

$$\boldsymbol{\mathcal{K}}_{ab}^{up} = -\int_{\Omega_e} (\boldsymbol{B}_a^s)^t \alpha \mathcal{N}_b d\Omega_e \tag{E.2.4}$$

$$\boldsymbol{\mathcal{K}}_{ab}^{u\phi^i} = -\int_{\Omega_e} (\boldsymbol{B}_a^s)^t K \mathcal{N}_b d\Omega_e \tag{E.2.5}$$

$$\boldsymbol{\mathcal{M}}_{ab}^{uu} = \int_{\Omega_e} \mathcal{N}_a \rho \mathcal{N}_b \boldsymbol{I} d\Omega_e \tag{E.2.6}$$

Furthermore, the viscoelasticity must be considered in wave propagation. Then, the constitutive equation should add the term $\boldsymbol{\sigma}^v = \boldsymbol{C^v} : \dot{\boldsymbol{\varepsilon}}$ and the capacity matrix is added:

$$\boldsymbol{\mathcal{C}}_{ab}^{uu} = \int_{\Omega_e} (\boldsymbol{\mathcal{B}}_a^s)^t \boldsymbol{C}^v \boldsymbol{\mathcal{B}}_b^s d\Omega_e \tag{E.2.7}$$

E.3 Fluid pressure

$$\frac{1}{M}\frac{\partial p}{\partial t} + \alpha \frac{\partial \varepsilon_v}{\partial t} = -\nabla \cdot \boldsymbol{q} + \Gamma^F, \tag{E.3.1}$$

where $\boldsymbol{q} = -\boldsymbol{k} \cdot \nabla p$, $\Gamma^F = k_v \Big[(p_v - p) - \omega(\pi_v - \pi_l) \Big] - k_l (p - p_l)$, and $k_l = \Big[1 - (\phi^T - \phi^{T0}) \Big] k_{ln}$.

$$\begin{aligned} \boldsymbol{\mathcal{R}}_a^p = \int_{\Omega_e} \boldsymbol{\mathcal{B}}_a^p \boldsymbol{q} d\Omega_e + \oint_{\Gamma_e} \mathcal{N}_a q d\Gamma_e - \int_{\Omega_e} \mathcal{N}_a \frac{1}{M}\frac{dp}{dt} d\Omega_e \\ - \int_{\Omega_e} \mathcal{N}_a \alpha \frac{d\varepsilon_v}{dt} d\Omega_e + \int_{\Omega_e} \mathcal{N}_a \Gamma^F d\Omega_e, \end{aligned} \tag{E.3.2}$$

with $\boldsymbol{\mathcal{B}}_a^p = (N_{a,1}, N_{a,2}, N_{a,3})$.

$$\boldsymbol{\mathcal{K}}_{ab}^{pp} = \int_{\Omega_e} (\boldsymbol{\mathcal{B}}_a^p)^t \boldsymbol{k} \boldsymbol{\mathcal{B}}_a^p d\Omega_e + \int_{\Omega_e} \mathcal{N}_a (k_v + k_l) \mathcal{N}_b d\Omega_e \tag{E.3.3}$$

$$\boldsymbol{\mathcal{K}}_{ab}^{p\phi^T} = -\int_{\Omega_e} \mathcal{N}_a (p - p_l) k_{ln} \mathcal{N}_b d\Omega_e \tag{E.3.4}$$

$$\boldsymbol{\mathcal{C}}_{ab}^{pp} = \int_{\Omega_e} \mathcal{N}_a \frac{1}{M} \mathcal{N}_b d\Omega_e \tag{E.3.5}$$

$$\boldsymbol{\mathcal{C}}_{ab}^{pu} = \int_{\Omega_e} \mathcal{N}_a \alpha \boldsymbol{\mathcal{B}}_b^p d\Omega_e \tag{E.3.6}$$

$$\boldsymbol{\mathcal{C}}_{ab}^{p\phi^i} = -\int_{\Omega_e} \mathcal{N}_a \alpha \mathcal{N}_b d\Omega_e \tag{E.3.7}$$

E.4 Tumor cells phase

$$\frac{\partial \phi^T}{\partial t} = \nabla \cdot \left(D^T \mathcal{M}^T \phi^T \nabla \phi^T \right) + \mathcal{M} T \phi^F \phi^T \Gamma^T T^T \tag{E.4.1}$$

$$\begin{aligned} \boldsymbol{\mathcal{R}}_a^{\phi^T} = & - \int_{\Omega_e} (\boldsymbol{\mathcal{B}}_a^g)^t D^T \mathcal{M}^T \phi^T \nabla \phi^T d\Omega_e \\ & + \oint_{\Gamma_e} \mathcal{N}_a D^T \mathcal{M}^T \phi^T \nabla \phi^T d\Gamma_e \\ & + \int_{\Omega_e} \mathcal{N}_a \Big(\frac{d\phi^T}{dt} - \mathcal{M}^T \phi^F \phi^T \Gamma^T T^T \Big) d\Omega_e \end{aligned} \tag{E.4.2}$$

$$\begin{aligned} \boldsymbol{\mathcal{K}}_a^{\phi^T \phi^T} = & \int_{\Omega_e} (\boldsymbol{\mathcal{B}}_a^g)^t D^T \mathcal{M}^T (\mathcal{N}_b \nabla \phi^T + \phi^T \boldsymbol{\mathcal{B}}_b^g) d\Omega_e \\ + \int_{\Omega_e} \mathcal{N}_a \mathcal{M}^T T^T & \Big[\Gamma^T (\phi^F - \alpha \phi^T) - \alpha^{TT} \phi^F \phi^T \Big] \mathcal{N}_b d\Omega_e, \end{aligned} \tag{E.4.3}$$

with $\boldsymbol{\mathcal{B}}_a^g = (N_{a,1}, N_{a,2}, N_{a,3})$.

$$\boldsymbol{\mathcal{K}}_a^{\phi^T \phi^H} = - \int_{\Omega_e} \mathcal{N}_a \mathcal{M}_T T^T \Big[\phi^T (\alpha \Gamma^T + \alpha^{TH} \phi^F) \Big] \mathcal{N}_b d\Omega_e \tag{E.4.4}$$

$$\boldsymbol{\mathcal{K}}_a^{\phi^T \phi^M} = - \int_{\Omega_e} \mathcal{N}_a \mathcal{M}_T T^T \Big[\phi^T (\alpha \Gamma^T + \alpha^{TM} \phi^F) \Big] \mathcal{N}_b d\Omega_e \tag{E.4.5}$$

$$\boldsymbol{\mathcal{K}}_a^{\phi^T p} = \int_{\Omega_e} \mathcal{N}_a \frac{1}{M} \mathcal{M}_T T^T \phi^T \Gamma^T \mathcal{N}_b d\Omega_e \tag{E.4.6}$$

$$\boldsymbol{\mathcal{C}}_{ab}^{\phi^T \phi^T} = - \int_{\Omega_e} \mathcal{N}_a \mathcal{N}_b d\Omega_e \tag{E.4.7}$$

Mechanotransduction function $\mathcal{M}_T(u)$ is assumed to be constant during one day of development, and since the growth model is updated daily, it can be considered constant with respect to displacements during a day.

E.5 Healthy cells phase

$$\frac{\partial \phi^H}{\partial t} = \mathcal{M}_H \phi^F \phi^H \Gamma^H T^H, \tag{E.5.1}$$

$$\boldsymbol{\mathcal{R}}_a^{\phi^H} = \int_{\Omega_e} \mathcal{N}_a \Big(\frac{d\phi^H}{dt} - \mathcal{M}_H \phi^F \phi^H \Gamma^H T^H \Big) d\Omega_e \tag{E.5.2}$$

$$\boldsymbol{\mathcal{K}}_a^{\phi^H \phi^H} = \int_{\Omega_e} \mathcal{N}_a \mathcal{M}_H T^H \Big[\Gamma^H (\phi^F - \alpha \phi^H) - \alpha^{HH} \phi^F \phi^H \Big] N b d\Omega_e \tag{E.5.3}$$

$$\boldsymbol{\mathcal{K}}_a^{\phi^H \phi^T} = - \int_{\Omega_e} \mathcal{N}_a \mathcal{M}_H T^H \Big[\phi^H (\alpha \phi^H + \alpha^{HT} \phi^F) \Big] \mathcal{N}_b d\Omega_e \tag{E.5.4}$$

$$\boldsymbol{\mathcal{K}}_a^{\phi^H \phi^M} = - \int_{\Omega_e} \mathcal{N}_a \mathcal{M}_H T^H \Big[\phi^H (\alpha \Gamma^H + \alpha^{HM} \phi^F) \Big] \mathcal{N}_b d\Omega_e \tag{E.5.5}$$

$$\boldsymbol{\mathcal{K}}_a^{\phi^H p} = \int_{\Omega_e} \mathcal{N}_a \frac{1}{M} \mathcal{M}_H T^H \phi^H \Gamma^H \mathcal{N}_b d\Omega_e \tag{E.5.6}$$

$$\boldsymbol{\mathcal{C}}_{ab}^{\phi^H \phi^H} = - \int_{\Omega_e} N_a N_b d\Omega_e \tag{E.5.7}$$

Mechanotransduction $\mathcal{M}_H(u)$ is assumed to be constant during one day of development, and since the growth model is updated daily, it can be considered constant with respect to displacements during a day.

E.6 Extracellular matrix

$$\frac{\partial \phi^M}{\partial t} = \beta^T \phi^T + \beta^H \phi^H - \delta^M \phi^M \Gamma^M \tag{E.6.1}$$

$$\boldsymbol{\mathcal{R}}_a^{\phi^M} = \int_{\Omega_e} \mathcal{N}_a \Big(\frac{d\phi^M}{dt} - \beta^T \phi^T - \beta^H \phi^H + \delta^M \phi^M \Gamma^M \Big) d\Omega_e \tag{E.6.2}$$

$$\boldsymbol{\mathcal{K}}_a^{\phi^M \phi^T} = \int_{\Omega_e} \mathcal{N}_a (\beta^T - \delta^M \phi^M \alpha^{MT}) \mathcal{N}_b d\Omega_e \tag{E.6.3}$$

$$\boldsymbol{\mathcal{K}}_a^{\phi^M \phi^H} = \int_{\Omega_e} \mathcal{N}_a (\beta^H - \delta^M \phi^M \alpha^{MH}) \mathcal{N}_b d\Omega_e \tag{E.6.4}$$

$$\boldsymbol{\kappa}_a^{\phi^M \phi^M} = -\int_{\Omega_e} \mathcal{N}_a \delta^M (\alpha^{MT} \phi^T + \alpha^{MH} \phi^H) \mathcal{N}_b d\Omega_e \tag{E.6.5}$$

$$\boldsymbol{c}_{ab}^{\phi^M \phi^M} = -\int_{\Omega_e} \mathcal{N}_a \mathcal{N}_b d\Omega_e \tag{E.6.6}$$

Part V

REFERENCES

References

[1] Hyuna Sung, Jacques Ferlay, Rebecca L Siegel, Mathieu Laversanne, Isabelle Soerjomataram, Ahmedin Jemal, and Freddie Bray. Global cancer statistics 2020: Globocan estimates of incidence and mortality worldwide for 36 cancers in 185 countries. *CA Cancer J. Clin.*

[2] Sociedad Española de Oncología Médica. Las cifras del cáncer en España 2022, 2022.

[3] World Health Org. Int Agency Res Cancer, 2020.

[4] K Robin Yabroff, Jennifer Lund, Deanna Kepka, and Angela Mariotto. Economic burden of cancer in the united states: estimates, projections, and future research. *Cancer Epidemiol. Biomarkers Prev.*, 20(10):2006–2014, 2011.

[5] Thomas Hofmarcher, Peter Lindgren, Nils Wilking, and Bengt Jönsson. The cost of cancer in europe 2018. *Eu. J. Cancer*, 129:41–49, 2020.

[6] X Badía, M Tort, A-G Manganelli, C Camps, and E Díaz-Rubio. The burden of cancer in spain. *Clin. Transl. Oncol.*, 21:729–734, 2019.

[7] Ramon Luengo-Fernandez, Jose Leal, Alastair Gray, and Richard Sullivan. Economic burden of cancer across the european union: a population-based cost analysis. *Lancet Oncol.*, 14(12):1165–1174, 2013.

[8] Paula Andrade, Jose A Sacristan, and Tatiana Dilla. The economic burden of cancer in spain: a literature review. *Health. Econ. Outcome Res.*, 3(1):1–8, 2017.

[9] Natasha B Leighl, Sharon Nirmalakumar, Doreen A Ezeife, and Bishal Gyawali. An arm and a leg: the rising cost of cancer drugs and impact on access. *ASCO Educ. Bk*, 41:e1–e12, 2021.

[10] Oliver Wyman. El impacto económico y social del cáncer en españa. *Asociación Española Contra el Cáncer. AECC*, 2020.

[11] Charles Heidelberger. Chemical carcinogenesis. *Annu. Rev. Bioch.*, 44(1):79–121, 1975.

[12] I Bernard Weinstein. The origins of human cancer: molecular mechanisms of carcinogenesis and their implications for cancer prevention and treatment—twenty-seventh gha clowes memorial award lecture. *Cancer Res.*, 48(15):4135–4143, 1988.

[13] Amy Y Chow. Cell cycle control by oncogenes and tumor suppressors: driving the transformation of normal cells into cancerous cells. *Nat. Edu.*, 3(9):7, 2010.

[14] Hyuk-Jin Cha and Hyungshin Yim. The accumulation of dna repair defects is the molecular origin of carcinogenesis. *Tumor Biol.*, 34:3293–3302, 2013.

[15] Emmanuel N Kontomanolis, Antonios Koutras, Athanasios Syllaios, Dimitrios Schizas, Aikaterini Mastoraki, Nikolaos Garmpis, Michail Diakosavvas, Kyveli Angelou, Georgios Tsatsaris, Athanasios Pagkalos, et al. Role of oncogenes and tumor-suppressor genes in carcinogenesis: a review. *Anticancer Res.*, 40(11):6009–6015, 2020.

[16] Keith R Loeb and Lawrence A Loeb. Significance of multiple mutations in cancer. *Carcinogenesis*, 21(3):379–385, 2000.

[17] Partha M Das and Rakesh Singal. Dna methylation and cancer. *J. Clin. Oncol.*, 22(22):4632–4642, 2004.

[18] Andrew P Feinberg. The epigenetics of cancer etiology. In *Seminars in cancer biology*, volume 14, pages 427–432. Elsevier, 2004.

[19] A Chatterjee, E Mambo, and D Sidransky. Mitochondrial dna mutations in human cancer. *Oncogene*, 25(34):4663–4674, 2006.

[20] M Brandon, P Baldi, and DC Wallace. Mitochondrial mutations in cancer. *Oncogene*, 25(34):4647–4662, 2006.

[21] Manel Esteller. Epigenetics in cancer. *N. Engl. J. Med.*, 358(11):1148–1159, 2008.

[22] Marta Kulis and Manel Esteller. Dna methylation and cancer. *Adv. Genet.*, 70:27–56, 2010.

[23] Shikhar Sharma, Theresa K Kelly, and Peter A Jones. Epigenetics in cancer. *Carcinogenesis*, 31(1):27–36, 2010.

[24] Suganya Ilango, Biswaranjan Paital, Priyanka Jayachandran, Palghat Raghunathan Padma, and Ramalingam Nirmaladevi. Epigenetic alterations in cancer. *Front. Biosci. (Landmark Ed.)*, 25(6):1058–1109, 2020.

[25] Bruce N Ames. Identifying environmental chemicals causing mutations and cancer. *Biol. Revol.: Appl. Cell Biol.*, pages 117–148, 1979.

[26] Stephen S Hecht. Tobacco carcinogens, their biomarkers and tobacco-induced cancer. *Nat. Rev. Cancer*, 3(10):733–744, 2003.

[27] Paolo Boffetta and Mia Hashibe. Alcohol and cancer. *Lancet Oncol.*, 7(2):149–156, 2006.

[28] Tom Walsh and Mary-Claire King. Ten genes for inherited breast cancer. *Cancer Cell*, 11(2):103–105, 2007.

[29] Darren L Roberts, Caroline Dive, and Andrew G Renehan. Biological mechanisms linking obesity and cancer risk: new perspectives. *Annu. Rev. Med.*, 61:301–316, 2010.

[30] Deevya L Narayanan, Rao N Saladi, and Joshua L Fox. Ultraviolet radiation and skin cancer. *Int. J. Dermat.*, 49(9):978–986, 2010.

[31] Iarc - cancer fact sheets. `https://www.iarc.who.int/cancer-topics/`.

[32] Selcuk Colak and Jan P Medema. Cancer stem cells–important players in tumor therapy resistance. *FEBS J.*, 281(21):4779–4791, 2014.

[33] María Auxiliadora Olivares-Urbano, Carmen Griñán-Lisón, Juan Antonio Marchal, and María Isabel Núñez. Csc radioresistance: A therapeutic challenge to improve radiotherapy effectiveness in cancer. *Cells*, 9(7):1651, 2020.

[34] Monica Marzagalli, Fabrizio Fontana, Michela Raimondi, and Patrizia Limonta. Cancer stem cells—key players in tumor relapse. *Cancers*, 13(3):376, 2021.

[35] Andreas Trumpp and Otmar D Wiestler. Mechanisms of disease: cancer stem cells—targeting the evil twin. *Nat. Clin. Pract. Oncol.*, 5(6):337–347, 2008.

[36] Catherine Adell O'Brien, Antonija Kreso, and Catriona HM Jamieson. Cancer stem cells and self-renewal. *Clin. Cancer Res.*, 16(12):3113–3120, 2010.

[37] Min Yu, Aditya Bardia, Ben S Wittner, Shannon L Stott, Malgorzata E Smas, David T Ting, Steven J Isakoff, Jordan C Ciciliano, Marissa N Wells, Ajay M Shah, et al. Circulating breast tumor cells exhibit dynamic changes in epithelial and mesenchymal composition. *Sci.*, 339(6119):580–584, 2013.

[38] Alexandra Flemming. Targeting the root of cancer relapse. *Nat. Rev. Drug Discov.*, 14(3):165–165, 2015.

[39] Lan Thi Hanh Phi, Ita Novita Sari, Ying-Gui Yang, Sang-Hyun Lee, Nayoung Jun, Kwang Seock Kim, Yun Kyung Lee, and Hyog Young Kwon. Cancer stem cells (cscs) in drug resistance and their therapeutic implications in cancer treatment. *Stem Cells Int.*, 2018, 2018.

[40] F Stephen Hodi, Martin C Mihm, Robert J Soiffer, Frank G Haluska, Marcus Butler, Michael V Seiden, Thomas Davis, Rochele Henry-Spires, Suzanne MacRae, Ann Willman, et al. Biologic activity of cytotoxic t lymphocyte-associated antigen 4 antibody blockade in previously vaccinated metastatic melanoma and ovarian carcinoma patients. *Proc. Natl. Acad. Sci.*, 100(8):4712–4717, 2003.

[41] Angela B Mariotto, K Robin Yabroff, Yongwu Shao, Eric J Feuer, and Martin L Brown. Projections of the cost of cancer care in the united states: 2010–2020. *J. Natl. Cancer Inst.*, 103(2):117–128, 2011.

[42] Daniel M Geynisman, Chun-Ru Chien, Fabrice Smieliauskas, Chan Shen, and Ya-Chen Tina Shih. Economic evaluation of therapeutic cancer vaccines and immunotherapy: a systematic review. *Hum. Vaccin. Immunother.*, 10(11):3415–3424, 2014.

[43] Padmanee Sharma and James P Allison. The future of immune checkpoint therapy. *Sci.*, 348(6230):56–61, 2015.

[44] Amy S Codd, Takayuki Kanaseki, Toshihiko Torigo, and Zsuzsanna Tabi. Cancer stem cells as targets for immunotherapy. *Immunology*, 153(3):304–314, 2018.

[45] Rakesh K Jain, John D Martin, and Triantafyllos Stylianopoulos. The role of mechanical forces in tumor growth and therapy. *Annu. Rev. Biomed. Eng.*, 16:321–346, 2014.

[46] Anika Nagelkerke, Johan Bussink, Alan E Rowan, and Paul N Span. The mechanical microenvironment in cancer: how physics affects tumours. In *Semin. Cancer Biol.*, volume 35, pages 62–70. Elsevier, 2015.

[47] Jason J Northey, Laralynne Przybyla, and Valerie M Weaver. Tissue force programs cell fate and tumor aggression. *Cancer Discov.*, 7(11):1224–1237, 2017.

[48] Hadi T Nia, Lance L Munn, and Rakesh K Jain. Physical traits of cancer. *Sci.*, 370(6516):eaaz0868, 2020.

[49] Valentin Gensbittel, Martin Kräter, Sébastien Harlepp, Ignacio Busnelli, Jochen Guck, and Jacky G Goetz. Mechanical adaptability of tumor cells in metastasis. *Dev. Cell*, 56(2):164–179, 2021.

[50] Christiana M Neophytou, Myrofora Panagi, Triantafyllos Stylianopoulos, and Panagiotis Papageorgis. The role of tumor microenvironment in cancer metastasis: Molecular mechanisms and therapeutic opportunities. *Cancers*, 13(9):2053, 2021.

[51] Larry A Taber. *Continuum Modeling in Mechanobiology*. Springer, 2020.

[52] Davide Ambrosi, Martine Ben Amar, Christian J Cyron, Antonio DeSimone, Alain Goriely, Jay D Humphrey, and Ellen Kuhl. Growth and remodelling of living tissues: perspectives, challenges and opportunities. *J. R. Soc. Interface*, 16(157):20190233, 2019.

[53] Marcelo Epstein. Mathematical characterization and identification of remodeling, growth, aging and morphogenesis. *J. Mech. Phys. Solids*, 84:72–84, 2015.

[54] Larry A Taber. Biomechanics of growth, remodeling, and morphogenesis. *Appl. Mech. Rev.*, 48(8):487, 1995.

[55] Boris I Shraiman. Mechanical feedback as a possible regulator of tissue growth. *Proc Natl Acad Sci*, 102(9):3318–3323, 2005.

[56] Xavier Trepat, Michael R Wasserman, Thomas E Angelini, Emil Millet, David A Weitz, James P Butler, and Jeffrey J Fredberg. Physical forces during collective cell migration. *Nat. Phys.*, 5(6):426–430, 2009.

[57] Kenneth D Irvine and Boris I Shraiman. Mechanical control of growth: ideas, facts and challenges. *Dev*, 144(23):4238–4248, 2017.

[58] Pere Roca-Cusachs, Vito Conte, and Xavier Trepat. Quantifying forces in cell biology. *Nat. Cell Biol.*, 19(7):742–751, 2017.

[59] A Wayne Orr, Brian P Helmke, Brett R Blackman, and Martin A Schwartz. Mechanisms of mechanotransduction. *Dev. Cell*, 10(1):11–20, 2006.

[60] Jihye Seong, Ning Wang, and Yingxiao Wang. Mechanotransduction at focal adhesions: from physiology to cancer development. *J. Cell Mol. Med.*, 17(5):597–604, 2013.

[61] LiKang Chin, Yuntao Xia, Dennis E Discher, and Paul A Janmey. Mechanotransduction in cancer. *Curr. Opin. Chem. Eng.*, 11:77–84, 2016.

[62] Nuh N Rahbari, Dmitriy Kedrin, Joao Incio, Hao Liu, William W Ho, Hadi T Nia, Christina M Edrich, Keehoon Jung, Julien Daubriac, Ivy Chen, et al. Anti-vegf therapy induces ecm remodeling and mechanical barriers to therapy in colorectal cancer liver metastases. *Sci. Trans. Med.*, 8(360):360ra135–360ra135, 2016.

[63] Triantafyllos Stylianopoulos, Lance L Munn, and Rakesh K Jain. Reengineering the physical microenvironment of tumors to improve drug delivery and efficacy: from mathematical modeling to bench to bedside. *Trends Cancer*, 4(4):292–319, 2018.

[64] Andreas Blana, François J Murat, Bernhard Walter, Stefan Thuroff, Wolf F Wieland, Christian Chaussy, and Albert Gelet. First analysis of the long-term results with transrectal hifu in patients with localised prostate cancer. *Eur. Urol.*, 53(6):1194–1203, 2008.

[65] HD Liang, J Tang, and M Halliwell. Sonoporation, drug delivery, and gene therapy. *Proc. Inst. Mech. Eng. H*, 224(2):343–361, 2010.

[66] Jiale Qin, Tzu-Yin Wang, and Juergen K Willmann. Sonoporation: Applications for cancer therapy. *Therap. Ultr.*, pages 263–291, 2016.

[67] Ine Lentacker, Ine De Cock, R Deckers, SC De Smedt, and CTW Moonen. Understanding ultrasound induced sonoporation: definitions and underlying mechanisms. *Adv. Drug Deliv. Rev.*, 72:49–64, 2014.

[68] Ezekiel Maloney and Joo Ha Hwang. Emerging hifu applications in cancer therapy. *Int. J. Hyperthermia*, 31(3):302–309, 2015.

[69] William Lopez, Nhu Nguyen, Jessica Cao, Christine Eddow, K Kirk Shung, Nan Sook Lee, and Mosses SS Chow. Ultrasound therapy, chemotherapy and their combination for prostate cancer. *Tech. Cancer Res. Treat.*, 20:15330338211011965, 2021.

[70] David R Mittelstein, Jian Ye, Erika F Schibber, Ankita Roychoudhury, Leyre Troyas Martinez, M Houman Fekrazad, Michael Ortiz, Peter P Lee, Mikhail G Shapiro, and Morteza Gharib. Selective ablation of cancer cells with low intensity pulsed ultrasound. *Appl. Phys. Lett.*, 116(1):013701, 2020.

[71] Stefanie Heyden and Michael Ortiz. Oncotripsy: Targeting cancer cells selectively via resonant harmonic excitation. *J. Mech. Phys. Solids*, 92:164–175, 2016.

[72] S Heyden and M Ortiz. Investigation of the influence of viscoelasticity on oncotripsy. *Comput. Meth. Appl. Mech. Eng.*, 314:314–322, 2017.

[73] Jianhao Lin, Shoulong Dong, Wencheng Peng, Hongmmei Liu, Penghao Zhang, Haoxiang Lv, Liang Yu, and Chenguo Yao. Low-intensity pulsed ultrasound for killing tumor cells: The physical and biological mechanism. In *The Proceedings of the 16th Annual Conference of China Electrotechnical Society*, pages 812–820. Springer, 2022.

[74] Donatella Lucchetti, Luigi Perelli, Filomena Colella, Claudio Ricciardi-Tenore, Gian Luca Scoarughi, Gaetano Barbato, Alma Boninsegna, Ruggero De Maria, and Alessandro Sgambato. Low-intensity pulsed ultrasound affects growth, differentiation, migration, and epithelial-to-mesenchymal transition of colorectal cancer cells. *J. Cell. Physiol.*, 235(6):5363–5377, 2020.

[75] Amit Katiyar, Jenna Osborn, Malaya DasBanerjee, Lijie Grace Zhang, Kausik Sarkar, and Krishna Pada Sarker. Inhibition of human breast cancer cell proliferation by low-intensity ultrasound stimulation. *J. Ultr. Med.*, 39(10):2043–2052, 2020.

[76] Valeria Carina, Viviana Costa, Stefania Pagani, Angela De Luca, Lavinia Raimondi, Daniele Bellavia, Stefania Setti, Milena Fini, and Gianluca Giavaresi. Inhibitory effects of low intensity pulsed ultrasound on osteoclastogenesis induced in vitro by breast cancer cells. *J. Exper. Clin. Cancer Res.*, 37(1):1–11, 2018.

[77] Itziar González, Jon Luzuriaga, Alba Valdivieso, Jesús Frutos, Jaime López, Luis Hernández, Luis Rodríguez-Lorenzo, Virginia Yagüe, Jose Luis Blanco, Alberto Pinto, et al. Low-intensity ultrasound inhibits the long-term migration of cancer cells. 2021.

[78] Itziar González, Jon Luzuriaga, Alba Valdivieso, Jesús Frutos, Jaime López, Luis Hernández, Luis M Rodríguez-Lorenzo, Virginia Yagüe, José Luis Santiago Blanco, Alberto Pinto, et al. Low-intensity continuous ultrasound to inhibit cancer cell migration. *Front. Cell Dev. Biol.*, 2023.

[79] Aditi Singh, Ajay Tijore, Felix Margadant, Chloe Simpson, Deepak Chitkara, Boon Chuan Low, and Michael Sheetz. Enhanced tumor

cell killing by ultrasound after microtubule depolymerization. *BioEng. Transl. Med.*, 6(3):e10233, 2021.

[80] Ajay Tijore, Felix Margadant, Mingxi Yao, Anushya Hariharan, Claire Alexandra Zhen Chew, Simon Powell, Glenn Kunnath Bonney, and Michael Sheetz. Ultrasound-mediated mechanical forces selectively kill tumor cells. *BioRxiv*, 2020.

[81] Kumbakonam R Rajagopal and Luoyi Tao. *Mechanics of mixtures*, volume 35. World Scientific, 1995.

[82] Davide Ambrosi and L Preziosi. On the closure of mass balance models for tumor growth. *Math. Mod. Meth. Appl. Sci.*, 12(05):737–754, 2002.

[83] Tiina Roose, S Jonathan Chapman, and Philip K Maini. Mathematical models of avascular tumor growth. *SIAM Rev.*, 49(2):179–208, 2007.

[84] AR Carotenuto, A Cutolo, A Petrillo, R Fusco, C Arra, M Sansone, D Larobina, L Cardoso, and M Fraldi. Growth and in vivo stresses traced through tumor mechanics enriched with predator-prey cells dynamics. *J. Mech. Behav. Biomed. Mater.*, 86:55–70, 2018.

[85] Anyue Yin, Dirk Jan AR Moes, Johan GC van Hasselt, Jesse J Swen, and Henk-Jan Guchelaar. A review of mathematical models for tumor dynamics and treatment resistance evolution of solid tumors. *CPT: Pharmacomet. Syst. Pharmacol.*, 8(10):720–737, 2019.

[86] Robyn P Araujo and DL Sean McElwain. A history of the study of solid tumour growth: the contribution of mathematical modelling. *Bull Math. Biol.*, 66(5):1039–1091, 2004.

[87] Triantafyllos Stylianopoulos. The solid mechanics of cancer and strategies for improved therapy. *J. Biomech. Eng.*, 139(2), 2017.

[88] Ender Konukoglu, Olivier Clatz, Bjoern H Menze, Bram Stieltjes, Marc-André Weber, Emmanuel Mandonnet, Hervé Delingette, and Nicholas Ayache. Image guided personalization of reaction-diffusion type tumor growth models using modified anisotropic eikonal equations. *IEEE Trans. Med. Imaging*, 29(1):77–95, 2009.

[89] Jared A Weis, Michael I Miga, Lori R Arlinghaus, Xia Li, A Bapsi Chakravarthy, Vandana Abramson, Jaime Farley, and Thomas E Yankeelov. A mechanically coupled reaction–diffusion model for predicting the response of breast tumors to neoadjuvant chemotherapy. *Phys. Med. Biol.*, 58(17):5851, 2013.

[90] David A Hormuth, Jared A Weis, Stephanie L Barnes, Michael I Miga, Erin C Rericha, Vito Quaranta, and Thomas E Yankeelov. A mechanically coupled reaction–diffusion model that incorporates intra-tumoural heterogeneity to predict in vivo glioma growth. *J. R. Soc. Interface*, 14(128):20161010, 2017.

[91] Guillermo Lorenzo, Michael A Scott, Kevin Tew, Thomas JR Hughes, Yongjie Jessica Zhang, Lei Liu, Guillermo Vilanova, and Hector Gomez. Tissue-scale, personalized modeling and simulation of prostate cancer growth. *Proc. Natl. Acad. Sci.*, 113(48):E7663–E7671, 2016.

[92] Guillermo Lorenzo, Thomas JR Hughes, Pablo Dominguez-Frojan, Alessandro Reali, and Hector Gomez. Computer simulations suggest that prostate enlargement due to benign prostatic hyperplasia mechanically impedes prostate cancer growth. *Proc. Natl. Acad. Sci.*, 116(4):1152–1161, 2019.

[93] Shea N Gardner. Modeling multi-drug chemotherapy: tailoring treatment to individuals. *J. Theor. Biol.*, 214(2):181–207, 2002.

[94] Sandeep Sanga, John P Sinek, Hermann B Frieboes, Mauro Ferrari, John P Fruehauf, and Vittorio Cristini. Mathematical modeling of cancer progression and response to chemotherapy. *Expert Rev. Anticancer Ther.*, 6(10):1361–1376, 2006.

[95] KR Raghavan and Andrew E Yagle. Forward and inverse problems in elasticity imaging of soft tissues. *IEEE Trans. Nucl. Sci.*, 41(4):1639–1648, 1994.

[96] Samuel W Key and Raymond D Krieg. Comparison of finite-element and finite-difference methods. In *Numerical and Computer Methods in Structural Mechanics*, pages 337–352. Elsevier, 1973.

[97] Olgierd Cecil Zienkiewicz, Robert Leroy Taylor, and Robert Leroy Taylor. *The finite element method: solid mechanics*, volume 2. Butterworth-heinemann, 2000.

[98] Robert L Taylor. Feap-a finite element analysis program, 2014.

[99] Maren Freutel, Hendrik Schmidt, Lutz Dürselen, Anita Ignatius, and Fabio Galbusera. Finite element modeling of soft tissues: material models, tissue interaction and challenges. *Clin. Biomech.*, 29(4):363–372, 2014.

[100] Gareth H Williams and Kai Stoeber. The cell cycle and cancer. *J. Pathol.*, 226(2):352–364, 2012.

[101] Charles J Sherr. Cancer cell cycles. *Sci.*, 274(5293):1672–1677, 1996.

[102] Michael B Kastan and Jiri Bartek. Cell-cycle checkpoints and cancer. *Nature*, 432(7015):316–323, 2004.

[103] Gerard I Evan and Karen H Vousden. Proliferation, cell cycle and apoptosis in cancer. *Nature*, 411(6835):342–348, 2001.

[104] James D Brierley, Mary K Gospodarowicz, and Christian Wittekind. *TNM classification of malignant tumours*. John Wiley & Sons, 2017.

[105] Alan W Partin, Michael W Kattan, Eric NP Subong, Patrick C Walsh, Kirk J Wojno, Joseph E Oesterling, Peter T Scardino, and Jay D Pearson. Combination of prostate-specific antigen, clinical stage, and gleason score to predict pathological stage of localized prostate cancer: a multi-institutional update. *Jama*, 277(18):1445–1451, 1997.

[106] Scott Valastyan and Robert A Weinberg. Tumor metastasis: molecular insights and evolving paradigms. *Cell*, 147(2):275–292, 2011.

[107] Jamal Majidpoor and Keywan Mortezaee. Steps in metastasis: an updated review. *Med. Oncol.*, 38:1–17, 2021.

[108] ME Menezes, SK Das, I Minn, L Emdad, X-Y Wang, D Sarkar, MG Pomper, and PB Fisher. Detecting tumor metastases: The road to therapy starts here. *Adv. Cancer Res.*, 132:1–44, 2016.

[109] MAJ Chaplain. Avascular growth, angiogenesis and vascular growth in solid tumours: The mathematical modelling of the stages of tumour development. *Math. Comput. Model.*, 23(6):47–87, 1996.

[110] Judah Folkman. Angiogenesis. *Biol. Endothel.*, pages 412–428, 1984.

[111] Judah Folkman. Angiogenesis. *Annu. Rev. Med.*, 57:1–18, 2006.

[112] Diane R Bielenberg and Bruce R Zetter. The contribution of angiogenesis to the process of metastasis. *Cancer J.*, 21(4):267–273, 2015.

[113] Cameron Walker, Elijah Mojares, and Armando del Río Hernández. Role of extracellular matrix in development and cancer progression. *Int. J. Mol. Sci.*, 19(10):3028, 2018.

[114] Paolo A Netti, David A Berk, Melody A Swartz, Alan J Grodzinsky, and Rakesh K Jain. Role of extracellular matrix assembly in interstitial transport in solid tumors. *Cancer Res.*, 60(9):2497–2503, 2000.

[115] Cheryl A Sherman-Baust, Ashani T Weeraratna, Leticia BA Rangel, Ellen S Pizer, Kathleen R Cho, Donald R Schwartz, Teresa Shock, and Patrice J Morin. Remodeling of the extracellular matrix through overexpression of collagen vi contributes to cisplatin resistance in ovarian cancer cells. *Cancer cell*, 3(4):377–386, 2003.

[116] Ting Wu and Yun Dai. Tumor microenvironment and therapeutic response. *Cancer Lett.*, 387:61–68, 2017.

[117] Masoud Najafi, Bagher Farhood, and Keywan Mortezaee. Extracellular matrix (ecm) stiffness and degradation as cancer drivers. *J. Cell. Biochem.*, 120(3):2782–2790, 2019.

[118] John D Hood and David A Cheresh. Role of integrins in cell invasion and migration. *Nat. Rev. Cancer*, 2(2):91–100, 2002.

[119] David J Sieg, Christof R Hauck, Dusko Ilic, Candice K Klingbeil, Erik Schaefer, Caroline H Damsky, and David D Schlaepfer. FAK integrates growth-factor and integrin signals to promote cell migration. *Nat. Cell Biol.*, 2(5):249–256, 2000.

[120] Martin Alexander Schwartz. Integrins and extracellular matrix in mechanotransduction. *CSH Perspect. Biol.*, 2(12):a005066, 2010.

[121] Masanori Ii, Hiroyuki Yamamoto, Yasushi Adachi, Yumiko Maruyama, and Yasuhisa Shinomura. Role of matrix metalloproteinase-7 (matrilysin) in human cancer invasion, apoptosis, growth, and angiogenesis. *Exp. Biol. Med*, 231(1):20–27, 2006.

[122] Yoshifumi Itoh and Hideaki Nagase. Matrix metalloproteinases in cancer. *Essays Biochem.*, 38:21–36, 2002.

[123] Yoshifumi Itoh. Mt1-mmp: A key regulator of cell migration in tissue. *IUBMB Life*, 58(10):589–596, 2006.

[124] Chrisostomi Gialeli, Achilleas D Theocharis, and Nikos K Karamanos. Roles of matrix metalloproteinases in cancer progression and their pharmacological targeting. *FEBS J.*, 278(1):16–27, 2011.

[125] Caitlin Collins, Aleksandra K Denisin, Beth L Pruitt, and W James Nelson. Changes in e-cadherin rigidity sensing regulate cell adhesion. *Proc. Natl. Acad. Sci.*, 114(29):E5835–E5844, 2017.

[126] Alisha M Mendonsa, Tae-Young Na, and Barry M Gumbiner. E-cadherin in contact inhibition and cancer. *Oncogene*, 37(35):4769–4780, 2018.

[127] M Angela Nieto, Ruby Yun-Ju Huang, Rebecca A Jackson, and Jean Paul Thiery. Emt: 2016. *Cell*, 166(1):21–45, 2016.

[128] Thomas Brabletz, Raghu Kalluri, M Angela Nieto, and Robert A Weinberg. Emt in cancer. *Nat. Rev. Cancer*, 18(2):128–134, 2018.

[129] Sarah Heerboth, Genevieve Housman, Meghan Leary, Mckenna Longacre, Shannon Byler, Karolina Lapinska, Amber Willbanks, and Sibaji Sarkar. Emt and tumor metastasis. *Clin. Transl. Med.*, 4(1):1–13, 2015.

[130] Zhan-Qi Cao, Zhi Wang, and Ping Leng. Aberrant n-cadherin expression in cancer. *Biomed. Pharmacother.*, 118:109320, 2019.

[131] Chin-Yap Loh, Jian Yi Chai, Ting Fang Tang, Won Fen Wong, Gautam Sethi, Muthu Kumaraswamy Shanmugam, Pei Pei Chong, and Chung Yeng Looi. The e-cadherin and n-cadherin switch in epithelial-to-mesenchymal transition: signaling, therapeutic implications, and challenges. *Cells*, 8(10):1118, 2019.

[132] Ramsey A Foty and Malcolm S Steinberg. The differential adhesion hypothesis: a direct evaluation. *Dev. Biol.*, 278(1):255–263, 2005.

[133] Ruben C Boot, Gijsje H Koenderink, and Pouyan E Boukany. Spheroid mechanics and implications for cell invasion. *Adv. Phys.*, 6(1):1978316, 2021.

[134] Alice Blumlein, Noel Williams, and Jennifer J McManus. The mechanical properties of individual cell spheroids. *Sci. Rep.*, 7(1):7346, 2017.

[135] N. E. Timmins and L. K. Nielsen. Generation of multicellular tumor spheroids by the hanging-drop method. *Tissue Eng.*, pages 141–151, 2007.

[136] Na-Eun Ryu, Soo-Hong Lee, and Hansoo Park. Spheroid culture system methods and applications for mesenchymal stem cells. *Cells*, 8(12):1620, 2019.

[137] Kazuyoshi Shiga, Masayasu Hara, Takaya Nagasaki, Takafumi Sato, Hiroki Takahashi, and Hiromitsu Takeyama. Cancer-associated fibroblasts: their characteristics and their roles in tumor growth. *Cancers*, 7(4):2443–2458, 2015.

[138] Rui Wei, Si Liu, Shutian Zhang, Li Min, Shengtao Zhu, et al. Cellular and extracellular components in tumor microenvironment and their application in early diagnosis of cancers. *Anal. Cell. Pathol.*, 2020, 2020.

[139] Arthur W. Lambert, Christopher Fiore, Yogesh Chutake, Elisha R. Verhaar, Patrick C. Strasser, Mei Wei Chen, Daneyal Farouq, Sunny Das, Xin Li, Elinor Ng Eaton, Yun Zhang, Joana Liu Donaher, Ian Engstrom, Ferenc Reinhardt, Bingbing Yuan, Sumeet Gupta, Bruce Wollison, Matthew Eaton, Brian Bierie, John Carulli, Eric R. Olson, Matthew G. Guenther, and Robert A. Weinberg. Np63/p73 drive metastatic colonization by controlling a regenerative epithelial stem cell program in quasi-mesenchymal cancer stem cells. *Devel. Cell*, 57(24):2714–2730.e8, 2022.

[140] Tannishtha Reya, Sean J Morrison, Michael F Clarke, and Irving L Weissman. Stem cells, cancer, and cancer stem cells. *Nature*, 414(6859):105–111, 2001.

[141] Barbara Muz, Pilar de la Puente, Feda Azab, and Abdel Kareem Azab. The role of hypoxia in cancer progression, angiogenesis, metastasis, and resistance to therapy. *Hypoxia*, 3:83, 2015.

[142] Michael Hockel and Peter Vaupel. Tumor hypoxia: definitions and curr clinical, biologic and molecular aspects. *J. Natl. Cancer Inst.*, 93(4):266–276, 2001.

[143] Peter Vaupel. The role of hypoxia-induced factors in tumor progression. *Oncologist*, 9(S5):10–17, 2004.

[144] Michael Höckel and Peter Vaupel. Biological consequences of tumor hypoxia. In *Semin. Oncol.*, volume 28, pages 36–41. Elsevier, 2001.

[145] Robert S Kerbel. Tumor angiogenesis. *N. Engl. J. Med.*, 358(19):2039–2049, 2008.

[146] Judah Folkman. Tumor angiogenesis: therapeutic implications. *N. Engl. J. Med.*, 285(21):1182–1186, 1971.

[147] Josette M Northcott, Ivory S Dean, Janna K Mouw, and Valerie M Weaver. Feeling stress: The mechanics of cancer progression and aggression. *Front. Cell Dev. Biol.*, 6:17, 2018.

[148] Borros Arneth. Tumor microenvironment. *Medicina*, 56(1):15, 2019.

[149] TL Whiteside. The tumor microenvironment and its role in promoting tumor growth. *Oncogene*, 27(45):5904–5912, 2008.

[150] D Ambrosi and Francesco Mollica. On the mechanics of a growing tumor. *Int. J. Eng. Sci.*, 40(12):1297–1316, 2002.

[151] Tina Roose, Paolo A Netti, Lance L Munn, Yves Boucher, and Rakesh K Jain. Solid stress generated by spheroid growth estimated using a linear poroelasticity model. *Microvasc. Res.*, 66(3):204–212, 2003.

[152] Jonas Ranft, Maryam Aliee, Jacques Prost, Frank Jülicher, and Jean-François Joanny. Mechanically driven interface propagation in biological tissues. *New J. Phys.*, 16(3):035002, 2014.

[153] Benoît Perthame, Fernando Quirós, and Juan Luis Vázquez. The hele–shaw asymptotics for mechanical models of tumor growth. *Arch. Nat. Mech. Anal.*, 212(1):93–127, 2014.

[154] Gabriel Helmlinger, Paolo A Netti, Hera C Lichtenbeld, Robert J Melder, and Rakesh K Jain. Solid stress inhibits the growth of multicellular tumor spheroids. *Nat. Biotechnol.*, 15(8):778, 1997.

[155] Gang Cheng, Janet Tse, Rakesh K Jain, and Lance L Munn. Microenvironmental mechanical stress controls tumor spheroid size and morphology by suppressing proliferation and inducing apoptosis in cancer cells. *PloS ONE*, 4(2):e4632, 2009.

[156] Fabien Montel, Morgan Delarue, Jens Elgeti, Danijela Vignjevic, Giovanni Cappello, and Jacques Prost. Isotropic stress reduces cell proliferation in tumor spheroids. *New J. Phys.*, 14(5):055008, 2012.

[157] Morgan Delarue, Fabien Montel, Danijela Vignjevic, Jacques Prost, Jean-François Joanny, and Giovanni Cappello. Compressive stress inhibits proliferation in tumor spheroids through a volume limitation. *Biophys. J.*, 107(8):1821–1828, 2014.

[158] Pietro Mascheroni, Cinzia Stigliano, Melania Carfagna, Daniela P Boso, Luigi Preziosi, Paolo Decuzzi, and Bernhard A Schrefler. Predicting the growth of glioblastoma multiforme spheroids using a multiphase porous media model. *Biomech. Mod. Mechanobiol.*, 15(5):1215–1228, 2016.

[159] C Bonnet-Gonnet, L Belloni, and B Cabane. Osmotic pressure of latex dispersions. *Langmuir*, 10(11):4012–4021, 1994.

[160] M Tse Janet, Gang Cheng, James A Tyrrell, Sarah A Wilcox-Adelman, Yves Boucher, Rakesh K Jain, and Lance L Munn. Mechanical compression drives cancer cells toward invasive phenotype. *Proc. Natl. Acad. Sci.*, 109(3):911–916, 2012.

[161] Kévin Alessandri, Bibhu Ranjan Sarangi, Vasily Valérïévitch Gurchenkov, Bidisha Sinha, Tobias Reinhold Kießling, Luc Fetler, Felix Rico, Simon Scheuring, Christophe Lamaze, Anthony Simon, et al. Cellular capsules as a tool for multicellular spheroid production and for investigating the mechanics of tumor progression in vitro. *Proc. Natl. Acad. Sci.*, 110(37):14843–14848, 2013.

[162] Maria Kalli and Triantafyllos Stylianopoulos. Defining the role of solid stress and matrix stiffness in cancer cell proliferation and metastasis. *Front. Oncol.*, 8:55, 2018.

[163] Triantafyllos Stylianopoulos, John D Martin, Vikash P Chauhan, Saloni R Jain, Benjamin Diop-Frimpong, Nabeel Bardeesy, Barbara L Smith, Cristina R Ferrone, Francis J Hornicek, Yves Boucher, et al. Causes, consequences, and remedies for growth-induced solid stress in murine and human tumors. *Proc. Natl. Acad. Sci.*, 109(38):15101–15108, 2012.

[164] Vikash P Chauhan, Yves Boucher, Christina R Ferrone, Sylvie Roberge, John D Martin, Triantafyllos Stylianopoulos, Nabeel Bardeesy, Ronald A DePinho, Timothy P Padera, Lance L Munn, et al. Compression of pancreatic tumor blood vessels by hyaluronan is caused by solid stress and not interstitial fluid pressure. *Cancer Cell*, 26(1):14, 2014.

[165] Arlizan B Ariffin, Patrick F Forde, Saleem Jahangeer, Declan M Soden, and John Hinchion. Releasing pressure in tumors: what do we know so far and where do we go from here? A Rev. *Cancer Res.*, 74(10):2655–2662, 2014.

[166] Ariel Ramírez-Torres, Reinaldo Rodríguez-Ramos, José Merodio, Raimondo Penta, Julián Bravo-Castillero, Raúl Guinovart-Díaz, Federico J Sabina, Catherine García-Reimbert, Igor Sevostianov, and Aura Conci. The influence of anisotropic growth and geometry on the stress of solid tumors. *Int. J. Eng. Sci.*, 119:40–49, 2017.

[167] Markus Basan, Thomas Risler, Jean-François Joanny, Xavier Sastre-Garau, and Jacques Prost. Homeostatic competition drives tumor growth and metastasis nucleation. *HFSP J.*, 3(4):265–272, 2009.

[168] Jonas Ranft, Markus Basan, Jens Elgeti, Jean-François Joanny, Jacques Prost, and Frank Jülicher. Fluidization of tissues by cell division and apoptosis. *Proc. Natl. Acad. Sci.*, 107(49):20863–20868, 2010.

[169] Beatriz Blanco, Juan Campos, Juan Melchor, and Juan Soler. Modeling interactions among migration, growth and pressure in tumor dynamics. *Math.*, 9(12):1376, 2021.

[170] Michela Verbeni, O Sánchez, Emanuela Mollica, Irène Siegl-Cachedenier, Alan Carleton, I Guerrero, A Ruiz i Altaba, and Juan Soler. Morphogenetic action through flux-limited spreading. *Phys. Life Rev.*, 10(4):457–475, 2013.

[171] Sergio Casas-Tintó and Marta Portela. Cytonemes, their formation, regulation, and roles in signaling and communication in tumorigenesis. *Int. J. Mol. Sci.*, 20(22):5641, 2019.

[172] Raimon Sunyer and Xavier Trepat. Durotaxis. *Curr. Biol.*, 30(9):R383–R387, 2020.

[173] Elisabeth G Rens and Roeland MH Merks. Cell shape and durotaxis explained from cell-extracellular matrix forces and focal adhesion dynamics. *Sci.*, 23(9):101488, 2020.

[174] Benjamin Yeoman, Gabriel Shatkin, Pranjali Beri, Afsheen Banisadr, Parag Katira, and Adam J Engler. Adhesion strength and contractility enable metastatic cells to become adurotactic. *Cell Rep.*, 34(10):108816, 2021.

[175] Ben Harland, Sam Walcott, and Sean X Sun. Adhesion dynamics and durotaxis in migrating cells. *Phys. Biol.*, 8(1):015011, 2011.

[176] Valeria Panzetta, Sabato Fusco, and Paolo A Netti. Cell mechanosensing is regulated by substrate strain energy rather than stiffness. *Proc. Natl. Acad. Sci.*, 116(44):22004–22013, 2019.

[177] Lance L Munn and Hadi T Nia. Mechanosensing tensile solid stresses. *Proc. Natl. Acad. Sci.*, 116(44):21960–21962, 2019.

[178] Chrysovalantis Voutouri and Triantafyllos Stylianopoulos. Accumulation of mechanical forces in tumors is related to hyaluronan content and tissue stiffness. *PloS ONE*, 13(3):e0193801, 2018.

[179] Richard Skalak, Stephen Zargaryan, Rakesh K Jain, Paolo A Netti, and Anne Hoger. Compatibility and the genesis of residual stress by volumetric growth. *J. Math .Biol.*, 34(8):889–914, 1996.

[180] D Ambrosi, Simone Pezzuto, Davide Riccobelli, T Stylianopoulos, and Pasquale Ciarletta. Solid tumors are poroelastic solids with a chemo-mechanical feedback on growth. *J. Elast.*, 129(1-2):107–124, 2017.

[181] Hadi Nia, Hao Liu, Giorgio Seano, Meenal Datta, Dennis Jones, Nuh Rahbari, Joao Incio, Vikash Chauhan, Keehoon Jung, John Martin, et al. Solid stress and elastic energy as measures of tumor mechanopathology. *Nat. Biomed. Eng.*, 1(0004), 2017.

[182] Qiong Huang, Xingbin Hu, Wanming He, Yang Zhao, Shihui Hao, Qijing Wu, Shaowei Li, Shuyi Zhang, and Min Shi. Fluid shear stress and tumor metastasis. *Am. J. Cancer Res.*, 8(5):763, 2018.

[183] J Matthew Barnes, Jones T Nauseef, and Michael D Henry. Resistance to fluid shear stress is a conserved biophysical property of malignant cells. *PloS ONE*, 7(12):e50973, 2012.

[184] Adrian C Shieh and Melody A Swartz. Regulation of tumor invasion by interstitial fluid flow. *Phys. Biol.*, 8(1):015012, 2011.

[185] Takanori Tsuji, Soichiro Ibaragi, and Guo-fu Hu. Epithelial-mesenchymal transition and cell cooperativity in metastasis. *Cancer Res.*, 69(18):7135–7139, 2009.

[186] Triantafyllos Stylianopoulos, John D Martin, Matija Snuderl, Fotios Mpekris, Saloni R Jain, and Rakesh K Jain. Coevolution of solid stress and interstitial fluid pressure in tumors during progression: implications for vascular collapse. *Cancer Res.*, 73(13):3833–3841, 2013.

[187] Denis Wirtz, Konstantinos Konstantopoulos, and Peter C Searson. The phys of cancer: the role of physical interactions and mechanical forces in metastasis. *Nat. Rev. Cancer*, 11(7):512–522, 2011.

[188] Kelsey M Gray and Kimberly M Stroka. Vascular endothelial cell mechanosensing: New insights gained from biomimetic microfluidic models. In *Semin. Cell Dev. Biol.*, volume 71, pages 106–117. Elsevier, 2017.

[189] Long Jian Liu, Stephen L Brown, James R Ewing, Brigitte D Ala, Kenneth M Schneider, and Mordechay Schlesinger. Estimation of tumor interstitial fluid pressure (TIFP) noninvasively. *PloS ONE*, 11(7):e0140892, 2016.

[190] Saminathan S Nathan, Gene R DiResta, Jorge E Casas-Ganem, Bang H Hoang, Rebecca Sowers, Rui Yang, Andrew G Huvos, Richard Gorlick,

and John H Healey. Elevated physiologic tumor pressure promotes proliferation and chemosensitivity in human osteosarcoma. *Clin. Cancer Res.*, 11(6):2389–2397, 2005.

[191] Matthias Hofmann, Maike Guschel, August Bernd, Jürgen Bereiter-Hahn, Roland Kaufmann, Christa Tandi, Helge Wiig, and Stefan Kippenberger. Lowering of tumor interstitial fluid pressure reduces tumor cell proliferation in a xenograft tumor model. *Neoplasia*, 8(2):89–95, 2006.

[192] Hyeon-gi Kim, A Ram Yu, Jae Joon Lee, Yong-Jin Lee, Sang Moo Lim, and Jin Su Kim. Measurement of tumor pressure and strategies of imaging tumor pressure for radioimmunotherapy. *Nucl. Med. Mol. Imaging*, pages 1–7, 2019.

[193] Michael Markl, Wolf Wallis, and Andreas Harloff. Reproducibility of flow and wall shear stress analysis using flow-sensitive four-dimensional MRI. *J. Magn. Reson. Imaging*, 33(4):988–994, 2011.

[194] Wouter V Potters, Henk A Marquering, Ed VanBavel, and Aart J Nederveen. Measuring wall shear stress using velocity-encoded MRI. *Curr. Cardiovasc. Imaging Rep.*, 7(4):1–12, 2014.

[195] Giorgio Seano, Hadi T Nia, Kyrre E Emblem, Meenal Datta, Jun Ren, Shanmugarajan Krishnan, Jonas Kloepper, Marco C Pinho, William W Ho, Mitrajit Ghosh, et al. Solid stress in brain tumours causes neuronal loss and neurological dysfunction and can be reversed by lithium. *Nat. Biomed. Eng.*, 3(3):230, 2019.

[196] Gautier Follain, David Herrmann, Sébastien Harlepp, Vincent Hyenne, Naël Osmani, Sean C Warren, Paul Timpson, and Jacky G Goetz. Fluids and their mechanics in tumour transit: shaping metastasis. *Nat. Rev. Cancer*, 20(2):107–124, 2020.

[197] G Lorenzo, TJR Hughes, A Reali, and H Gomez. A numerical simulation study of the dual role of 5α-reductase inhibitors on tumor growth in prostates enlarged by benign prostatic hyperplasia via stress relaxation and apoptosis upregulation. *Comput. Methods Appl. Mech. Eng*, 362:112843, 2020.

[198] Kiran R Nandalur, Robert Colvin, David Walker, Sirisha R Nandalur, Brian Seifman, David Gangwish, and Jason Hafron. Benign prostate hyperplasia as a potential protective factor against prostate cancer: Insights from a magnetic resonance imaging study of compositional characteristics. *Prostate*, 81(14):1097–1104, 2021.

[199] Charlotte Alibert, Bruno Goud, and Jean-Baptiste Manneville. Are cancer cells really softer than normal cells? *Cell Biol.*, 109(5):167–189, 2017.

[200] Ryota Masuzaki, Ryosuke Tateishi, Haruhiko Yoshida, Takahisa Sato, Takamasa Ohki, Tadashi Goto, Hideo Yoshida, Shinpei Sato, Yosuke Sugioka, Hitoshi Ikeda, et al. Assessing liver tumor stiffness by transient elastography. *Hepatol. Int.*, 1(3):394–397, 2007.

[201] Richard G Barr, Richard Memo, and Carl R Schaub. Shear wave ultrasound elastography of the prostate: initial results. *Ultrasound Q.*, 28(1):13–20, 2012.

[202] Matthew C Murphy, John Huston, Kevin J Glaser, Armando Manduca, Fredric B Meyer, Giuseppe Lanzino, Jonathan M Morris, Joel P Felmlee, and Richard L Ehman. Preoperative assessment of meningioma stiffness using magnetic resonance elastography. *J. Neurosurg.*, 118(3):643–648, 2013.

[203] Yuri M Efremov, Mirian Velay-Lizancos, Cory J Weaver, Ahmad I Athamneh, Pablo D Zavattieri, Daniel M Suter, and Arvind Raman. Anisotropy vs isotropy in living cell indentation with AFM. *Sci. Rep.*, 9(1):1–12, 2019.

[204] CT Lim, EH Zhou, and ST Quek. Mechanical models for living cells?a rev. *J. Biomech.*, 39(2):195–216, 2006.

[205] Ralph Sinkus, Mickael Tanter, Tanja Xydeas, Stefan Catheline, Jeremy Bercoff, and Mathias Fink. Viscoelastic shear properties of in vivo breast lesions measured by MR elastography. *Magn. Reson. Imaging*, 23(2):159–165, 2005.

[206] Kay M Pepin and Kiaran P McGee. Quantifying tumor stiffness with magnetic resonance elastography: the role of mechanical properties for detection, characterization, and treatment stratification in oncol. *Top. Magn. Reson. Imaging*, 27(5):353–362, 2018.

[207] AE Bohte, JL Nelissen, JH Runge, O Holub, SA Lambert, L de Graaf, S Kolkman, S Van Der Meij, J Stoker, GJ Strijkers, et al. Breast magnetic resonance elastography: a rev of clinical work and future perspectives. *NMR Biomed.*, 31(10):e3932, 2018.

[208] Kaspar-Josche Streitberger, Ledia Lilaj, Felix Schrank, Jürgen Braun, Karl-Titus Hoffmann, Martin Reiss-Zimmermann, Josef A Käs, and

Ingolf Sack. How tissue fluidity influences brain tumor progression. *Proc. Natl. Acad. Sci.*, 117(1):128–134, 2020.

[209] Alberto Elosegui-Artola. The extracellular matrix viscoelasticity as a regulator of cell and tissue dynamics. *Curr. Opin. Cell. Biol.*, 72:10–18, 2021.

[210] Philip Geoffrey Saffman and Geoffrey Ingram Taylor. The penetration of a fluid into a porous medium or hele-shaw cell containing a more viscous liquid. *Proc. R. Soc.*, 245(1242):312–329, 1958.

[211] George M Homsy. Viscous fingering in porous media. *Annu. Rev. Fluid Mech.*, 19(1):271–311, 1987.

[212] Kaspar-Josche Streitberger, Martin Reiss-Zimmermann, Florian Baptist Freimann, Simon Bayerl, Jing Guo, Felix Arlt, Jens Wuerfel, Jürgen Braun, Karl-Titus Hoffmann, and Ingolf Sack. High-resolution mechanical imaging of glioblastoma by multifrequency magnetic resonance elastography. *PloS ONE*, 9(10):e110588, 2014.

[213] Guillermo Rus, Inas H Faris, Jorge Torres, Antonio Callejas, and Juan Melchor. Why are viscosity and nonlinearity bound to make an impact in clinical elastographic diagnosis? *Sensors*, 20(8):2379, 2020.

[214] Chuen-Mao Yang, Chin-Sung Chien, Chung-Chen Yao, Li-Der Hsiao, Yu-Chen Huang, and Chou Bing Wu. Mechanical strain induces collagenase-3 (MMP-13) expression in MC3T3-E1 osteoblastic cells. *J. Biol. Chem.*, 279(21):22158–22165, 2004.

[215] Florence Broders-Bondon, Thanh Huong Nguyen Ho-Bouldoires, Maria-Elena Fernandez-Sanchez, and Emmanuel Farge. Mechanotransduction in tumor progression: the dark side of the force. *J. Cell Biol.*, 217(5):1571–1587, 2018.

[216] Wei Huang, Hui Hu, Qiong Zhang, Xian Wu, Fuxiang Wei, Fang Yang, Lu Gan, Ning Wang, Xiangliang Yang, and An-Yuan Guo. Regulatory networks in mechanotransduction reveal key genes in promoting cancer cell stemness and proliferation. *Oncogene*, 38(42):6818–6834, 2019.

[217] Bing Han, Xiao-Hui Bai, Monika Lodyga, Jing Xu, Burton B Yang, Shaf Keshavjee, Martin Post, and Mingyao Liu. Conversion of mechanical force into biochem.ical signaling. *J. Biol. Chem.*, 279(52):54793–54801, 2004.

[218] Brenton D Hoffman, Carsten Grashoff, and Martin A Schwartz. Dynamic molecular processes mediate cellular mechanotransduction. *Nature*, 475(7356):316–323, 2011.

[219] Sungsoo Na, Olivier Collin, Farhan Chowdhury, Bernard Tay, Mingxing Ouyang, Yingxiao Wang, and Ning Wang. Rapid signal transduction in living cells is a unique feature of mechanotransduction. *Proc. Natl. Acad. Sci.*, 105(18):6626–6631, 2008.

[220] Martin A Schwartz and Douglas W DeSimone. Cell adhesion receptors in mechanotransduction. *Curr. Opin. Cell Biol.*, 20(5):551–556, 2008.

[221] Viola Vogel. Mechanotransduction involving multimodular proteins: converting force into biochemical signals. *Annu. Rev. Biophys. Biomol. Struct.*, 35:459–488, 2006.

[222] Miki Hieda. Signal transduction across the nuclear envelope: role of the linc complex in bidirectional signaling. *Cells*, 8(2):124, 2019.

[223] Fabiana Martino, Ana R Perestrelo, Vladimír Vinarskỳ, Stefania Pagliari, and Giancarlo Forte. Cellular mechanotransduction: from tension to function. *Front. Physiol.*, 9:824, 2018.

[224] Benjamin Geiger, Joachim P Spatz, and Alexander D Bershadsky. Environmental sensing through focal adhesions. *Nat. Rev. Mol. Cell Biol.*, 10(1):21–33, 2009.

[225] Zeinab Jahed, Hengameh Shams, Mehrdad Mehrbod, and Mohammad RK Mofrad. Mechanotransduction pathways linking the extracellular matrix to the nucleus. In *Int. Rev. Cell Mol. Biol.*, volume 310, pages 171–220. Elsevier, 2014.

[226] Haguy Wolfenson, Bo Yang, and Michael P Sheetz. Steps in mechanotransduction pathways that control cell morphology. *Annu. Rev. Physiol.*, 81:585–605, 2019.

[227] Joshua T Morgan, Christopher J Murphy, and Paul Russell. What do mechanotransduction, Hippo, Wnt, and TGFβ have in common? YAP and TAZ as key orchestrating molecules in ocular health and disease. *Exp. Eye Res.*, 115:1–12, 2013.

[228] Joan Massagué. TGFβ in cancer. *Cell*, 134(2):215–230, 2008.

[229] Charles J David, Yun-Han Huang, Mo Chen, Jie Su, Yilong Zou, Nabeel Bardeesy, Christine A Iacobuzio-Donahue, and Joan Massagué. TGF-β tumor suppression through a lethal EMT. *Cell*, 164(5):1015–1030, 2016.

[230] Joan Seoane and Roger R Gomis. TGF-β family signaling in tumor suppression and cancer progression. *CSHP Biol.*, 9(12):a022277, 2017.

[231] Jiri Zavadil and Erwin P Böttinger. TGF-beta and epithelial-to-mesenchymal transitions. *Oncogene*, 24(37):5764–5774, 2005.

[232] P Singh, JD Wig, R Srinivasan, et al. The Smad family and its role in pancreatic cancer. *Indian J. Cancer*, 48(3):351, 2011.

[233] Mauricio Burotto, Victoria L Chiou, Jung-Min Lee, and Elise C Kohn. The MAPK pathway across different malignancies: a new perspective. *Cancer*, 120(22):3446–3456, 2014.

[234] Joan Massagué. TGFβ signalling in context. *Nat. Rev. Mol. Cell Biol.*, 13(10):616–630, 2012.

[235] Sanjit K Roy, Rakesh K Srivastava, and Sharmila Shankar. Inhibition of PI3K/AKT and MAPK/ERK pathways causes activation of FOXO transcription factor, leading to cell cycle arrest and apoptosis in pancreatic cancer. *J. Mol. Signaling*, 5(1):1–13, 2010.

[236] Robert L Furler, Douglas F Nixon, Christine A Brantner, Anastas Popratiloff, and Christel H Uittenbogaart. TGF-β sustains tumor progression through Biochem.ical and mechanical signal transduction. *Cancers*, 10(6):199, 2018.

[237] Jennifer L Leight, Michele A Wozniak, Sophia Chen, Michelle L Lynch, and Christopher S Chen. Matrix rigidity regulates a switch between TGF-β1–induced apoptosis and epithelial-mesenchymal transition. *Mol. Biol. Cell*, 23(5):781–791, 2012.

[238] Mitsuru Futakuchi, Kris Lami, Yuri Tachibana, Yukari Yamamoto, Masahiro Furukawa, and Junya Fukuoka. The effects of TGF-β signaling on cancer cells and cancer stem cells in the bone microenvironment. *Int. J. Mol. Sci.*, 20(20):5117, 2019.

[239] Carl-Henrik Heldin, Michael Vanlandewijck, and Aristidis Moustakas. Regulation of EMT by TGFβ in cancer. *FEBS Lett.*, 586(14):1959–1970, 2012.

[240] Spencer C Wei, Laurent Fattet, Jeff H Tsai, Yurong Guo, Vincent H Pai, Hannah E Majeski, Albert C Chen, Robert L Sah, Susan S Taylor, Adam J Engler, et al. Matrix stiffness drives epithelial–mesenchymal transition and tumour metastasis through a TWIST1–G3BP2 mechanotransduction pathway. *Nat. Cell Biol.*, 17(5):678–688, 2015.

[241] Jun-Lin Guan. Role of focal adhesion kinase in integrin signaling. *Int. J. Biochem. Cell Biol.*, 29(8-9):1085–1096, 1997.

[242] Armando Del Rio, Raul Perez-Jimenez, Ruchuan Liu, Pere Roca-Cusachs, Julio M Fernandez, and Michael P Sheetz. Stretching single talin rod molecules activates vinculin binding. *Sci.*, 323(5914):638–641, 2009.

[243] Arianne Heinrichs. Switch and stretch. *Nat. Rev. Mol. Cell Biol.*, 10(3):163–163, 2009.

[244] Michael P Sheetz, Dan P Felsenfeld, and Catherine G Galbraith. Cell migration: regulation of force on extracellular-matrix-integrin complexes. *Trends Cell Biol.*, 8(2):51–54, 1998.

[245] Ingrid A Mayer and Carlos L Arteaga. The PI3K/AKT pathway as a target for cancer treatment. *Annu. Rev. Med.*, 67:11–28, 2016.

[246] Hong Yang, Liuyuan Guan, Shun Li, Ying Jiang, Niya Xiong, Li Li, Chunhui Wu, Hongjuan Zeng, and Yiyao Liu. Mechanosensitive caveolin-1 activation-induced PI3K/Akt/mTOR signaling pathway promotes breast cancer motility, invadopodia formation and metastasis in vivo. *Oncotarget*, 7(13):16227, 2016.

[247] Keith Burridge, Elizabeth Monaghan-Benson, and David M Graham. Mechanotransduction: from the cell surface to the nucleus via RhoA. *Philos. Trans. R. Soc.*, 374(1779):20180229, 2019.

[248] Camillo Porta, Chiara Paglino, and Alessandra Mosca. Targeting PI3K/Akt/mTOR signaling in cancer. *Front. Oncol.*, 4:64, 2014.

[249] Jurgen Behrens and Barbara Lustig. The Wnt connection to tumorigenesis. *Int. J. Dev. Biol.*, 48(5-6):477–487, 2004.

[250] A Kikuchi, H Yamamoto, A Sato, and S Matsumoto. Wnt5a: its signalling, functions and implication in diseases. *Acta Physiol.*, 204(1):17–33, 2012.

[251] B Lustig and J Behrens. The Wnt signaling pathway and its role in tumor dev. *J. Cancer Res. Clin. Oncol.*, 129(4):199–221, 2003.

[252] Hans Clevers. Wnt/β-catenin signaling in developement and disease. *Cell*, 127(3):469–480, 2006.

[253] Ian Ackers and Ramiro Malgor. Interrelationship of canonical and non-canonical Wnt signalling pathways in chronic metabolic diseases. *Diab. Vasc. Dis. Res.*, 15(1):3–13, 2018.

[254] Charite Universitatsmedizin Berlin Campus Charite Mitte and Charite Universitatsmedizin Berlin. The Piezo1 Mechanosensitive Ion Channel Promotes Melanoma Malignant Progression by Activating PI3K-AKT Signaling. 2021.

[255] Simei Zhang, Shuang Cao, Mengyuan Gong, Wunai Zhang, Weifan Zhang, Zeen Zhu, Shuai Wu, Yangyang Yue, Weikun Qian, Qingyong Ma, et al. Mechanically activated ion channel Piezo1 contributes to melanoma malignant progression through AKT/mTOR signaling. *Cancer Biol. Ther.*, 23(1):336–347, 2022.

[256] Yu Han, Chao Liu, Dongfang Zhang, Hongchao Men, Lifang Huo, Qiaowei Geng, Shengnan Wang, Yiting Gao, Wei Zhang, Yongjian Zhang, et al. Mechanosensitive ion channel Piezo1 promotes prostate cancer Dev through the activation of the Akt/mTOR pathway and acceleration of cell cycle. *Int. J. Oncol.*, 55(3):629–644, 2019.

[257] Jennifer L Freese, Darya Pino, and Samuel J Pleasure. Wnt signaling in development and disease. *Neurobiol. Dis.*, 38(2):148–153, 2010.

[258] Beibei Wu, Steve P Crampton, and Christopher CW Hughes. Wnt signaling induces matrix metalloproteinase expression and regulates T cell transmigration. *Immunity*, 26(2):227–239, 2007.

[259] Elyssa M Rubin, Yi Guo, Khoa Tu, Jun Xie, Xiaolin Zi, and Bang H Hoang. Wnt Inhibitory Factor 1 (WIF-1) decreases tumorigenesis and metastasis in osteosarcoma. *Mol. Cancer Ther.*, 9(3):731–741, 2010.

[260] David S Yee, Yaxiong Tang, Xuesen Li, Zhongbo Liu, Yi Guo, Samia Ghaffar, Peter McQueen, Dash Atreya, Jun Xie, Anne R Simoneau, et al. The Wnt inhibitory factor 1 restoration in prostate cancer cells was associated with reduced tumor growth, decreased capacity of cell migration and invasion and a reversal of epithelial to mesenchymal transition. *Mol. cancer*, 9(1):1–14, 2010.

[261] Dan Huang and Xiang Du. Crosstalk between tumor cells and microenvironment via Wnt pathway in colorectal cancer dissemination. *World J. Gastroenterol.*, 14(12):1823, 2008.

[262] Janine Wörthmüller and Curzio Rüegg. The crosstalk between FAK and Wnt signaling pathways in cancer and its therapeutic implication. *Int. J. Mol. Sci.*, 21(23):9107, 2020.

[263] Christoph Wissmann, Peter Johannes Wild, Simone Kaiser, Stefan Roepcke, Robert Stoehr, Matthias Woenckhaus, Glen Kristiansen, Jen-Chih Hsieh, Ferdinand Hofstaedter, Arndt Hartmann, et al. WIF1, a component of the Wnt pathway, is down-regulated in prostate, breast, lung, and bladder cancer. *J Pathol.*, 201(2):204–212, 2003.

[264] Yu-Ching Lin, Liang You, Zhidong Xu, Biao He, Cheng-Ta Yang, Jan-Kan Chen, Iwao Mikami, Geneviève Clément, Yihui Shi, Kristopher Kuchenbecker, et al. Wnt inhibitory factor-1 gene transfer inhibits melanoma cell growth. *Hum. Gene Ther.*, 18(4):379–386, 2007.

[265] Gandhi TK Boopathy and Wanjin Hong. Role of hippo pathway-YAP/TAZ signaling in angiogenesis. *Front. Cell Dev. Biol.*, 7:49, 2019.

[266] Stefano Piccolo, Dupont Sirio, and Michelangelo Cordenonsi. The Biol of YAP/TAZ: hippo signaling and beyond. *Phys. Rev.*, 94(4):1287–1312, 2014.

[267] Yu-Chiuan Chang, Jhen-Wei Wu, Chueh-Wen Wang, and Anna C-C Jang. Hippo signaling-mediated mechanotransduction in cell movement and cancer metastasis. *Front. Mol. Biosci.*, 6:157, 2020.

[268] Fa-Xing Yu and Kun-Liang Guan. The hippo pathway: regulators and regulations. *Genes Dev.*, 27(4):355–371, 2013.

[269] Philamer C Calses, James J Crawford, Jennie R Lill, and Anwesha Dey. Hippo pathway in cancer: aberrant regulation and therapeutic opportunities. *Trends Cancer*, 5(5):297–307, 2019.

[270] Wantae Kim and Eek-hoon Jho. The history and regulatory mechanism of the Hippo pathway. *BMB Rep.*, 51(3):106, 2018.

[271] Fernando Calvo, Nil Ege, Araceli Grande-Garcia, Steven Hooper, Robert P Jenkins, Shahid I Chaudhry, Kevin Harrington, Peter Williamson, Emad Moeendarbary, Guillaume Charras, et al. Mechanotransduction and YAP-dependent matrix remodelling is required for the generation and maintenance of cancer-associated fibroblasts. *Nat. Cell Biol.*, 15(6):637–646, 2013.

[272] Xiaomin Cai, Kuei-Chun Wang, and Zhipeng Meng. Mechanoregulation of YAP and TAZ in cellular homeostasis and disease progression. *Front. Cell Dev. Bio.*, 9:673599, 2021.

[273] Sirio Dupont, Leonardo Morsut, Mariaceleste Aragona, Elena Enzo, Stefano Giulitti, Michelangelo Cordenonsi, Francesca Zanconato, Jimmy

Le Digabel, Mattia Forcato, Silvio Bicciato, et al. Role of YAP/TAZ in mechanotransduction. *Nat*, 474(7350):179–183, 2011.

[274] Jin Hao, Yueling Zhang, Dian Jing, Yu Li, Juan Li, and Zhihe Zhao. Role of Hippo signaling in cancer stem cells. *J. Cell Physiol.*, 229(3):266–270, 2014.

[275] Barry J Thompson. YAP/TAZ: drivers of tumor growth, metastasis, and resistance to therapy. *Bioessays*, 42(5):1900162, 2020.

[276] Ahmed Elbediwy, Zoé I Vincent-Mistiaen, and Barry J Thompson. YAP and TAZ in epithelial stem cells: a sensor for cell polarity, mechanical forces and tissue damage. *Bioessays*, 38(7):644–653, 2016.

[277] Janine SA Warren, Yuxuan Xiao, and John M Lamar. YAP/TAZ activation as a target for treating metastatic cancer. *Cancers*, 10(4):115, 2018.

[278] Corinne Bouvier, Nicolas Macagno, Quy Nguyen, Anderson Loundou, Carine Jiguet-Jiglaire, Jean-Claude Gentet, Jean-Luc Jouve, Alexandre Rochwerger, Jean-Camille Mattei, Daniel Bouvard, et al. Prognostic value of the Hippo pathway transcriptional coactivators YAP/TAZ and β1-integrin in conventional osteosarcoma. *Oncotarget*, 7(40):64702, 2016.

[279] Pilar Sanchez, Virginie Clement, and Ariel Ruiz i Altaba. Therapeutic targeting of the Hedgehog-GLI pathway in prostate cancer. *Cancer Res.*, 65(8):2990–2992, 2005.

[280] M Michael Cohen Jr. The hedgehog signaling network. *Am. J. Med. Genet. A.*, 123(1):5–28, 2003.

[281] Emanuela Heller, Michelle A Hurchla, Jingyu Xiang, Xinming Su, Sara Chen, Jochen Schneider, Kyu-Sang Joeng, Marcos Vidal, Leah Goldberg, Hongju Deng, et al. Hedgehog signaling inhibition blocks growth of resistant tumors through effects on tumor microenvironment. *Cancer Res.*, 72(4):897–907, 2012.

[282] Jin Jiang and Chi-chung Hui. Hedgehog signaling in dev and cancer. *Dev. Cell*, 15(6):801–812, 2008.

[283] Aamir Ahmad, Ma'in Y Maitah, Kevin R Ginnebaugh, Yiwei Li, Bin Bao, Shirish M Gadgeel, and Fazlul H Sarkar. Inhibition of Hedgehog signaling sensitizes NSCLC cells to standard therapies through modulation of EMT-regulating miRNAs. *J. Hematol. Oncol.*, 6(1):1–10, 2013.

[284] Yuriko Katoh and Masaru Katoh. Hedgehog signaling, epithelial-to-mesenchymal transition and miRNA. *Int. J. Mol. Med.*, 22(3):271–275, 2008.

[285] Yiwei Li, Ma'in Y Maitah, Aamir Ahmad, Dejuan Kong, Bin Bao, and Fazlul H Sarkar. Targeting the Hedgehog signaling pathway for cancer therapy. *Expert Opin. Ther. Targets*, 16(1):49–66, 2012.

[286] Li Song, Zhuo-Yu Li, Wei-Ping Liu, and Mei-Rong Zhao. Crosstalk between Wnt/β-catenin and Hedgehog/Gli signaling pathways in colon cancer and implications for therapy. *Cancer Biol. Ther.*, 16(1):1–7, 2015.

[287] Delphine Javelaud, Marie-Jeanne Pierrat, and Alain Mauviel. Crosstalk between TGF-β and hedgehog signaling in cancer. *FEBS Lett.*, 586(14):2016–2025, 2012.

[288] Young A Yoo, Myoung Hee Kang, Hyun Joo Lee, Baek-hui Kim, Jong Kuk Park, Hyun Koo Kim, Jun Suk Kim, and Sang Cheul Oh. Sonic hedgehog pathway promotes metastasis and lymphangiogenesis via activation of Akt, EMT, and MMP-9 pathway in gastric cancer. *Cancer Res.*, 71(22):7061–7070, 2011.

[289] Jillian Brechbiel, Karen Miller-Moslin, and Alex A Adjei. Crosstalk between hedgehog and other signaling pathways as a basis for combination therapies in cancer. *Cancer Treat. Rev.*, 40(6):750–759, 2014.

[290] Adrián Aguirre-Tamaral, Manuel Cambón, David Poyato, Juan Soler, and Isabel Guerrero. Predictive model for cytoneme guidance in Hedgehog signaling based on Ihog-Glypicans interaction. *Nat. Comm.*, 13(1):1–14, 2022.

[291] Yun Qi, Han Liu, Kang Zhang, Yihui Wu, Chenghao Shen, and Xinhua Lin. Ihog proteins contribute to integrin-mediated focal adhesions. *Sci. China Life Sci.*, pages 1–10, 2022.

[292] HP Greenspan. Models for the growth of a solid tumor by diffusion. *Stud. Appl. Math.*, 51(4):317–340, 1972.

[293] HP Greenspan. On the growth and stability of cell cultures and solid tumors. *J. Theor. Biol.*, 56(1):229–242, 1976.

[294] DLS McElwain and PJ Ponzo. A model for the growth of a solid tumor with non-uniform oxygen consumption. *Math. Biosci.*, 35(3-4):267–279, 1977.

[295] DLS McElwain and LE Morris. Apoptosis as a volume loss mechanism in mathematical models of solid tumor growth. *Math. Biosci.*, 39(1-2):147–157, 1978.

[296] Helen M Byrne and Mark AJ Chaplain. Mathematical models for tumour angiogenesis: numerical simulations and nonlinear wave solutions. *Bull. Math. Biol.*, 57(3):461–486, 1995.

[297] Robert A Gatenby and Philip K Maini. Mathematical oncology: cancer summed up. *Nature*, 421(6921):321–321, 2003.

[298] HM Byrne, T Alarcon, MR Owen, SD Webb, and PK Maini. Modelling aspects of cancer dynamics: a review. *Philos. Trans. R. Soc. A*, 364(1843):1563–1578, 2006.

[299] Helen M Byrne. Dissecting cancer through mathematics: from the cell to the animal model. *Nat. Rev. Cancer*, 10(3):221–230, 2010.

[300] Angela M Jarrett, Ernesto ABF Lima, David A Hormuth, Matthew T McKenna, Xinzeng Feng, David A Ekrut, Anna Claudia M Resende, Amy Brock, and Thomas E Yankeelov. Mathematical models of tumor cell proliferation: A review of the literature. *Expert Rev. Anticancer Ther.*, 18(12):1271–1286, 2018.

[301] Prashant Dogra, Joseph D Butner, Yao-li Chuang, Sergio Caserta, Shreya Goel, C Jeffrey Brinker, Vittorio Cristini, and Zhihui Wang. Mathematical modeling in cancer nanomedicine: a review. *Biomed. Microdevices*, 21:1–23, 2019.

[302] Sophie Bekisz and Liesbet Geris. Cancer modeling: From mechanistic to data-driven approaches, and from fundamental insights to clinical applications. *J. Comput. Sci.*, 46:101198, 2020.

[303] John Metzcar, Yafei Wang, Randy Heiland, and Paul Macklin. A review of cell-based computational modeling in cancer biology. *JCO Clin. Cancer Inform.*, 2:1–13, 2019.

[304] Massimiliano Fraldi and Angelo R Carotenuto. Cells competition in tumor growth poroelasticity. *J. Mech. Phys. Solids*, 112:345–367, 2018.

[305] G Albano and V Giorno. A stochastic model in tumor growth. *J. Theor. Biol.*, 242(2):329–336, 2006.

[306] Juan Luis Vázquez. *The porous medium equation: mathematical theory*. Oxford University Press, 2007.

[307] Juan Calvo, Juan Campos, Vicent Caselles, O Sánchez, and Juan Soler. Pattern formation in a flux limited reaction–diffusion equation of porous media type. *Invent. Math.*, 206(1):57–108, 2016.

[308] J Campos and J Soler. Qualitative behavior and traveling waves for flux-saturated porous media equations arising in optimal mass transportation. *Nonlinear Anal.*, 137:266–290, 2016.

[309] Martina Conte, Sergio Casas-Tintò, and Juan Soler. Modeling invasion patterns in the glioblastoma battlefield. *PLoS Comp. Biol.*, 17(1):e1008632, 2021.

[310] Juan Calvo, Juan Campos, Vicent Caselles, Óscar Sánchez, and Juan Soler. Flux-saturated porous media equations and applications. *EMS Surveys Math. Sci.*, 2(1):131–218, 2015.

[311] Juan Calvo, Juan Campos, Vicent Caselles, Óscar Sánchez, and Juan Soler. Qualitative behaviour for flux-saturated mechanisms: travelling waves, waiting time and smoothing effects. *J. Math. Biol.*, 19(2):441–472, 2017.

[312] Juan Campos, Pilar Guerrero, Óscar Sánchez, and Juan Soler. On the analysis of traveling waves to a nonlinear flux limited reaction–diffusion equation. In *Annales de l'IHP Analyse non linéaire*, volume 30, pages 141–155, 2013.

[313] Lutz Claes and Bettina Willie. The enhancement of bone regeneration by ultrasound. *Prog. Biophys. Mol. Biol.*, 93(1-3):384–398, 2007.

[314] Seyed Jamaleddin Mousavi, Mohamed Hamdy Doweidar, and Manuel Doblaré. 3d computational modelling of cell migration: A mechano-chemo-thermo-electrotaxis approach. *J. Theor. Biol.*, 329:64–73, 2013.

[315] Jacobo Ayensa-Jiménez, Marina Pérez-Aliacar, Teodora Randelovic, Sara Oliván, Luis Fernández, José Antonio Sanz-Herrera, Ignacio Ochoa, Mohamed H Doweidar, and Manuel Doblaré. Mathematical formulation and parametric analysis of in vitro cell models in microfluidic devices: application to different stages of glioblastoma evolution. *Sci. Rep.*, 10(1):21193, 2020.

[316] Martina Conte and Christina Surulescu. Mathematical modeling of glioma invasion: acid-and vasculature mediated go-or-grow dichotomy and the influence of tissue anisotropy. *Appl. Math. Comput.*, 407:126305, 2021.

[317] Myriam Labelle and Richard O Hynes. The initial hours of metastasis: The importance of cooperative host–tumor cell interactions during hematogenous disseminationhost–tumor cell interactions during metastatic dissemination. *Cancer Discov.*, 2(12):1091–1099, 2012.

[318] John S Lowengrub, Hermann B Frieboes, Fang Jin, Yao-Li Chuang, Xiangrong Li, Paul Macklin, Steven M Wise, and Vittorio Cristini. Nonlinear modelling of cancer: bridging the gap between cells and tumours. *Nonlinearity*, 23(1):R1, 2009.

[319] Edward K Rodriguez, Anne Hoger, and Andrew D McCulloch. Stress-dependent finite growth in soft elastic tissues. *J. Biomech.*, 27(4):455–467, 1994.

[320] Lev Davidovich Landau, Evgenij M Lifšic, Evegnii Mikhailovich Lifshitz, Arnold Markovich Kosevich, and Lev Petrovich Pitaevskii. *Theory of elasticity*, volume 7. Elsevier, 1986.

[321] Chrysovalantis Voutouri, Fotios Mpekris, Panagiotis Papageorgis, Andreani D Odysseos, and Triantafyllos Stylianopoulos. Role of constitutive behavior and tumor-host mechanical interactions in the state of stress and growth of solid tumors. *PloS ONE*, 9(8):104717, 2014.

[322] Fotios Mpekris, Chrysovalantis Voutouri, Panagiotis Papageorgis, and Triantafyllos Stylianopoulos. Stress alleviation strategy in cancer treatment: Insights from a mathematical model. *ZAMM-J. Appl. Math. Mech.*, 98(12):2295–2306, 2018.

[323] Chysovalantis Voutouri and Triantafyllos Stylianopoulos. Evolution of osmotic pressure in solid tumors. *J. Biomech.*, 47(14):3441–3447, 2014.

[324] Fotios Mpekris, Stelios Angeli, Athanassios P Pirentis, and Triantafyllos Stylianopoulos. Stress-mediated progression of solid tumors: effect of mechanical stress on tissue oxygenation, cancer cell proliferation, and drug delivery. *BioMech. Mod. Mechanobiol.*, 14(6):1391–1402, 2015.

[325] Stephen C Cowin. *Continuum mechanics of anisotropic materials*. Springer Science & Business Media, 2013.

[326] Helen Byrne and Luigi Preziosi. Modelling solid tumour growth using the theory of mixtures. *Math. Med. Biol.*, 20(4):341–366, 2003.

[327] JD Humphrey and KR Rajagopal. A constrained mixture model for growth and remodeling of soft tissues. *Math. Mod. Meth. App. Sci.*, 12(03):407–430, 2002.

[328] Clifford Truesdell. Sulle basi della termomeccanica. *Rend. Lincei*, 22(8):33–38, 1957.

[329] Alan J Bray. Theory of phase-ordering kinetics. *Adv. Phys.*, 51(2):481–587, 2002.

[330] Angelo Rosario Carotenuto, Arsenio Cutolo, Stefania Palumbo, and Massimiliano Fraldi. Lyapunov stability of competitive cells dynamics in tumor mechanobiol. *Acta Mech. Sin.*, 37(2):244–263, 2021.

[331] Cosmina Hogea, Christos Davatzikos, and George Biros. An image-driven parameter estimation problem for a reaction–diffusion glioma growth model with mass effects. *J. Math. Biol.*, 56(6):793–825, 2008.

[332] Angela M Jarrett, David A Hormuth, Stephanie L Barnes, Xinzeng Feng, Wei Huang, and Thomas E Yankeelov. Incorporating drug delivery into an imaging-driven, mechanics-coupled reaction diffusion model for predicting the response of breast cancer to neoadjuvant chemotherapy: theory and preliminary clinical results. *Phys Med Biol*, 63(10):105015, 2018.

[333] Si-Fan Yin, Shi-Lei Xue, Bo Li, and Xi-Qiao Feng. Bio–chemo–mechanical modeling of growing biological tissues: Finite element method. *Int. J. Non Linear Mech.*, 108:46–54, 2019.

[334] Ariel Ramírez-Torres, Reinaldo Rodríguez-Ramos, Rainer Glüge, Julián Bravo-Castillero, Raúl Guinovart-Díaz, and Rocío Rodríguez-Sanchez. Biomechanic approach of a growing tumor. *Mech. Res. Comm.*, 51:32–38, 2013.

[335] A Ramírez-Torres, R Rodríguez-Ramos, José Merodio, Julián Bravo-Castillero, R Guinovart-Díaz, and Juan Carlos López Alfonso. Action of body forces in tumor growth. *Int. J. Eng. Sci.*, 89:18–34, 2015.

[336] Xinjian Chen, Ronald M Summers, and Jianhua Yao. Kidney tumor growth prediction by coupling reaction–diffusion and biomechanical model. *IEEE Trans. Biomed. Eng.*, 60(1):169–173, 2012.

[337] Maurice A Biot. General theory of three-dimensional consolidation. *J. Appl. Phys.*, 12(2):155–164, 1941.

[338] Emmanuel Detournay and Alexander H-D Cheng. Fundamentals of poroelasticity. In *Analysis and design methods*, pages 113–171. Elsevier, 1993.

[339] Stephen C Cowin and Stephen B Doty. *Tissue mechanics*. Springer, 2007.

[340] Rakesh K Jain, Ricky T Tong, and Lance L Munn. Effect of vascular normalization by antiangiogenic therapy on interstitial hypertension, peritumor edema, and lymphatic metastasis: insights from a mathematical model. *Cancer Res.*, 67(6):2729–2735, 2007.

[341] David A Hormuth, Caleb M Phillips, Chengyue Wu, Ernesto ABF Lima, Guillermo Lorenzo, Prashant K Jha, Angela M Jarrett, J Tinsley Oden, and Thomas E Yankeelov. Biologically-based mathematical modeling of tumor vasculature and angiogenesis via time-resolved imaging data. *Cancers*, 13(12):3008, 2021.

[342] Min Wu, Hermann B Frieboes, Mark AJ Chaplain, Steven R McDougall, Vittorio Cristini, and John S Lowengrub. The effect of interstitial pressure on therapeutic agent transport: coupling with the tumor blood and lymphatic vascular systems. *J Theor Biol*, 355:194–207, 2014.

[343] P Mascheroni, M Carfagna, A Grillo, DP Boso, and BA Schrefler. An avascular tumor growth model based on porous media mechanics and evolving natural states. *Math. Mech. Solids*, 23(4):686–712, 2018.

[344] Shi-Lei Xue, Bo Li, Xi-Qiao Feng, and Huajian Gao. Biochemechanical poroelastic theory of avascular tumor growth. *J. Mech. Phys. Solids*, 94:409–432, 2016.

[345] Davide Ambrosi and Luigi Preziosi. Cell adhesion mechanisms and stress relaxation in the mechanics of tumours. *Biomech. Mod. Mechanbiol.*, 8(5):397, 2009.

[346] Mark AJ Chaplain, Luigi Graziano, and Luigi Preziosi. Mathematical modelling of the loss of tissue compression responsiveness and its role in solid tumour dev. *Math. Med. Biol.*, 23(3):197–229, 2006.

[347] Daoxiang Huang and Satoru Kidoaki. Stiffness-optimized drug-loaded matrix for selective capture and elimination of cancer cells. *J. Drug Deliv. Sci. Technol.*, 55:101414, 2020.

[348] Rakesh K Jain and Triantafyllos Stylianopoulos. Delivering nanomedicine to solid tumors. *Nat. Rev. Clin. Oncol.*, 7(11):653, 2010.

[349] Christiana Polydorou, Fotios Mpekris, Panagiotis Papageorgis, Chrysovalantis Voutouri, and Triantafyllos Stylianopoulos. Pirfenidone normalizes the tumor microenvironment to improve chemotherapy. *Oncotarget*, 8(15):24506, 2017.

[350] Hao-Li Liu, Mu-Yi Hua, Hung-Wei Yang, Chiung-Yin Huang, Po-Chun Chu, Jia-Shin Wu, I-Chou Tseng, Jiun-Jie Wang, Tzu-Chen Yen, Pin-Yuan Chen, et al. Magnetic resonance monitoring of focused ultrasound/magnetic nanoparticle targeting delivery of therapeutic agents to the brain. *Proc. Natl. Acad. Sci.*, 107(34):15205–15210, 2010.

[351] Adam J Cole, Victor C Yang, and Allan E David. Cancer theranostics: the rise of targeted magnetic nanoparticles. *Trends Biotechnol.*, 29(7):323–332, 2011.

[352] Yuqi Wu, Xiaobing Liu, Zizhen Qin, Li Hu, and Xiangwei Wang. Low-frequency ultrasound enhances chemotherapy sensitivity and induces autophagy in PTX-resistant PC-3 cells via the endoplasmic reticulum stress-mediated PI3K/Akt/mTOR signaling pathway. *Onco Targets Ther.*, 11:5621, 2018.

[353] Natalya Y Rapoport, Anne M Kennedy, Jill E Shea, Courtney L Scaife, and Kweon-Ho Nam. Controlled and targeted tumor chemotherapy by ultrasound-activated nanoemulsions/microbubbles. *J. Control Release*, 138(3):268–276, 2009.

[354] Scott Schoen Jr, M Sait Kilinc, Hohyun Lee, Yutong Guo, F Levent Degertekin, Graeme F Woodworth, and Costas Arvanitis. Towards controlled drug delivery in brain tumors with microbubble-enhanced focused ultrasound. *Adv. Drug Deliv. Rev.*, 180:114043, 2022.

[355] CA Speed. Therapeutic ultrasound in soft tissue lesions. *Rheumatology*, 40(12):1331–1336, 2001.

[356] Irene Tirado-Cabrera, Eduardo Martin-Guerrero, Sara Heredero-Jimenez, Juan A Ardura, and Arancha R Gortázar. PTH1R translocation to primary cilia in mechanically-stimulated ostecytes prevents osteoclast formation via regulation of CXCL5 and IL-6 secretion. *J. Cell Physiol.*, 2022.

[357] Pawel Piotr Dobrakowski, Agnieszka Kamila Machowska-Majchrzak, Beata Łabuz-Roszak, Krzysztof Grzegorz Majchrzak, Ewa Kluczewska, and Krystyna Barbara Pierzchała. MR-guided focused ultrasound: a new generation treatment of Parkinson's disease, essential tremor and neuropathic pain. *Interv. Neuroradiol.*, 20(3):275–282, 2014.

[358] Sebastien Crouzet, Jean Yves Chapelon, Olivier Rouvière, Florence Mege-Lechevallier, Marc Colombel, Hélène Tonoli-Catez, Xavier Martin, and Albert Gelet. Whole-gland ablation of localized prostate cancer with high-intensity focused ultrasound: oncologic outcomes and morbidity in 1002 patients. *Eur. Urol.*, 65(5):907–914, 2014.

[359] Andrew KW Wood and Chandra M Sehgal. A review of low-intensity ultrasound for cancer therapy. *Ultr. Med. Biol.*, 41(4):905–928, 2015.

[360] Tinghe Yu, Zhibiao Wang, and Timothy J Mason. A review of research into the uses of low level ultrasound in cancer therapy. *Ultrason. Sonochem.*, 11(2):95–103, 2004.

[361] Marlies Christina Hoelzl, Marco Fiorito, Ondrej Holub, Gilbert Fruhwirth, and Ralph Sinkus. Oscillatory shear strain impacts metastatic cancer cell spread. In *Proc. Int. Soc. Magn. Reson. Med*, page 2813, 2016.

[362] Marlies Glatz. *Low frequency shear waves as a potential mechanotherapy approach in cancer*. PhD thesis, King's College London, 2019.

[363] Marlies Christina Hoelzl, Frederic Festy, Gilbert Fruhwirth, and Ralph Sinkus. Impacting cancer cells via mechanical waves: can we change cellular behaviour? In *Proc. Int. Soc. Magn. Reson. Med.*, page 4363, 20167.

[364] Yu Ling Huang, Yujie Ma, Cindy Wu, Carina Shiau, Jeffrey E Segall, and Mingming Wu. Tumor spheroids under perfusion within a 3D microfluidic platform reveal critical roles of cell-cell adhesion in tumor invasion. *Sci. Rep.*, 10(1):1–11, 2020.

[365] Antonio Jesús Gómez Fernández. *Transurethral shear wave elastography for prostate cancer*. PhD thesis, UCL (University College London), 2018.

[366] Jose M Carcione. Viscoelastic effective rheologies for modelling wave propagation in porous media. *Geophys. prospect.*, 46(3):249–270, 2008.

[367] Thomas S Brown, Shukai Du, Hasan Eruslu, and Francisco-Javier Sayas. Analysis of models for viscoelastic wave propagation. *Appl. Math. Nonlinear Sci.*, 3(1):55–96, 2018.

[368] Antonio Manuel Callejas Zafra et al. Feasibility of using torsional waves to assess viscoelasticity of cervical tissue. 2019.

[369] Raghu Kalluri, Robert A Weinberg, et al. The basics of epithelial-mesenchymal transition. *J. Clin. Inv.*, 119(6):1420–1428, 2009.

[370] Felipe-Andrés Ramírez-Weber and Thomas B Kornberg. Cytonemes: cellular processes that project to the principal signaling center in drosophila imaginal discs. *Cell*, 97(5):599–607, 1999.

[371] Marcos Julián Cardozo, Luisa Sánchez-Arrones, Africa Sandonis, Cristina Sánchez-Camacho, Gaia Gestri, Stephen W Wilson, Isabel Guerrero, and Paola Bovolenta. Cdon acts as a hedgehog decoy receptor during proximal-distal patterning of the optic vesicle. *Nat. Comm.*, 5(1):1–13, 2014.

[372] Thomas B Kornberg and Lilach Gilboa. Nanotubes in the niche. *Nat*, 523(7560):292–293, 2015.

[373] Hai Huang, Songmei Liu, and Thomas B Kornberg. Glutamate signaling at cytoneme synapses. *Sci.*, 363(6430):948–955, 2019.

[374] Laura González-Méndez, Irene Seijo-Barandiarán, and Isabel Guerrero. Cytoneme-mediated cell-cell contacts for hedgehog reception. *Elife*, 6:e24045, 2017.

[375] J Casas-Vázquez and D Jou. Nonequilibrium temperature versus local-equilibrium temperature. *Phys. Rev. E.*, 49(2):1040, 1994.

[376] Tomasz Dębiec, Benoît Perthame, Markus Schmidtchen, and Nicolas Vauchelet. Incompressible limit for a two-species model with coupling through brinkman's law in any dimension. *J. Math. Pures Appl.*, 145:204–239, 2021.

[377] Benoît Perthame, Fernando Quirós, Min Tang, and Nicolas Vauchelet. Derivation of a hele-shaw type system from a cell model with active motion. *Interface Free Bound.*, 16:489–508, 2014.

[378] Vlado A Lubarda and Anne Hoger. On the mechanics of solids with a growing mass. *Int. J. Solids Struct.*, 39(18):4627–4664, 2002.

[379] F. Andreu, J. Calvo, J. M. Mazón, and J. Soler. On a nonlinear flux-limited equation arising in the transport of morphogens. *J. Differential Equations*, 252(10):5763–5813, 2012.

[380] M. Arias, J. Campos, and J. Soler. Cross-diffusion and traveling waves in porous-media flux-saturated keller–segel models. *Math. Models Methods Appl. Sci.*, 28(11):2103–2129, 2018.

[381] Juan Campos, Claudia García, and Juan Soler. Kinks and solitons in linear and nonlinear-diffusion keller-segel type models with logarithmic sensitivity. *arXiv preprint arXiv:2102.13480*, 2021.

[382] Yuanyuan Liu, Chi-Wang Shu, and Mengping Zhang. High order finite difference weno schemes for nonlinear degenerate parabolic equations. *SIAM J. Sci. Comput.*, 33(2):939–965, 2011.

[383] Bernardo Cockburn, Chi-Wang Shu, Claes Johnson, Eitan Tadmor, and Chi-Wang Shu. *Essentially non-oscillatory and weighted essentially non-oscillatory schemes for hyperbolic conservation laws*. Springer, 1998.

[384] Chi-Wang Shu. Essentially non-oscillatory and weighted essentially non-oscillatory schemes for hyperbolic conservation laws. In *Adv. Num. Approx. Nonlinear Hyperbolic Eq.*, pages 325–432. Springer, 1998.

[385] Chi-Wang Shu. Essentially non-oscillatory and weighted essentially non-oscillatory schemes. *Acta Numerica*, 29:701–762, 2020.

[386] Manuel A. Diaz. Weighted essentially non-oscillatory (weno) scheme. https://www.mathworks.com/matlabcentral/fileexchange/44639-weighted-essentially-non-oscillatory-weno-scheme, 2021. MATLAB Central File Exchange. Retrieved March 10, 2020.

[387] Kidong Park, Larry J Millet, Namjung Kim, Huan Li, Xiaozhong Jin, Gabriel Popescu, NR Aluru, K Jimmy Hsia, and Rashid Bashir. Measurement of adherent cell mass and growth. *Proc. Natl. Acad. Sci.*, 107(48):20691–20696, 2010.

[388] Katarzyna Pogoda, LiKang Chin, Penelope C Georges, FitzRoy J Byfield, Robert Bucki, Richard Kim, Michael Weaver, Rebecca G Wells, Cezary Marcinkiewicz, and Paul A Janmey. Compression stiffening of brain and its effect on mechanosensing by glioma cells. *New J. Phys.*, 16(7):075002, 2014.

[389] Andrei S Dukhin and Philip J Goetz. Bulk viscosity and compressibility measurement using acoustic spectroscopy. *J. Chem. Phys.*, 130(12):124519, 2009.

[390] Leander Claes, René Spencer Chatwell, Elmar Baumhögger, Tim Hetkämper, Henning Zeipert, Jadran Vrabec, and Bernd Henning. Measurement procedure for acoustic absorption and bulk viscosity of liquids. *Measurement*, 184:109919, 2021.

[391] F. T. d'Astous and F. S. Foster. Frequency dependence of ultrasound attenuation and backscatter in breast tissue. *Ultrasound Med. Biol.*, 12(10):795–808, 1986.

[392] Linda R Taggart, Ralph E Baddour, Anoja Giles, Gregory J Czarnota, and Michael C Kolios. Ultrasonic characterization of whole cells and isolated nuclei. *Ultr. Med. Biol.*, 33(3):389–401, 2007.

[393] Elie Nader, Sarah Skinner, Marc Romana, Romain Fort, Nathalie Lemonne, Nicolas Guillot, Alexandra Gauthier, Sophie Antoine-Jonville, Céline Renoux, Marie-Dominique Hardy-Dessources, et al. Blood rheology: key parameters, impact on blood flow, role in sickle cell disease and effects of exercise. *Front. Physiol.*, 10:1329, 2019.

[394] M. V. Shirmanova, L. E. Shimolina, M. M. Lukina, E. V. Zagaynova, and M. K. Kuimova. Live cell imaging of viscosity in 3d tumour cell models. *Multi-Parametric Live Cell Microscopy of 3D Tissue Models*, pages 143–153, 2017.

[395] Saying Li, Min Chen, Wenchao Wang, Weifeng Zhao, Jianye Wang, Xuna Zhao, and Cheng Zhou. A feasibility study of mr elastography in the diagnosis of prostate cancer at 3.0 t. *Acta Radiolog.*, 52(3):354–358, 2011.

[396] R. L. Taylor. FEAP - finite element analysis program, 2014.

[397] John Lysmer and Roger L Kuhlemeyer. Finite dynamic model for infinite media. *J. Eng. Mech.*, 95(4):859–877, 1969.

[398] Guillermo Rus. Nature of acoustic nonlinear radiation stress. *Appl. Phys. Lett.*, 105(12):121904, 2014.

[399] Jirair K Kevorkian and Julian D Cole. *Multiple scale and singular perturbation methods*, volume 114. Springer Science & Business Media, 2012.

[400] Min Wu, Hermann B Frieboes, Steven R McDougall, Mark AJ Chaplain, Vittorio Cristini, and John Lowengrub. The effect of interstitial pressure on tumor growth: coupling with the blood and lymphatic vascular systems. *J. Theor. Biol.*, 320:131–151, 2013.

[401] Yasuhiro Takeuchi. *Global dynamical properties of Lotka-Volterra systems*. World Scientific, 1996.

[402] Mario de Lucio, Miguel Bures, Arezoo M Ardekani, Pavlos P Vlachos, and Hector Gomez. Isogeometric analysis of subcutaneous injection of monoclonal antibodies. *Comp. Meth. Appl. Mech. Eng.*, 373:113550, 2021.

[403] Maurice A Biot. Generalized theory of acoustic propagation in porous dissipative media. *J. Acoust. Soc. Am.*, 34(9A):1254–1264, 1962.

[404] OC Zienkiewicz and T Shiomi. Dynamic behaviour of saturated porous media; the generalized biot formulation and its numerical solution. *nt. J. Numer. Anal. Meth. Geomech*, 8(1):71–96, 1984.

[405] Martin Schanz. Poroelastodynamics: linear models, analytical solutions, and numerical methods. *Appl. Mech. Rev.*, 62(3), 2009.

"Como no estás experimentado en las cosas del mundo, todas las cosas que tienen algo de dificultad te parecen imposibles; confía en el tiempo, que suele dar dulces salidas a muchas amargas dificultades."

Don Quijote de la Mancha